

①

AD-A230 972



# RESPONSE OF LOW-RISE FRAME STRUCTURE TO DYNAMIC SOIL MOTIONS

J. E. Higgins

November 1990

Final Report

DTIC  
ELECTE  
JAN 30 1991  
E D

Approved for public release; distribution unlimited.

Weapons Laboratory  
Air Force Systems Command  
Kirtland Air Force Base, NM 87117-6008

91 1 29 088

This final report was prepared by the Weapons Laboratory, Kirtland Air Force Base, New Mexico, under Job Order 8809131M. Captain John E. Higgins (NTES) was the Laboratory Project Officer-in-Charge.

When Government drawings, specifications, or other data are used for any purpose other than in connection with a definitely Government-related procurement, the United States Government incurs no responsibility or any obligation whatsoever. The fact that the Government may have formulated or in any way supplied the said drawings, specifications, or other data, is not to be regarded by implication, or otherwise in any manner construed, as licensing the holder, or any other person or corporation; or as conveying any rights or permission to manufacture, use, or sell any patented invention that may in any way be related thereto.

This report has been authored by an employee of the United States Government. Accordingly, the United States Government retains a nonexclusive royalty-free license to publish or reproduce the material contained herein, or allow others to do so, for the United States Government purposes.

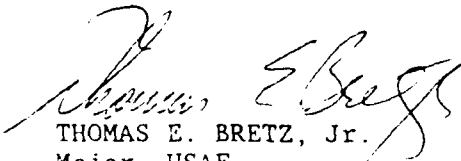
This report has been reviewed by the Public Affairs Office and is releasable to the National Technical Information Service (NTIS). At NTIS, it will be available to the general public, including foreign nationals

If your address has changed, if you wish to be removed from our mailing list, or if your organization no longer employs the addressee, please notify WL/NTES, Kirtland AFB, NM 87117-6C08 to help us maintain a current mailing list.

This report has been reviewed and is approved for publication.

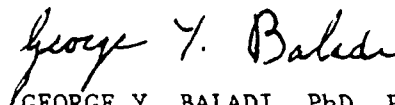


JOHN E. HIGGINS  
Capt, USAF  
Project Officer



THOMAS E. BRETZ, Jr.  
Major, USAF  
Chief, Civil Engineering Research Div

FOR THE COMMANDER



GEORGE Y. BALADI, PhD, PE  
Technical Advisor  
Civil Engineering Research Div

DO NOT RETURN COPIES OF THIS REPORT UNLESS CONTRACTUAL OBLIGATIONS OR NOTICE ON A SPECIFIC DOCUMENT REQUIRES THAT IT BE RETURNED.

# REPORT DOCUMENTATION PAGE

Form Approved  
GSA FPMR (41 CFR) 101-11.6

1. AGENCY USE ONLY (Leave blank)		2. REPORT DATE November 1990	3. REPORT TYPE AND DATES COVERED Final - Jun 88-Dec 89
4. TITLE AND SUBTITLE RESPONSE OF LOW-RISE FRAME STRUCTURE TO DYNAMIC SOIL MOTIONS		5. FUNDING NUMBERS PR: 8809 TA: 13 WU: 1M PE: 62601F	
6. AUTHOR(S)  Higgins, John E.		8. PERFORMING ORGANIZATION REPORT NUMBER  WL-TR-90-86	
7. PERFORMING ORGANIZATION NAME(S) AND ADDRESS(ES) Weapons Laboratory Kirtland AFB, NM 87117-6008		9. SPONSORING MONITORING AGENCY NAME(S) AND ADDRESS(ES)	
9. SPONSORING MONITORING AGENCY NAME(S) AND ADDRESS(ES)		10. SPONSORING MONITORING AGENCY REPORT NUMBER	
11. SUPPLEMENTARY NOTES Dissertation in partial fulfillment of the requirements for the degree of Doctor of Philosophy.			
12a. DISTRIBUTION AVAILABILITY STATEMENT Approved for public release; distribution unlimited.		12b. DISTRIBUTION CODE	
13. ABSTRACT (Maximum 200 words) The major objective of this study was to develop a simplified model to simulate the response of low-rise structures subjected to dynamic loads. This model incorporates the influence of soil and floor flexibility and is based upon underlying assumptions of static portal frame analysis. Ultimately, this study was extended to incorporate mono-symmetric structures (with and without setback) subject to self-induced torsion, as well as asymmetric frames. This model provides estimates of any desired force or displacement which might be determined in a corresponding space frame model. For selected design parameters, including maximum base shear and torque, maximum horizontal roof deflection, and maximum beam forces (shear, moment, and torque), the average errors for all comparisons to space frame calculations were less than ten percent.  Prior to development of the simplified model, preliminary studies assessed the impact of linear soil-structure interaction effects (SSI) upon the response of space frames with flexible mat foundations and composite beam/slab floor systems. Within the limits of linear analysis of uniformly applied horizontal soil loads, mat flexibility was found significant only to the response of the mat foundation of the structure. Structure forces and displacements above the mat are only slightly affected by soil and mat flexibility.			
14. SUBJECT TERMS Earthquake                      Torsion                      Soil-Structure Interaction Dynamic Response              Setback                      Structural Analysis Simplified Analysis              Frame			15. NUMBER OF PAGES 274
			16. PRICE CODE
17. SECURITY CLASSIFICATION OF REPORT Unclassified	18. SECURITY CLASSIFICATION OF THIS PAGE Unclassified	19. SECURITY CLASSIFICATION OF ABSTRACT Unclassified	20. LIMITATION OF ABSTRACT

Prior to development of the simplified model, preliminary studies assessed the impact of linear soil-structure interaction effects (SSI) upon the response of space frames with flexible mat foundations and composite beam/slab floor systems. An extensive parameter study of representative space frames was conducted, in which response of the frames supported on a modest soil volume of finite elements was used to determine an effective distribution of equivalent soil springs. With the equivalent soil spring distribution in place, each frame was then subjected to one or more earthquake loads using modal analysis and appropriate mode combination techniques. Investigation of flexible mat foundations was limited to frames loaded in the direction of a horizontal axis of symmetry. Accuracy of the space frame parameter study model was compared to published analytical results and found to be sufficiently accurate to support the following broad conclusions. Within the limits of linear analysis of uniformly applied horizontal soil loads, mat flexibility is significant only to the response of the mat foundation of the structure. Structure forces and displacements above the mat are only slightly affected by soil and mat flexibility. This preliminary study provided baseline space frame calculations for comparisons with the simplified model.

or	
<input checked="" type="checkbox"/> <input type="checkbox"/> <input type="checkbox"/>	
Justification	
By _____	
Distribution/	
Availability Codes	
Disc.	Avail and/or Special
A-1	

## TABLE OF CONTENTS

	Page
TABLE OF CONTENTS . . . . .	v
LIST OF FIGURES . . . . .	viii
LIST OF TABLES . . . . .	xii
LIST OF SYMBOLS . . . . .	xiii
CHAPTER	
I            INTRODUCTION . . . . .	1
Overview . . . . .	1
Background . . . . .	2
Current Design Practice . . . . .	6
Research Outline . . . . .	14
II           ANALYSIS AND MODELING OF FRAME STRUCTURES . . . . .	18
Overview . . . . .	18
Space Frame Response . . . . .	19
Stick Frame Response . . . . .	35
Summary of Calculations Performed . . . . .	57
III          RESULTS OF PRELIMINARY INVESTIGATION OF SOIL-STRUCTURE INTERACTION . . . . .	67
Preliminary Soil Model Verification . . . . .	67
Frame Structures with Flexible Mat Foundations Excited along a Plane of Symmetry . . . . .	79

CHAPTER	Page
IV RESULTS OF SIMPLIFIED DYNAMIC PORTAL FRAME MODEL . . . . .	88
Superstructure Response of Frames Loaded in the Direction of an Axis of Symmetry (Primary Forces and Displacements) . . . . .	88
Superstructure Response of Frames Loaded in the Direction of an Axis of Symmetry (Individual Member Forces) . . . . .	97
Eccentric Frame Structures with Rigid Mat Foundations Excited in Horizontal Directions Insuring Self-Induced Torsion . . . . .	106
V CONCLUSIONS . . . . .	114
Phase 1 - Preliminary Study of Soil-Structure Interaction . . . . .	114
Phase 2 - Portal Frame Model with Loading in the Direction of an Axis of Symmetry . . . . .	120
Phase 3 - Portal Frame Model With Torsion Allowed . . . . .	123
Application of Portal Frame Model to Design . . . . .	126
REFERENCES . . . . .	132
APPENDIX	
A NET FLOOR DISPLACEMENTS AND FORCES . . . . .	142
B MAT VERTICAL DEFLECTION PROFILES . . . . .	175
C EQUIVALENT SOIL SPRING STIFFNESS . . . . .	208

APPENDIX	Page
D      SUMMARY OF ANSYS ANALYSIS PROCEDURES . . . . .	221
Reduced Modal Analysis . . . . .	222
Direct Harmonic Response Analysis . . . . .	222
Pseudo-Velocity Spectrum Response . . . . .	224
Guyan Reduction to Specified Master Degrees of Freedom and Superelement Formation . . . . .	227
E      EXAMPLE PORTAL FRAME ANALYSIS . . . . .	230
VITA . . . . .	254

## LIST OF FIGURES

FIGURE		Page
1.1	Conceptual illustration of stick, planar, and space frame models . . . . .	3
2.1	Displacement conditions on a plane of antisymmetry . . . . .	20
2.2	Comparison of finite element and equivalent soil spring models . . . . .	22
2.3	Soil volume dimensions . . . . .	27
2.4	Comparison of earthquakes selected for study . . .	34
2.5	General soil spring model for rigid mat foundation . . . . .	36
2.6	Portal frame model (symmetric loading and asymmetric loading with torsion) . . . . .	37
2.7	Model for computing effective floor springs of stick model . . . . .	40
2.8	Model for computing effective torsional column stiffness of stick model of moment resisting frame . . . . .	46
2.9	Doubly symmetric, monosymmetric, and asymmetric floor plans with soil loading directions . . . . .	63
3.1	Overall stiffness (rocking mode) for massless, rigid mat on soft soil ( $v_s = 500$ fps) . . . . .	70

FIGURE	Page
3.2 Overall radiation damping (rocking mode) for massless, rigid mat on soft soil ( $v_s = 500$ fps) . . . . .	70
3.3 Comparison of proposed model values of stiffness and damping intensity along a square mat centerline to values derived from Whittaker and Christiano (56) data ( $K=.004, a_0=0.0$ ) . . . . .	73
3.4 Comparison of proposed model values of stiffness and damping intensity along a square mat centerline to values derived from Whittaker and Christiano (56) data ( $K=3.3, a_0=0.0$ ) . . . . .	73
3.5 Comparison of proposed model values of stiffness and damping intensity along a square mat centerline to values derived from Whittaker and Christiano (56) data ( $K=.004, a_0=2.5$ ) . . . . .	74
3.6 Comparison of proposed model values of stiffness and damping intensity along a square mat centerline to values derived from Whittaker and Christiano (56) data ( $K=3.3, a_0=2.5$ ) . . . . .	74
3.7 Simple comparison models (half-space and quarter-space) . . . . .	76
3.8 Comparison of soil deflection profile ( $u_x$ ) below mat center for quarter and half slab calculations ( $a_0 = .29$ ) . . . . .	78
3.9 Interpretation of negative equivalent springs . . . . .	81

FIGURE	Page
3.10 Horizontal floor deflection variation with soil shear wave velocity (series 10/1:1/0500-1500/E-C) . . . . .	85
3.11 Total column shear variation with soil shear wave velocity (series 10/1:1/0500-1500/E-C) . . . . .	85
4.1 Mode 1 frequencies (series N/1:1/0500) . . . . .	89
4.2 Mode 1 frequencies normalized to 3-D data (series N/1:1/0500) . . . . .	89
4.3 Mode frequency comparisons 3-D versus portal frame (series N/1:1/0500) . . . . .	91
4.4 Mode frequency comparisons 3-D versus portal frame (series N/1:1.75/0500) . . . . .	91
4.5 Comparison of computed mode 1 frequencies for series N/1:1/0500 to ANSI field data for steel frames . . . . .	92
4.6 Horizontal floor deflection with cantilever beam bounding estimate (series 5/1:1/0500/E-C) . . . . .	94
4.7 Total column shear with cantilever beam bounding estimate (series 5/1:1/0500/E-C) . . . . .	94
4.8 Comparison of maximum beam shear location and magnitude normalized to portal frame values for typical quadrant . . . . .	103
4.9 Comparison of maximum beam moment location and magnitude normalized to portal frame values for typical quadrant . . . . .	104

FIGURE

Page

- 4.10 Comparison of maximum beam torque location and magnitude normalized to portal frame values for typical quadrant . . . . . 105

## LIST OF TABLES

TABLE		Page
2.1	Loading in a plane of symmetry . . . . .	58
2.2	Structural details . . . . .	61
3.1	Comparison of overall rigid mat rocking stiffness (computed from proposed soil model) to Dobry and Gazetas (14) recommendations . . . . .	69
4.1	Comparison of important response values from space frame and portal frame analysis . . . . .	98
4.2	Summary comparison of important response values from space frame and portal frame analysis . . . . .	101
4.3	Comparison of important response values from space frame and portal frame analysis with torsion response allowed . . . . .	107

## LIST OF SYMBOLS

The important symbols and notations used in this dissertation are defined where they are first used in the text and given below:

$A_k$	=	Effective area of $k^{\text{th}}$ column of planar frame model
$A_{kj}$	=	Area of $j^{\text{th}}$ column of $k^{\text{th}}$ floor of space frame model
$a_0$	=	Dimensionless frequency
$a_t$	=	Tributary area at soil boundary node in computing $c_{ni}$ and $c_{ti}$
$b$	=	Mat width in direction of loading
$C_T$	=	.035 for steel frames
CCC	=	Complete quadratic mode combination
$C$	=	Damping matrix
$c$	=	Mat width in direction normal to loading
$c_{ni}$	=	Normal boundary damper viscosity
$c_0$	=	Compression wave soil velocity
$c_s$	=	Shear wave soil velocity
$c_{ti}$	=	Tangential boundary damper viscosity
$D$	=	Maximum lateral dimension of structure
$D$	=	Unit direction vector for spectral excitation
$d$	=	Equivalent dashpot viscosity

$\tilde{d}$	=	Complex mat vertical deflection at link
$E_b$	=	Elastic modulus of beams
$E_c$	=	Elastic modulus of columns
$E_m$	=	Elastic strain energy of material m
$E_{mat}$	=	Elastic modulus of mat
E-C	=	EI Centro earthquake spectral loading
e	=	Static column eccentricity
$e_m$	=	Damping ratio for material m
$e'$	=	Effective modal damping
$F_{max}$	=	Force vector amplitude
$F(t)$	=	Force vector
f	=	Frequency (cycles/sec)
$\tilde{f}$	=	Complex link axial force
G	=	Column shear modulus
$G_s$	=	Shear modulus of soil
h	=	Mat thickness
$h_n$	=	Overall structure height
$I_b$	=	Beam moment of inertia
$I_c$	=	Column moment of inertia

- $I_{kji}$  = Moment of inertia of  $j^{\text{th}}$  column of  $k^{\text{th}}$  floor in  $i$  direction for space frame model
- $I_{kl}$  = Effective moment of inertia of  $k^{\text{th}}$  floor column in  $l$  direction for planar frame model
- $J_{\text{eff}}$  = Effective portal frame column polar moment of inertia
- $K$  = Mat to soil stiffness ratio
- $K_{fi}$  = Equivalent rotational stiffness for floor  $f$  about axis direction  $i$
- $K_t$  = Overall torsional floor stiffness
- $K_{\theta jx}$  = Individual column joint rotation stiffness due to floor system
- $K$  = Stiffness matrix
- $k$  = Equivalent spring stiffness
- $L$  = Floor height
- $L_b$  = Beam length
- $L_c$  = Column length
- M.C. <sub>$i$</sub>  = Mode coefficient ratio for mode  $i$
- M-C = Mexico City earthquake spectral loading
- $M$  = Mass matrix
- $m$  = Material type
- $m_i^s$  = Spectral multiplier for mode  $i$

- $\rho_{min}$  = Minimum mat reinforcement ratio
- $R_a$  = Total modal response
- $R_i$  = Maximum modal response of mode  $i$
- $r$  = Ratio of frequencies for coupled modes  $i$  and  $j$  in computing  $\epsilon_{ij}$
- $S_{vi}$  = Interpolated spectral velocity of mode  $i$
- SRSS = Square root of sum of squares mode combination
- SSI = Soil-structure interaction
- $T_1$  = Fundamental period of structure
- $T$  = Stick model column member torque
- $\mathbf{u}$  = Nodal displacement vector
- $\mathbf{u}_{max}$  = Nodal displacement vector amplitude
- $v_s$  = Shear wave velocity of soil
- $V_{ij}$  = Net column  $i$  shear in direction  $l$
- $V_{tij}$  = Column  $i$  shear in direction  $l$  due to torque
- $V_{vit}$  = Column  $i$  shear in direction  $l$  due to shear
- $x_i$  = Column  $i$  x-coordinate relative to origin at center of rigidity
- $z_i$  = Column  $i$  z-coordinate relative to origin at center of rigidity
- $\alpha$  = Soil wave angle of incidence to boundary normal vector

- $\beta$  = angle from x-axis to column i radius with origin at center of rigidity
- $\gamma_{il}$  = Portal frame moment coefficient for column i in direction l
- $\epsilon_{ij}$  = Coupling coefficient for modes i and j
- $\lambda_i$  = Participation factor for mode i
- $\mu_p$  = Poisson's ratio for mat
- $\mu_s$  = Poisson's ratio for soil
- $\xi_i$  = Effective damping ratio for mode i
- $\rho$  = Joint rotation index
- $\rho_s$  = Soil density
- $\phi$  = Displacement vector phase shift
- $\psi$  = Mode shape vector
- $\Omega$  = Forcing function natural frequency
- $\omega$  = Frequency (radians/sec)
- $\omega_i$  = Frequency (radians/sec) for mode i

## CHAPTER I

### INTRODUCTION

#### OVERVIEW

To better understand the response of civil structures to dynamic soil loading, recent research has focused on two means of improving analysis: refining soil and structure material models and expanding computer representation of material and structural details. Budget and schedule constrain the application of such improved analyses in the design process. These constraints bear heavily in the design of most low-rise framed structures--hotels, office buildings, and parking garages. Running counter to this trend, the major objective of this research was to generate recommendations for a reliable simplified design model for low-rise frames. A preliminary objective of this research was to assess the impact of linear soil-structure interaction (SSI) effects upon the response of space frames with flexible mat foundations. An extensive parameter study of doubly symmetric frame structures analyzed by advanced techniques provided the basis for simplified model recommendations.

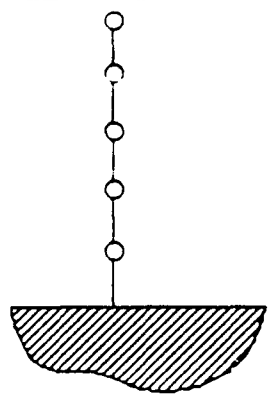
-----  
This dissertation conforms to the style of the Journal of the Engineering Mechanics Division, ASCE.

## **BACKGROUND**

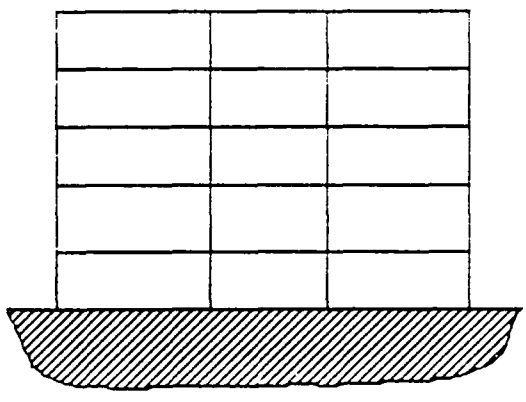
### **Comparison of Stick, Planar, and Space Frame Models**

Where practical, structural designers have progressed from simple stick models to more sophisticated planar frame and space frame models (see Figure 1.1). The stick models capture principal features of response for many conventional architectures. In frame structures, such models permit calculation of displacements at each floor elevation and net shear forces and bending moments in connecting columns. Planar frame models permit supplementary calculation of net axial column forces due to ground motion, as well as net beam and floor slab forces, moments, and displacements directed in the plane of ground motion. Space frame models permit calculation of forces, moments, and displacements--acting in all members and in all directions. Principal benefits of planar and space frame structural models are two-fold. First, improved dimensional modeling allows direct calculation of secondary or supplemental displacements and stresses in structures. These secondary responses may control structural design for certain architectures. For instance, space frame analysis can assess the torsional response characteristic of asymmetric floor plans. Second, the expansion of degrees of freedom into multiple dimensions mobilizes additional flexibility inherent in an actual structural frame. This enhanced flexibility typically increases deflections while reducing forces and moments in members.

stick frame



planar frame



space frame

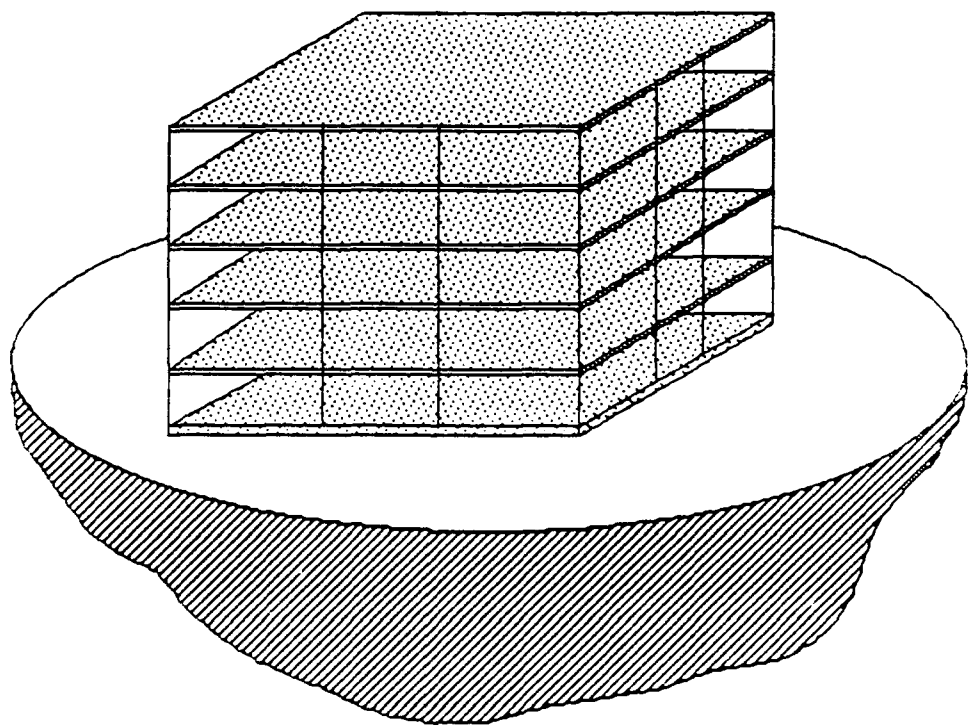


Figure 1.1 Conceptual illustration of stick, planar, and space frame models

Conversely, the simplified models tend to yield conservative estimates of member forces, but may significantly underestimate critical displacements of the structure.

### **Soil-Structure Interaction Models**

In the past, research and design engineers have frequently ignored SSI effects. They have simply applied uniform free-field ground motions directly to the base of structural frames. As with restrictions on model dimensionality, restrictions on soil flexibility also tended to yield conservatively low estimates of structural strength, as well as unconservatively low estimates of structure displacements. Subsequent studies (relying upon improved computer capabilities) have demonstrated reasonable economy in analysis by introducing progressively improved soil models. Soil motions dangerous to typical civil structures can induce large soil shear-strains and nonlinear material response (e.g., 20, 31, 49). Additionally, if applied loads are strong enough to cause partial uplift of the structure from the soil, geometric soil-structure non-linearity will occur (e.g., 1, 5, 11, 16, 35, 41, 47, 57, 61). To directly account for material and geometric non-linearity, program enhancements increase computer memory requirements and computational expense compared to linear solution techniques. To include these non-linear behavior mechanisms, engineers use cost-effective approximations. Based on non-linear SSI studies (e.g., 20, 31, 49) and response of actual

structures to earthquake and ground shock loading (e.g., 19, 44, 46), they may select linear soil properties which simulate expected overall soil stiffness and damping. Within acceptable design tolerances, they may reduce the problem of progressive loss of soil-structure contact (uplift) using a simplified two-spring soil model suggested by Psycharis and Jennings (35).

#### **Advanced Finite Element Modeling Features of Interest**

Published SSI computations for frame structures typically feature simple stick models. However, recent developments in general purpose finite element analysis codes can allow convenient improvement of space frame models with acceptable computational effort for purposes of research. As implemented in ANSYS and other general purpose finite element programs, the Guyan-reduction algorithm (e.g., 12, 24, 45) retains much of the fundamental character of a space frame structure. This algorithm systematically redistributes mass, stiffness and damping in a consistent manner. Mode frequencies and shapes are generated based on a limited number of active coordinates. Mass, stiffness, and damping contributions for all nodal coordinates are accounted for in the formation of effective matrices to represent these properties for the reduced set of coordinates. With reasonable selection of active coordinates, lowest mode effects are usually well represented. Loss of fidelity for higher modes typically subtracts little from overall response of large civil

engineering structures. The Guyan-reduction algorithm provides a convenient programming environment for analysis of frame structures which incorporate both three-dimensionality and linear SSI effects.

Additionally, the Guyan-reduction can be combined with substructuring techniques to simplify SSI analysis. With these features a supporting soil region may be modeled as a substructure once, and then loaded with various frame superstructures in separate calculations, thus limiting the cost of repeated element formation in parametric studies. The number of degrees of freedom of the substructure may be easily adjusted to accommodate changes in frequency sensitivity for various soil-structure systems evaluated in this way. Again, with reasonable distributions of active coordinates, lower mode fidelity of the soil substructure can be well preserved., see Chopra and Gutierrez (10) for further discussion.

## **CURRENT DESIGN PRACTICE**

### **Critical Structures**

To satisfy continuing interest, research engineers have conducted limited investigations of simple non-linear soil-structure systems (e.g., 20, 31, 49). However, finding non-linear SSI calculations to be cost prohibitive for routine tasks, design engineers frequently make the following approach to structure

design. For critically important axisymmetric structures (such as nuclear power plant containment vessels or large cooling towers), the designer may undertake SSI calculations using site representative linear soil properties consistent with the design ground motions and anticipated soil shear-strain levels. Sometimes the designer will use a simple stick model of the superstructure, but retain a full three-dimensional representation of the soil and substructure. The massive mat substructures required to support these architectures are approximately rigid. However, secondary responses, such as structure accelerations at equipment anchorage locations, change significantly when analysis accounts for slight mat flexibility (e.g., 23, 36, 58). For critical structures lacking axisymmetry, designers frequently simplify SSI analysis by retaining stick frame or planar frame models of the superstructure, but reduce the soil and substructure model to a two dimensional form.

### **Low and Medium-Rise Frames**

#### **Prominent Analysis Methods**

To further reduce computer usage requirements in a highly competitive design environment, designers of ordinary frame structures generally select from two analysis methods. They may apply dynamic ground motions to simple stick frame models of the structural frame (e.g., 2, 39, 48). For the vast majority of frames designed by this method, the soil is assumed rigid--free-

field ground motion is input directly to the base of the frame. Such stick frame analysis generally yields conservative estimates of net column forces, but may under-predict story deflections. This trend is dependent upon relatively uniform distributions of dynamic input with frequency. No other forces or displacements are directly inferred. A significant counter example to this trend may occur with torsional loading or self-induced torsion resulting from asymmetric geometry, see Todorovska, Lee, and Trifunac (43). In this case, uniform base motion does not allow amplification of asymmetric modes, thereby leading to possibly unconservative force estimates. Alternatively, and most commonly, designers may apply code-specified equivalent lateral static loads to mass concentrations in one, two, or three-dimensional frame models (e.g., 3). These statically loaded models tend to yield member forces and deflections which are lower than typical peak values computed from dynamic analysis. Resulting frame designs rely upon implicit relief of forces and moments through energy dissipation at plastic hinges in the frame. Since hinging is assumed but not explicitly modeled, deflections can be significantly under computed, regardless of the level of dimensionality and structural detail.

### Stick Frame Modeling in Dynamic Analysis

The extent to which the peak excursions in computed forces accurately reflect the need for non-linear energy dissipation in an actual design is limited by the accuracy of the specific linear model used in dynamic analysis. The simplest stick frame model regularly used to assess response of frame structures is the shear building model. For this model, the entire horizontal flexibility of the frame is attributed to bending (and slight shear) deformation in the columns. Because the floor system is considered rigid, joints connecting columns at floor elevations are locked against rotation. If subjected to a dynamic loading with a uniform distribution of spectral energy with respect to frequency, this model can be expected to develop greater shearing forces than a careful three-dimensional model of the same structure. The three-dimensional model introduces additional flexibility, primarily through deflection of the floor system in low-rise structures. Flexibility in the floor system effectively softens the structure response by allowing column rotation.

Another even simpler stick frame model, the cantilever beam, relaxes all restraint against rotation of column nodes at floor elevations. These continuous, but unrestrained, joint connections simulate a structure with no floor stiffness. This model can be used to good effect in approximating response of shearwall structures (where floor systems contribute little to lateral

resistance). However, this model is generally far too limber for typical moment-resisting frames. For such frames, the cantilever beam model will grossly over-predict deflections and under-predict shear forces compared to a careful three-dimensional model. This trend is sensitive to the same loading considerations described for the shear building model.

In a model proposed by Blume (8) in 1968, improvement in stick frame response was sought by artificially adjusting the bending stiffness of columns in the shear beam model. This adjustment relied upon assessment of the ratio of column to beam flexibility, at the mid-height floor of the frame. This ratio was referred to as the joint rotation index ( $\rho$ ):

$$\rho = \frac{\sum_{1}^{\text{all}} \frac{I_b}{L_b}}{\sum_{1}^{\text{all}} \frac{I_c}{L_c}} \quad \text{eq. 1.1}$$

where  $I_c$  and  $I_b$  are the individual column and girder moments of inertia, and  $L_c$  and  $L_b$  are the individual column and girder lengths of the mid-height floor of the frame. Studies, conducted at the time this model was proposed, suggested credible simulation of modal responses for the first three modes, with deterioration at

higher modes. The model may only be used to compute those structural response features predicted by the shear beam model: net column shears, moments, and horizontal floor deflections. The joint rotation index ( $\rho$ ) has been applied as recently as 1986, by Cruz and Chopra (13), to assess practical ranges of floor flexibility; however, no recent applications of the Blume model were found in the literature. A principle objective of the present study was to develop an alternative stick model with a larger number of degrees of freedom to more directly model the influence of floor system flexibility on lateral and torsional flexibility. Ultimately, techniques were also developed to assess forces and displacements in any structural element, not just net column response.

### **Soil Modeling in Dynamic Analysis**

#### Prominent Analysis Methods

Where dynamic SSI calculations are to be performed, designers often select from two basic approaches for modeling the soil. Various authors (e.g., 6, 7, 15, 22, 25, 26, 29, 30, 32, 37, 42, 52, 54) refer to these methods as finite element and lumped mass analysis, or similar names. More recently, research (e.g., 15, 17) has demonstrated the feasibility of boundary element methods in assessing SSI effects. However, for design of routine frame structures, practical application of this method awaits the development of general purpose programs which combine boundary

element and finite element techniques. Another recently introduced method of analysis, the flexible volume method, has been applied to flexible foundations by Ostadan, Tseng, and Lilhanand (34).

#### Finite Element Models

With the finite element method of SSI analysis (used primarily in the United States), the soil foundation is most often treated as a two-dimensional material confined by plane-strain conditions. Appropriate vertical and horizontal dashpots attenuate waves emanating from the soil-structure interface in a manner simulating out-of-plane radiation damping. This two-dimensional method of analysis of soil interaction effects is almost exclusively implemented with FLUSH, a program authored by Lysmer, Udaka, Tsai, and Seed (28). This program minimizes the lateral extent of the two-dimensional soil volume through special infinite elements. These infinite elements accurately represent the far field, but only for two-dimensional geometries. Because the emphasis of this program is on wide ranging linear soil effects, including layered geologies, the actual planar frame representation is rather crude. Frequently, soil-structure interface motions found with FLUSH are used to drive detailed frame models, using more general finite element programs. The FLUSH program assumes most energy radiates from the structure in planes closely aligned with the direction of propagation of the

free-field soil disturbances. Because of this alignment, two-dimensional approximation is generally valid.

Where large additional design costs are justified, designers may extend the finite element procedure and model the soil foundation with a convenient and effective bounding geometry, such as a rectangular or hemispherical soil volume. For such models the structure is located at or near the center of the free surface of this volume. The other extremities of the soil volume are constrained by combinations of springs and dashpots approximating the far field of a soil half-space (e.g., 50, 51).

#### Lumped Mass Method (Rigid Foundations - Linear Soil Springs)

The lumped mass method (frequently applied in Europe and Japan) assesses Green's influence function to arrive at an equivalent elastic foundation. This foundation is defined by a complex, frequency-dependent impedance function distributed over the substructure interface. Several researchers have shown direct calculation of Green's influence function to be practical for a structure supported by a rigid mat (e.g., 27, 54, 59). With rigid mat foundations, the complex impedance function can be replaced with a combination of six frequency dependent springs and dashpots. The actual variation of frequency dependence in these equivalent springs and dashpots is both structure and soil dependent (see Wolf (58) for numerous examples).

## **RESEARCH OUTLINE**

### **Overview**

The goal of this research was to promote improved earthquake and ground shock design practice for low-rise structural frames, such as office buildings, laboratories, hotels, and parking structures. To achieve this goal, an efficient space frame model accounting for SSI effects was first developed. Analysis performed with this model included an extensive parametric study of typical low-rise frame structures. Study parameters embraced a representative range of floor plans, elevations, soil stiffnesses, and soil loadings. By comparing the response of typical stick models to the space frame response of the parameter study, a modified design model was sought which reflects the response characteristics of more exact analysis. Finally the study culminated in an assessment of the impact of various findings on current design practices.

### **Chronologic Organization**

Phase 1 - preliminary investigation of space frames with flexible mat foundations - included a comprehensive evaluation of the following parameters:

1. Structural frame elevations ranging from 5 to 20 stories.
2. Rectangular floor plans with overall length to width ratios ranging from 0.5 to 2.0.

3. Soil conditions consistent with shear-wave velocities of 500 to 1500 fps.
4. Diverse earthquake types (El Centro, 1940--Mexico City, 1986).
5. Structures uniformly loaded in a horizontal direction, parallel to a plane of symmetry.

Phase 2 - development of a simplified structural model - was limited to simulation of space frame response for structures uniformly loaded in the direction of a plane of symmetry. The types of issues addressed with these models include:

1. Appropriate distribution of structural inertia and stiffness in the frame.
2. Acceptable representation of soil-structure interaction using simple, equivalent springs and dashpots.
3. Significance of frequency dependence of soil properties in the response of frame structures.
4. Assessment of superstructure forces and deflections.

Phase 3 - extension of the simplified model - assessed the influence of other loading cases and architectures including:

1. Doubly symmetric frames uniformly loaded in an arbitrary horizontal direction.

2. Self-induced torsion in mono-symmetric floor plans, uniformly loaded in an arbitrary horizontal direction.
3. The influence of setback frame profiles in mono-symmetric floor plans subject to self-induced torsion.
4. Self-induced torsion in asymmetric floor plans, uniformly loaded in a horizontal direction.

Final design recommendations were statistically evaluated to delineate the degree of conservatism inherent the proposed design procedures. Additionally, areas in which these procedures were unconservative, or fail to predict significant aspects of structure response, were highlighted.

#### **A Key Technical Approximation of the Study**

A secondary objective of this parametric study was to measure the importance of the SSI effect to overall three-dimensional response of frame structures with flexible foundations. To measure the importance of this phenomenon in a practical manner, analysis of a modest soil volume provided frequency-independent distributions of effective springs and dashpots. Ghaffar-Zadeh and Chapel (18) have demonstrated that frequency-independent impedances can provide "a satisfactory approximation of the exact solution over a wide frequency range" for circular foundations. These impedances were selected for correct response at the fundamental frequency of soil-structure

system. Earlier work suggested the same approximation to be valid for more arbitrary floor plans (e.g., 6, 21). Experimental work by Weissman (55), suggests that regardless of the foundation shape or level of embedment, "the amount of radiation damping depends on the natural frequency of the vibrating modes of the structure relative to the fundamental frequency of the soil layer". Convergence tests were performed for the present study to insure the soil model provided an accurate distribution of relative soil stiffness and viscosity over the base of the frame. In the interests of economy, absolute overall stiffness and viscosity of the resulting soil model were allowed to vary from independently verified rigid-mat examples by as much as one-third. The sensitivity of rigid-mat structural response to soil model error was assessed by comparing the results of the present study with published analytical analyses (e.g., 14, 56, 59). This error sensitivity was further assessed for flexible mat calculations by comparing the approximate results of the finite element analysis of the soil volume over a wide range of relative soil to mat foundation stiffness ratios.

## CHAPTER II

### ANALYSIS AND MODELING OF FRAME STRUCTURES

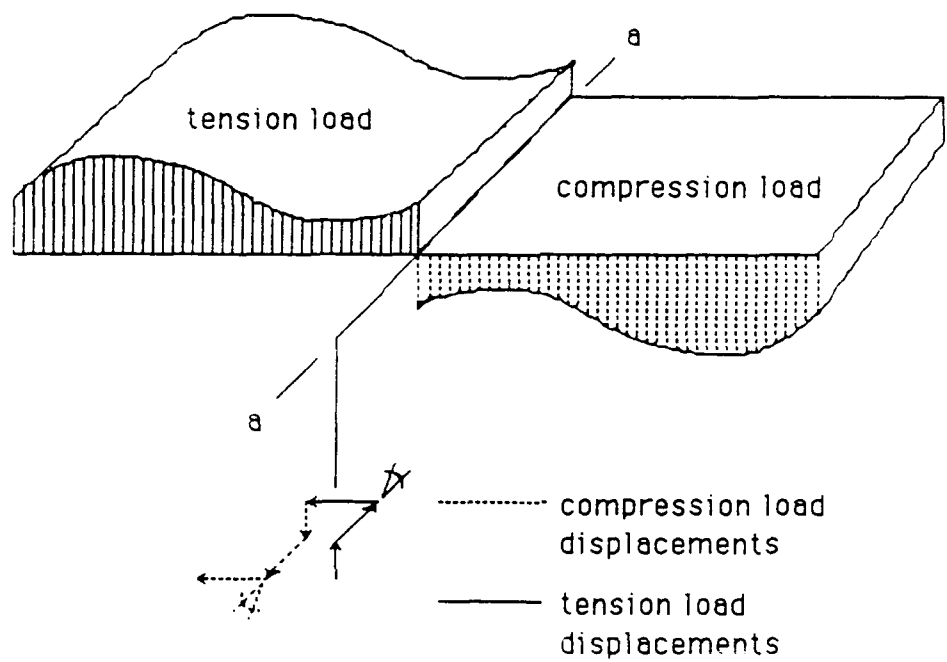
#### OVERVIEW

Phase 1 preliminary investigation of response of space frames with flexible mat foundations provided baseline comparisons for simpler stick frame analogs (phase 2). Phase 1 also supplied the rationale for modeling mono-symmetric and asymmetric space frames with rigid mat foundations - for comparison with corresponding stick frame analogs (phase 3). For phase 1, three to twenty story rectangular plan structures rested upon flexible mat foundations supported by an elastic soil island of prismatic finite elements. Each frame resisted horizontal soil loading directed along a plane of symmetry. Findings of phase 1 calculations suggested more practical soil and foundation models for use with phase 2 and 3 structures. In the procedure description to follow, and in later chapters, these phases are referenced to clarify which models were developed first and how results obtained from each phase influenced later models. The remainder of this chapter is organized to demonstrate space frame model details, stick frame model details, and itemization of specific calculations and structural details, in that order.

## **SPACE FRAME RESPONSE**

### **Symmetric Loading of Rectangular Frames**

The symmetry of phase 1 floor plans decreased computer costs significantly. Force and displacement distributions in these frames must vary symmetrically in opposing halves of the structure. Prohibiting out-of-plane displacement and rotation of the structure at the plane of symmetry (in the direction of loading), reduced the model size by half. Even with this soil volume reduction, conventional finite element modeling of soil in dynamic analysis requires an extensive soil volume beneath the mat foundation to insure accurate representation. By examining the soil response of an elastic half-space to an arbitrary loading couple distributed about a free surface axis (axis a-a, see Figure 2.1) certain boundary conditions are easily recognized. In the vertical plane through this axis dividing the coupled loading, any vertical displacement resulting from a region of compression on one side of the dividing axis is exactly balanced by a tension counterpart on the opposite side of the dividing axis. Similarly, in-plane horizontal displacements and rotations balance to zero. If the soil stiffness and surface load on one side of the axis of symmetry is neglected, the complete set of equivalent boundary conditions at the plane of anti-symmetry must be prescribed to insure the response of the remaining quarter region is unchanged. Similar arguments can be made for the



Note: no net displacement or rotation in the plane of antisymmetry

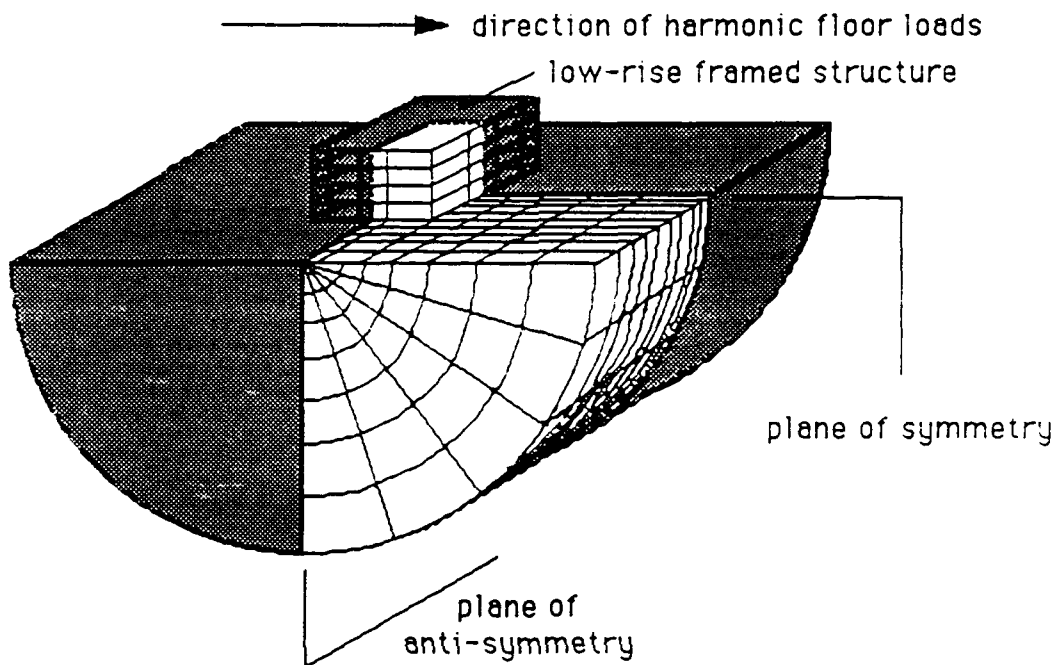
Figure 2.1 Displacement conditions on a plane of antisymmetry

response of the quarter-superstructure. By implementing approximate boundary conditions along this vertical plane of anti-symmetric response (no in-plane displacements or rotations), harmonic rocking forces could be applied to just a quarter region of the soil-structure model (see Figure 2.2). As demonstrated in Chapter III, this simplification provided adequate representation of soil-structure interaction at reduced cost. The results from harmonic loading analysis permitted calculation of approximate vertical spring distributions at the interface between the mat foundation and soil infinity. Distributed springs were required to accurately represent vertical soil stresses applied over the face of the flexible mat. Once determined, the vertical soil springs supported a half frame structure subjected to pseudo-velocity response spectrum loadings (see Figure 2.2).

To compute vertical soil spring distributions, a quarter region of each structure and supporting soil volume were modeled within the bounds of two vertical planes passing through opposing mid-side points of a given floor plan. In-plane deflection and rotation restraint approximated actual conditions on the mid-plane normal to the direction of harmonic loading (plane of anti-symmetry). Recognizing that mode combination schemes generally approximate phase differences by describing peak responses as a computed norm

Structure-soil volume model

(shaded region implied by boundary conditions)



Equivalent structure-soil springs and dashpots model

(shaded region implied by boundary conditions)

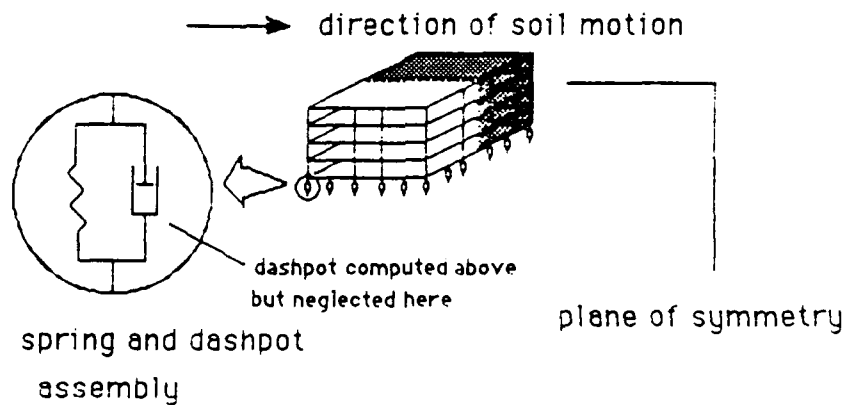


Figure 2.2 Comparison of finite element and equivalent soil spring models

of all significant modes, the combined modal response can be viewed as the peak (stationary) response of a single effective 'mode'. This interpretation is best justified if the structure is dominated by one mode, or a few modes with relatively closely spaced frequencies. To assess the accuracy of these assumptions, comparisons of small half-space and quarter-space calculations, as well as comparisons of detailed quarter-space calculations and elasticity-based solutions for rigid and flexible mats, are presented below (Chapter III).

Where direct finite element modeling of soil is undertaken in dynamic soil-structure analysis, a hemispherical region, or other convenient geometry, frequently describes the soil-infinity boundary (see Niwa, Katayama, and Penzien; Vaughan and Isenberg; and Wolf (33, 50, 58) for representative implementations). If, as described by Wolf (58), all waves strike normal to the far-field boundary, soil waves propagating from the structure to the extreme soil boundary can be perfectly damped (with no reflection) by appropriately selected dampers isolating each boundary node. By modeling a sufficiently large radius for the soil region and locating the structure over the vertex of the region, waves propagating from the structure do impinge upon the spherical boundary at approximate right angles at first reflection. Regardless of

direction of propagation, this angle of incidence is roughly constant for all waves emanating from the structure.

As shown by Wolf (58), longitudinal waves striking a perpendicular surface attenuate perfectly when each boundary node at this surface is constrained by a normal damper of magnitude:

$$c_{ni} = \rho_s a_t c_p \quad \text{eq. 2.1}$$

where  $c_{ni}$  is the viscosity of the damper at boundary node  $i$ ,  $\rho_s$  is the soil density,  $a_t$  is the tributary area of the soil boundary at node  $i$ , and  $c_p$  is the compression wave soil velocity. Additionally, shear waves attenuate perfectly when each boundary node at this perpendicular surface is constrained by a pair of dampers, oriented normal to each other and tangent to the soil surface, of magnitude:

$$c_{ti} = \rho_s a_t c_s \quad \text{eq. 2.2}$$

where  $c_{ti}$  is the viscosity of each damper at boundary node  $i$  and  $c_s$  is the shear-wave soil velocity. These values of  $c_{ni}$  and  $c_{ti}$  are appropriate for a homogeneous, linearly elastic, isotropic continuum.

To further reduce the required volume of the soil, rocking forces on the structure were noted to result in soil wave energy propagated in directions nearly normal to the axis of rocking. This assumption is consistent with the justification for two-dimensional plane-strain analysis in the standard soil-structure program, Flush (28). Following this assumption, the soil region was bounded by a cylindrical surface. As described above, three mutually orthogonal dampers restrained nodes on the far-field surface. Nodes on a vertical plane parallel to the plane of symmetry, and located beyond the extreme reach of the widest floor plan investigated, were constrained to prevent out-of-plane displacement and rotation. As described above a pair of tangential dampers attenuated reflected shear waves at this vertical boundary plane. However, an average angle of incidence was taken into account for elements at varying radial locations from the rocking axis of the soil volume. Following the theory elaborated by Wolf (58), the viscosity values for attenuation of shear waves striking surfaces at an arbitrary angle is given by:

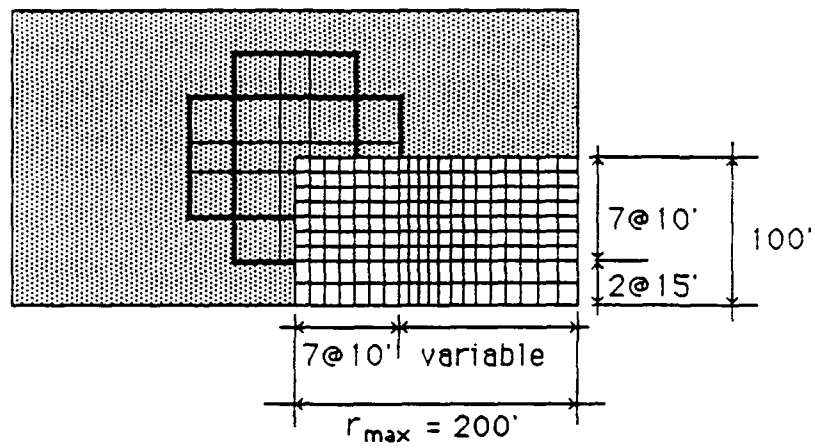
$$c_{ij} = \rho_s a_t c_s \cos(\alpha) \quad \text{eq. 2.3}$$

where  $\alpha$  is the angle of incidence between the wave direction of propagation and the normal to the reflecting surface. The maximum length and width of floor plans in this investigation

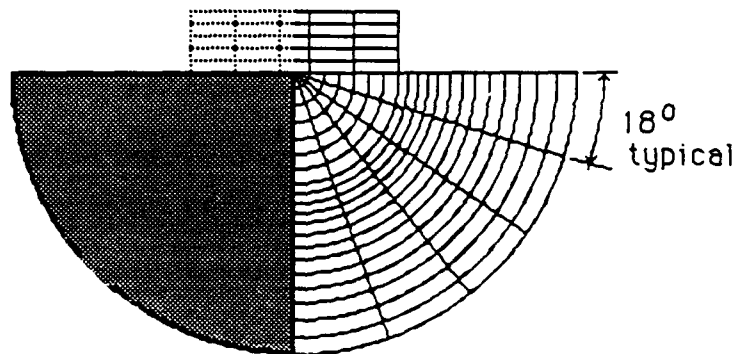
did not exceed 140 feet. Consistent with the findings of Vaughan, Wojcik, and Isenberg (51), a soil cylinder radius of 200 feet, or 2.86 times the maximum half-length of any floor plan, provided volume sufficient for acceptable accuracy (see Chapter I). The width of the soil region, about the axis of rocking, was 100 feet--1.43 times the maximum half-width of any floor plan. See Figure 2.3 for details.

Ten vertical planes, six radial planes, and twenty cylindrical surfaces sub-divided the soil region, with an element node located at the intersections of all bounding or subdividing surfaces. Linear-elastic quadrilateral soil elements connected adjacent soil nodes. The spacing of sub-dividing planes and surfaces concentrated soil elements beneath the mat foundations and avoided element aspect ratios exceeding 4:1:1. The elements with maximum aspect ratios were isolated along the  $r=0.0$  axis and the  $r_{max}$  surface. Displacements at the  $r=0.0$  axis were essentially zero for all calculations, and the  $r_{max}$  surface was located far from the superstructure and also experienced very small displacements. For these reasons, any inaccuracy induced by the high aspect ratio elements was substantially mitigated.

Classical (undamped) modal analysis subjected this soil-structure system to vertically distributed harmonic loads.



plan view



elevation view

—————> direction of soil motion

Figure 2.3 Soil volume dimensions

This distribution applied concentrated loads at the centroid of each floor level, horizontally in the plane of symmetry. The load magnitude at each floor, including the mat foundation level, scaled in proportion to the building mass at that floor level. All forces acted in phase with one another at the fundamental frequency of the soil-structure system. An approximate value of this frequency converged rapidly with simple iteration, as described below. The combined modal response of the soil and structure produced complex forces in link elements, between the soil and structure, and complex vertical displacements of the floor mat, at each link connection. Complex division of these forces and associated displacements provided equivalent vertical soil spring and damper distributions for harmonic loading. This distribution replaced the soil volume in subsequent earthquake spectral loading calculations. The equivalent spring and damper distributions were computed at each soil-mat interface node as follows:

$$\tilde{f} / \tilde{d} = [k + i d / (2 \omega)] \quad \text{eq. 2.4}$$

where  $\tilde{f}$  is the complex link axial force,  $\tilde{d}$  is the complex mat vertical deflection at the link,  $k$  is the equivalent spring stiffness,  $d$  is the equivalent dashpot viscosity, and  $\omega = 2\pi f$ .

where  $f$  is the natural frequency of the harmonic forces applied to the structure.

The appropriate distribution of vertical springs and dashpots needed to resist rocking at the fundamental period of the soil-structure system was unique for each frame design and soil specification investigated. Standard code recommendations provided good first estimates for the fundamental system frequency:

$$T_1 = C_T h_n^{3/4} \quad (\text{Eq. 9B}) \quad \text{ANSI A58.1-1982 (3)}$$

where,  $T_1$ , is the fundamental period of the structure,  $C_T = .035$  for steel frames and  $h_n$  is the overall structure height (in feet). Typically, the assumed input frequency and the computed fundamental mode frequency converged within five percent of each other before the third iteration.

Link elements between the soil and mat foundation provided vertical (axial) rigidity but very low horizontal (shear) resistance. These conditions are consistent with the bulk of previous research describing vertical continuity with no horizontal friction between the soil and mat foundation, see Dobry and Gazetas; Luco and Westmann; Veletsos and Meek;

Whittaker and Christiano; and Wong and Luco (14, 27, 52, 59) for examples.

For all harmonic loading analysis, a single superelement with two hundred internally distributed degrees of freedom modeled the entire soil volume. The number and distribution of these internal degrees of freedom provided sufficient mass points per radially-oriented wavelength to assure accuracy consistent with other limitations of the model. Nodes at the ground level of the soil volume aligned with mat element vertices for all architectures to be considered. Thus the soil island superelement mass and stiffness matrices were computed only three times, for soil shear wave velocities of 500, 1000 and 1500 fps. This superelement implementation significantly reduced overall computer costs for multiple frame response calculations.

With equivalent soil springs and dampers computed, each frame was remodeled as a half-structure truncated at the plane of symmetry in the direction of ground shaking. As will be demonstrated in Chapter III, soil springs were computed with acceptable accuracy at the fundamental frequency of each soil-structure system; however, dashpot magnitudes approached qualitative accuracy only at higher frequencies ( $\omega_0 = \omega b/v_s \geq 5$ , where  $b$  is the maximum plan dimension in the

direction of loading). For strong dynamic soil loading, actual radiation damping was considered to be small compared to material damping, (see Vaughan and Isenberg (50) for estimates of 2% radiation damping for a typical nuclear containment structure). Consequently, for structural analysis of response to earthquake spectral velocities, only distributed vertical springs (with no parallel radiation dampers) supported the flexible mat foundation. For square mat foundations and rectangular foundations with the long dimension oriented in the direction of ground motion, a single spring restrained the structure at the mat center, thus representing horizontal soil stiffness. For rectangular foundations with the long dimension oriented normal to the direction of ground motion, a line of horizontal stiffness springs restrained the structure along the mat axis parallel to that longest dimension. In the latter case, the horizontal spring distribution varied according to tributary area in the direction of loading. In both cases, the total magnitude of horizontal soil stiffness equaled the value computed for a rigid, massless mat, see Dobry and Gazetas (14).

For all earthquake spectrum loadings, a weighted value of viscous damping was adjusted for each mode. The selected ANSYS damping option provides an effective modal damping value as follows:

$$e' = \frac{\sum_1^m (e_m E_m)}{\sum_1^m E_m} \quad \text{eq. 2.5}$$

where  $m$  is the material identifier,  $e_m$  is the damping ratio, and  $E_m$  is the elastic strain energy ( $\frac{1}{2}\{\mathbf{u}\}^T[\mathbf{K}]\{\mathbf{u}\}$ ) for material  $m$ . Here  $\mathbf{u}$  is the nodal displacement vector for elements of material  $m$ , and  $\mathbf{K}$  is the composite stiffness matrix for these elements. Viscous damping for soil was 10%, concrete 5% and steel 2% of critical damping. As will be shown in Chapter III, the bulk of strain energy for the most significant modes was concentrated in the steel columns of the frame, resulting in effective damping ratios ( $e'$ ) slightly larger than 2%.

As described in Table 2.1, two earthquake spectral loadings were selected for use in this study. The El Centro 1940 north-south component of motion was applied to every structure and soil combination. This earthquake has been extensively applied in past studies, and is fairly representative of earthquakes forming the basis for current design spectrum recommendations. For comparison, the Mexico City 1984 east-west component of motion was applied to all square plan doubly symmetric frames resting on soft soil ( $v_s = 500$  fps). This earthquake is not only of unusually high intensity, but has a peculiar distribution of motion amplitude over the range of

observed frequencies. The majority of the input for this earthquake is limited to a band of frequencies ranging from about .3 to .7 Hz. Figure 2.4 compares these earthquake in terms of pseudo-velocity versus frequency.

For each calculation the following items were examined:

- All mat displacements and selected floor displacements.
- Maximum shear, axial, moment and twisting forces for each member size of column and beam.
- All column forces for each floor.

For the doubly symmetric floor plans (no self-induced torsion), square root of sum of squares (SRSS) modal combination provided satisfactory estimates of all response values (see Chapter III).

#### **Eccentrically Loaded Space Frame Response**

Details and analysis of eccentrically loaded space frames, phase 3, were as described for symmetric loading of rectangular frames, with two significant simplifications. First, essentially rigid material properties characterized the mat foundation. Second, simple axial and torsional soil

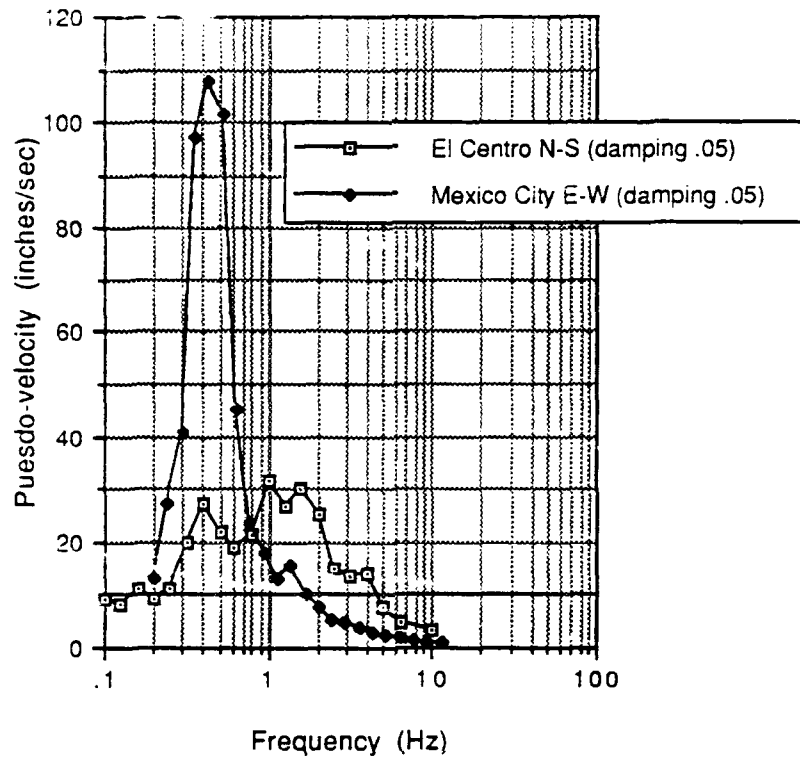


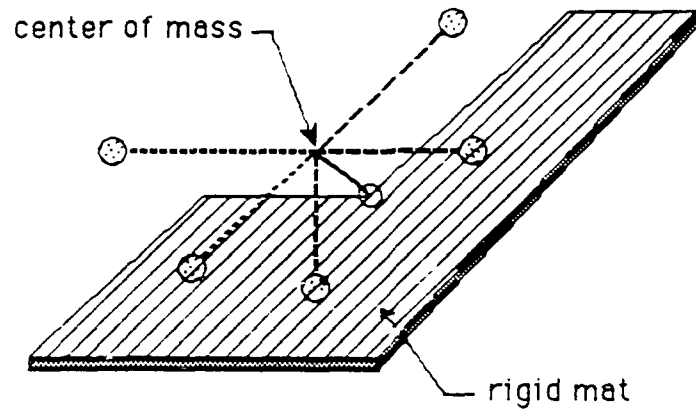
Figure 2.4 Comparison of earthquakes selected for study

springs, appropriate for a rigid, massless foundation, see Dobry and Gazetas (14), replaced the distributed soil springs for spectral analyses. This soil model required five springs to resist displacement and rotation along and about two horizontal axes and rotation about the vertical axis. All soil springs connected to a node at the center of mass of the mat foundation (see Figure 2.5). In cases where the center of mass was located off the actual mat, a centrally located mat node was constrained to rotate and displace in a plane containing this center of mass. Far field ends of soil springs were fixed an arbitrary distance from the center of mass along axes parallel to the global axes.

## **STICK FRAME RESPONSE**

### **Degrees of Freedom**

A stick model was constructed by interconnecting lumped masses using simple one-dimensional finite elements of appropriate bending and/or torsional stiffness (see Figure 2.6). For all such models developed for phase 2 and phase 3 calculations, the only independent degrees of freedom were located at the column ends. Degrees of freedom for symmetric structures loaded in a plane of symmetry included in-plane horizontal and vertical displacement, along with in-plane rotation. Non-symmetric floor plans, loaded in arbitrary directions, required five independent degrees of freedom at



- ..... translation spring
- torsion spring
- rigid connector
- ⊗ fixed spring joint

Figure 2.5 General soil spring model  
for rigid mat foundation

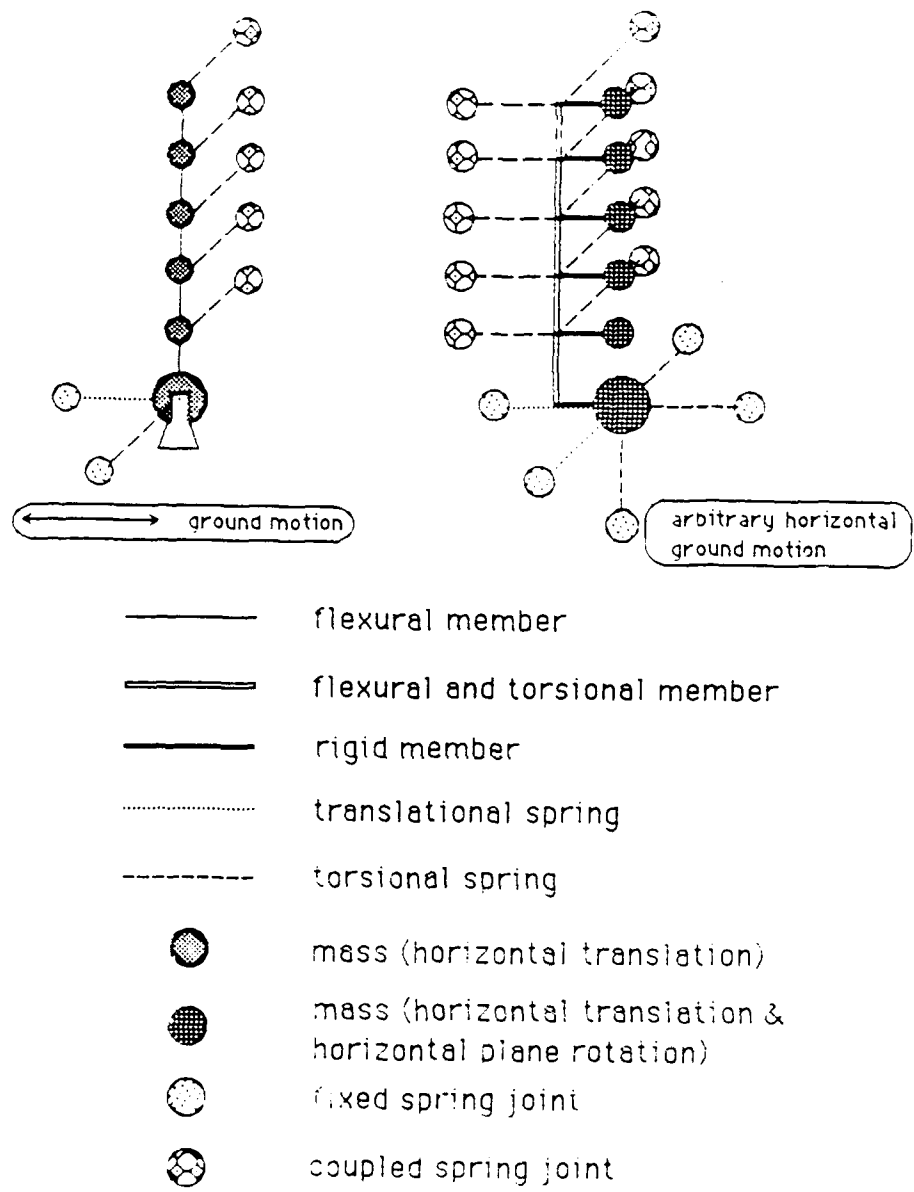


Figure 2.5 Portal frame model (symmetric loading and asymmetric loading with torsion)

column ends. For doubly symmetric frames with horizontal soil motion arbitrarily directed, vertical axis rotations were negligible--only small computed torsions accumulated from round-off errors. Axial strains and forces generated in the columns were similarly negligible, since vertical accelerations were not allowed.

#### **Equivalent Horizontal and Vertical Stiffness**

In all stick frames, horizontal column stiffness in the x and z-axis global directions resulted from summation of column stiffness of corresponding space frame floor plans:

$$I_{kl} = \sum_{j=1}^n (I_{kjl}) \quad \text{eq. 2.6}$$

where  $I_{kl}$  is the effective moment of inertia of the  $k^{\text{th}}$  column of the  $n$ -floor stick frame,  $I_{kjl}$  is the moment of inertia of the  $j^{\text{th}}$  column of the  $k^{\text{th}}$  floor of the space frame, and  $l$  is the direction of loading.

Similarly, vertical column stiffness resulted from summation of column areas in the corresponding space frame floor plan as follows:

$$A_k = \sum_{j=1}^n (A_{kj}) \quad \text{eq. 2.7}$$

where  $A_k$  is the effective area of the  $k^{\text{th}}$  column of the  $n$ -floor stick frame and  $A_{kj}$  is the area of the  $j^{\text{th}}$  column of the  $k^{\text{th}}$  floor of the space frame. This model was influenced very little by axial stiffness of the columns, since vertical accelerations, including gravity, were neglected. Also, in the eccentric models, vertical mass was neglected for reasons given below.

#### **Equivalent Rotational Stiffness of the Floor System (Horizontal Axes)**

For stick frames loaded in the direction of an axis of symmetry, estimated rotational stiffness at column ends resulted from summing the approximate static stiffness of the individual column joints in the corresponding three-dimension floor plan. A static two-dimensional finite element analysis of each unique floor system of the frame provided acceptable inputs for this estimate. Because, for frames exceeding ten floors, each floor design was modified only once, no more than two such analyses were required per frame. Moment resisting beams were reduced in capacity for the upper floors of taller frames. In each static calculation, the floor system replicated exactly the corresponding space frame model details (see Figure 2.7). Column interface nodes rigidly restrained vertical displacement of the floor. A minimum of in-plane displacement constraints at free edges of the floor model prevented in-plane "rigid body" displacements and rotations.

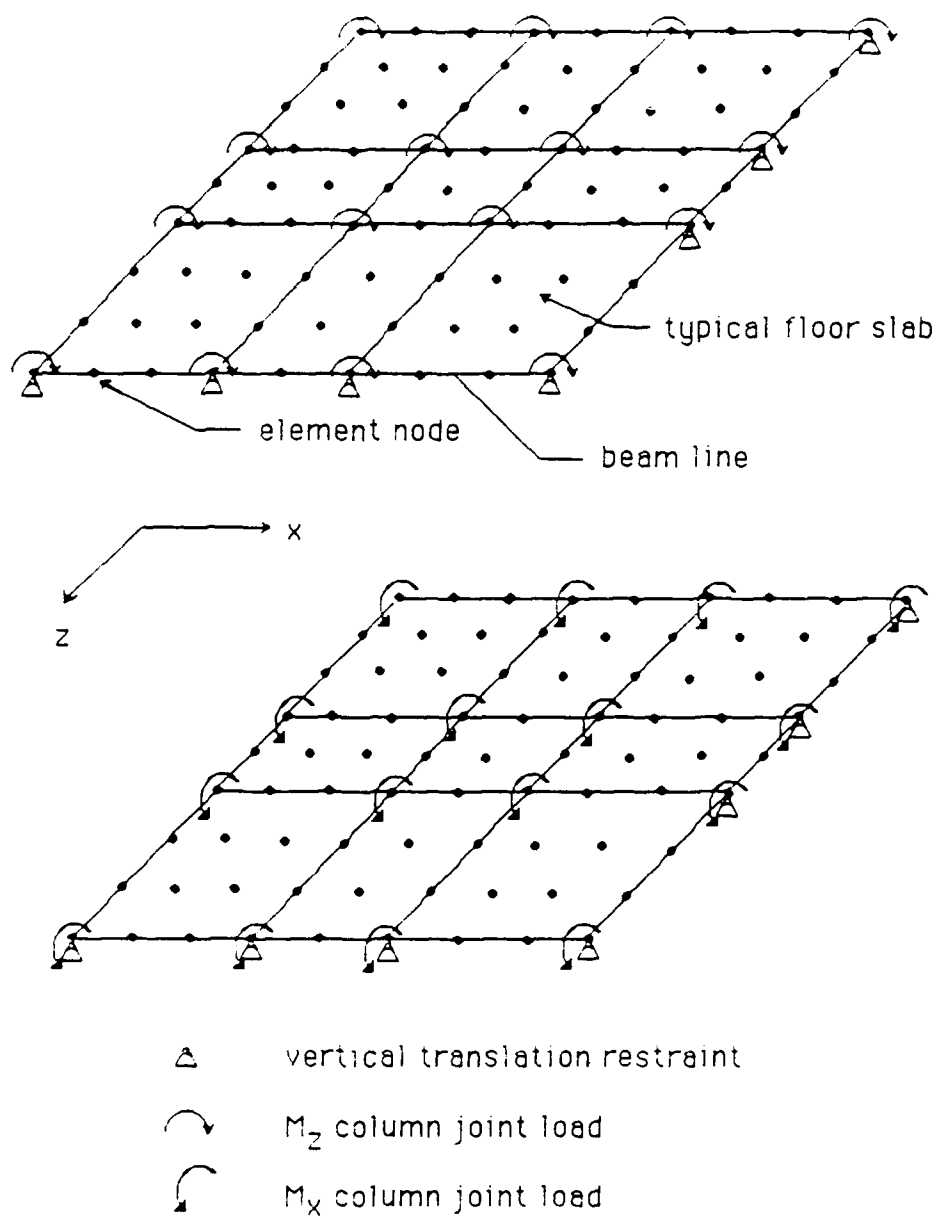


Figure 2.7 Model for computing effective floor springs of stick model

For symmetric structures, a half structure model terminated at a line of symmetry normal to the axes of applied loads. At each column interface node, an applied static moment forced rotation about the axis of required rotational stiffness. The magnitude of rotational stiffness at that joint resulted from division of the applied load by the computed rotation. The applied moment at each joint scaled in proportion to the assumptions of portal frame analysis, for which a general description of features and limitations were published by ASCE (4) in 1940, and in typical frame analysis text books of that era. Where all columns in the space frame act as if hinged at mid-height of each floor, shear along a given column line in the direction of soil motion distributes in proportion to the tributary area of floor supported by the columns along the line. These conditions are a reasonable approximation of dynamic frame response at the instant of peak displacement, provided the overall frame response is dominated by a single, fundamental mode. The resulting individual rotational stiffnesses were summed into a single torsional stiffness oriented to resist rotation of the column ends about a horizontal axis perpendicular to the direction of soil motion. One end of each torsional spring was attached to the appropriate column interface node, while the other end was fixed in five degrees of freedom. The remaining degree of freedom was slaved to maintain identical rotations with the

mat foundation mass about the axis of torsional spring alignment. The dependent rotation of this far-field end prevented undue "floor moment" from being generated by rigid body rotations of the frame about the mat foundation.

In frames subjected to soil motions not aligned with an axis of horizontal symmetry, the above procedure was repeated for moments applied about the remaining horizontal axis of column alignment. Together these calculations produced a pair of mutually perpendicular torsional springs oriented along global axes in the plane of each floor of the frame (compare Figures 2.6 and 2.7). As above, the far-field axial rotation of each torsional spring duplicated the rotation of the mat foundation about a similarly oriented global axis.

An alternative approximation of the above equivalent rotational stiffness can be found by treating each line of column nodes in direction  $l$  (x or z) as an independent portal frame. Here the equivalent rotational stiffness ( $K_{fl}$ ), for floor  $f$  and direction  $l$ , is found by summing the rotation stiffness of individual beams at the column nodes  $j$  as follows:

$$K_{fl} = \sum_{j=1}^{\text{all}} \left[ \gamma_j \sum_{b=1}^{\text{all}} \frac{6E_b I_b}{L_b} \right] \quad \text{eq. 2.8}$$

where  $E_b$ ,  $I_b$ , and  $L_b$  are the elastic modulus, moment of inertia, and length of individual beams (b) framing into column (j) along the normal to direction (l). The coefficient  $\gamma_j$  is found by normalizing portal frame moments applied to the joint j such that  $\gamma=1.0$  for an end column in a corresponding frame of equal length and equal number of spans, but of constant span length. The  $\gamma$  values for the original portal frame are then found by scaling arbitrarily computed values for the original frame such that the sum of applied column joint moments ( $\sum \gamma_i$ ) for both frames are equal. This empirical normalization of the joint moment factors was found to provide an excellent prediction of the previous analysis for all structures examined (see Chapter III). This approximation is intended to simplify preliminary portal frame calculations for plans with orthogonal beam lines, in which specific floor forces are not needed, and floor stiffness is clearly dominated by moment resisting beams with low torsional stiffness.

#### **Equivalent Torsional Stiffness of an Individual Story (Vertical Axis)**

When maximum torque about the vertical axis was sought in frames lacking double symmetry (phase 3), horizontal soil motion was applied in a direction normal to the line connecting the centers of rigidity and mass for the mat foundation. The torsional resistance of the stick frame columns was found by

approximating the combined stiffness of individual columns of the space frame as follows. To estimate the story stiffness between floors, a single full structure static space frame analysis was conducted with an arbitrary torque about the y-axis applied at the center of rigidity of the roof. Division of the applied moment by differential floor rotation about the vertical axis provided an estimate of overall static torsional stiffness of each story. The differential rotation was computed from displacements of corner nodes of the structure. To compensate for slight in-plane shear of the floor, the differential rotation along two orthogonal boundaries was averaged before computing the torsional stiffness of the floor of columns.

With the above calculation providing an estimate of the overall static torsional resistance of each floor, the static column stiffness of the corresponding portal frame was computed as follows:

$$J_{\text{eff}} = \frac{K_t L}{G} \quad \text{eq. 2.9}$$

where  $J_{\text{eff}}$  is the static column polar moment of inertia,  $G$  is the column shear modulus, and  $K_t$  is the overall torsional stiffness of the corresponding floor of the space frame model.

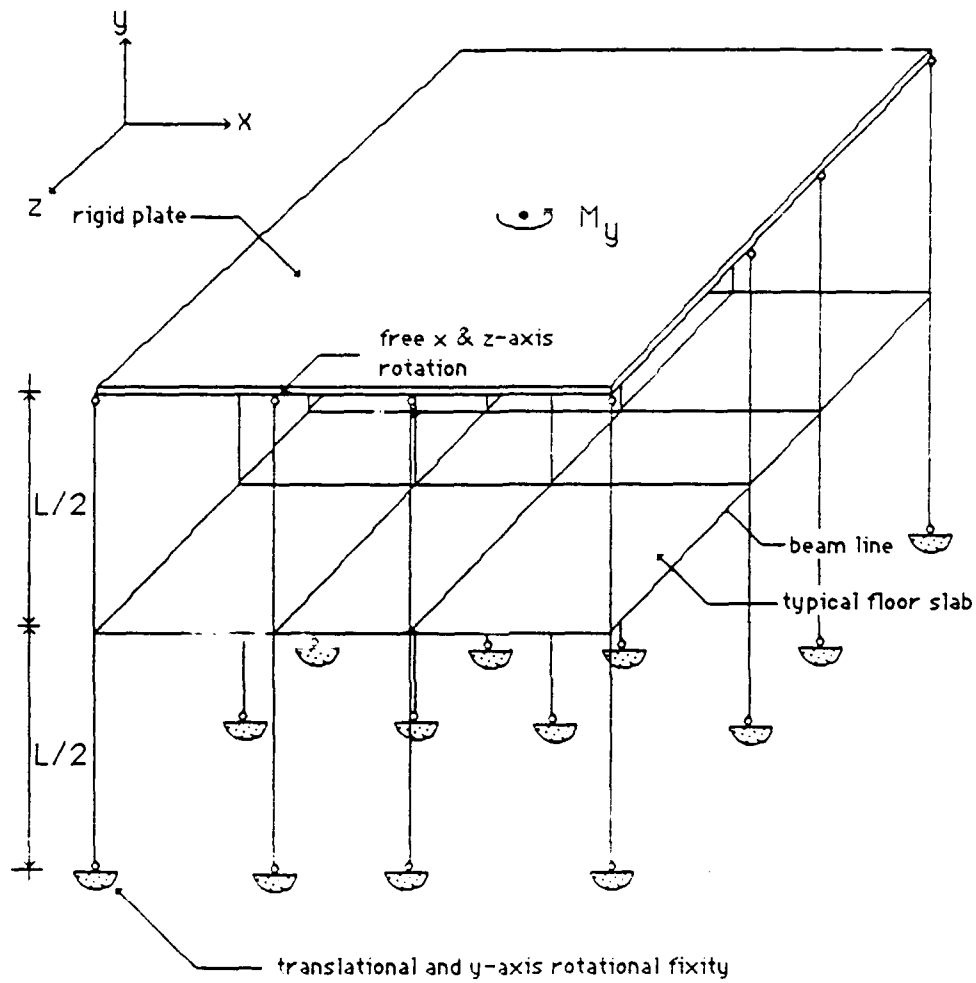
An alternative approximation for the overall torsional stiffness of a single floor space frame model is found by accepting the assumptions of eq. 2.8. Here, the individual column joint rotation stiffness ( $K_{\theta jx}$ ) at joint  $j$  in direction  $x$  is computed as follows:

$$K_{\theta jx} = \gamma_j \sum_{b=1}^{\text{all}} \frac{6E_b I_b}{L_b} \quad \text{eq. 2.10}$$

Where  $E_b$ ,  $I_b$  and  $L_b$  are the elastic modulus, moment of inertia, and length of beam  $b$  framing into column joint  $j$  along the  $x$  direction. Referring to Figure 2.8, the displacement  $\delta_{jx}$  in direct  $x$  of the top joint of any upper half-column  $j$  may be estimated from contributions due to column bending and floor slab rotation,

$$\delta_{jx} = \frac{P_{jx} L^3}{12E_c I_{cz}} + \frac{P_{jx} L^2}{2K_{\theta jx}} \quad \text{eq. 2.11}$$

where  $E_c$ ,  $I_{cz}$ , and  $L$  are the elastic modulus, moment of inertia about the  $z$ - $z$  axis, and length of the half-column  $j$ .  $P_{jx}$  is the undetermined shear at the point of deflection in direction  $x$ . Since the top plane of joints for this model rotate rigidly about the center of rigidity of the floor plan, as described



note:  $L =$  story height

Figure 2.8 Model for computing effective torsional column stiffness of stick model of moment resisting frame

above, these deflections are also explicitly defined by the rotation ( $\phi$ ) of this rigid plane and the projection of the radius from the center of rigidity to the top joint of column  $j$  in the  $z$  direction:

$$\delta_{jx} = \phi r_{jz} \quad \text{eq. 2.12}$$

Thus,

$$P_{jx} = \left( \frac{12E_c I_{cz} K_{\theta jx}}{K_{\theta jx} L^3 + 6E_c I_{cz} L^2} \right) r_{jz} \theta \quad \text{eq. 2.13}$$

Noting  $r_{jz} = r_j \cos(\beta)$  and  $r_{jx} = r_j \sin(\beta)$ , where  $\beta$  is the angle between  $r_j$  (radius to top joint of column  $j$ ) and the  $x$ -axis, and summing moments due to column shears  $P_{jx}$  and  $P_{jz}$  about the center of rigidity, the arbitrary rotation  $\theta$  may be eliminated. In final form  $K_t$  may be summarized as:

$$K_t = \sum_{j=1}^{\text{all}} \left( \frac{12E_c I_{cz} K_{\theta jx}}{K_{\theta jx} L^3 + 6E_c I_{cz} L^2} \right) r_j^2 \sin^2(\beta) + \sum_{j=1}^{\text{all}} \left( \frac{12E_c I_{cx} K_{\theta jz}}{K_{\theta jz} L^3 + 6E_c I_{cx} L^2} \right) r_j^2 \cos^2(\beta)$$

eq. 2.14

This approximation is also intended for use in preliminary estimates of plans with orthogonal beam lines, where specific floor forces are not needed, and floor stiffness is clearly dominated by moment resisting beams with low torsional stiffness.

Clearly, the magnitude of torsional stiffness will vary with each floor, even if column sizes are constant with elevation. In the structures examined in this study, the approximate value of  $K_t$  found from eq. 2.14 provided a reasonable average value for all stories, and so was applied uniformly with elevation. For comparison, dynamic response was computed for each structure based on the equivalent torsional stiffness distribution of a full static frame calculation, as well as the uniform distribution of obtained from eq. 2.14.

For frames designed with eccentricity between the static center of rigidity and the center of mass at each floor, the stick structure compensated in the following way. Each column attached to nodes located at the center of rigidity of the bounding floors. With the lumped mass of the floor positioned at a center of mass node, an effectively rigid beam connected the column ends and lumped mass. The lumped mass was assigned appropriate in-plane rotational inertia and horizontal translational inertia. Out of plane rotational

inertia was neglected because floor rotations were very small. Vertical translational inertia was neglected to prevent development of vertical modes peculiar to this stick frame analog (i.e. vertical vibration of the lumped masses on the short cantilever beams). Lateral torsion "floor" springs connected to the structure at the centers of rigidity of each floor (column ends).

### **Soil Model**

Equivalent soil springs resisted independent displacements and rotations. These springs were appropriate to rigid, massless foundations as described by Dobry and Gazetas (14). For frames loaded in a plane of symmetry, the mat foundation node rigidly resisted vertical displacement at the mat center of gravity. A horizontal spring acting in the direction of motion and a torsional spring acting about a horizontal axis perpendicular to the direction of soil motion, further restrained this center of gravity node. The magnitude of soil spring stiffness was adjusted i., each frame as appropriate for the computed soil-structure system fundamental mode. Selection of soil springs required no more than two iterations of the modal analysis for any frame to reduce the difference between assumed and computed fundamental mode frequency to less than five percent. As described above, initial mode

estimates were based on standard building code recommendations.

For eccentrically loaded structures, an additional pair of horizontal springs provided resistance to horizontal mat displacement and rotation along and about the other horizontal global axis. Additionally, a vertical torsional soil spring was provided to resist rotation about this axis. The latter spring was clearly superfluous in doubly symmetric structures, since only small "numerical" torsion was induced in these structures.

All soil springs connected to a center of mass node of the mat foundation. The far-field ends connected to rigid nodes at an arbitrary distance along appropriate axes of orientation. These members had stiffness only along or about the member axis as needed.

### **Portal Frame Estimates of Individual Member Forces**

#### **Column Forces**

Column shears and torque in the single column of the portal frame model may be used to compute shear in individual columns of the real structure through superposition in the following way. Horizontal shears for the moment resisting frames of this study--with constant floor beam details--share

shear approximately equally among parallel lines of columns. Space frame calculations indicate perimeter lines of columns carry 10 to 15% less than interior lines of columns. By assuming uniform distribution among parallel column lines, perimeter columns are strengthened, providing additional torsional resistance to the structure. Thus individual column shears may be assessed as:

$$V_{vij} = \frac{\gamma_{ij} V_i}{\sum_{j=1}^{\text{all}} \gamma_{ij}} \quad \text{eq. 2.15}$$

where  $V_{vij}$  is column (i) shear in principal direction (l) resulting from the stick frame column shear,  $\gamma_{ij}$  is the associated normalized distribution shear distribution factor described above, and  $V_i$  is the total shear of the portal frame column in direction (l)

Assuming rigid diaphragm action in the plane of each floor, individual column shears resulting from torque of the stick frame column may be derived as follows:

$$T = \sum_{i=1}^{\text{all}} V_{tix} z_i + \sum_{i=1}^{\text{all}} V_{tiz} x_i \quad \text{eq. 2.16}$$

Where  $V_{tix}$  and  $V_{tiz}$  are the column shears in principal directions (x) and (z),  $x_i$  and  $z_i$  are the column ordinates with the origin located at the center of rigidity of the floor, and  $T$  is the stick frame column torque. Assuming these column shears to be proportional to the corresponding moment arm to the center of rigidity and proportional to the portal frame distribution factor of the column:

$$\frac{V_{tix}}{z_i \gamma_{ix}} = \frac{V_{tiz}}{x_i \gamma_{iz}} \quad \text{eq. 2.17}$$

These individual shears are further related through simple geometry by:

$$\frac{V_{tix}}{V_{tiz}} = \frac{z_i}{x_i} \quad \text{eq. 2.18}$$

Substituting eq. 2.17 and eq. 2.18 into eq. 2.16 and eliminating one shear results in:

$$V_{tix} = \frac{T}{\frac{\sum_{i=1}^{\text{all}} (\gamma_{ix} z_i^2)}{\gamma_{ix} z_i} + \frac{\sum_{i=1}^{\text{all}} (\gamma_{iz} x_i^2)}{\gamma_{iz} x_i}} \quad \text{eq. 2.19}$$

Through superposition the total shear ( $V_{ij}$ ) in direction (I) for each column (i) is found to be:

$$V_{ij} = V_{vij} + V_{tij} \quad \text{eq. 2.20}$$

Similar approximations can be developed for floor systems with varying beam member sizes, torsionally stiff edge beams or other stiffness features influencing the distribution of shear in the columns. For each type of floor system, the distribution of column shears, and the appropriateness of static portal frame analysis, should be confirmed by independent static space frame analysis.

Column axial force estimates may be obtain directly from the results of dynamic portal frame analysis in a manner consistent the techniques described above. The axial force in any column results from the accumulation of vertical shear forces in the floors above the column. Because the quality of force estimates in the floor system are relatively poor, the estimate of accumulated shear in the important lower floors of the structure is unsatisfactory. Acceptable estimates of this force, as well as all other important member forces, may be obtained from the method described in the following subsection beginning of page 53.

### Beam (and Other Floor Element) Forces and Displacements

Combining results of stick frame modal analysis and two and three-dimensional static analysis provided estimates of member forces and displacements for all floor elements. To illustrate this process, the simplest case of loading through a plane of symmetry will be described first. Loading in an arbitrary direction, including eccentric loading, requires more extensive post processing of data, but is conceptually similar.

#### Loading about a plane of symmetry

To implement the stick frame model described above, a two-dimensional static floor system analysis first assessed the magnitude of equivalent torsional floor springs. Post processing of this static calculation retained all member forces and displacements. The results of the subsequent stick frame dynamic calculation then allowed scaling of the floor system response to values consistent with peak space frame spectral loading response. Floor system response is obtained by scaling the static response (stress, force or displacement) of any floor member to the ratio of net computed torsional spring moment of the dynamic analysis to the sum of applied moments of the static floor analysis.

### Non-eccentric loading of frames in arbitrary directions

For this configuration of frame layout and loading, two static calculations provided individual column node rotational stiffness in two horizontal directions. Distributed column end moments acted along different major horizontal axes of the frame in each calculation. With member responses recorded for both calculations, the results of subsequent stick frame modal analysis can be applied twice to obtain the net member response of all floor members. Floor system member response is obtained from two separate scaling processes, rather than the one described for symmetric frames. These processes must be algebraically summed to obtain a net estimate of the space frame member responses. To perform this algebraic summation, the effective modal frame displacement pattern must be cautiously examined to evaluate whether positive or negative floor spring moments are appropriate. This caution is necessary because modal combination generates only positive values of force and displacement. Appropriate displacement patterns are not obvious from results of mode combination procedures. These procedures predict only the peak (positive) magnitude of each displacement. Appropriate signs for these magnitudes were found by deducing displacement patterns consistent with column shear forces and essentially rigid floor diaphragm displacements.

### Eccentric loading of frames

For eccentrically loaded frames, two static calculations provide individual column node rotational stiffness in two horizontal directions. In addition, a static space frame analysis of the full structure subjected to pure torsional loading (described in detail above) provides an effective torsional column stiffness for stick frame analysis. With member responses retained for all three of these static calculations, results of the subsequent stick frame modal analysis can be applied three times to obtain the net member response of all floor members.

Algebraic combination of static two-dimensional calculations, used to determine effective horizontal torsion member stiffnesses, may be carried out as described above. The results of the static space frame calculation may be scaled by the ratio of net effective stick frame column torque acting above and below the floor of interest and the applied torque of the static full space frame calculation. Appropriate algebraic combination of all three floor system responses provides an estimate of three dimensional dynamic response. Again, because of the ambiguity of sign in modally combined parameters, the sign of floor spring and column torque must be independently deduced as described above.

### **Static Space Frame Estimate of Forces and Displacements (Equivalent Portal Frame Loading)**

An estimate of all superstructure forces and displacements can be computed by applying an equivalent static load at the center of rigidity of each floor of space frame model. The equivalent static shear loads are taken to be the difference between the shear in the portal frame columns above and below the floor for which differential loading is to be computed. The equivalent static torque load is taken to be the difference between the torque in the portal frame columns above and below the floor for which differential loading is to be computed. The direction (sign) of the equivalent shears and torques may be determined from the directions of column deflection and rotation in the portal frame model.

### **SUMMARY OF CALCULATIONS PERFORMED**

#### **Structures Loaded Parallel to a Single Plane of Symmetry**

A matrix of 52 stick frame and space frame calculations were performed for doubly symmetric frames loaded in a plane of symmetry. As detailed in Table 2.1, the parameters studied included: number of floors, soil shear wave velocity, earthquake spectral velocity distribution and intensity, and floor plan aspect ratio. In addition to this basic matrix, several calculations evaluated response of simple massless

Table 2.1 Loading in a plane of symmetry

N floors	Aspect Ratio (x:z)			Earthquake		Vs (fps)		
	(1:1	1:1.75	1.75:1)	(E - C	M - C)	(500	1000	1500)
3	X			X		X		
5	X			X		X		
10	X			X		X		
15	X			X		X		
20	X			X		X		
3	X			X			X	
5	X			X			X	
10	X			X			X	
15	X			X			X	
20	X			X			X	
3	X			X				X
5	X			X				X
10	X			X				X
15	X			X				X
20	X			X				X
3	X				X	X		
5	X				X	X		
10	X				X	X		
15	X				X	X		
20	X				X	X		
3		X		X		X		
5		X		X		X		
10		X		X		X		
3		X		X				X
5		X		X				X
10		X		X				X
3			X	X				X
5			X	X				X
10			X	X				X

mat foundations, with no superstructure, in order to demonstrate the quantitative similarity of this calculational procedure compared with analytical examples from the literature. Also one transitional calculation evaluated the response of a five story frame with a square floor plan, overlying soft soil (500 fps). This frame included an effectively rigid mat supported by two simple soil springs resisting horizontal and rocking motions.

The design of each doubly symmetric frame proceeded in the following manner. Each structure was subjected to an equivalent horizontal static loading, as described in the ANSI A58.1-1982 (3) building code. Space frame analysis was performed repetitively with trial beam and column sizes, to determine members designs consistent with horizontal frame deflection requirements of ANSI A58.1-1982 and combined stress requirements of AISC steel building code of 1978 (40). A similar check of the beam and column selection process was performed for gravity loads, and bounding forces for each member were derived from superposition. Member sizes were then upgraded as needed to limit combined stresses. The concrete floors were not detailed, but the floor thickness was selected to insure compliance with the ACI 318-83 (9) concrete building code requirements for static slab deflection. The concrete mat thickness was also selected in according

with ACI 318-83 consistent with the design philosophy described below.

Table 2.2 summarizes the structural design details for all structures of this study. In each point design, floor systems included moment resisting beams spanning both principal directions between columns. Column lay out for all doubly symmetric structures provided for a central beam span of 20 feet, with exterior beam spans of 30 feet. All structural steel designs assumed a minimum yield strength of  $f_y = 36$  ksi. Floor slabs supported a total of 100 psf (distributed inertia with no gravity). Floor slab depth was 8.25 inches, sufficient to prevent excessive static deflections under a distributed gravity load of 50 psf dead load and 50 psf live load. To simulate the effects of negative bending on a composite beam/slab system, the vertical location of the beam center varied linearly with distance from the column location. At column nodes, the beam center and slab center coincided, simulating the reduced section properties of a slab cracked in negative bending. At distances of ten feet or greater from column nodes, the beam center displaced below the slab center, so the top of the beam coincided with the bottom of the slab at node locations.

Table 2.2 Structural details

Total Stories	Floor Range	Columns	Floor Range	Beams
3	1 -- 3	ST12x12x.375"	1 -- 3	W21x62
5	1 -- 5	W12x72w/.5" *	1 -- 5	W21x62
10	1--5	W12x136w/.625"	1--10	W21x62
	5--10	W12x72w/.5"		
15	1--5	W12x210w/1.0"	1 -- 5	W21x68
	6--10	W12x136w/.625"	6--15	W21x62
	11--15	W12x72w/.5"		
20	1 -- 5	W12x252w/1.25"	1--1	W21x68
	6 -- 10	W12x210w/1.0"	11-- 20	W21x62
	11--15	W12x136w/.625"		
	16--20	W12x72w/.5"		

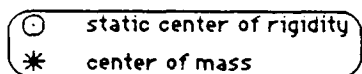
\* refers to built-up section W12x72 with .5" plates spanning in web direction at edges of flanges to effectively form a tubular section with two compartments.

Mat foundation designs insured concrete alone would be sufficient to resist punching shear. In designs controlled by bending forces, steel percentages slightly exceeded  $p_{min}=.005$ , based on Grade 40 reinforcement. For the 3, 5, 10, 15 and 20 story structures, mat depths were 22, 25, 36, 45 and 54 inches respectively. All concrete material properties derived from an assumed compression strength of  $f'_c=3$  ksi for normal weight concrete.

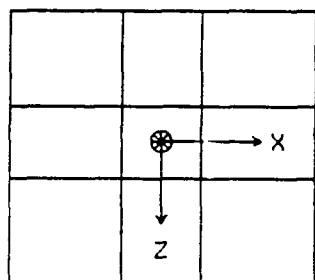
#### **Structures Loaded in Arbitrary Directions with Self-Induced Torsion Possible**

A total of six space frame calculations and eleven stick frame calculations were performed to assess the ability of the portal frame model to predict the response of frames subject to self-induced torsion. Three of four structures examined were five floors in height, one was ten stories in height with the top five floors set back by one thirty foot span in the x direction. All structures rested upon soft soil ( $v_s=500$  fps) and were subjected to the El Centro velocity spectrum described above.

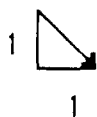
The first space frame and stick frame calculations predicted response for the square, doubly symmetric floor plan previously detailed. This structure was loaded along a horizontal direction bisecting the principal axes of the plan (see Figure 2.9 for plan views described in this section). The



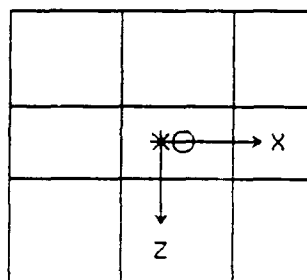
Doubly Symmetric Frame



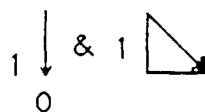
horizontal loading



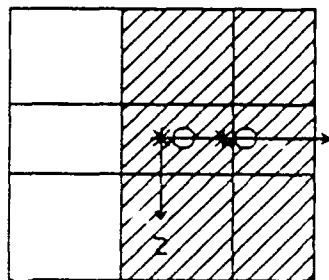
Mono-Symmetric Frame



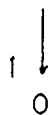
horizontal loading



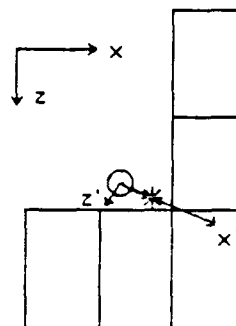
Mono-Symmetric Frame with Setback



horizontal loading



Asymmetric Frame



horizontal loading



.5625

Figure 2.9 Doubly symmetric, mono-symmetric, and asymmetric floor plans with soil loading directions

purpose of this comparison was to identify any unexpected interactions which might be produced in extending the portal frame model to include two orthogonal torsional "floor" springs per floor location.

A space frame and two stick frame calculations were performed for a square, mono-symmetric floor plan in which bay widths were rearranged in the x direction to produce eccentricity between the center of rigidity and the center of mass. This structure was loaded in the z direction to induce maximum torque. The two stick frame calculations for this structure differed in their distribution of effective column torsional stiffnesses. One portal frame calculation used a uniform vertical distribution of torsional stiffness (obtained from eq. 2.14). The other portal frame calculation scaled torsional stiffness at each floor based on the torsional response of a static space frame calculation, as described previously. This more elaborate distribution used middle floor stiffnesses equal to the average of those obtained for the full structure static analysis described above. Transition floor stiffnesses were equal to those of the full structure static stiffness distribution. These portal frame options in torsional stiffness distribution were exercised for each eccentric load case to follow.

These last three calculations were repeated with loads in a horizontal direction bisecting the principal axes of the floor plan. Since the structure stiffness varies significantly between the x and z directions, this loading was taken to be in a representative arbitrary direction.

A structure with significant setback conditions was created by extending the mono-symmetric design (described immediately above) to a height of ten floors, but omitting the thirty foot end span in the x-direction. This structure was loaded in the z-direction for maximum torsional response. One space frame and two portal frame comparisons were made in the manner detailed above.

A five story L-shaped floor plan was created to assess the ability of the portal frame model to predict the response of asymmetric floor plans. One space frame and two portal frame comparisons were made in the manner detailed above using CQC modal combination, with the first eigenvector of the portal frame calculations multiplied by -1, to match the shape of the corresponding space frame eigenvector. These three calculations were repeated using SRSS modal combination to overcome problems of reversed mode shapes between model types for this structure (see Chapter III for details).

For all frame designs described above, the steel and concrete strengths, mat thicknesses, and member sizes match those described earlier for doubly-symmetric structures of the same height.

## CHAPTER III

### RESULTS OF PRELIMINARY INVESTIGATION OF SOIL-STRUCTURE INTERACTION

#### PRELIMINARY SOIL MODEL VERIFICATION

To ascertain the limits of accuracy of the proposed method of soil-structure interaction analysis with flexible mat foundations supporting frame superstructures, several simpler calculations were compared to published results. These calculations simulated analytic investigations for rigid massless mats resting upon a linear soil half-space, Dobry and Gazetas (14), as well as a flexible massless mat resting upon a linear soil half-space, Whittaker and Christiano (56). For both types of calculations, elements with high axial stiffness in the vertical direction, but low lateral stiffness, linked adjacent mat and soil nodes. This arrangement simulated a frictionless soil-mat interface. In all cases, a pair of vertical concentrated loads of equal magnitude and opposite direction applied a harmonic couple to the mat. This force couple acted at middle third points along an axis of symmetry of each mat.

For the rigid mat comparisons, the range of mat aspect ratios soil shear wave velocities, and harmonic loading frequencies corresponded closely with those selected for the frame buildings of this research. Equivalent rocking spring stiffnesses and

dashpot viscosities resulted from summing the products of individual vertical spring stiffnesses and dashpot viscosities with corresponding moment arms about the center of each mat. These rocking spring stiffnesses and dashpot viscosities were then compared directly with values computed from recommendations given by Dobry and Gazetas (14). As detailed in Table 3.1, greatest accuracy in rocking stiffness (relative to Dobry and Gazetas recommendations) resulted for square mats on stiff soil ( $v_s=1500$  fps). For mat aspect ratios above or below 1:1, and for softer soils, errors increased from a minimum of -.5% to as much as 35%, compared to stiffness values obtained from the published recommendations. As will be shown below, errors of this magnitude influenced response of the structural frames only slightly. However, the proposed technique grossly overestimated dashpot viscosities. In a separate series of calculations (see Figures 3.1 and 3.2), a square rigid mat (of width  $b$ ) with insignificant mass was supported by soil of stiffness such that:

$$v_s = 500 \text{ fps}$$
$$\text{and } \mu_s = .333$$

This mat was subjected to a range of loading frequencies. As  $a_c = \omega b v_s$  increased, the viscosity approached accepted values. Dobry and Gazetas (14), only for frequencies ( $\omega$ ) much higher than the

Table 3.1 Comparison of overall rigid mat rocking stiffness (computed from proposed soil model) to Dobry and Gazetas (14) recommendations

Mat/Soil Identifier (see key below)*	K <sub>y</sub> Proposed (kip-in/rad)	K <sub>y</sub> Dobry and Gazetas (kip-in/rad)	Difference (%)
3/1:1/0500	4.711E12	3.833E12	22.9
5/1:1/0500		3.960E12	
10/1:1/0500		4.130E12	
15/1:1/0500		4.170E12	
20/1:1/0500	5.080E12	4.174E12	21.7
3/1:1/1000		1.630E13	
5/1:1/1000		1.650E13	
10/1:1/1000		1.670E13	
15/1:1/1000		1.700E13	
20/1:1/1000		1.700E13	
3/1:1/1500	3.857E13	3.767E13	2.4
5/1:1/1500		3.800E13	
10/1:1/1500		3.880E13	
15/1:1/1500		3.880E13	
20/1:1/1500	3.862E13	3.881E13	- .5
3/1:1.75/0500	7.826E12	5.832E12	34.2
5/1:1.75/0500		6.030E12	
10/1:1.75/0500	8.321E12	6.352E12	31.0
3/1:1.75/1500	6.318E13	5.712E13	10.6
5/1:1.75/1500		5.770E13	
10/1:1.75/1500	6.310E13	5.832E13	8.2
3/1.75:1/0500	1.659E13	1.260E13	31.7
5/1.75:1/0500		1.320E13	
10/1.75:1/0500	1.780E13	1.395E13	27.6
3/1.75:1/1500	1.413E14	1.282E14	10.2
5/1.75:1/1500		1.310E14	
10/1.75:1/1500	1.398E14	1.323E14	5.7

\* Identifier Key: (Total Floors/Mat Aspect Ratio/Soil v<sub>s</sub>)

Note: Comparisons were selected to represent the range of story heights (soil-structure fundamental frequencies) and soil stiffnesses (soil shear-wave velocities) for each mat aspect ratio examined in this study.

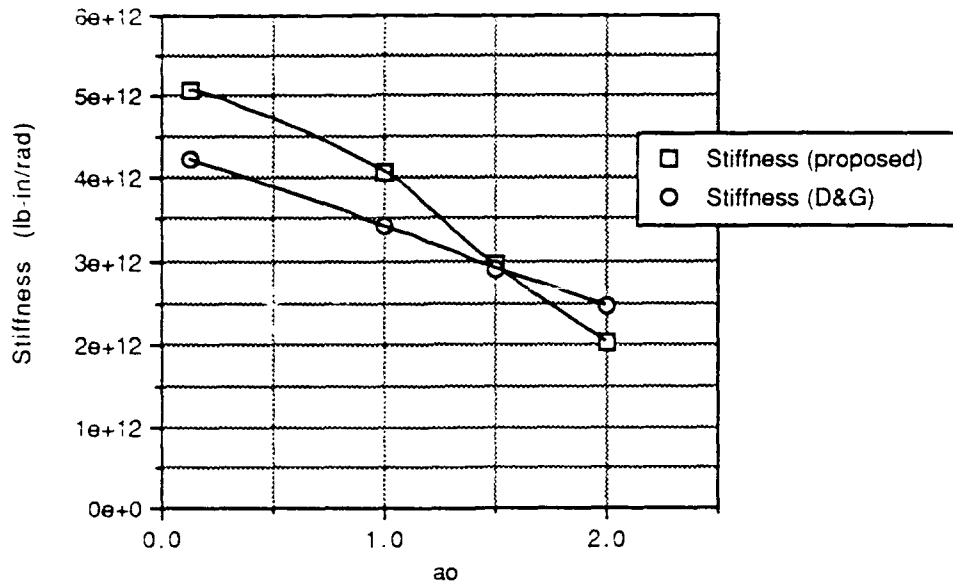


Figure 3.1 Overall stiffness (rocking mode) for massless, rigid mat on soft soil (vs=500fps)

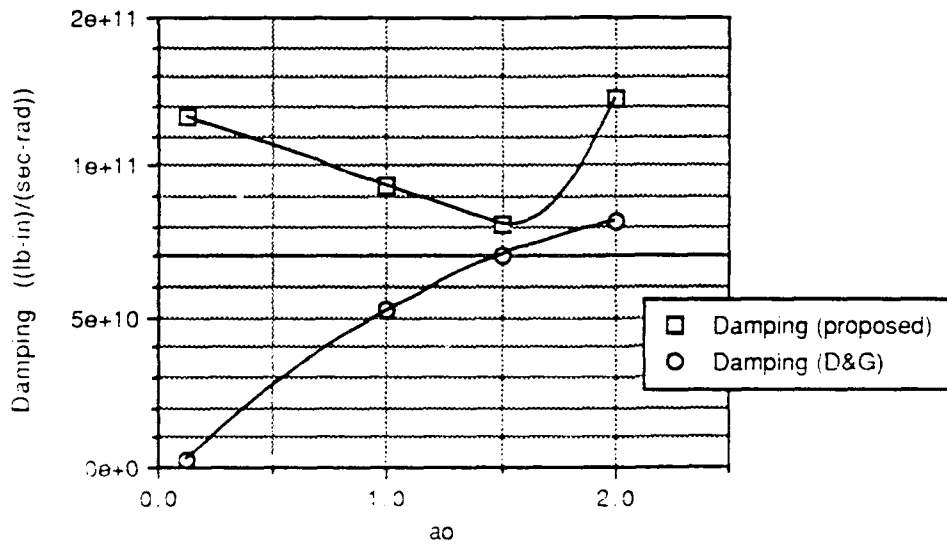


Figure 3.2 Overall radiation damping (rocking mode) for massless, rigid mat on soft soil (vs=500 fps)

fundamental modes of low-rise frames. Subsequent frame calculations neglected radiation damping due to rocking for two reasons. First, these values are typically small (see Vaughan and Isenberg (50) for one careful estimate of 2.5% of critical damping for the fundamental mode of a very rigid structure). Second, radiation damping could not be reliably computed by the proposed model. However, substantial viscous material damping (10% of critical) was allocated for the equivalent soil springs. For cohesionless soils with the structural properties described above, this level of material damping correlates with maximum shear-strain levels in soil of about .01 (see Seed, Wong, Idriss, and Tokimatsu (38)). These moderately non-linear strain levels were used here to approximate the overall material damping of the entire affected soil region. Given the rocking action of the structure, maximum soil strains would be expected to be greatest near the mat and least near the far-field soil boundary. Given that linear analysis is implemented in all calculations of this research, the above assumptions of global viscous damping in the soil are a first order approximation, which attempts to introduce a reasonable level of soil damping without requiring higher order analysis. In fact, the effective damping ratios for the more important modes of each analysis (greatest mode coefficients--see Appendix D) were dominated by damping in the steel columns. The bulk of the soil-structure strain energy was concentrated in the columns. Consequently, the effective soil-structure damping

for each calculation was slightly more than 2%, the value prescribed for the columns. Rigid mat calculations provided an insight into the sensitivity of overall rocking response in the frame due to errors in the soil model, but did not assess the local error in force distribution within the mat foundation.

By comparing published data, a typical error range for mat deformations and force distributions was found for the proposed soil-structure interaction model. The complex quotient of force over displacement intensity functions, given by Whittaker and Christiano (56) for a square flexible mat with insignificant mass, was used to determine equivalent spring intensities for selected points along a line of symmetry parallel to the loading plane. Spring values along this line of symmetry were divided by the corresponding tributary areas to determine average spring intensities for the region. Thus, independently derived distributions of stiffness intensities were compared for three values of soil stiffness (see Figures 3.3 to 3.6 for distributions of  $k$  and  $\omega d$ ). The error in stiffness intensities increased with decreasing soil stiffness. Peak errors at perimeter nodes approached 30%. The qualitative distribution of soil stiffness intensity is accurately reflected by the proposed method in all calculations.

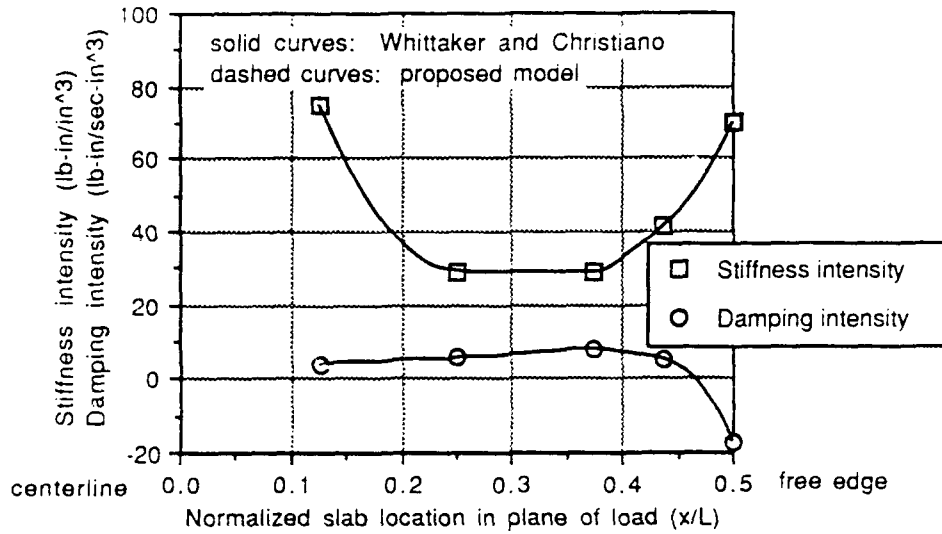


Figure 3.3 Comparison of proposed model values of stiffness and damping intensity along a square mat centerline to values derived from Whittaker and Christiano (56) data ( $K=.004$ ,  $a_0=0.0$ )

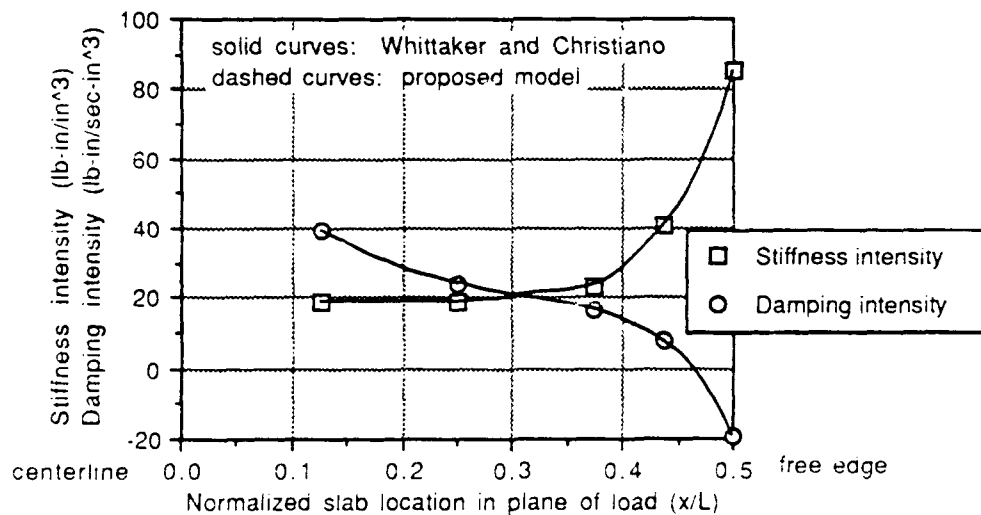


Figure 3.4 Comparison of proposed model values of stiffness and damping intensity along a square mat centerline to values derived from Whittaker and Christiano (56) data ( $K=3.3$ ,  $a_0=0.0$ )

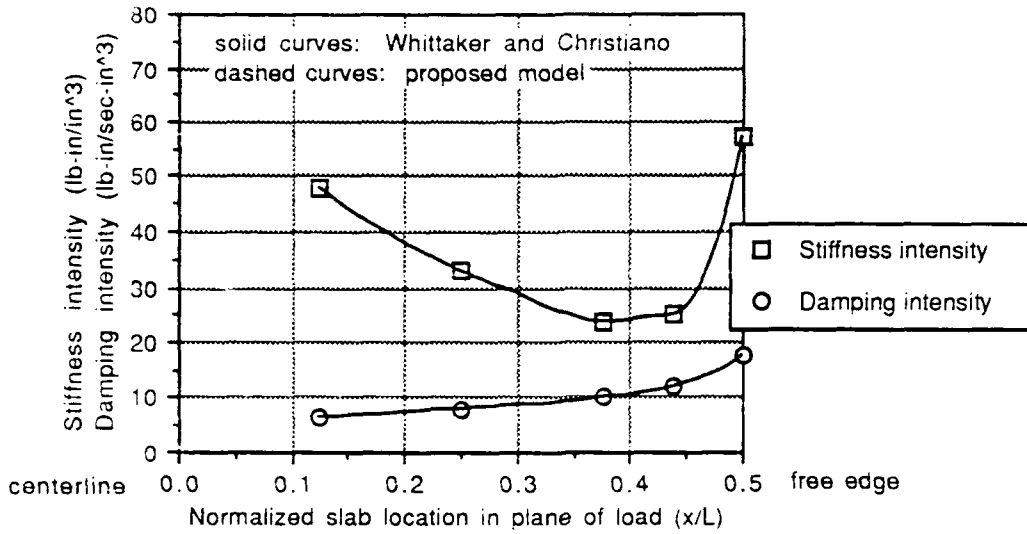


Figure 3.5 Comparison of proposed model values of stiffness and damping intensity along a square mat centerline to values derived from Whittaker and Christiano (56) data ( $K=.004$ ,  $a_0=2.5$ )

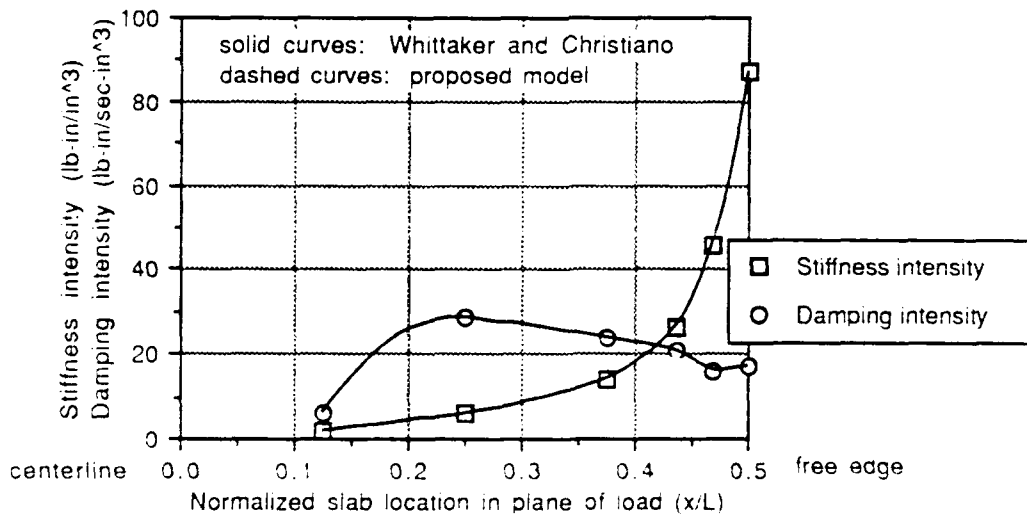
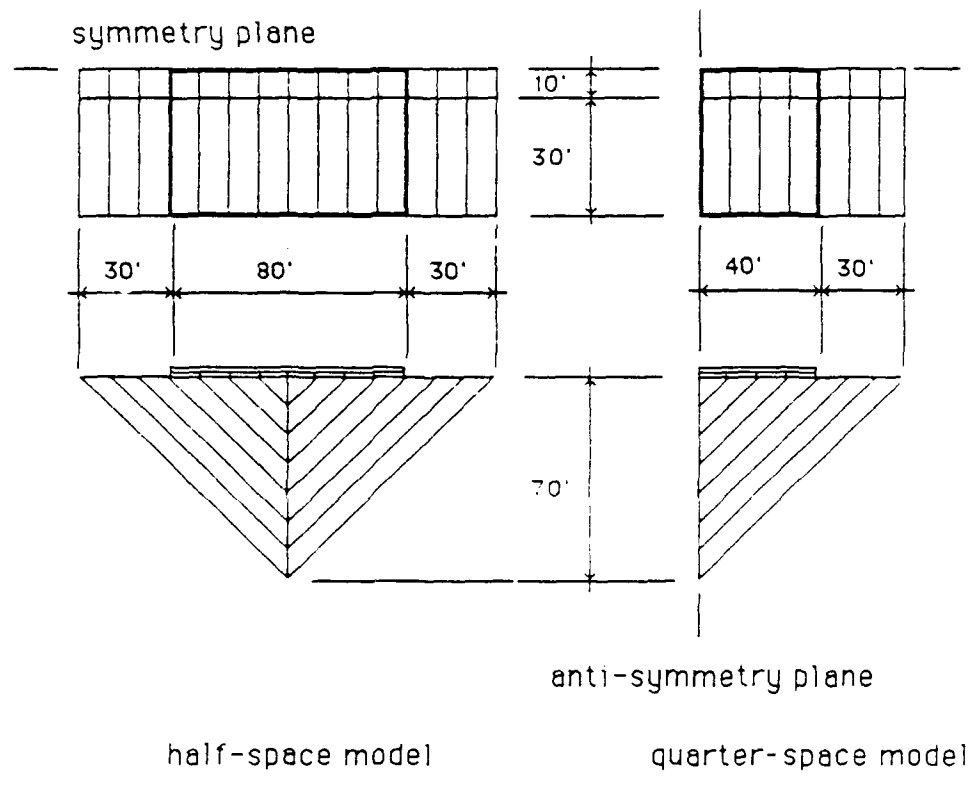


Figure 3.6 Comparison of proposed model values of stiffness and damping intensity along a square mat centerline to values derived from Whittaker and Christiano (56) data ( $K=3.3$ ,  $a_0=2.5$ )

In addition to the model verification tests performed above, a simple check was made of the relative accuracy provided by a quarter-space bounded by planes of symmetry and anti-symmetry, compared to a half-space bounded by a plane of symmetry. Imposing these constraints as described in Chapter II, a very simple soil island of low fidelity (few soil elements with extremely large aspect ratios--see Figure 3.7) grossly over-estimated overall rocking stiffness. However, relative comparison of results between models was quite good. Comparing the quarter-space model to the half-space model for two values of  $a_0$  (.29 to 1.15), individual vertical link forces were not more than 2.2% low for the lowest values of  $a_0$ , but varied in sign and magnitude, by as much as 2250%, for the highest values of  $a_0$ . Individual vertical displacements of mat nodes were not more than .3% low for the lowest values of  $a_0$ , but were more than 90.4% low for the highest values of  $a_0$ . The break down in fidelity for the highest values of  $a_0$  resulted from computation of extensive negative forces in the links with the quarter-space model. These negative forces were not representative of actual contact stresses in a rigid slab, (see Whittaker and Christiano (56)). They occur much less frequently and are of much lower magnitude in the half-space model. Consequently, comparisons of overall rocking stiffness were .3% low for the lowest value of  $a_0$ , and 79.7% low for the highest value of  $a_0$ . A survey of link force distributions for two intermediate values of  $a_0$  (.58 and .86)



Note: square rigid massless mat  
soft soil ( $v_s = 450$  fps  
 $\mu_s = 333$ )

Figure 3.7 Simple comparison models  
(half-space and quarter-space)

disclosed no negative link forces for either the quarter or half-space models. A gradual divergence of force magnitudes occurred between the two models, with maximum disparity at nodes near the rocking axis. Link forces at nodes farthest from the rocking axis, which contribute most to overall rocking stiffness, were not more than 9.6% low for the quarter-space model (for  $a_0 = .86$ ). These observations suggest that both models degrade for high values of  $a_0$ , with results for the quarter-slab model being far worse at these highest frequencies. Soil stiffness is probably underestimated for high frequency modes; however, even for the course model presented here, differences in response between the quarter and half-space models were not great at moderate to low values of  $a_0$ . For comparison, the computed fundamental mode frequencies of the soil structure systems investigated in this study will be shown not to exceed 1.3 Hz for square mat structures on soft soil (see Chapter IV). This fundamental frequency corresponds to a maximum value of .25 for  $a_0$ . Only high, and relatively insignificant, modes may be expected to be greatly affected by errors introduced in assuming anti-symmetry conditions for the quarter-slab model. Also, Figure 3.8 demonstrates good comparison in the horizontal soil deflection profile along the negative y-axis nodes of the quarter and half-space models. The partial boundary conditions imposed by the assumptions of anti-symmetry appear sufficiently accurate for the proposed analysis. The resulting model simplification is

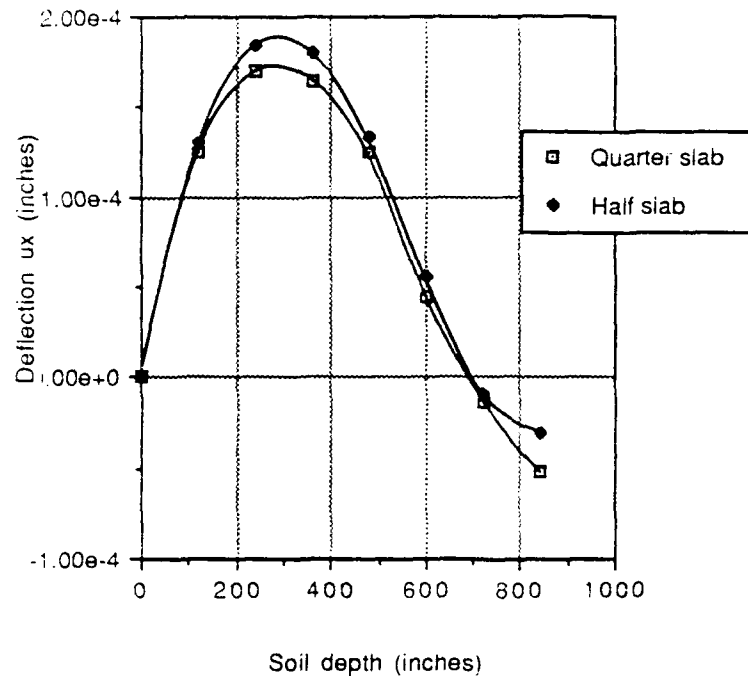


Figure 3.8 Comparison of soil deflection profile ( $u_x$ ) below mat center for quarter and half slab calculations ( $a_0=.29$ )

justified by significant computer cost savings.

## **FRAME STRUCTURES WITH FLEXIBLE MAT FOUNDATIONS EXCITED ALONG A PLANE OF SYMMETRY**

### **Foundation Response and Interaction Effect**

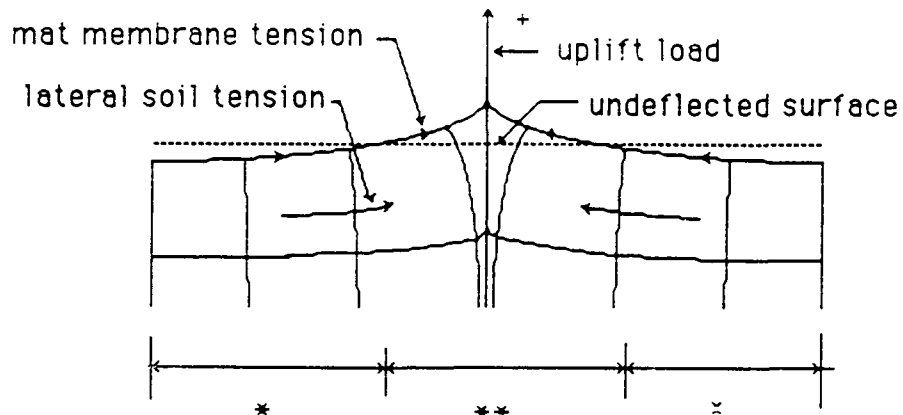
Appendix C contains profiles for equivalent soil springs for a representative sample of frame structure calculations (13 of 34 flexible mat calculations). In general, these spring distributions approximated values for rigid slabs, Dobry and Gazetas (14), when comparing results for taller frames with thick mat foundations supported by soft soils. As the mat to soil stiffness decreased, these spring distributions became more complex in profile. Negative spring values were often large. One difficulty in assessing physical significance of these springs results from the fact that the equivalent spring technique forces a finite number of independent vertical soil springs to represent the diverse interaction of a three-dimensional volume of soil elements. In the limit, a soft mat may be thought of as a film (with no bending stiffness) adhering to the surface of a solid half-space. If a concentrated vertical uplift were applied to this surface within the region of the film, Ahlvin and Ulery analysis (see Yoder and Witczak (60)) demonstrates that the deflected profile of the film and half-space surface would be upward very near the load, but downward due to Poisson effects (resistance to volume change) away from the load. The opposite was true for a compressive

vertical loading. To produce this deflection reversal away from the load with a distribution of independent vertical springs, springs in the region of this reversal were required to be of negative magnitude to simulate the influence of lateral soil tension tending to resist an excessive increase in soil volume (see Figure 3.9). Positive equivalent soil spring stiffness tended to increase toward the mat perimeter and at column nodes. Negative equivalent soil springs were greatest at or near the mat perimeter but away from columns. The principal benefit of identifying and implementing equivalent soil springs by the proposed technique was to reduce calculation effort for multiple loadings.

Appendix B contains vertical mat deflections for each of thirty-four frame structure calculations. Several generalizations emerge from this data. First, the qualitative distribution of displacements approached those of a rigid slab for softer soils and taller structures requiring thicker foundations. Whittaker and Christiano (56) express the influence of relative soil to mat stiffness for flexible, massless, square mats in terms of the stiffness ratio:

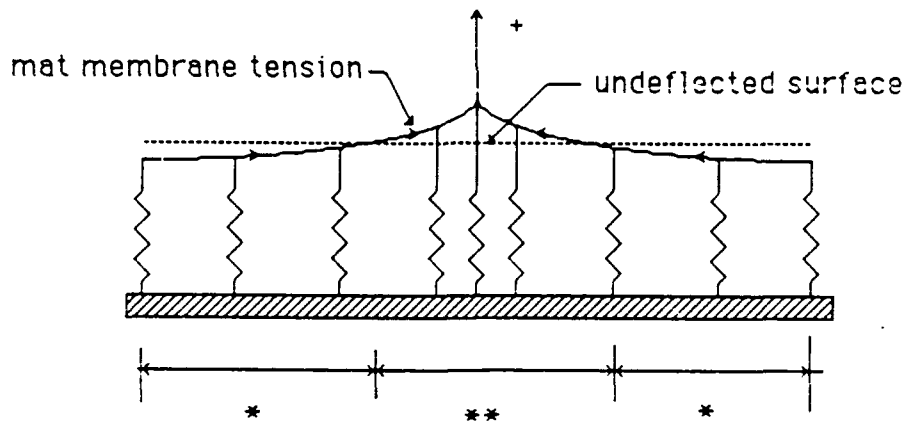
$$K = \frac{Eh^3(1-\mu_s)}{12(1-\mu_p^2)G_s(b)^3}$$

Membrane on soil:



- \* negative surface deflection--lateral soil tension component and lateral mat membrane tension effect exceeds positive vertical soil tension and positive vertical mat membrane effect
- \*\* positive surface deflection--uplift dominated

Membrane on effective vertical springs:



- \* negative surface deflection--large negative springs produce moderate negative deflection in response to slight positive vertical membrane force component
- \*\* positive surface deflection--uplift dominated

Figure 3.9 Interpretation of negative equivalent springs

where  $E$ ,  $\mu_p$ ,  $b$  and  $h$  are the elastic modulus, Poisson's ratio, width and thickness of a square mat, and  $G_s$  and  $\mu_s$  are the shear modulus and Poisson's ratio of the soil.

This stiffness factor was also a strong indicator of the response of mats with appropriate mass supporting flexible frames in the present study. As values of  $K$  decreased, multiple reversals of mat curvature and direction of deflection resulted. For these relatively soft mats, maximum upward displacements in the uplifted half of the mat occurred at columns. Mid-span mat nodes were relatively small, or even downward, on the uplifted half of the mat. The modal combination method, square root of sum of squares (SRSS), used to evaluate all of the flexible mat calculations, generates only positive values of all parameters. Regions of negative displacements were inferred from the deflected mat shape in harmonic loading analyses performed to assess the appropriate equivalent soil springs for these structures. In order for the computed soil spring distribution to be valid, the approximate deflected shape of the mat must be very similar for both harmonic and earthquake loadings. This similarity was generally the case, except in areas of negative deflection in the harmonic load response. In Appendix B, the dashed line profile in the z-axis view represents the deflected shape along the mat centerline arising from harmonic loading. These harmonic deflections are normalized such that

displacements along this profile are identical at the mat boundary (b). At points along this profile where the harmonic deflections are negative, the earthquake deflections also are negative. A profile view of harmonic displacements in the x-axis direction was also displayed for each calculation represented in Appendix B. The specific line of nodes graphed for these harmonic deflections varied with mat aspect ratio so as to present maximum negative displacements.

In two of the thirty-four calculations presented in this context, the deflected earthquake shape differed radically from that computed for harmonic loading. In these two instances, 10/1:1/1500/E-C and 10/1.75:1/1500/E-C, interior mat deflections were excessively high. The source of error was not identified for these cases. These particular structures have identical loading, soil conditions and profiles when viewed from the z-axis, perpendicular to the direction of loading.

The mat vertical displacement profiles were nearly identical in shape for comparisons between El Centro and Mexico City earthquake loadings. Despite extreme variations in frequency versus energy distributions between these loads, only the amplitudes, and not the deflected shapes, were affected significantly.

The presence of negative deflections on the uplift side of the mat for twelve of the thirty-four flexible mats is troublesome, and may point to a significant limitation of the proposed model in such cases. For these calculations, continuity was enforced at all link locations. Tensile separation of the mat from the soil, though physically possible, was not allowed. Within the limits of linear material response, this enforced continuity accurately represented the response of mats with significant, but finite, stiffness subjected to a vertical compression load. Continuity of the soil-structure interface is less likely in response to uplift. If mat separation should occur, a significant redistribution of mat forces and displacements would result. As shown by Psycharis and Jennings (35), a corresponding decrease in overall rocking stiffness could occur as a result of such a redistribution. Also, potentially significant vertical acceleration must be considered with uplift.

#### **Superstructure Response (Net Column Forces and Deflections)**

Although the distribution and magnitude of forces and displacements in the mat foundation were greatly affected by soil stiffness, superstructure response changed by no more than ten percent as the shear wave velocity increased by a factor of 3 (soil stiffness by a factor of 9). Figures 3.10 and 3.11 present a typical comparison of space frame calculations for identical

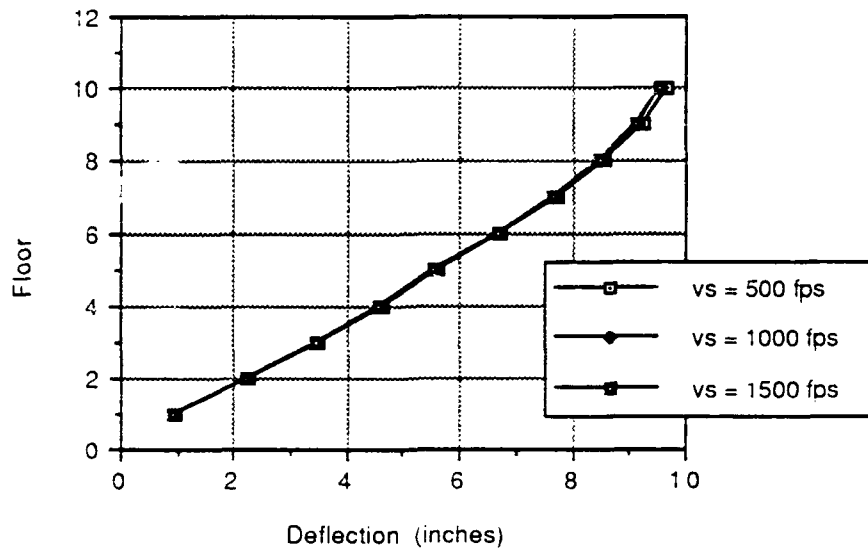


Figure 3.10 Horizontal floor deflection variation with soil shear wave velocity (series 10/1:1/0500-1500/E-C)

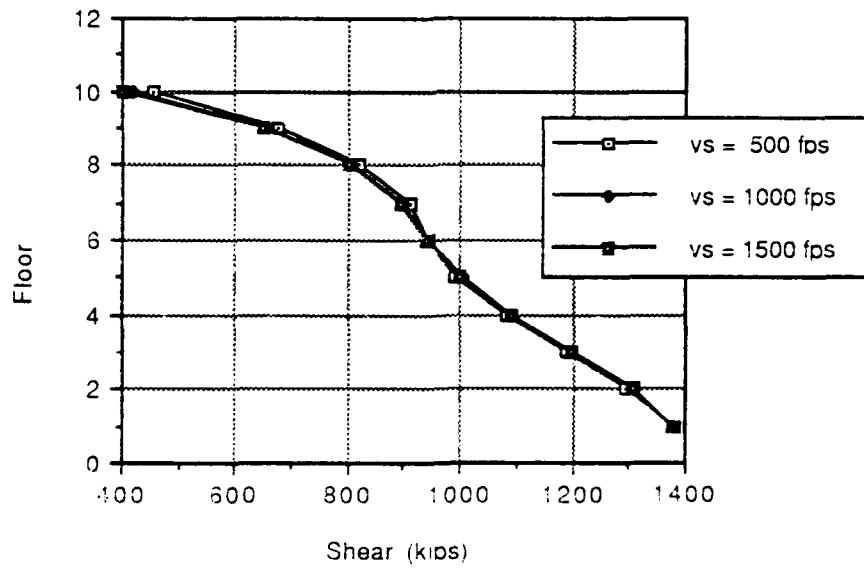


Figure 3.11 Total column shear variation with soil shear wave velocity (series 10/1:1/0500-1500/E-C)

structures supported by soils of varying stiffnesses. Increasing soil stiffness generally produced small increases or decreases in superstructure response depending upon the specific earthquake and structure height. The specific design of the superstructure had less bearing on the direction of change in response than either specific earthquake character or structure height.

Three calculations were performed in which the doubly symmetric five-floor frame was given an essentially rigid mat, but equivalent soil spring distributions were developed in the manner described above. The soil stiffness was adjusted with each run ( $v_s = 500, 1000, \text{ and } 1500$  fps). The differences in horizontal roof displacement decreased with increasing soil stiffness. The rigid mat values ranged from 3.6% high to .8% high compared to baseline flexible mat calculations. Similarly, base shear differences decreased with increasing soil stiffness. The rigid mat values ranged from 2.8% high to 2.3% high compared to baseline flexible mat calculations.

A single rigid mat calculation was performed for this same doubly symmetric five floor frame using the essentially rigid mat and substituting the pair of soft soil ( $v_s = 500$  fps) horizontal translation and rocking soil springs as recommended by Dobry and Gazetas (14). These springs were attached to the mat foundation at the center of mass node. In this calculation, maximum roof

displacement was .5% higher than the baseline flexible mat calculation--base shear was 1.4% higher.

## CHAPTER IV

### RESULTS OF SIMPLIFIED DYNAMIC PORTAL FRAME MODEL

#### SUPERSTRUCTURE RESPONSE OF FRAMES LOADED IN THE DIRECTION OF AN AXIS OF SYMMETRY (PRIMARY FORCES AND DISPLACEMENTS)

The space frame results of the previous chapter provide a baseline for measuring the performance of the simplified portal frame model. In Appendix A, superstructure response is summarized for eleven frame structures with flexible mats supported on the softest soil type considered ( $v_s=500$  fps). These results include horizontal floor deflection and total column shear for the full range of floor plans and story heights investigated. Each graph presents the results for: (a) a space frame calculation with flexible mat and linear soil volume; (b) a traditional shear building calculation with floor joints fixed against rotation; (c) the proposed portal frame model. This proposed model incorporated soil flexibility (see Wolf (58) for typical implementation), as well as floor system flexibility (based on assumptions of portal frame analysis). Figures 4.1 and 4.2 demonstrate the relative accuracy of these two stick models in approximating the fundamental frequency of the space frame calculations. While the shear building model error increases roughly linearly with height from 9 to 206% in the range of 5 to

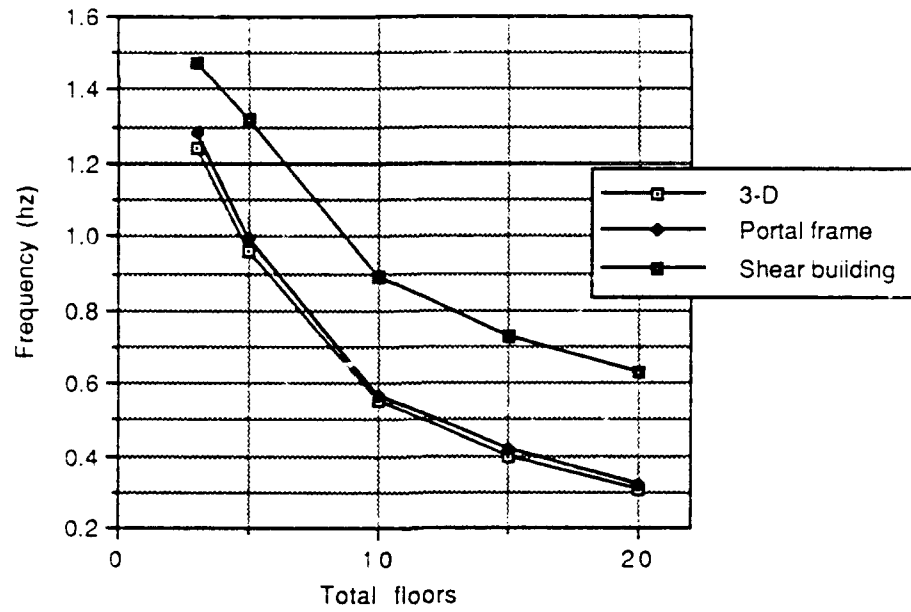


Figure 4.1 Mode 1 frequencies  
(series N/1:1/0500)

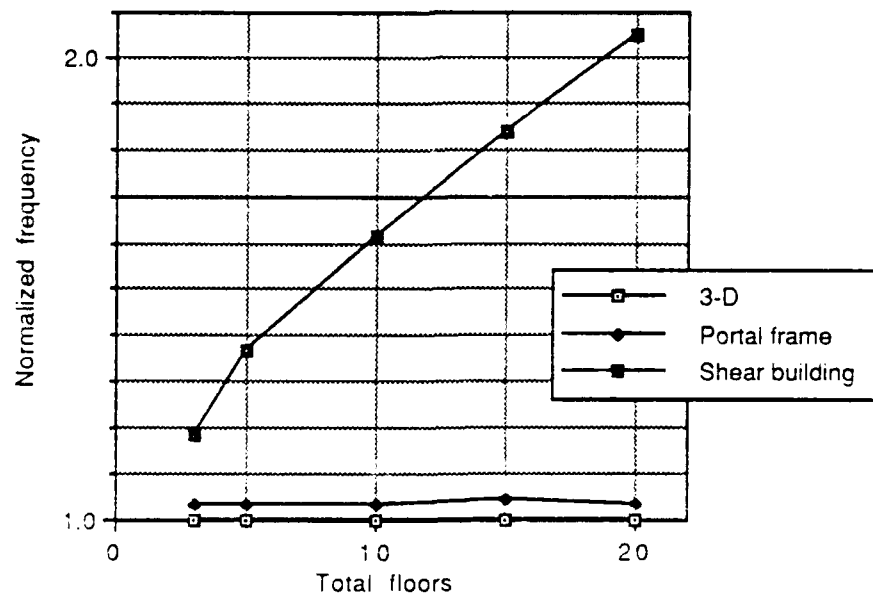


Figure 4.2 Mode 1 frequencies  
normalized to 3-D data (series N/1:1/0500)

20 floors for a square floor plan, the error in the portal frame remained relatively constant (3 to 5%). For a bounding comparison, response of building 5/1:1/0500/E-C was computed using a conventional cantilever model, with floor nodes unrestrained against rotation. The fundamental frequency for this structure was .159 Hz, roughly 84% below that of the space frame model. Figures 4.3 and 4.4 provide an expanded comparison of modal frequency error for the proposed model. The portal frame model provided improving accuracy for at least the first three additional significant modes, with the exception of the highest frequencies of the three floor structures. In these very short structures, the highest mode shown was only marginally significant and was the not the same mode selected as significant in the space frame calculation. Thus the apparent error in frequency calculation was really due to differences in computed modal significance between the two calculations. There was little resemblance between the modal frequencies computed for the higher modes of the shear frame analysis and the space frame analysis. All higher mode frequencies of this traditional stick model analysis were very high compared to the space frame analysis.

Figure 4.5 compares ANSI A58.1 (3) data on fundamental frequency responses for a representative steel frame structure to the computed fundamental frequencies of this investigation.

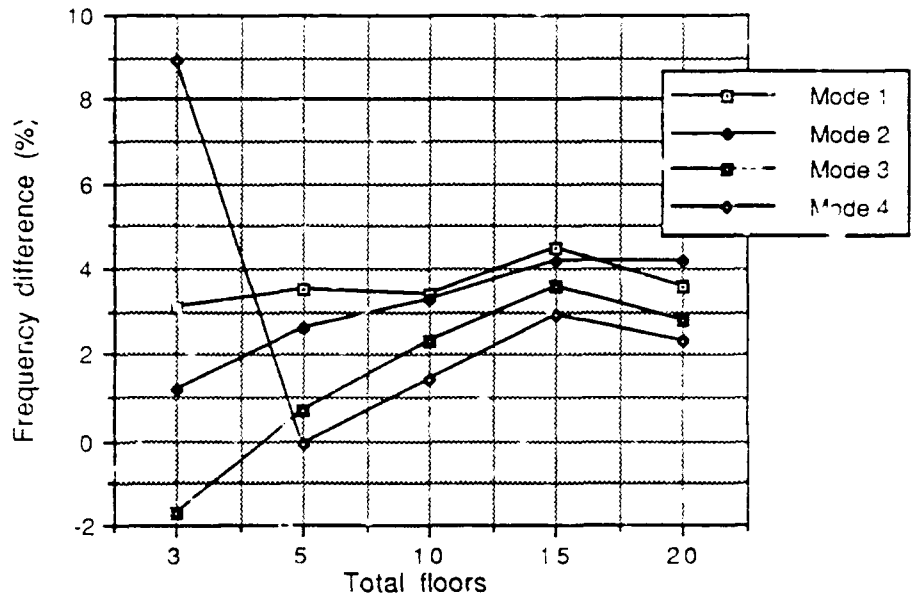


Figure 4.3 Mode frequency comparisons  
3-D versus portal frame  
(series N/1:1/0500)

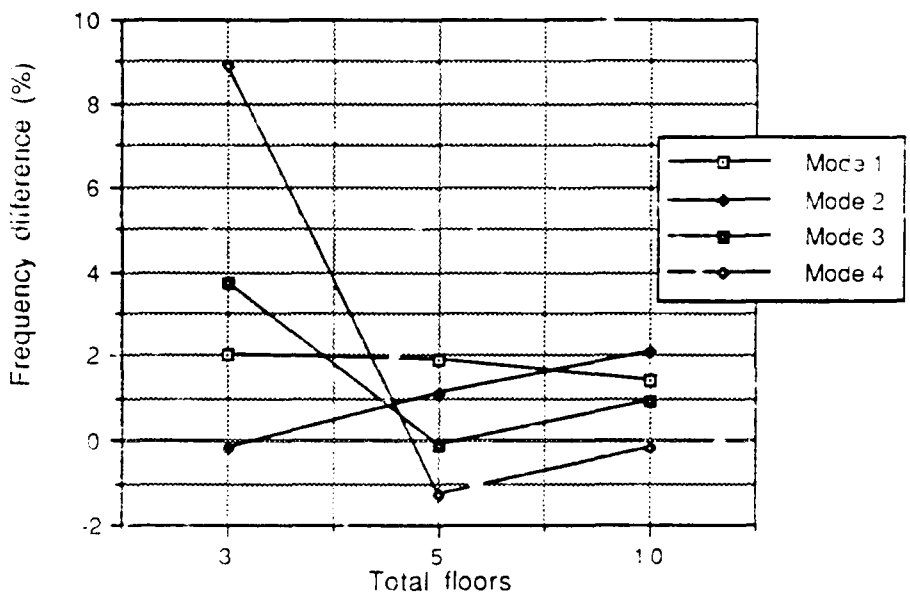


Figure 4.4 Mode frequency comparisons  
3-D versus portal frame  
(series N/1:1.75/0500)

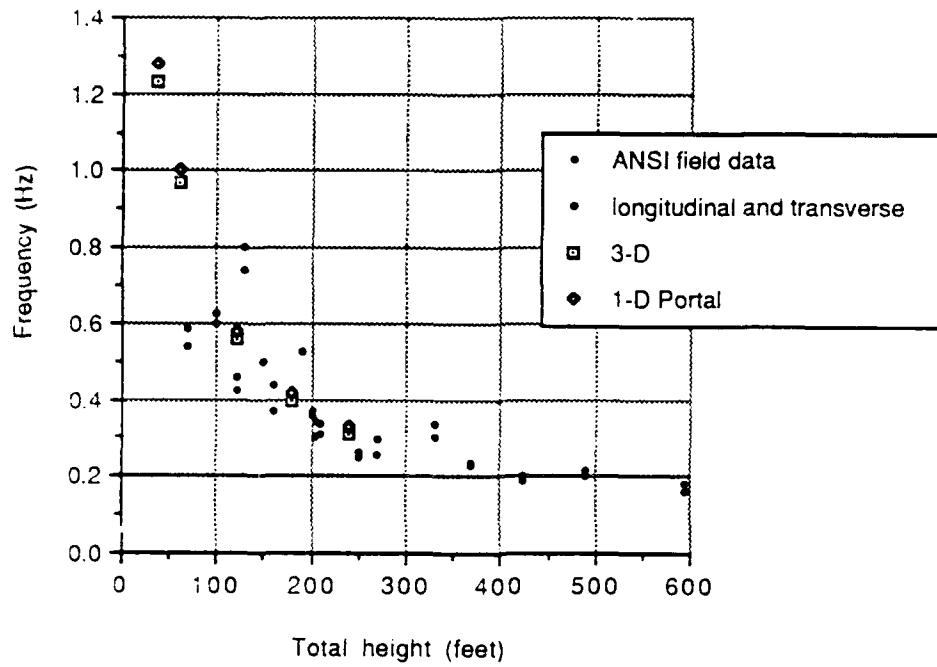


Figure 4.5 Comparison of computed mode 1 frequencies for series N/1:1/0500 to ANSI field data for steel frames

Frequencies for these representative frames were determined from direct field measurements. The computed frequencies for space frame and portal frame calculations fell in the mid range of this field data. Frequencies computed by the shear beam model were clearly too high. Again, errors for the shear beam model increased dramatically for taller structures. In the one case examined (5/1:1/0500/E-C), frequencies computed by the cantilever beam model were grossly low.

Figures 4.6 and 4.7 compared horizontal floor deflection and total column shear for structure 5/1:1/0500/E-C. For this single example, the results of space frame, portal frame, shear building, and cantilever building models are compared. This comparison clearly demonstrates the beneficial effect of carefully representing the flexibility of individual floor slabs. For the selected design, both deflection and shear are broadly bounded by perfectly rigid floor slab (shear building) and perfectly flexible floor slab (cantilever beam) assumptions. In Appendix A, horizontal floor deflection and total column shear are compared for the space frame, shear building, and the proposed portal frame analyses. Cantilever building frame analysis is not presented for these comparisons because the floor systems selected for this research are relatively flexible. These comparisons complement the findings of the frequency comparisons stated above. The traditional shear building model

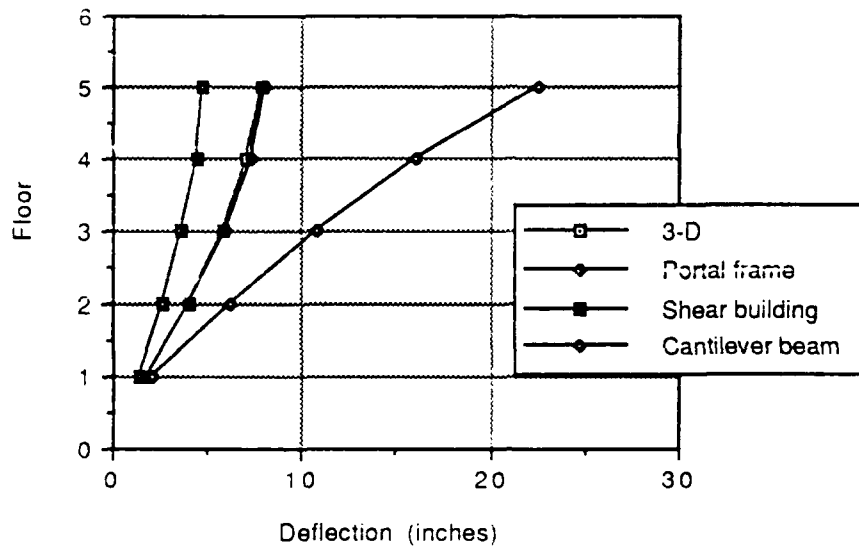


Figure 4.6 Horizontal floor deflection with cantilever beam bounding estimate (series 5/1:1/0500/E-C)

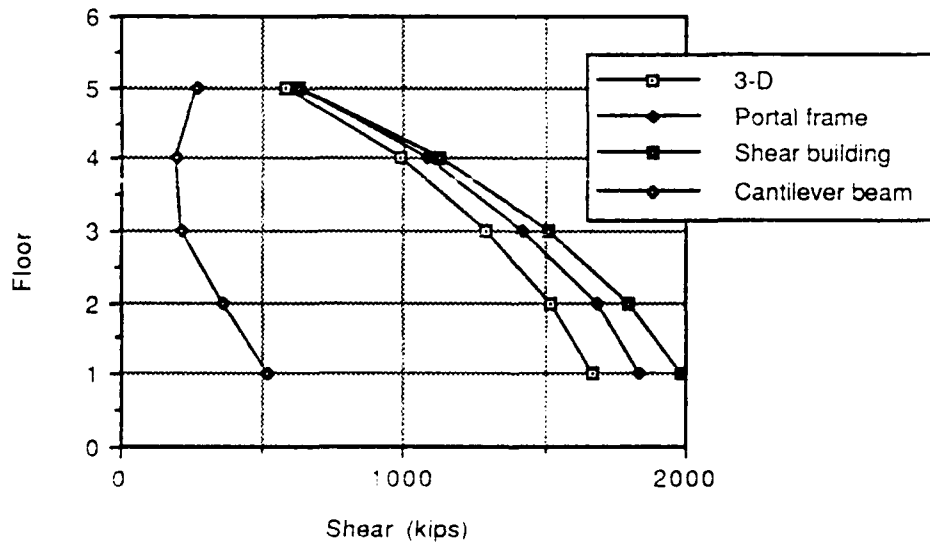


Figure 4.7 Total column shear with cantilever beam bounding estimate (series 5/1:1/0500/E-C)

was more stiff than the space frame model. Horizontal deflections with this model were too low, and column shear forces were too high with the El-Centro loading (which, as demonstrated in Chapter I, has a code-like spectral distribution of pseudo-velocities). For very low frames, this error would be acceptable for many design applications, but the differences grew to less acceptable levels for structures of ten floors or more. An important exception to this trend occurred in structures subjected to the Mexico City earthquake. For this loading, the largest pseudo-velocities were restricted to a relatively narrow band of frequencies (loading band). In the shorter frames (3 to 5 floors), the shear building and space frame calculations responded to similar pseudo-velocities for the fundamental mode. Here, the shear forces in the shear building model were significantly larger, as described for the El Centro loading. For the taller structures, differences in shear building and space frame fundamental frequencies were of the same order magnitude as the width of the loading band. Consequently, while the space frame calculations were responding to peak pseudo-velocities in the middle of the band, the shear building model responded to much lower pseudo-velocities at frequencies above the loading band (see Figures A.15 to A.18, ten and fifteen floor structures, square floor plan). For these structures, the shear building model grossly under-predicted the column shear forces. In the twenty floor structure, the space frame calculation was responding to

pseudo-velocities near the low frequency edge of the loading band. In this case the shear building model was responding to roughly similar pseudo-velocities at the high frequency edge of the loading band. Here, shear forces were again greater in the shear beam model.

The portal frame calculations provided good approximations of superstructure response for all soil types, loading, floor plans, and frame heights examined. Although maximum variations from the space frame horizontal roof deflection and total base column shear ranged from -15.5% to 21.6%, it was just as common for these comparisons to overlie each other. For horizontal roof deflection and total base column shear, average errors were -3.5 to 4.0% respectively. The modal frequency accuracy of this model prevented complications with the narrow loading pulse of the Mexico City earthquake. Horizontal deflections and column shears from this portal frame model were greater or less than those of the space frame model with roughly equal frequency. The amount and distribution of error found in these dynamic comparisons were consistent with typical comparisons of exact and traditional portal frame analyses for two-dimensional static analysis.

### **SUPERSTRUCTURE RESPONSE OF FRAMES LOADED IN THE DIRECTION OF AN AXIS OF SYMMETRY (INDIVIDUAL MEMBER FORCES)**

A technique for combining results of the portal frame analysis and extended member output from static space frame floor analysis (refer to Chapter II) was carried out for sixteen structures supported on soft soil ( $v_s=500$  fps) to obtain location and magnitude of maximum member forces of interest. These forces included total column moment and shear, as well as maximum beam moment, shear, and torque for each member size used in a given frame. Mean error with standard deviation for these forces, relative to corresponding space frame forces, are summarized in Table 4.1, along with comparisons of maximum base shear and horizontal roof deflection. Table 4.2 provides a summary of this data. Errors for individual member forces typically were larger than for total base shears and roof deflections. However sufficient accuracy remained for many design applications. Greatest individual errors were positive, tending to overestimate member forces. The largest errors, exceeding +30%, occurred most frequently for smaller member sizes in the upper floors of a structure. Standard deviations for all errors of a given member selection and force type did not exceed 15%. Mean errors for all parameters surveyed range from -3.5 to 11.1%. Similarly, mean standard deviations ranged from 7.2 to 16.2%.

Table 4.1 Comparison of important response values from space frame and portal frame analysis

Identifier	Roof deflection		Base Shear		Maximum Columns Forces		Maximum Beam Forces		
	(%)	(%)	(%)	(%)	Shear (%)	Mbment (%)	Shear (%)	Mbment (%)	Torque (%)
3/1:1/0500/E-C	-15.5	2.1	13.3	16.4	-3.7	-3.1	-5.2		
5/1:1/0500/E-C	2.5	10.3	15.9	21.3	17.0	15.8	14.6		
10/1:1/0500/E-C	-7.4	0.3	-1.8	9.1	15.0	8.7	7.9		
			0.1	-0.1					
15/1:1/0500/E-C	-7.0	0.3	-6.5	10.9	12.8	-5.7	5.4		
			-5.1	-4.8	-13.8	13.7	10.1		
			-0.2	-0.1					
20/1:1/0500/E-C	8.3	8.9	1.5	19.6	24.4	-1.3	14.5		
			-1.1	-0.2					
			3.2	4.7	300	24.3	20.2		
			13.8	10.0					
mean	-3.8	4.4	3.0	7.9	11.5	6.9	9.6		
standard deviation	9.3	4.8	7.8	8.8	15.0	11.3	8.2		

Table 4.1 (continued)

Identifier	Roof deflection (%)	Base Shear (%)	Maximum Columns Forces		Maximum Beam Forces		
			Shear (%)	Moment (%)	Shear (%)	Moment (%)	Torque (%)
3/1:1/0500/MC	0.1	8.1	19.5	22.9	5.2	2.5	0.1
5/1:1/0500/MC	-9.6	-2.4	1.7	7.2	-8.7	2.4	1.4
10/1:1/0500/MC	-17.7	-11.1	-17.3	-4.1	-21.8	-3.4	-3.9
			-12.2	-12.0			
15/1:1/0500/MC	-5.1	3.3	-6.7	11.1	-10.5	10.0	8.7
			-3.4	-3.5	-7.1	14.8	12.4
			2.1	2.6			
20/1:1/0500/MC	11.4	21.6	7.9	31.2	4.7	28.7	27.7
			9.4	10.6			
			14.6	14.3	12.4	36.7	33.3
			39.1	19.9			
mean	-4.2	3.9	5.0	9.1	-3.7	6.4	11.4
standard deviation	10.9	12.2	15.9	12.9	11.7	23.1	14.2

Table 4.1 (continued)

Identifier	Roof deflection (%)	Base Shear (%)	Maximum Columns Forces		Maximum Beam Forces		
			Shear (%)	Moment (%)	Shear (%)	Moment (%)	Torque (%)
3/1.75/0500/E-C	-8.0	15.5	10.5	13.4	-18.3	-10.2	-0.6
5/1.75/0500/E-C	0.5	3.7	9.6	13.0	-16.9	4.7	17.6
10/1.75/0500/E-C	0.6	-4	-1.0	3.3	-12.7	5.3	15.3
			1.7	1.5			
mean	-2.3	6.5	5.2	7.8	-16.0	-1	10.8
standard deviation	4.9	7.9	5.7	6.3	2.9	8.8	9.9
3/1.75:1/0500/E-C	-5.3	-0.5	17.6	22.6	-18.0	-10.9	12
5/1.75:1/0500/E-C	0.5	5.0	19.7	23.9	-15.3	3.9	19.4
10/1.75:1/0500/E-C	-4.5	-0.6	8.4	15.6	-22.3	5.7	21.2
			7.8	7.7			
mean	-3.1	1.3	13.4	17.5	18.5	-0.4	13.9
standard deviation	3.1	3.2	6.2	7.5	3.5	9.1	11.1

Table 4.2 Summary comparison of important response values from space frame and portal frame analysis

Response Type Identifier	Mean (%)	Standard Deviation (%)
Roof Deflection	-3.5	7.7
Base Shear	4.0	8.4
Maximum Column Shear	5.4	11.2
Maximum Column Moment	9.6	10.2
Maximum Beam Shear	-2.4	16.2
Maximum Beam Moment	7.1	12.5
Maximum Beam Torque	11.1	10.5

In addition to the maximum beam forces, maximum individual column shear was determined by use of equation 2.15 for each comparison of Table 4.1. Maximum individual column shear estimates from portal frame analysis were on average 5.3% higher than corresponding space frame values. The standard deviation for this error was 7.9%.

Figures 4.8 to 4.10 summarize errors in locating the position of the maximum member forces relative to those obtained from space frame calculations. Columns with maximum shear and moment were located correctly for all calculations. Maximum shear occurred at the first floor (and at the first transition floor) for columns. Maximum column moment occurred in one of the first three floors, with higher locations in taller structures. Beam shears were often highest, and nearly equal, at two locations in each floor plan. The combined analysis method incorrectly identified peak shear at the secondary maximum position in about 15% of the cases (maximums for each beam size). Similar errors occurred more frequently in selecting maximum beam moment locations (54%) and maximum beam torque (62%).

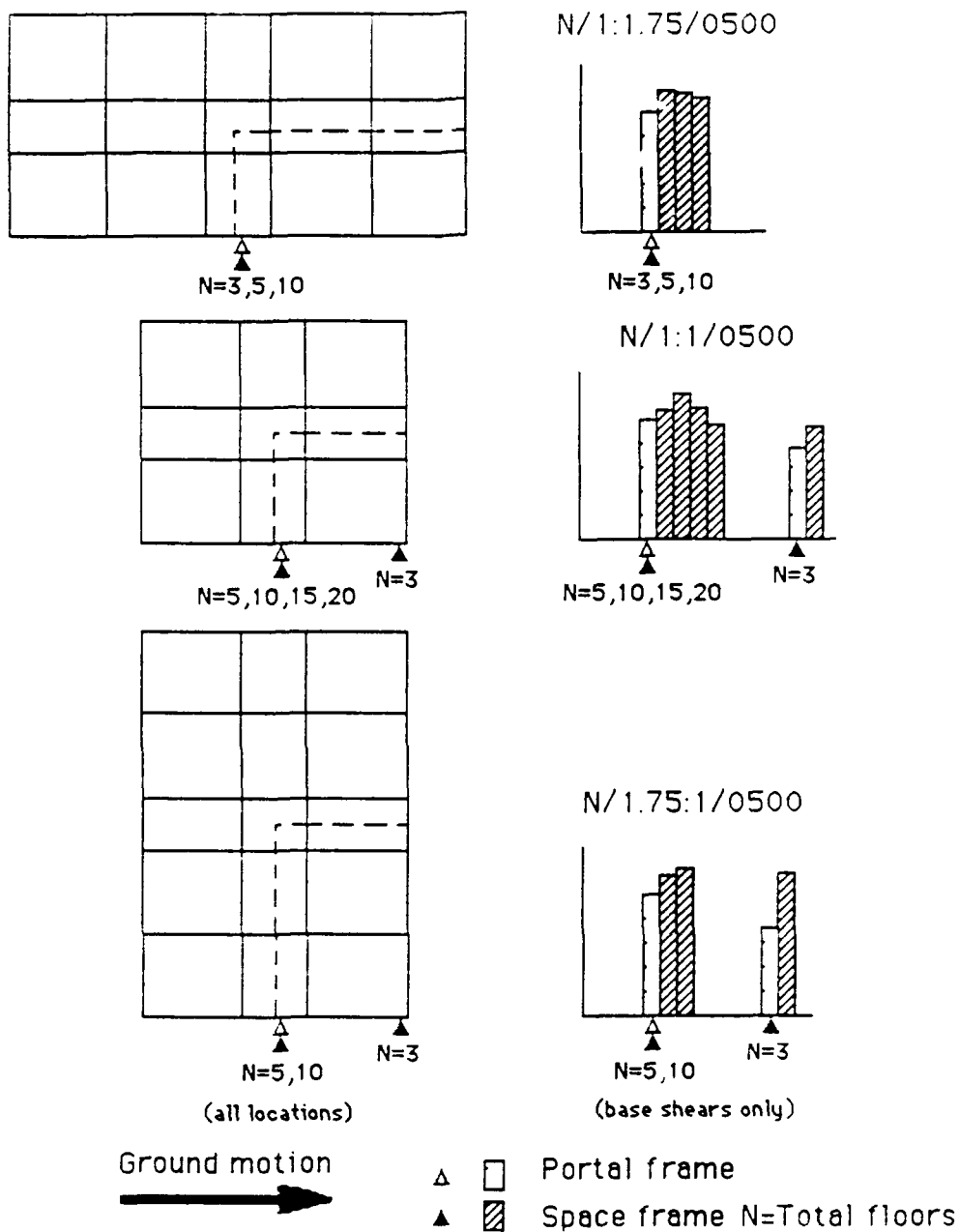


Figure 4.8 Comparison of maximum beam shear location and magnitude normalized to portal frame values for typical quadrant

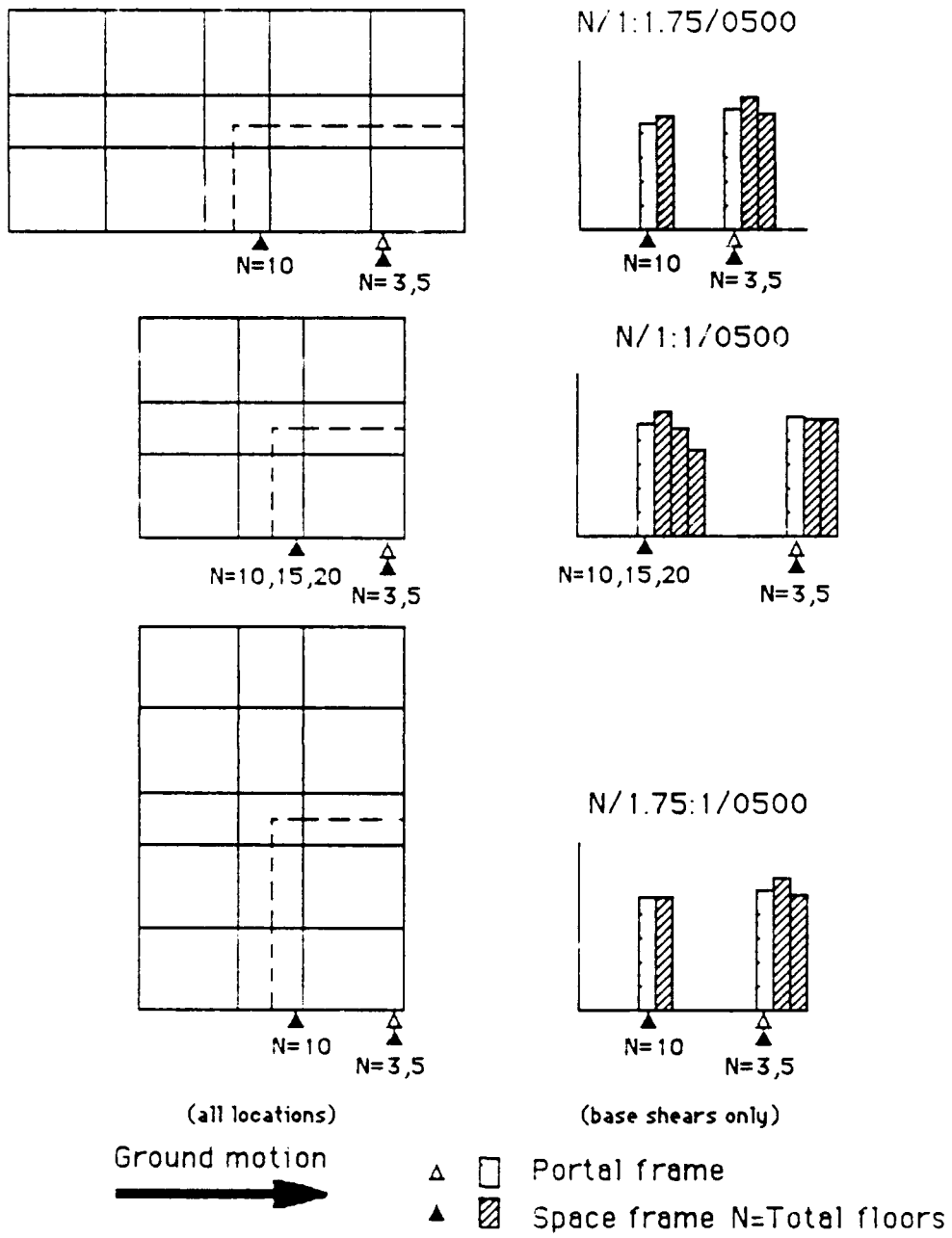


Figure 4.9 Comparison of maximum beam moment location and magnitude normalized to portal frame values for typical quadrant

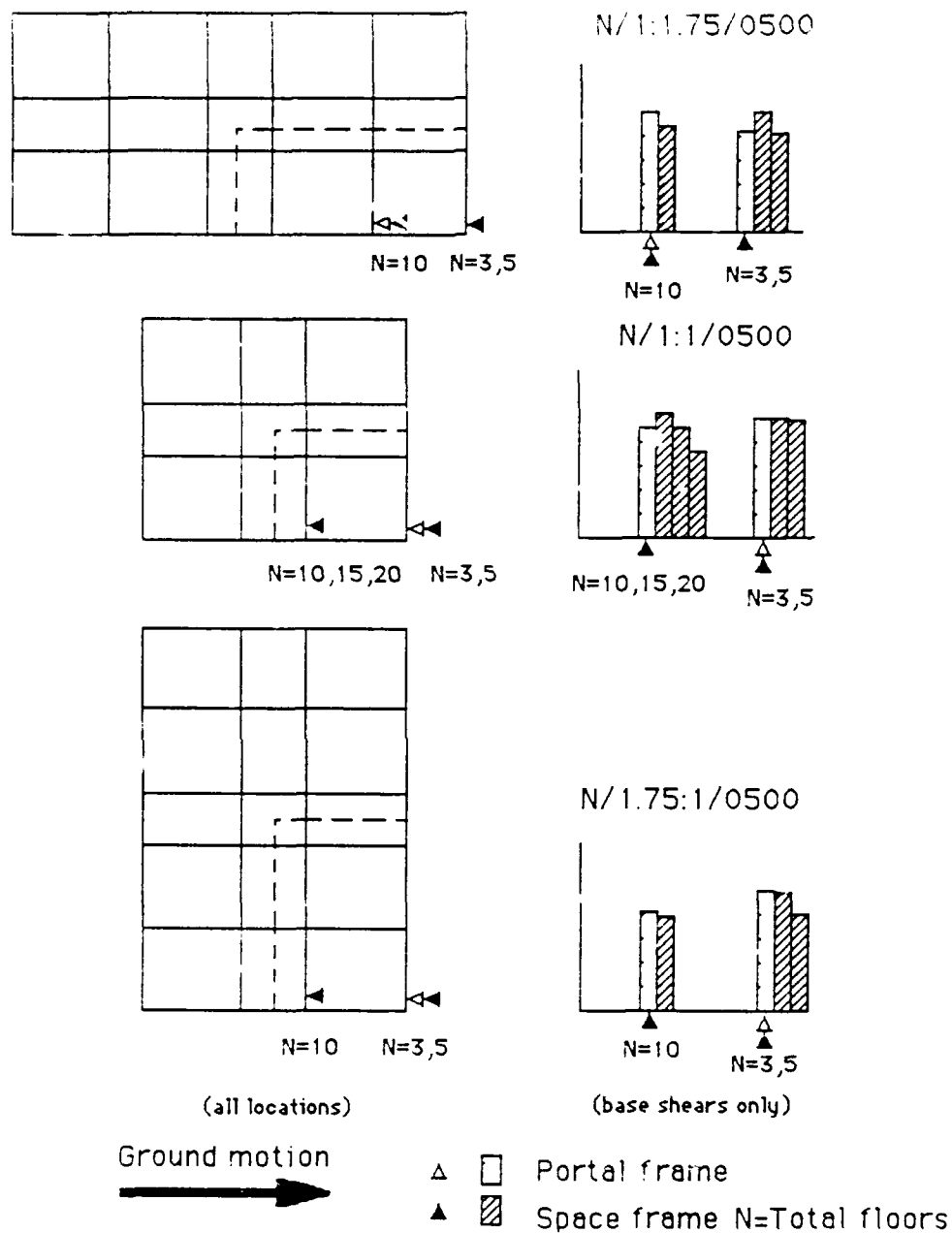


Figure 4.10 Comparison of maximum beam torque location and magnitude normalized to portal frame values for typical quadrant

## **ECCENTRIC FRAME STRUCTURES WITH RIGID MAT FOUNDATIONS EXCITED IN HORIZONTAL DIRECTIONS INSURING SELF-INDUCED TORSION**

### **Preliminary Non-Symmetric Horizontal Loading of a Doubly Symmetric Frame**

Prior to extending the portal frame model to include torsion effects, the technique of approximating floor stiffness effects with a single torsional spring was extended for loads applied in an arbitrary direction. Aligned along the principal axes of the columns, a pair of torsional springs proved sufficient to provide this enhancement (see Chapter III). Given the very limited effect of mat flexibility upon superstructure response for symmetrically loaded structures described above, rigid mat approximations were considered adequate for all subsequent space frame calculations. Portal frame and space frame calculations of the response of a single five-floor doubly-symmetric frame of square floor plan confirmed earlier observations. Responses of this structure and subsequent eccentric structures are summarized in Table 4.3. Appendix A provides graphic profiles of deflected shapes, as well as shear and torque. The first three pairs of portal frame modal frequencies ranged from 3.6 to 4.1% higher than those obtained from space frame calculations. In the principal directions, base shears averaged 10.4% high and horizontal roof deflections averaged 4.7% high in the portal frame model. No significant

Table 4.3 Comparison of important response values from space frame and portal frame analysis with torsion response allowed

Identifier	Roof deflection		Base shear/torque		
	x-def (%)	z-def (%)	x-shr (%)	z-shr (%)	y-tor (%)
doubly symmetric frames					
5/1:1/0500/E-C(1,1)	4.8	4.5	10.7	10.1	n/a
mono-symmetric frames					
5/1:1E/0500/E-C(0,1)	n/a	3.4	n/a	8.5	3.7
5/1:1E/0500/E-C(1,1)	4.1	3.5	4.1	7.0	-5.2
10/1:1ESB/0500/E-C(0,1)	n/a	-10.1	n/a	-2.2	-9.9
asymmetric frame					
5/3:2L/0500/E-C(.5625,.1.0)--CQC(1)	-18.6	-4.5	-10.8	-8.7	8.5
5/3:2L/0500/E-C(.5625,.1.0)--CQC(2)	-17.5	.7	-8.8	20.6	-8.0
5/3:2L/0500/E-C(.5625,.1.0)--SRSS(1)	-5.5	-13.7	4.0	-1.7	-3.3
5/3:2L/0500/E-C(.5625,.1.0)--SRSS(2)	-13.5	6.5	-2.3	25.6	-18.0
mean	-7.7	-1.2	-5	7.4	-4.6
standard deviation	10.5	7.4	8.3	11.6	8.8

n/a -- not applicable for this structure, loading, or statistical summary

- Trailing identifiers for asymmetric calculations
- CQC -- CQC modal combination (see Appendix D)
- SRSS -- SRSS modal combination (see Appendix D)
- (1) -- Torsional stiffness varied with elevation
- (2) -- Torsional stiffness from eq. 2.14 uniformly applied

torsion developed in either model. This comparison suggests no additional complications result from arbitrary loading directions, so long as torsion is slight.

### **Non-Symmetric Horizontal Loading of Mono-Symmetric Frames**

To assess the response of a relatively simple frame to self-induced torsion with the extended portal frame technique described in Chapter III, a mono-symmetric frame of square floor plan was selected. This frame was loaded in two horizontal directions (at  $90^\circ$  and  $45^\circ$  to the axis of symmetry) in separate calculations. For this comparison, and all comparisons of this section, two portal frame calculations were performed (one with a vertical distribution of torsional stiffness proportioned to results of a full space frame analysis, and one with a uniform stiffness distribution determined from eq. 2.14). These portal frame results were so similar for the mono-symmetric structures of this section that only the simplified analysis is reported in detail here (see Appendix A for comparisons of different portal frame analyses).

The  $90^\circ$  loading (referred to as 5/1:1E/0500/E-C{0,1} in Appendix A) generated maximum lateral-torsional response. Comparing portal frame and space frame responses for this loading, portal frame frequencies were 2.9 to 3.2% high for modes

1, 3 and 7 (dominated by combined lateral and torsional response). Similarly, frequencies were 6.1% and 1.3% high for modes 3 and 6 (dominated by torsional response). In the direction of loading, horizontal roof deflection was 3.4% high, base shear was 8.5% high, and base torque (at the static center of rigidity) was 3.7% high for the portal frame calculation.

For the 90° loading only, forces and displacements were also determined by the method of equivalent static portal frame loading applied to a space frame model of the structure (refer to Chapter II). The equivalent portal frame forces for this calculation were obtained from a portal frame model based on the simple stiffness estimates of equations 2.8 and 2.14. Horizontal roof displacement in the direction of loading, determined by this method, was 6.0% greater than in the corresponding portal frame analysis, and 10.5% greater than in the corresponding dynamic space frame analysis. Primary structure forces correlated exactly with those of the dynamic portal frame model (from which the equivalent static space frame loads are derived). Maximum member forces were compared between the static and dynamic space frame analyses. Maximum shear and moment (in both principal directions), axial force, and torque for columns and beams averaged 19% higher in the static space frame with a standard deviation of 11.2%. The higher maximum forces in the static space frame are partially explained by differences in

modal combination between the dynamic portal frame model and dynamic space frame model. As explained in Chapter II, portal frame column torque was determined for each significant mode prior to CQC modal combination. The resulting dynamic portal frame base torque, for instance, is 14.2% greater than the base torque determined directly from CQC column shears and torques of the dynamic space frame analysis.

Very similar frequency errors were noted for the 45° loading (referred to as 5/1:1E/0500/E-C{1,1} in Appendix A). Independent lateral modes were added for motion parallel to the plane of symmetry (in the x-direction). Portal frame roof deflections were 4.1% high in the x-direction (3.5% high in the z-direction). Portal frame base shears were 4.1% high in the x-direction (7.0% high in the z-direction). Base torque error was 5.2% low in the portal frame model.

Finally, a ten floor mono-symmetric frame with the top five stories set back thirty feet (referred to as 10/1:1ESB/0500/E-C{0,1} in Appendix A) was loaded perpendicular to the axis of symmetry. Comparing portal frame and space frame responses for this loading, portal frame frequencies were 3.7 to 5.1% high for modes 1, 4 and 7 (dominated by combined lateral and torsional response). Similarly, frequencies were 9.0% and 4.7% high for modes 3 and 6 (dominated by torsional response). In the direction

of loading, horizontal roof deflection was 10.1% low, base shear was 2.2% low, and base torque was 9.9% high for the portal frame calculation.

### **Horizontal Loading of an Asymmetric Frame**

An asymmetric frame of L-shaped floor plan (referred to as 5/3:2L/0500/E-C in Appendix A) was investigated by direct application of the portal frame model, with the axes of column moments of inertia and floor/soil springs not aligned with the line connecting the centers of mass and rigidity of the structure. The magnitudes of horizontal displacement and column shears in the x and z directions were found to be qualitatively reversed compared to space frame values. Torque was too low, and all three parameters differed from the space frame values by not less than 25%. Subsequent investigation revealed the tendency for small changes in lateral or torsional stiffness to cause a discrete fluctuation between the two sets of results described above. This fluctuation was generated in both the space frame and portal frame models. This problem was traced to the sensitivity of the CQC modal combination to sign reversal in combined eigenvectors. The first three mode shapes were examined for this structure. The sign of the eigenvector of the first mode, as computed by the Householder technique, was found to be very sensitive to small fluctuations in structure stiffness. The CQC generated comparisons of this section and Figures A.50

through A.52 were made by artificially reversing the sign of the first eigenvector of the portal frame model. To further insure that the problem described above was not the result of other factors as well, the space frame and portal frame calculations of this section were repeated using SRSS modal combination, which is not sensitive to the sign of the eigenvector.

Comparing responses of the space frame and portal frame with torsional stiffness varying with elevation, portal frame frequencies were 8.2 to 6.4% high for modes 1, 2, 4 and 5 (dominated by combined lateral and torsional response). Similarly, frequencies were 6.5% and 9.5% low for modes 3 and 6 (dominated by torsional response). For CQC modal combination, horizontal roof deflection was 18.6% low in the x-direction and 4.5% low in the z-direction. Base shear was 10.8% low in the x-direction and 8.7% low in the z-direction. Base torque was 8.5% high for the portal frame calculation. For SRSS modal combination, horizontal roof deflection was 5.5% low in the x-direction and 13.7% low in the z-direction. Base shear was 4.0% high in the x-direction and 1.7% low in the z-direction. Base torque was 3.3% low for the portal frame calculation.

Comparing responses of the space frame and portal frame with uniform torsional stiffness determined by the approximate method of eq. 2.14, portal frame frequencies were 8.7 to 9.8%

high for modes 1, 2, 4 and 5 (dominated by combined lateral and torsional response). Similarly, frequencies were 2.7% high and .5% low for modes 3 and 6 (dominated by torsional response). For CQC modal combination, horizontal roof deflection was 17.5% low in the x-direction and .7% high in the z-direction. Base shear was 8.8% low in the x-direction and 20.6% high in the z-direction. Base torque was 8.0% low for the portal frame calculation. For SRSS modal combination, horizontal roof deflection was 13.5% low in the x-direction and 6.5% high in the z-direction. Base shear was 2.3% low in the x-direction and 25.6% high in the z-direction. Base torque was 18.0% low for the portal frame calculation.

## CHAPTER V

### CONCLUSIONS

#### PHASE 1 - PRELIMINARY STUDY OF SOIL-STRUCTURE INTERACTION

##### Comparison to Published Data

In most respects the space frame model satisfied the preliminary objectives of this research. This model provided good qualitative representation of response features of the mat foundation. Although overall soil rocking stiffness was high by as much as one third for certain soil-structure combinations, these errors did not prevent consistent and quantitatively justified details of the response of the superstructure.

Compared to published analytical results of Dobry and Gazetas (14), error in overall rocking stiffness resulting from soil and mat interaction ranged from less than 1% error to as much as 35% error. The error increased as soil stiffness decreased and mat aspect ratios varied from 1.0 (square plan). Rocking stiffness was assessed for approximately rigid massless mats excited by harmonic couples applied at the fundamental frequencies of the proposed structures. For a given mat, the amount of error in rocking stiffness was a function of rocking frequency. For values of  $a_0$  corresponding to frequencies in the range of the fundamental

frequencies of the structures investigated, results of three-dimensional mat analysis were generally stiffer than analytic results. Radiation damping, computed using the three-dimensional mat model, did not approach the values of Dobry and Gazetas (14), except at frequencies far higher than the fundamental mode frequencies of typical low-rise structures supported by moment resisting frames. Radiation damping was not directly modeled for earthquake loading. Instead, viscous damping of 10% was applied to the equivalent soil springs. Even this relatively large amount of rocking viscosity had little influence on the overall response of the superstructure. Structural damping was dominated by the amount of viscous damping assigned to the frame columns (2%), since the bulk of strain energy stored in the soil-structure system was concentrated in the columns.

The three-dimensional mat model also compared acceptably with analytical data published for flexible mat foundations, see Whittaker and Christiano (56). Results were compared for mats which were nearly rigid as well as quite flexible (soil stiffness ratios of  $K=3.3$  and  $.004$ ). The distribution of soil spring intensity was computed along the axis of symmetry in the direction of loading for a square mat. Three-dimensional mat model results compared better with analytic solutions as  $K$  increased. Maximum error in spring intensity for the softer mat

was about 30% at the mat perimeter. As with overall rocking damping, the distribution of soil damping intensity did not agree well with analytical results. The damping distributions of the three-dimensional mat model were typically low in magnitude, and qualitatively different in distribution, compared to analytical solutions. Somewhat better qualitative agreement of overall rocking damping resulted for higher frequency comparisons ( $a_0 = 2.5$ ).

The application of anti-symmetry conditions--to reduce the model size to a quarter of the full frame and soil volume--had little effect on structure response. Comparison of quarter and half-space calculations demonstrated differences of less than 1% in overall rocking stiffness for low frequency harmonic excitations, near the fundamental soil-structure frequencies studied ( $a_0=.21$ ). Gradual divergence between these models occurred as  $a_0$  was increased to about .85, with more rapid deterioration of this comparison at higher frequencies.

### **Limitations**

Soil plasticity was not modeled explicitly. The application of 10% viscous soil damping was assumed consistent with moderate levels of non-linear soil strain (.001) for cohesive soils. The three-dimensional mat model, and subsequent space frame model, does not account for soil tension cut-off--vertical accelerations

including gravity were neglected and linear analysis was performed. Negative springs generate soil tension forces on the compression side of the rocking axis, and compression forces on the tension side. Future study may suggest whether this effect changes the net tendency of a flexible mat to uplift.

Equivalent soil springs were determined for a particular distribution of harmonic loads acting in phase (see Chapter II). These spring distributions are only applicable to earthquake loadings provided mat displacement profiles from earthquake analysis are similar to those obtained under harmonic loading. From data presented in Appendix B, best correlation of mat displacement profiles occurred for thick mats (tall frames) with square floor plans supported on stiff soil ( $v_s = 1500$  fps). Moderate deterioration of profile comparisons occurred for thin mats and rectangular floor plans supported by softer soils. Severe exceptions to these trends occurred for two calculations: (10/1:1/1500/E-C) and (10/1.75:1/1500/E-C). For these two calculations, profile comparisons are much worse than for five floor structures with the same mat aspect ratios and soil stiffnesses, and for ten floor structures with the same mat aspect ratios but softer soil ( $v_s = 500$  fps). Space frame mat displacements and forces for these two calculations are highly suspect. As will be discussed below, frame response was insensitive to mat response and only moderately sensitive to

overall soil rocking stiffness. Consequently, results of frame response in these two calculations were retained for comparison with other structures.

### **Findings for Space Frame with Flexible Mat**

Mat flexibility is very important to mat response, but is of little consequence to superstructure response. Mat designs were based on the assumption that, for low to medium-rise structures, best economy and serviceability are obtained from concrete mats featuring minimal steel percentages. Such designs provide maximum rigidity from relatively thick concrete sections, good ductility resulting from under-reinforcement, and extensive redundancy insured by biaxial reinforcement at all mat locations. Considering factors such as these, a greater concern in design becomes the response of the superstructure. For this study, mat vertical deflections were reported to assess the importance of these deflections upon response of the superstructure. Clearly, as mat flexibility increased, the deflection patterns of the mat became more intricate, with multiple reversals of curvature. These deflection patterns and corresponding extreme variations in equivalent soil spring intensity had very little effect on the major response features of the superstructure. For all structures in which mat flexibility was assessed, 300% variations in soil shear-wave velocity produced no more than 7.1% and 6.6% variation in horizontal roof deflection and total base shear.

Typical variations were about half of these extreme values for horizontal roof deflection and total base shear. This soil shear-wave velocity variation corresponded to a soil stiffness variations of 900% (with a constant Poisson's ratio of .333). Given that the qualitative distribution of equivalent soil springs compared well with published data, even the maximum errors of 35% in overall rocking stiffness in the foundation were of little consequence to the response of the frame. These low maximum superstructure response variations resulted in part from applying uniform spectral loading to the far-field nodes of the soil springs. Sivakumaran and Balendra (39) found larger variations in deflection and shear distributions in stick frame models not accounting for mat flexibility (up to about 30% variation over similar ranges of soil stiffness). These larger variations result from applying a spectral rocking moment to ridge (single node) foundations (see Veletsos and Verbic (53)). The amount and variation in mat deflection and soil-spring intensities computed in this investigation suggest much greater variation in frame response should be expected, if mat flexibility were in fact important. Additionally, limited comparisons were made of flexible mat space frames supported by equivalent soil spring distributions to (a) rigid mat space frames supported by equivalent soil spring distributions and (b) rigid mat space frames supported by simple two spring soil models. Differences in roof deflection and base shear did not exceed 4%. All of the

above comparisons suggest that neither soil nor mat flexibility is of great significance to the superstructure response.

## **PHASE 2 - PORTAL FRAME MODEL WITH LOADING IN THE DIRECTION OF AN AXIS OF SYMMETRY**

### **Comparison to Space Frame Model Results**

Fundamental mode frequencies of the portal frame model were slightly higher (3 to 5%) than fundamental mode frequencies computed for the same structure design analyzed by the space frame model. Higher modes of the portal frame model were also stiffer than corresponding modes of the space frame model. It is particularly interesting that frequency differences between the models decrease for higher modes, up to the point that direct correlation between the modes is possible. The two models differ as to the level of significance of the corresponding modes. Above modes four or five, these differences were sufficient to cause the retention of different modes for modal combination in each model. In such cases, the low level of significance of higher modes, and differences in relative significance levels between higher modes for a given model, resulted in different modes being retained for modal combination. In both models the fundamental mode dominated the response of the frame. The accuracy of a given model in computing the fundamental mode and mode-shape was extremely important in computing realistic response in

structures subjected to loads with strongest shaking limited to a narrow band of frequencies, as for the Mexico City earthquake.

Variation in error of the portal frame model for important response features approximated a normal distribution. Maximum horizontal roof deflection and base shear error averaged 3.5% low to 4.0% high for the portal frame model, with standard deviations of 7.7 and 8.4% respectively. Similarly, maximum column shear and moment error averaged 5.4% high and 9.6% high with standard deviations of 11.2% and 10.2%. Also, maximum beam shear, moment and torque error averaged 2.4% low, and 7.1% and 11.1% high, with standard deviations of 16.2%, 12.5%, and 10.5%. Axial column forces could not be accurately approximated from portal frame analysis; however, equivalent static loading of a space frame model provided good estimates of all important frame member forces (see page 122).

While floors experiencing maximum net column shears and moments were correctly located in all frames, maximum beam forces in each beam size were mis-located in 15 to 62% of cases examined, depending upon the type of beam force. These errors can occur because the static two-dimensional floor analysis, performed to derive the equivalent torsional floor spring stiffness of the portal frame models, can only locate one unique maximum for each response item. This location is constant

regardless of the number of floors of that particular design. However, for the space frame calculations the location of a maximum response can vary between frames with different numbers of floors. These location errors were not so serious considering that the alternate maximum locations found in dynamic space frame analysis always occurred at a point of near maximum response for the two-dimensional static floor analysis.

#### **Comparison to Other Stick Model Results**

As expected, the cantilever beam model was not appropriate to typical moment resisting frame designs. The response of this model was too soft--producing extremely low fundamental frequencies, low shear forces, and high horizontal floor displacements compared to the portal frame model and the space frame model. This model was briefly explored in this research to demonstrate the effect of no floor joint restraint in a stick model.

The shear building model provided a fair representation of response for very low-rise frames (not more than five floors). Compared to space frame calculations, the fundamental frequency was too high in all cases, with error increasing linearly with frame height, from 20 to 200% over a range of 3 to 20 floor frames. Higher mode frequencies for this model were far too high, reducing the fidelity of the approximation. Due to this

predictably stiff response, the computed column shear forces were generally too high and the horizontal floor deflections too low. However, for the Mexico City earthquake (dominated by a narrow frequency band of strong soil motions), this trend was dramatically altered. With this earthquake, frames of 3, 5 or 20 floors experienced column shear forces and horizontal deflections as described above. For frames with 10 and 15 floors, column shear forces in the shear building model were lower and horizontal floor deflections were very much lower than computed for the space frame model.

The Blume (8) model was not directly compared to the calculations of this study. However, conclusions of previous studies allow some casual comparisons. The Blume model is not reported to be effective in modeling the influence of more than the first three or four modes. Artificial rigidity of the floor nodes against rotation does not promote realistic column response. Because the model uses fewer degrees of freedom than the portal frame model, it should be easier to implement. This model does not predict floor member forces and is not applicable to torsion analysis without further modification.

### **PHASE 3 - PORTAL FRAME MODEL WITH TORSION ALLOWED**

A preliminary calculation, with double symmetry in the floor plan (and therefore no self-induced torsion), did not demonstrate any

compounding of errors in the portal frame method, when loaded in an arbitrary horizontal direction. Practically the same relative errors between portal frame and space frame analyses were found for this frame as were previously reported for single floor spring models loaded along an axis of symmetry.

In mono-symmetric frames eccentrically loaded, horizontal floor deflection and net column shear errors relative to space frame analysis did not vary significantly from results summarized above. For all mono-symmetric frames, base torque errors averaged 1.3% with a standard deviation of 5.2%. These statistics are cumulative for both variations of portal frame analysis described in Chapter II and Appendix A. About three times the effort is needed to obtain floor member forces and deflections from the portal frame model with significant torsion. The effort required to determine maximum force locations with torsion generated is much greater than described above for loading in the direction of an axis of symmetry, and the tendency to mis-locate maximums is at least as great.

The asymmetric L-shaped frame was modeled directly by the portal frame technique. Response of this structure was not dominated by a single mode to the extent of previous structures with significant torsional response. For this structure, the first lateral-torsional mode participation ranged from  $M.C._1 = .97$  to

1.0 depending upon the particular distribution of torsional stiffness in the portal frame model (see Appendix D). The second lateral-torsional mode participation ranged from  $M.C._2 = .54$  to 1.0. The first torsional mode participation ranged from by  $M.C._3 = .21$  to  $.28$ . In mono-symmetric torsion examples, only one lateral torsion mode was generated. Participation of this mode was  $M.C._1 = 1.0$  in all cases. For the first torsional mode participation was  $M.C._j = .06$  and  $.24$  for  $5/11E/0500/E-C\{0,1$  &  $1,1\}$  and  $10/11E/0500/E-C\{0,1\}$ . The greater participation of the second and third modes in the L-shaped plan may have contributed to greater sensitivity to error in lateral and torsional stiffness estimates. The results from calculations based on a variable distribution of torsional stiffness in the columns with elevation gave somewhat closer comparisons to the space frame response. This is particularly true for SRSS modal combination. Although some degeneration of accuracy was seen for this rather extreme geometry, the basic fidelity of the stick model appears to remain intact. Closer estimates of space frame response can reasonably be expected with the development of better approximations for the structural stiffness parameters of the model (i.e. the floor springs and distribution of column torsional stiffness).

## **APPLICATION OF THE PORTAL FRAME MODEL TO DESIGN**

### **Overview**

The basic forces and displacements of the dynamic portal frame model provide a good estimate of net floor displacement, shear, and torque. These parameters have intrinsic value in that they summarize the overall distribution of forces in the structure. However, for the designer, interested in forces of individual members, further post-processing of this data is required. Most, but not all, member forces may be extracted with good approximation directly from the response of the dynamic portal frame model. This type of analysis makes use of static analyses performed in assessing the various stiffness estimates required in the dynamic portal frame model, well as other simple static analyses based upon traditional portal frame assumptions. For many tasks the simple estimates thus obtained may be entirely sufficient. To develop a comprehensive design, the basic forces of the dynamic portal frame model may be used as equivalent static shear and torsion loads which may be applied simultaneously with gravity to a space frame model. In this way, forces and deflections of all members so modeled may be assessed.

### **Portal Frame Based Estimates**

For preliminary design estimates, where distributions of horizontal deflection, horizontal shears, and torque about a

vertical axis may be of most interest, the portal frame method may be conveniently applied, provided sufficiently conservative designs are selected. Although the total number of calculations and variety of architectures examined in this study were not sufficient to provide a comprehensive statistical basis for code recommendations, certain conclusions are strongly supported. Applying portal frame analysis to the typical moment resisting frame designs of this study, a reasonable safety margin of two standard deviations beyond the mean is obtained for average story forces and displacements, provided the performance of the selected design is at least 20% conservative. For instance, if five inches of horizontal roof deflection were considered acceptable in the design of a given ten story structure, the portal frame analysis should produce not more than four inches of deflection to insure a roughly 95% probability of meeting this performance criteria. Greater conservatism is indicated for extreme geometries with multiple lateral-torsional and torsional modes as strong participants.

Most element force estimates provide similar safety levels in the moment resisting frames of this study, if the values predicted by the portal frame method are at least 30% conservative. For instance, if a 100 kip-inches bending moment is considered the maximum acceptable for a given beam of the selected design, the portal frame moment for this beam should not exceed 70 kip-

inches to insure a roughly 95% probability of meeting this performance criteria. In general, determination of specific floor member forces by the portal frame method is recommended only for the simplest loading case (soil motion parallel to an axis of symmetry). Even in this case, the designer must consider the strong probability of maximum forces being mis-located. In all cases considered in this study, the location of maximum beam force by the portal frame method was also a location of maximum, or near maximum, force in the corresponding space frame analysis. Although procedures are described in Chapter II for obtaining floor member force estimates where torsion is present, determining maximum forces is much more difficult.

#### Limitations and Simplifications

The portal frame model developed for this study clearly demonstrates the influence of floor system flexibility upon the lateral and torsional stiffness of a moment resisting frame. This stick model has no provision for assessing the effects of axial column flexibility in taller structure. Because of this limitation, the portal frame model is not recommended for analysis of structures exceeding 20 floors (the traditional limit of static planar portal frame analysis).

Calculation of torsional moments in space frame calculations of this study were made by first determining the overall torque at

the center of rigidity of each floor for each mode. The combined modal estimate of torsion for the space frame calculation was then determined with torque identified as a typical parameter for modal combination. This process occurs automatically for the portal frame model since torque is a basic column "force" of the model. If torque in the space frame is assessed after modal combination has occurred, most torsion comparisons between portal frame and space frame analyses are dramatically degraded. The author suggests that the method of determining overall floor torque in this study is consistent with the assumptions of modal combination theory and provides estimates of floor torque and rotation which are consistent with the estimates of floor shear, deflection and other basic design parameters.

Static planar finite element analysis was introduced in Chapter II, as a means of assessing the overall floor stiffness of a general floor system. By this technique the designer is free to model a floor system with any required level of detail. For typical moment-resisting frames with orthogonal beam lines, the equivalent floor system stiffness may be estimated by summing the beam rotational stiffness at column faces. The summation is performed for all beams aligned in the horizontal direction for which the equivalent stiffness is sought. Bending stiffness of the concrete floor slab and torsional resistance of beams are neglected. This approximation is summarized in the development

of eq. 2.8. Comparing this approximation to the more detailed procedure, on average, the equivalent floor system stiffness by the approximate method was 2.8% low with a standard deviation of 5.3% (for all mat aspect ratios and beam selections).

Static three-dimensional finite element analysis of the full structure was introduced in Chapter II, as a means of assessing the torsional stiffness of each floor. By this technique the designer is free to model floor systems and columns with any required level of detail. Portal frame analysis by this technique provided good estimates of torque and can be recommended for general architectures.

For typical moment-resisting frames with orthogonal beam lines, the equivalent combined torsional stiffness of columns may be estimated by summing moments resulting from column shears about the center of rigidity of the floor plan for a typical single floor substructure of the space frame. As above, bending stiffness of the concrete floor slab and torsional resistance of beams are neglected. The development of eq. 2.14 summarizes this approximation. Comparing this approximation to the more detailed full structure static analysis, the equivalent column torsional stiffness was typically 15 to 25% higher than the lowest torsional stiffness of any corresponding floor as computed from the full structure static loading. When this

approximate stiffness was applied uniformly over portions of the structure for which the estimate was valid (same column and floor design), a good average estimate of space frame response was obtained for most structures. The asymmetric frame was an exception to this trend with error of as much as 25% (in base torque).

#### **General Method of Element Force Estimation**

The simple methods of element force estimation described above provide a partial set of needed design parameters. They may be applied to obtain acceptable preliminary estimates, particularly in very low rise frames for which column axial forces may be dominated by gravity. In general, all element forces may be obtained by applying static loads to the center of rigidity of each floor of a space frame. As described in Chapter II, these equivalent static loads are derived in a very simple way from the primary forces obtained from dynamic portal frame analysis. This static space frame analysis is directly analogous to conventional static design procedures, except that the equivalent loading includes torsional loading, as well as shear loading, and is derived specifically for the earthquake spectra and structure under investigation. These equivalent static shear and torsion loads may be applied simultaneously with gravity as desired.

## REFERENCES

1. Aik-Siong Koh, Spanos, P. D., and Roesset, J. M., "Harmonic Rocking of Rigid Block on Flexible Foundation," *Journal of Engineering Mechanics*, ASCE, Vol. 112, No. 11, Nov., 1986, pp. 1165-1180.
2. Ali, Mir M., "Seismic Design of Tall Steel Buildings," Third United States National Conference on Earthquake Engineering, EERI, Vol. 3, 1986, pp. 1743-1751.
3. *American National Standard Minimum Design Loads for Buildings and Other Structures*, American National Standards Institute, Inc., ANSI A58.1-1982.
4. ASCE, "Wind Bracing in Steel Buildings--Final Report of Subcommittee on Steel of the Structural Division," *Transactions of the American Society of Civil Engineers*, Paper No. 2095, Vol. 105, 1940, pp. 1713-1739.
5. Beucke, K., Werkle H., and Waas G., "Nonlinear Soil-Structure Interaction with Base Uplift," *Transactions of the Seventh International Conference on Structural Mechanics in Reactor Technology*, Vol. K(a), Aug., 1983, pp. 107-113.
6. Bielak, J., "Modal Analysis of Building-Soil Interaction." *Journal of Engineering Mechanics Division*, ASCE, Vol. 102, 1976, pp. 771-786.

7. Bielak, J., Sudarbo, H., and Morse, D. V., "Coupled Lateral-Rocking-Torsional Response of Structures with Embedded Foundations Due to SH-Waves," Third United States National Conference on Earthquake Engineering, EERI, Vol. 2, 1986, pp. 811-822.
8. Blume, J. A., "Dynamic Characteristics of Multistory Buildings," *Journal of Structural Division*, ASCE, Vol. 94, No. ST2, Feb., 1968, pp. 377-401.
9. *Building Code Requirements for Reinforced Concrete*, American Concrete Institute, ACI 318-83.
10. Chopra, A. K., and Gutierrez, J. A., "Earthquake Analysis of Structures including Structure-Soil Interaction by a Substructure Method," Transactions of the Fourth International Conference on Structural Mechanics in Reactor Technology, Vol. K(a), K 2/8, Aug., 1977.
11. Cofer, L. J., Kamil, H., Sharpe, R. L., and Hoggatt, D., "The Influence of Uplift and Sliding Nonlinearities on Seismic Response of Small Test Reactor Building," Transactions of the Fifth International Conference on Structural Mechanics in Reactor Technology, Vol. K(a), K 6/4, Aug., 1979, pp. 1-8.
12. Craig, R. R., *Structural Dynamics -- An Introduction to Computer Methods*. John Wiley and Sons, New York, N. Y., 1981.
13. Cruz and Chopra, "Elastic Earthquake Response of Building Frames," *Journal of Structural Engineering*, ASCE, Vol. 112, No. 3, Mar., 1986, pp. 443-459.

14. Dobry, R., and Gazetas, G., "Dynamic Response of Arbitrarily Shaped Foundations," *Journal of Geotechnical Engineering*, Vol. 112, No. 2, Feb., 1986, pp. 109-135.
15. Dominguez, J., "Dynamic Stiffness of Rectangular Foundations," National Science Foundation, Publication No. R78-20, Aug., 1978.
16. Fukuzawa, R., Chiba, O., Hatori T., and Tohdo M., "Rocking Vibration of Nuclear Power Plant Considering Up-lift and Yield of Supporting Soil," Transactions of the Sixth International Conference on Structural Mechanics in Reactor Technology, Vol. K(a), K 3/7, Aug., 1981.
17. Gaitanaros, A. P., and Karabalis, D. L., "Dynamic Analysis of 3-D Flexible Embedded Foundations By A Frequency Domain BEM-FEM," *Earthquake Engineering and Structural Dynamics*, Vol. 16, No. 5, Jul., 1988, pp. 653-674.
18. Ghaffar-Zadeh, M., and Chapel, F., "Frequency-Independent Impedances of Soil-Structure Systems in Horizontal and Rocking Modes," *Earthquake Engineering and Structural Dynamics*, Vol. 1, No. 4, Jul., 1983, pp. 523-540.
19. Housner, G. W., "Behavior of Structures During Earthquakes," *Journal of Engineering Mechanics Division*, ASCE, Vol 88, 1959, pp. 109-129.

20. Ichikawa, T., Hayashi, Y., and Nakai, S., "Earthquake Response Analysis of Embedded Reactor Building Considering Soil-Structure Separation and Nonlinearity of Soil," Transactions of the Ninth International Conference on Structural Mechanics in Reactor Technology, Vol. K1, Aug., 1987, pp. 323-328.
21. Jennings, P.C., and Bielak, J., "Dynamics of Building-Soil Interaction," *Bulletin of the Seismological Society of America*, Vol 63, 1973, pp. 9-48.
22. Kausel, E., Whitman, R. V., Murray, J. P., and Elsabee, F., "The Spring Method for Embedded Foundations," *Nuclear Engineering and Design*, Vol 48, 1978, pp. 377-392.
23. Kobatake, M., Hirashima, S., Narikawa, M., and Tanaka, H., "Influence of Flexible Foundation Slab on Seismic Response of Nuclear Reactor Building," Transactions of the Eighth International Conference on Structural Mechanics in Reactor Technology, Vol. K(a), Aug., 1985, pp. 299-304.
24. Kohnke, P. C. (Editor), *Ansys Engineering Analysis System -- Theoretical Manual*, Swanson Analysis Systems, Inc., Houston, Pa., 1987.
25. Kuen-Yaw Shye and Robinson, A. R., "Dynamic Soil-Structure Interaction -- Technical Research Report," University of Illinois, Urbana, Il., SRSN 484, Sep., 1980.
26. Lin, A. N., and Jennings, P. C., "Effect of Embedment on Foundation-Soil Impedances," *Journal of Engineering Mechanics*, Vol. 110, No. 7, Jul., 1984, pp. 1060-1075.

27. Luco, J. E., and Westmann, "Dynamic Response of Circular Footings," *Journal of Engineering Mechanics*, ASCE, Vol. 97, EM5, 1971, pp.1381-1395.
28. Lysmer, J., Udaka, T., Tsai, C.-F., and Seed, H. B., "Flush--A Computer Program for Approximate 3-D Analysis of Soil-Structure Interaction Problems," College of Engineering, University of California, Berkeley, Rept. No. EERC 75-30, Nov., 1975.
29. Meek, J. W., and Veletsos, A. S., "Simple Models For Foundations in Lateral and Rocking Motion," Proc. 5th World Conference on Earthquake Engineering, Rome, Vol. 2, 1973, pp. 2610-2613.
30. Morrow, W. M., "A Comparison of Responses from Different Seismic Soil-Structure Interaction Analyses," Transactions of the Sixth International Conference on Structural Mechanics in Reactor Technology, Vol. K(a), K 4/8, Aug., 1981.
31. Muto, K., Kobayashi, T., Motohashi, S., Mizuno, N., Moribe, I., Sugiyama, N., and Suzuki, T., "Nonlinear Rocking Analysis of Nuclear Reactor Building Simultaneously Subjected to Horizontal and Vertical Earthquake Motions," Transactions of the Seventh International Conference on Structural Mechanics in Reactor Technology, Vol. K(b), Aug., 1983, pp. 123-130.

32. Nelson, I., "Two Stage Approach to Dynamic Soil Structure Interaction," Transactions of the Sixth International Conference on Structural Mechanics in Reactor Technology, Vol. K(a), K 3/3, Aug., 1981.
33. Niwa, A., Katayama I., and Penzien J., "A Quantitative Evaluation of Radiation Damping in Soil-Structure Interaction Effects," Transactions of the Seventh International Conference on Structural Mechanics in Reactor Technology, Vol. K(a), K 8/9, Aug., 1983, pp. 61-71.
34. Ostadan, F., Tseng, W. S., and Lilhanand K., "Application of the Flexible Volume Method to Soil-Structure Interaction Analysis of Flexible and Embedded Foundations," Transactions of the Ninth International Conference on Structural Mechanics in Reactor Technology, Vol. K1, Aug., 1987, pp. 329-336.
35. Psycharis, I. N., and Jennings, P.C., "Dynamic Behavior of Rocking Structures Allowed to Uplift," *Earthquake Engineering and Structural Dynamics*, Vol. 11, No. 1, Jan., 1983, pp. 57-76.
36. Riggs, H. R., and Waas, G., "Influence of Foundation Flexibility on Soil-Structure Interaction," *Earthquake Engineering and Structural Dynamics*, Vol. 13, No. 5, Sep., 1985, pp. 597-615.
37. Seed, H. B., and Lysmer J., "Soil-Structure Interaction Analysis by Finite Element Methods State-of-the-Art," Transactions of the Fourth International Conference on Structural Mechanics in Reactor Technology, Vol. K(a), K 2/1, Aug., 1977.

38. Seed, H. B., Wong, R. T., Idriss, I. M., and Tokimatsu, K., "Moduli and Damping Factors for Dynamic Analyses of Cohesionless Soils," Report No. UBC/EERC-84/14, Sep., 1984.
39. Sivakumaran, K. S., and Balendra, T., "Seismic Response of Multi-Storey Buildings Including Foundation Interaction and P- $\Delta$  Effects," *Engineering Structures*, Vol. 9, Oct., 1987, pp. 277-284.
40. *Specification for the Design, Fabrication and Erection of Structural Steel for Buildings*, American Institute of Steel Construction, Nov., 1978.
41. Takaki, M., Kawamura, S., and Yamada, M., "Three Dimensional Uplift Response Analysis of a Nuclear Reactor Building," Transactions of the Eighth International Conference on Structural Mechanics in Reactor Technology, Vol. K(a), Aug., 1985, pp. 203-208.
42. Takemori, T., Kuwabara, Y., Ogivara, Y., and Suwabe A., "Comparison of Soil-Structure Interaction By Different Ground Models," Transactions of the Fifth International Conference on Structural Mechanics in Reactor Technology, Vol. K(a), K 5/5, Aug., 1979, pp. 1-8.
43. Todorovska, M. I., Lee, V. W., and Trifunac, M. D., "Investigation of Earthquake Response of Long Buildings," University of Southern California, Los Angeles, Ca., CE 88-02, Feb., 1988.

44. Tohma, J., Ohtomo, K., Kurimoto, M., and Arii, K., "Experimental Study on Dynamic Soil-Structure Interaction," Transactions of the Fifth International Conference on Structural Mechanics in Reactor Technology, Vol. K(a), Aug., 1985, pp. 287-292.
45. Torkamani, M. A. M., and Huang, J. T., "Consideration of Floor Flexibility in Dynamic Analysis of High-Rise Buildings," Third United States National Conference on Earthquake Engineering, EERI, Vol. 2, 1986, pp. 835-846.
46. Tsai, N. C., "A Review of Experimental Soil-Structure Interaction Damping," Transactions of the Sixth International Conference on Structural Mechanics in Reactor Technology, Vol. K(a), K 3/10, Aug., 1981.
47. Tseng, W. S., and Liou D. D., "Simplified Methods for Predicting Seismic Basemat Uplift of Nuclear Power Plant Structures," Transactions of the Sixth International Conference on Structural Mechanics in Reactor Technology, Vol. K(a), K 3/6, Aug., 1981.
48. Tso, W. K., and Meng V., "Torsional Provisions in Building Codes," *Canadian Journal of Civil Engineering*, Vol. 9, 1982, pp. 38-46.
49. Vaughan, D. K., and Isenberg, J., "Nonlinear Soil-Structure Interaction by Explicit Integration Methods," Transactions of the Sixth International Conference on Structural Mechanics in Reactor Technology, Vol. K(a), K 3/9, Aug., 1981.

50. Vaughan, D. K., and Isenberg, J., "Evaluation of Radiation Damping Using 3-D Finite Element Models," Transactions of the Seventh International Conference on Structural Mechanics in Reactor Technology, Vol. K(a), Aug., 1983, pp. 179-186.
51. Vaughan, D. K., Wojcik, G. L., and Isenberg, J., "Influence of Boundary Approximations on Soil-Structure Interaction Response," Transactions of the Eighth International Conference on Structural Mechanics in Reactor Technology, Vol. K(a), Aug., 1985, pp. 209-214.
52. Veletsos, A. S., and Meek, J. W., "Dynamic Behavior of Building Foundation Systems," *Earthquake Engineering and Structural Dynamics*, Vol. 3, No. 2, Oct.-Dec., 1974, pp. 121-138.
53. Veletsos, A. S., and Verbic, B., "Basic Response Function For Elastic Foundations," *Journal of the Engineering Mechanics Division*, ASCE, Vol. 100, 1974, pp. 189-202.
54. Waas G., and Weber, W., "Soil Structure Interaction Analyses by Different Methods," Transactions of the Fifth International Conference on Structural Mechanics in Reactor Technology, Vol. K(a), K 5/8, Aug., 1979, pp. 1.
55. Weissman, K., "A Study of Radiation Damping and Soil-Structure Interaction Effects in the Centrifuge," Technical Report NCEER-88-0013, National Center for Earthquake Engineering Research, May, 1988.

56. Whittaker, W. L., and Christiano, P., "Dynamic Response of Plate on Elastic Half-Space," *Journal of the Engineering Mechanics Division*, ASCE, Vol.108, No. EM1, Feb., 1982, pp. 133-153.
57. Wolf, J. P., "Approximate Soil-Structure Interaction with Separation of Base Mat from Soil (Lifting-Off)," Transactions of the Third International Conference on Structural Mechanics in Reactor Technology, Vol. K, K 3/6, Sep., 1975.
58. Wolf, J. P., *Dynamic Soil-Structure Interaction*, Prentice-Hall, Inc., Englewood Cliffs, N. J., 1985.
59. Wong, H. L., and Luco, J. E., "Dynamic Response of Rigid Foundations of Arbitrary Shape," *Earthquake Engineering and Structural Dynamics*, Vol. 4, No. 6, Oct.-Dec., 1976, pp. 579-587.
60. Yoder, E. J., and Witczak, M.W., *Principles of Pavement Design*, John Wiley and Sons, Inc., New York, N. Y., 1975.
61. Zinn, R., and Stangenberg, F., "Base Mat Uplift Effects on the Seismic Response of A Rectangular Nuclear Building," Transactions of the Seventh International Conference on Structural Mechanics in Reactor Technology, Vol. K(a), Aug., 1983, pp. 115-122.

## APPENDIX A

### NET FLOOR DISPLACEMENTS AND FORCES

This appendix summarizes net displacements and forces of interest for all calculations on soft soil ( $v_s = 500$  fps). For frames loaded along an axis of symmetry, total horizontal floor deflection at the center of rigidity and column shears are displayed at five floor intervals or less. For other load cases, these comparisons are supplemented by similar displays of total column torques about the static center of rigidity of the floor. Displacements correspond directly with floor levels specified along the vertical axis. For Figure A.45, two displacements are identified at floor five due to relative displacement of the centers of rigidity for columns above and below that floor (due to floor rotation). Shears and torques correspond with columns immediately below floor levels specified along the vertical axis.

Legend notes:

**3-D** implies space frame analysis on flexible mat foundation for Figures A.1 to A.32. **3-D** implies space frame analysis on rigid mat foundation for Figures A.33 to A.53. **Portal frame** and **Shear building** implies stick models detailed in Chapter II. For mono-symmetric floor plans, **Portal frame (1)** corresponds to  $J_{eff}$  based on the one-story space frame calculation depicted in Figure 2.8, but varying with elevation in proportion to a full structure static analysis, see Chapter II. **Portal frame (2)** corresponds to  $J_{eff}$  based on uniform vertical distribution of the eq. 2.15 estimate.

Series nomenclature: (N/X:Z/kkkk/E-Q{x,z})

**N** equals number of floors

**X:Z** equals floor plan ratio of dimensions in x and z directions

**kkkk** equals soil shear wave velocity in feet/sec

**E-Q** implies earthquake (E-C for El Centro and M-C for Mexico City)

**{x,z}** vector identifying the horizontal direction of earthquake loading

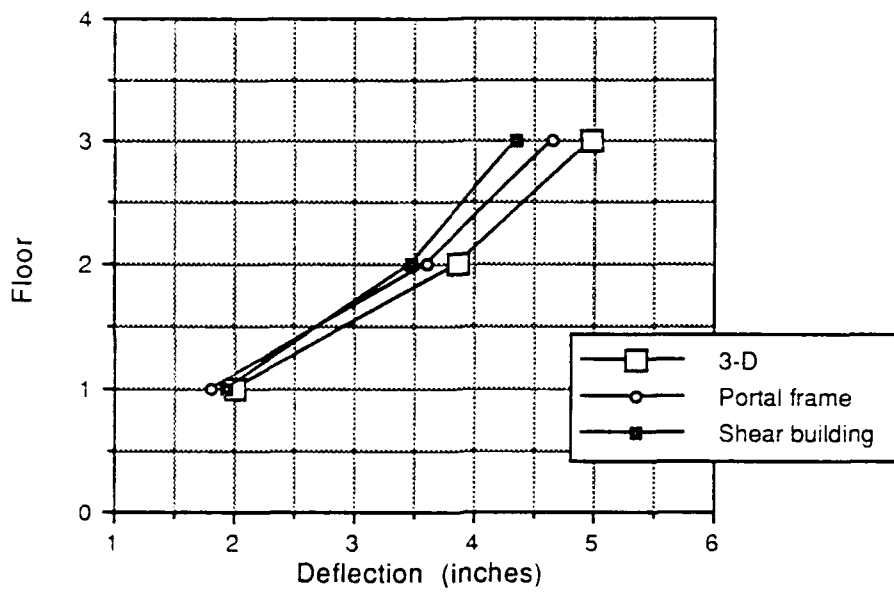


Figure A.1 Horizontal floor deflection (series 3/1:1/0500/E-C)

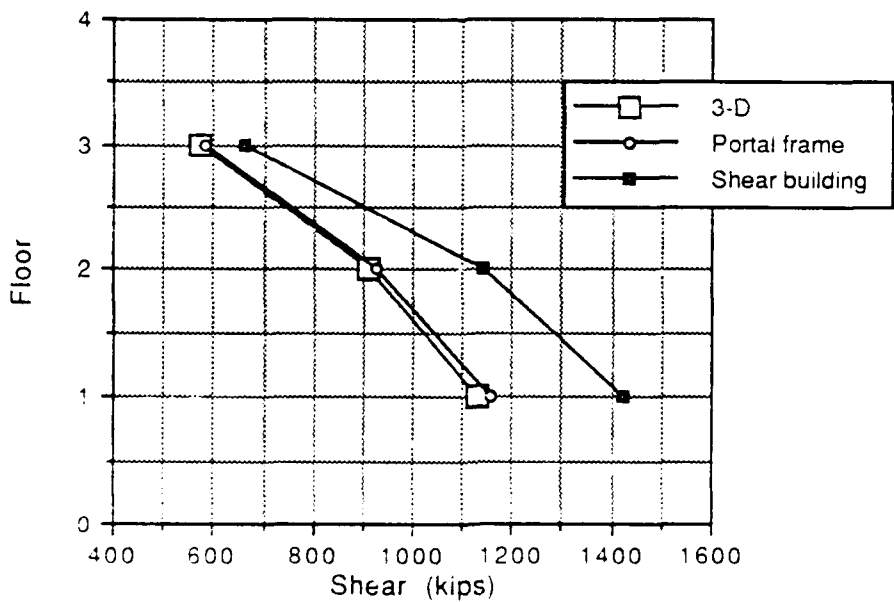


Figure A.2 Total column shear (series 3/1:1/0500/E-C)

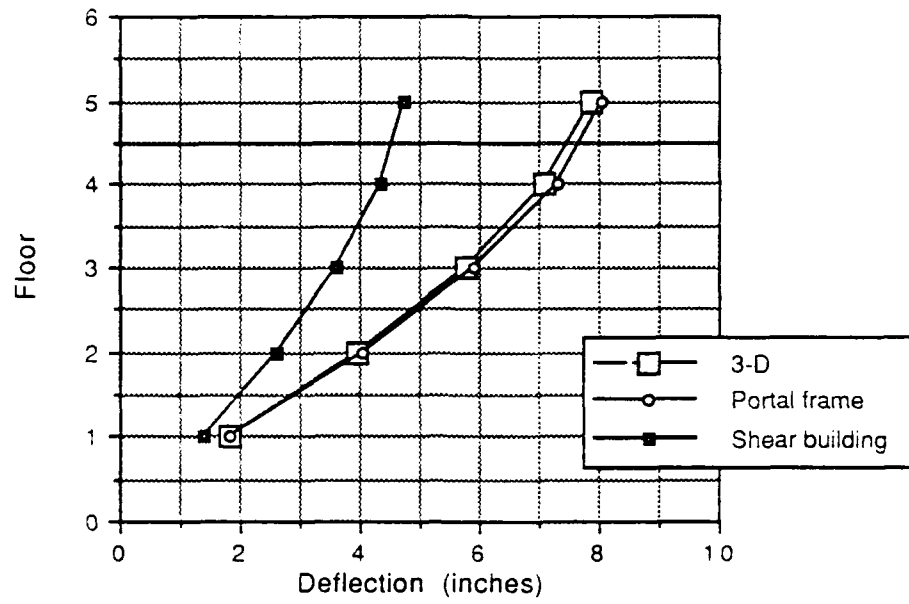


Figure A.3 Horizontal floor deflection  
(series 5/1:1/0500/E-C)

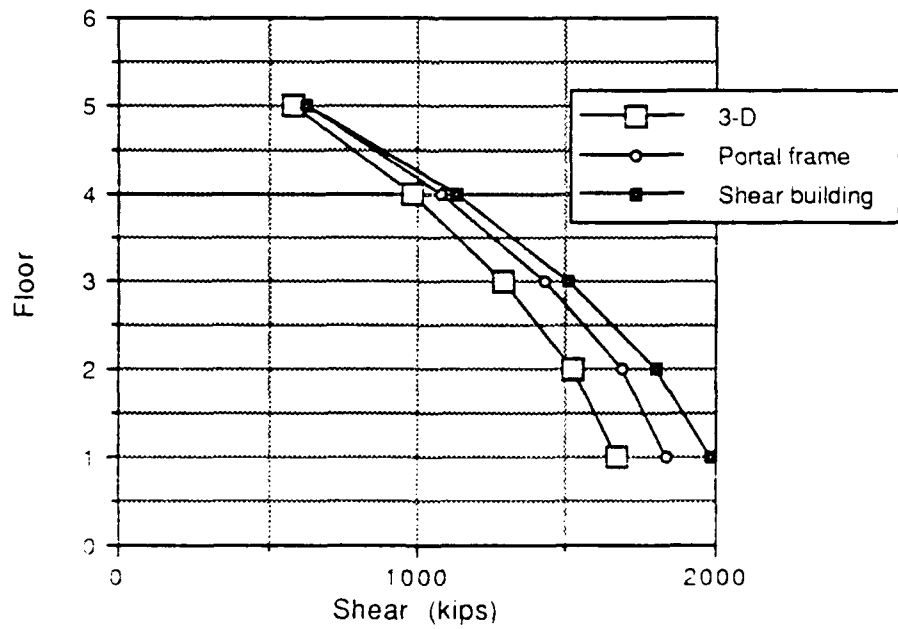


Figure A.4 Total column shear  
(series 5/1:1/0500/E-C)

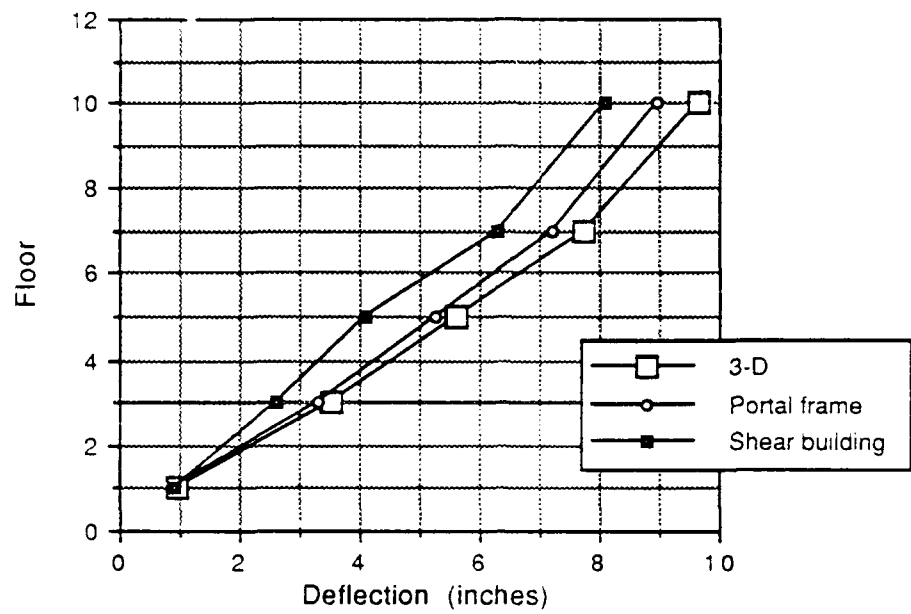


Figure A.5 Horizontal floor deflection (series 10/1:1/0500/E-C)

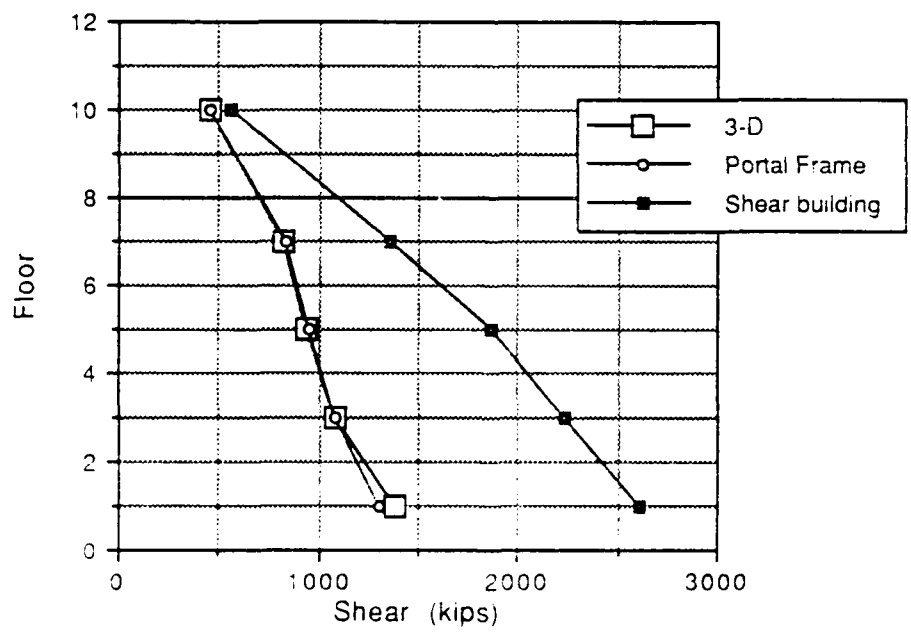


Figure A.6 Total column shear (series 10/1:1/0500/E-C)

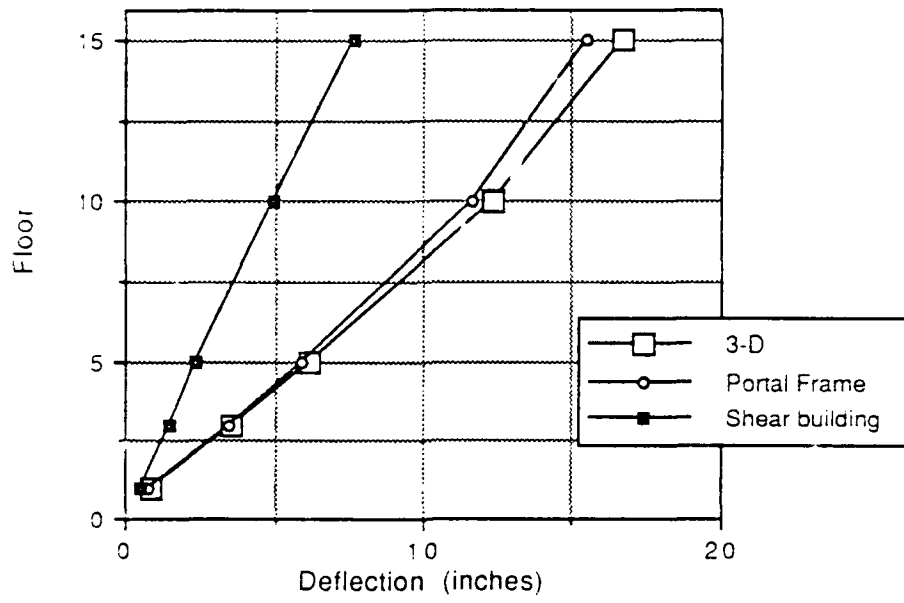


Figure A.7 Horizontal floor deflection (series 15/1:1/0500/E-C)

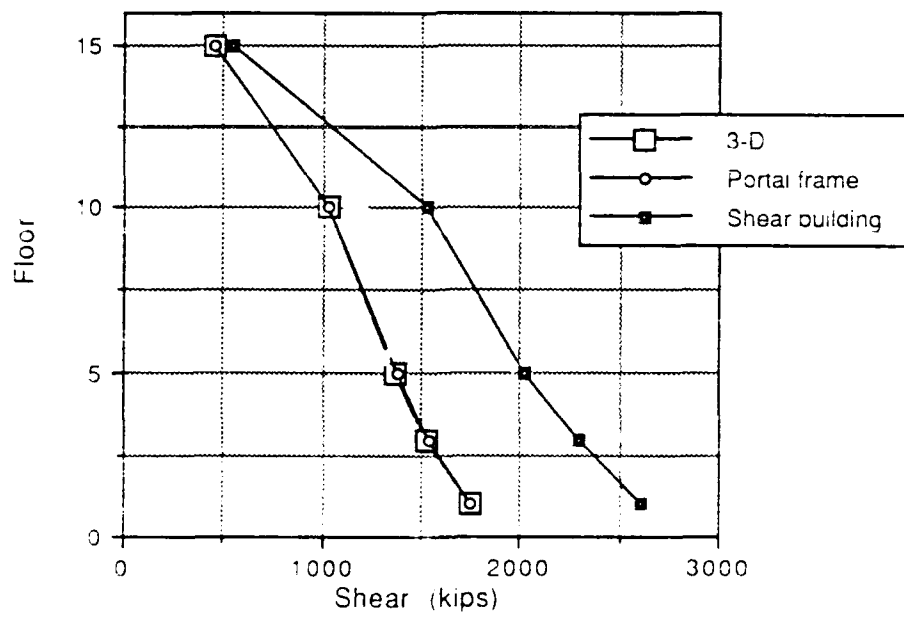


Figure A.8 Total column shear (series 15/1:1/0500/E-C)

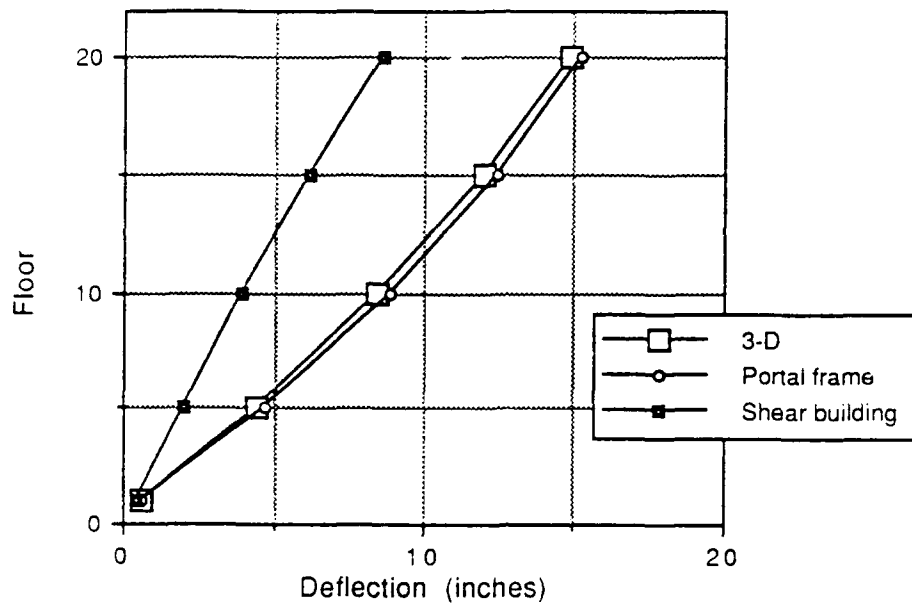


Figure A.9 Horizontal floor deflection  
(series 20/1:1/0500/E-C)

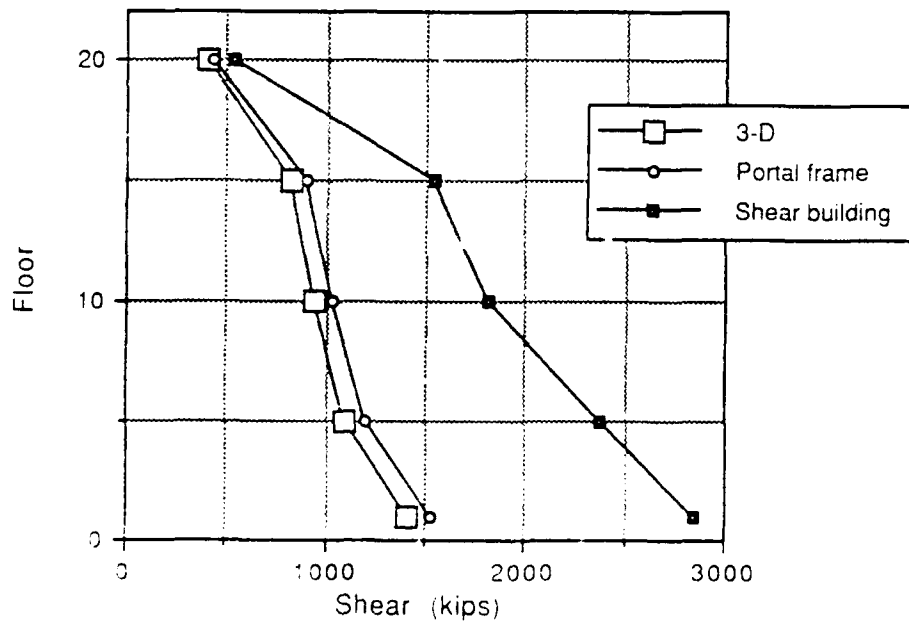


Figure A.10 Total column shear  
(series 20/1:1/0500/E-C)

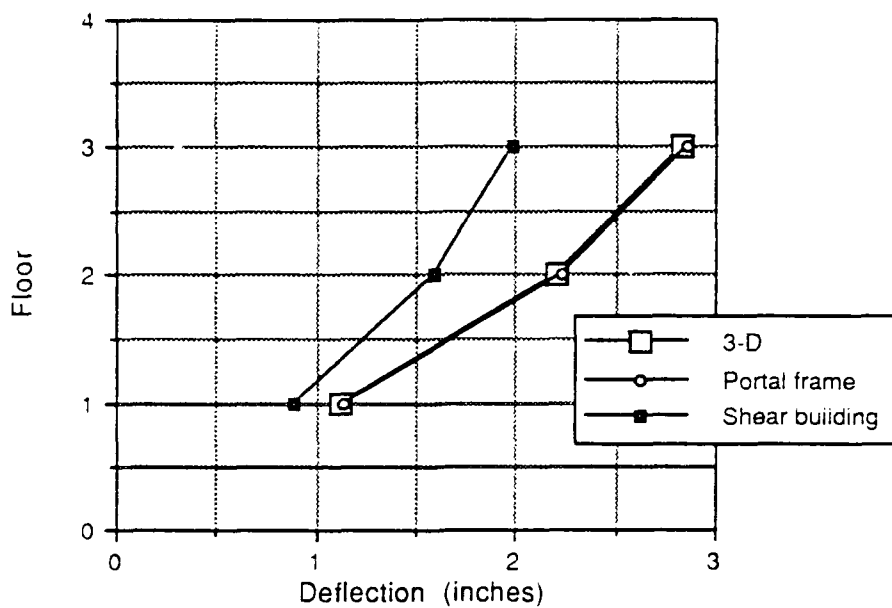


Figure A.11 Horizontal floor deflection  
(series 3/1:1/0500/M-C)

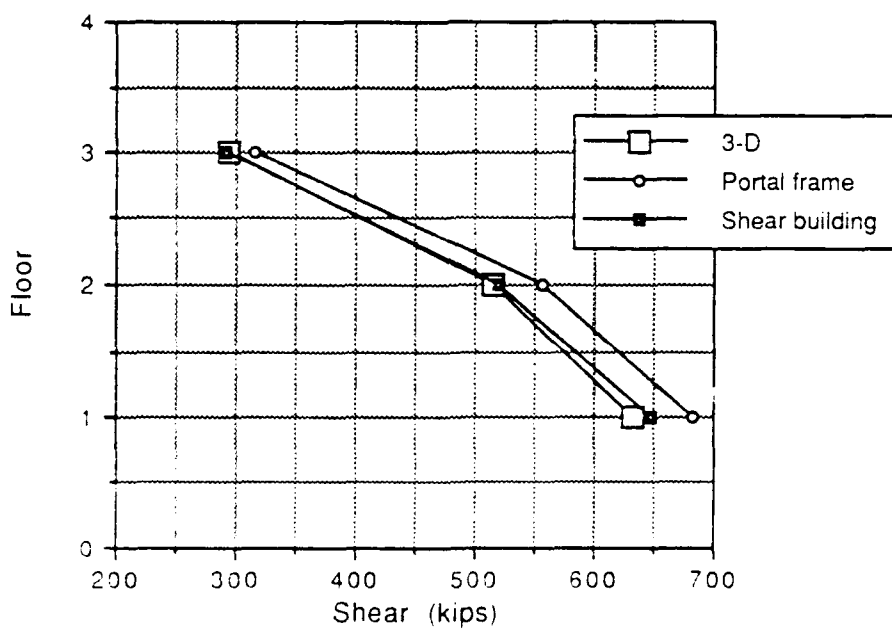


Figure A.12 Total column shear  
(series 3/1:1/0500/M-C)

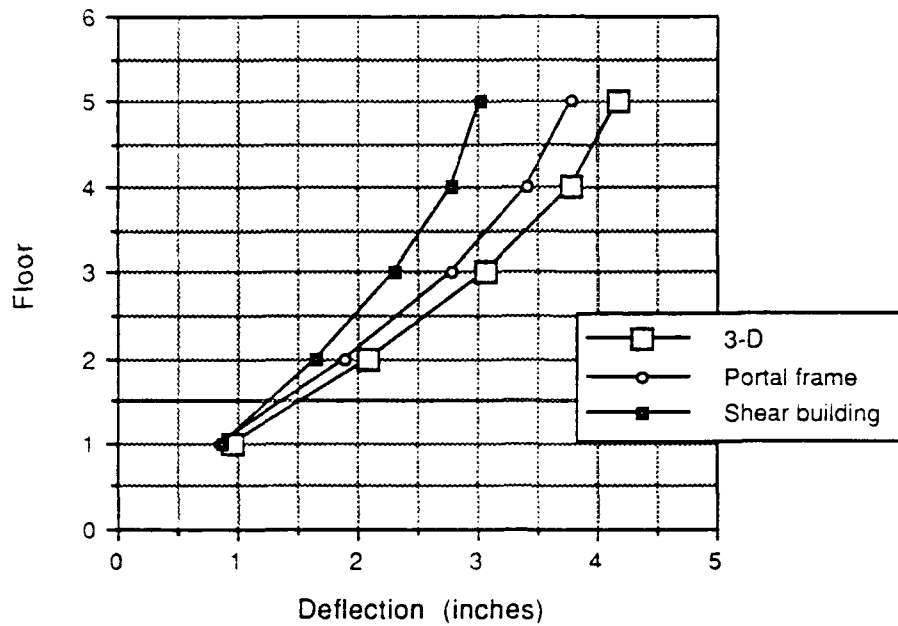


Figure A.13 Horizontal floor deflection (series 5/1:1/0500/M-C)

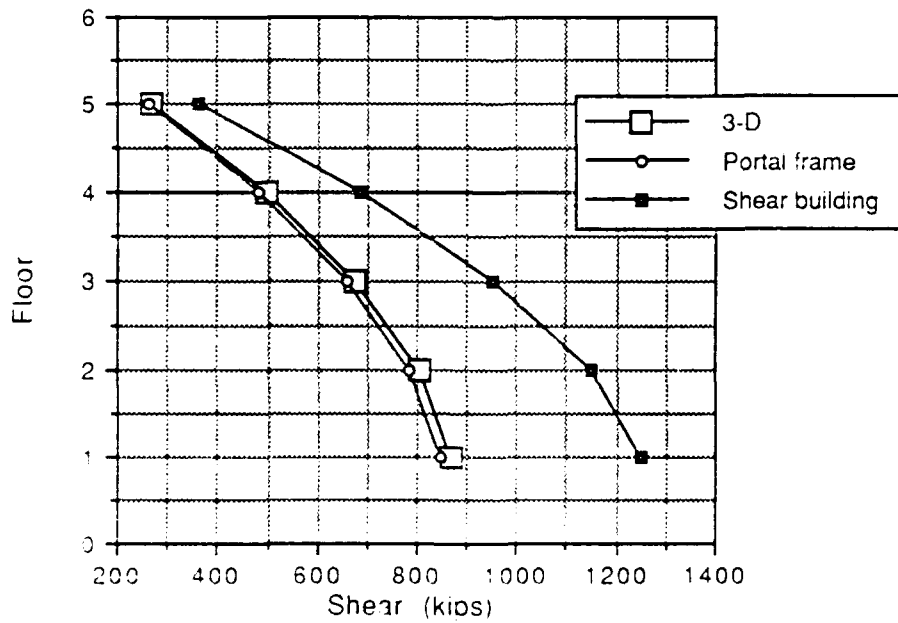


Figure A.14 Total column shear (series 5/1:1/0500/M-C)

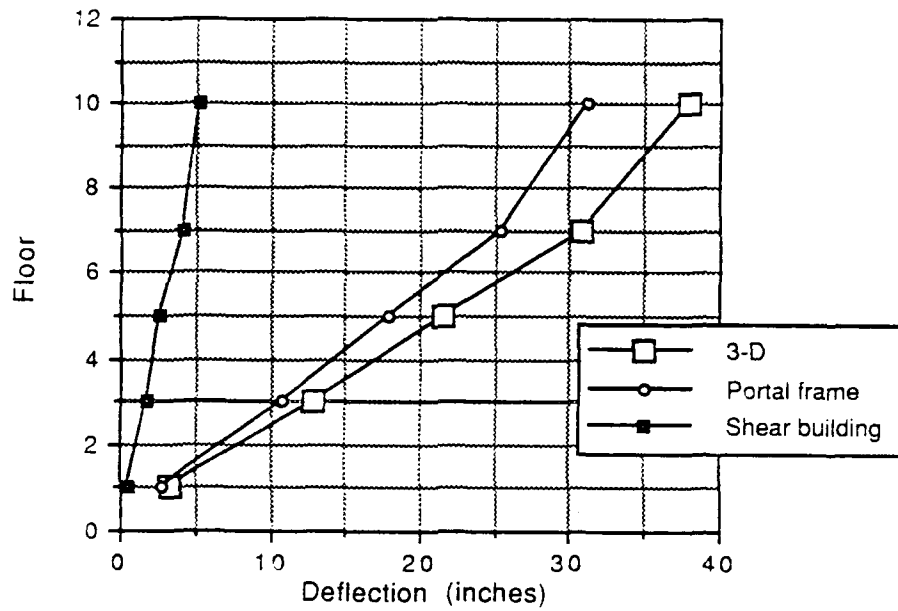


Figure A.15 Horizontal floor deflection (series 10/1:1/0500/M-C)

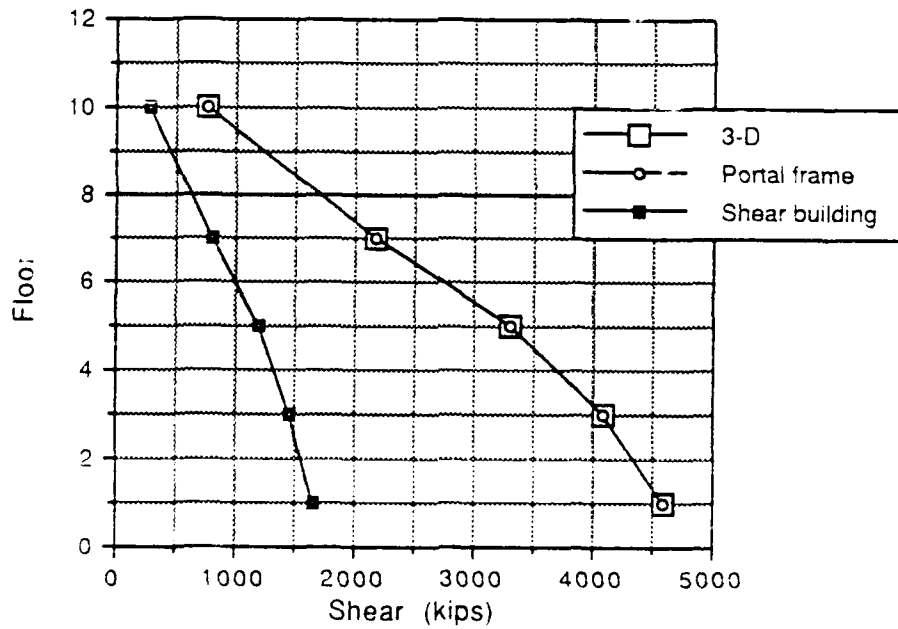


Figure A.16 Total column shear (series 10/1:1/0500/M-C)

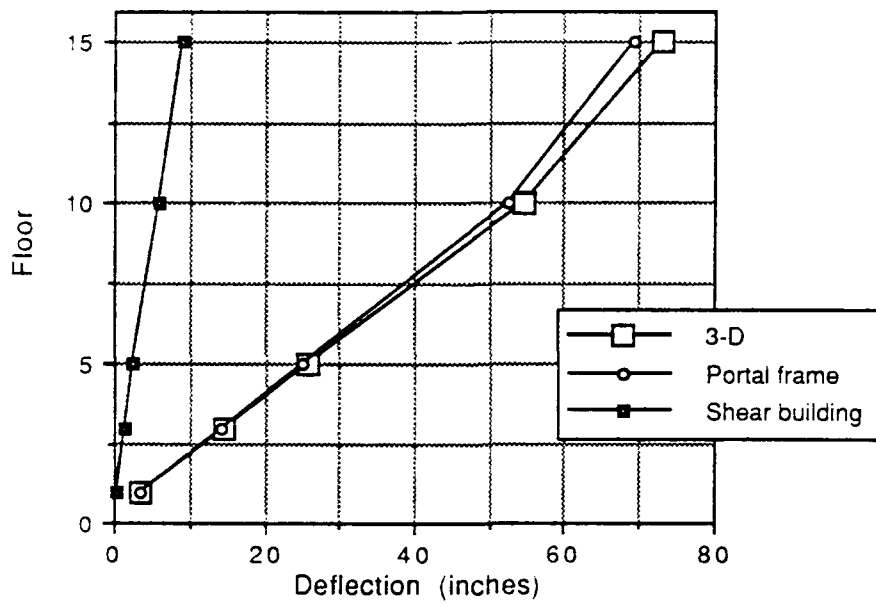


Figure A.17 Horizontal floor deflection  
(series 15/1:1/0500/M-C)

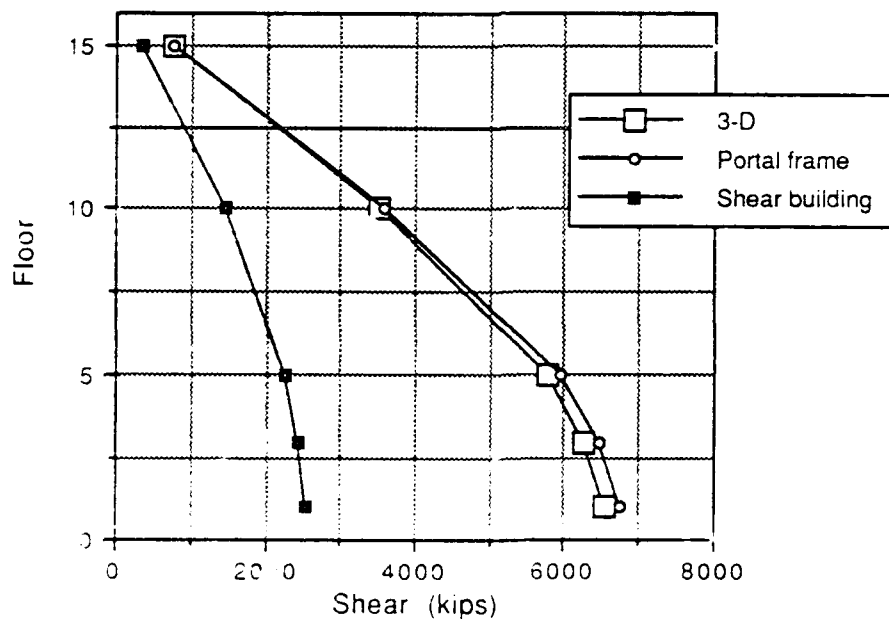


Figure A.18 Total column shear  
(series 15/1:1/0500/M-C)

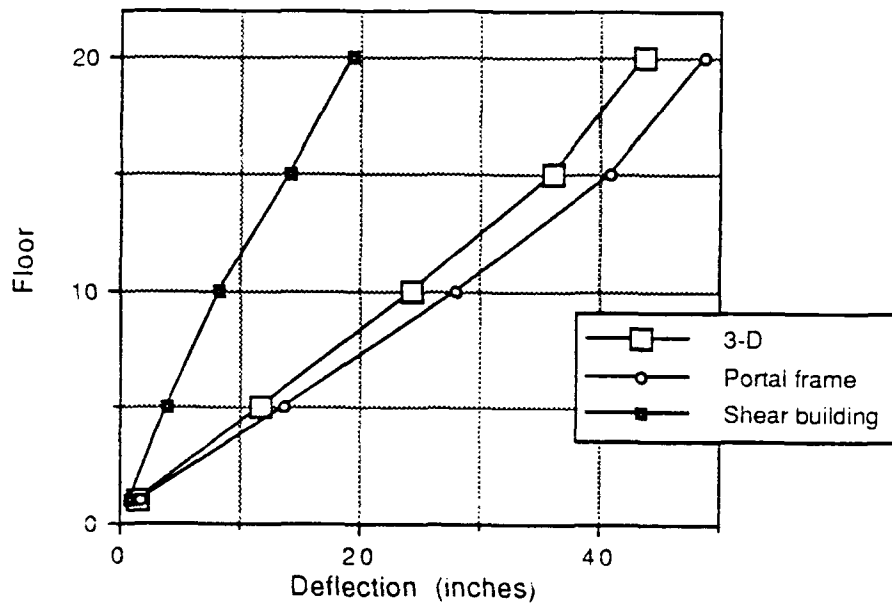


Figure A.19 Horizontal floor deflection (series 20/1:1/0500/M-C)

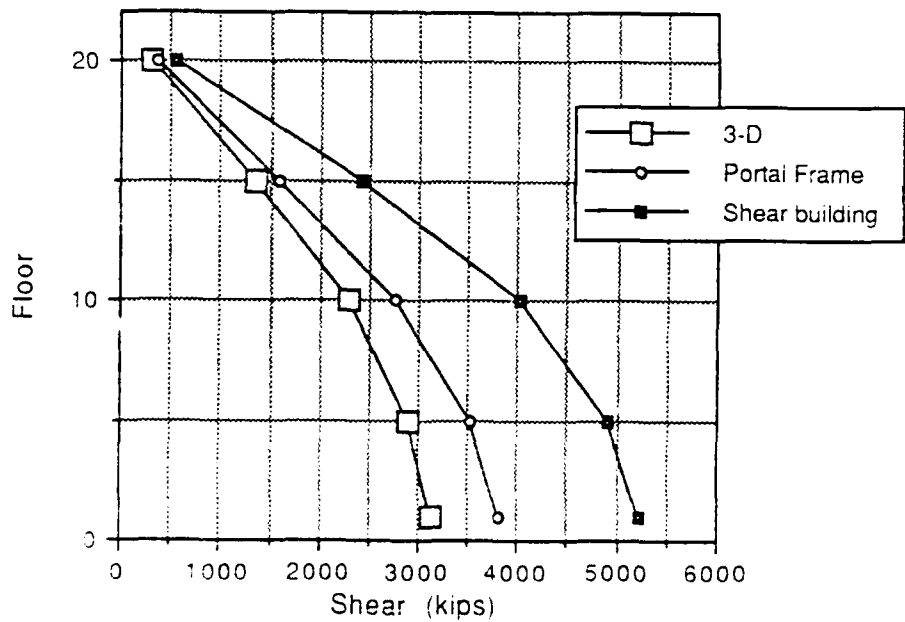


Figure A.20 Total column shear (series 20/1:1/0500/M-C)

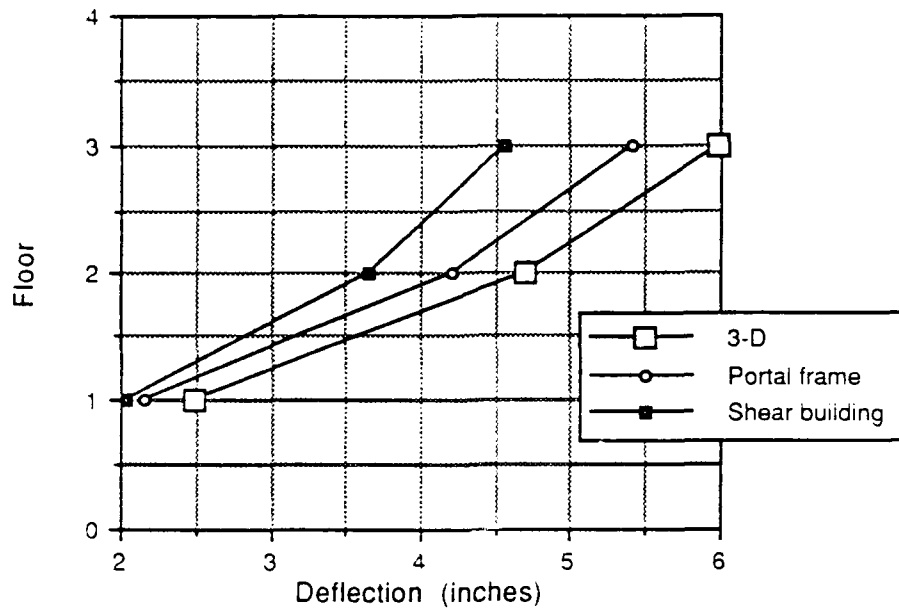


Figure A.21 Horizontal floor deflection  
(series 3/1:1.75/0500/E-C)

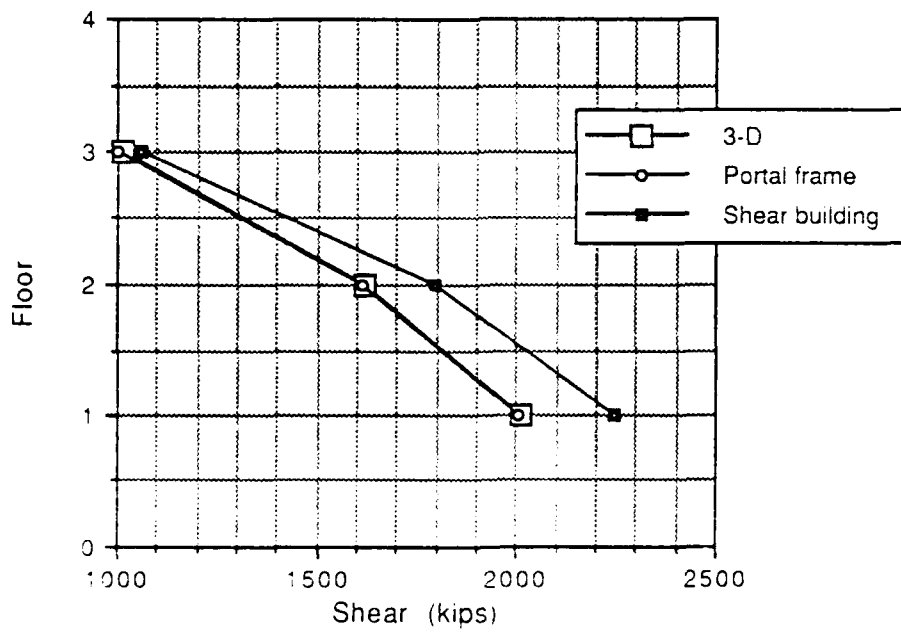


Figure A.22 Total column shear  
(series 3/1:1.75/0500/E-C)

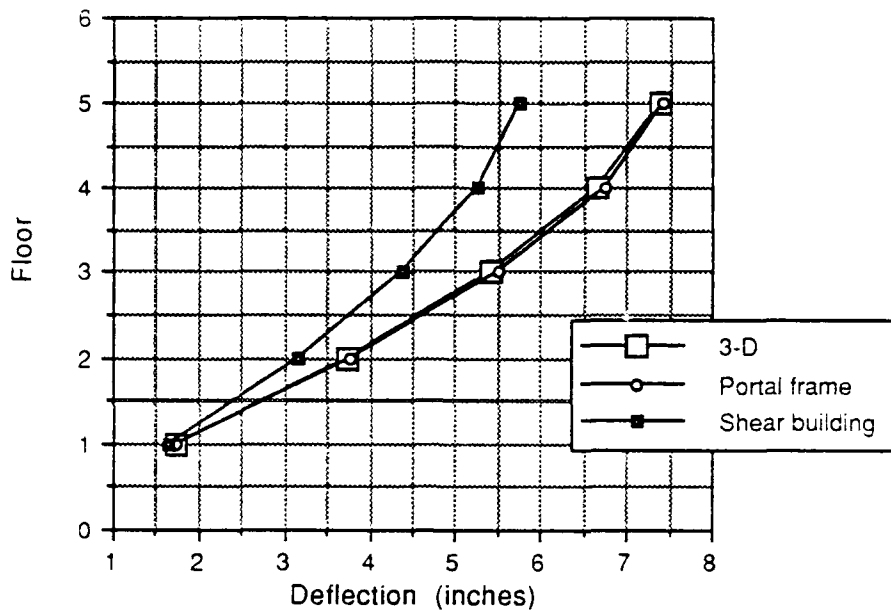


Figure A.23 Horizontal floor deflection (series 5/1:1.75/0500/E-C)

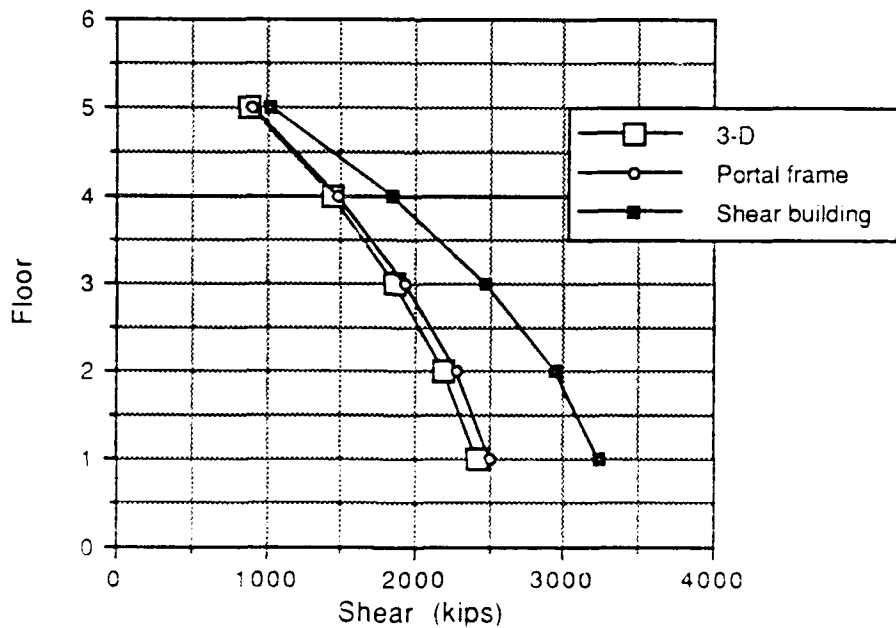


Figure A.24 Total column shear (series 5/1:1.75/0500/E-C)

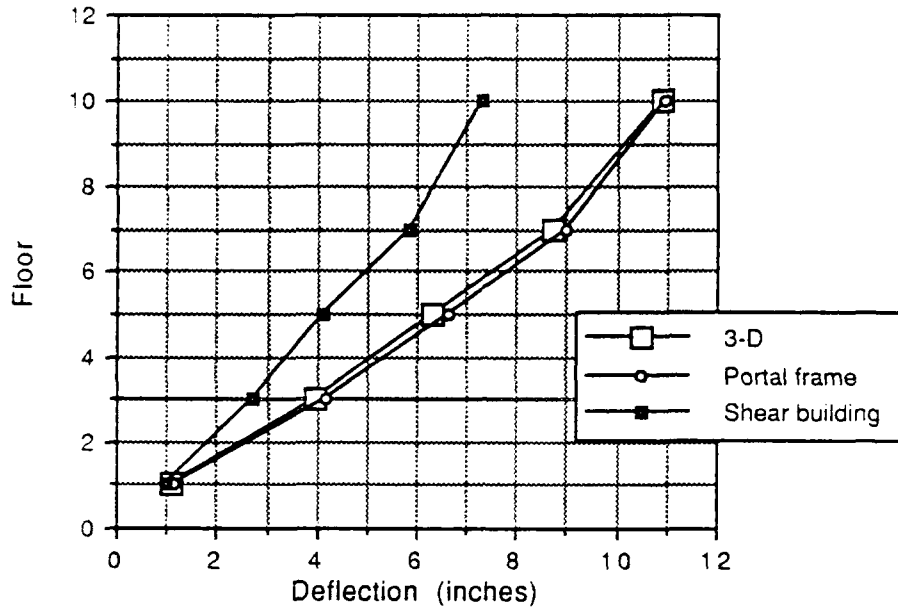


Figure A.25 Horizontal floor deflection (series 10/1:1.75/0500/E-C)

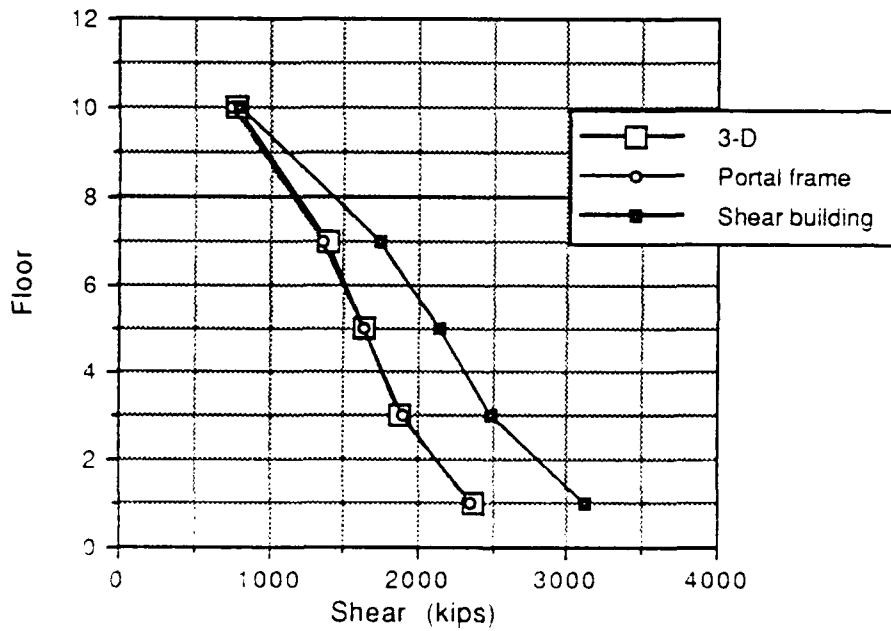


Figure A.26 Total column shear (series 10/1:1.75/0500/E-C)

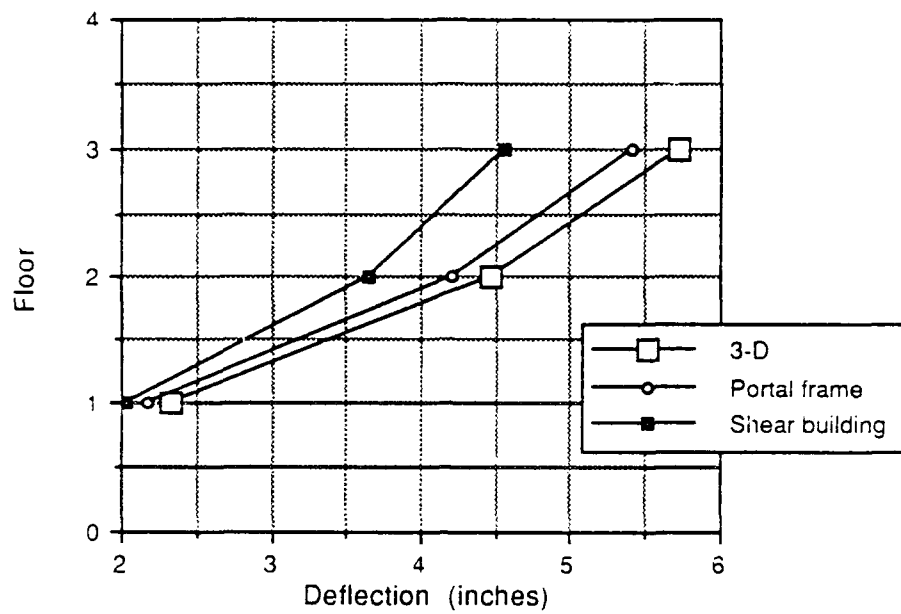


Figure A.27 Horizontal floor deflection  
(series 3/1.75:1/0500/E-C)

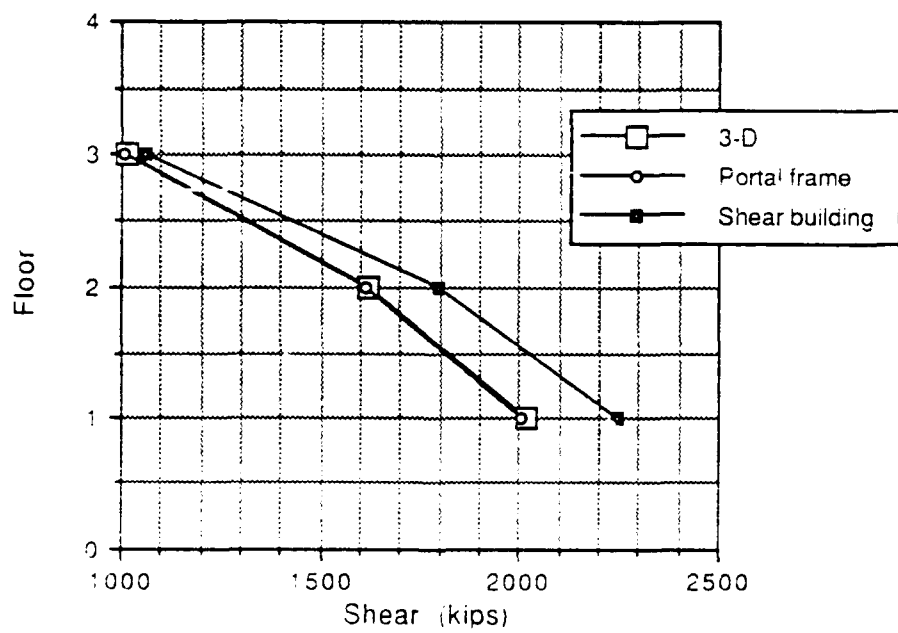


Figure A.28 Total column shear  
(series 3/1.75:1/0500/E-C)

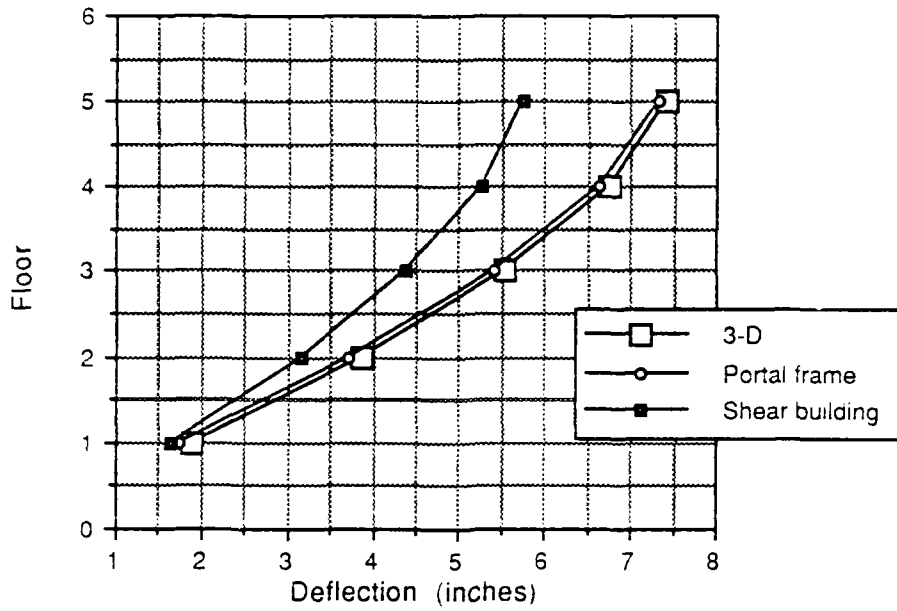


Figure A.29 Horizontal floor deflection (series 5/1.75:1/0500/E-C)

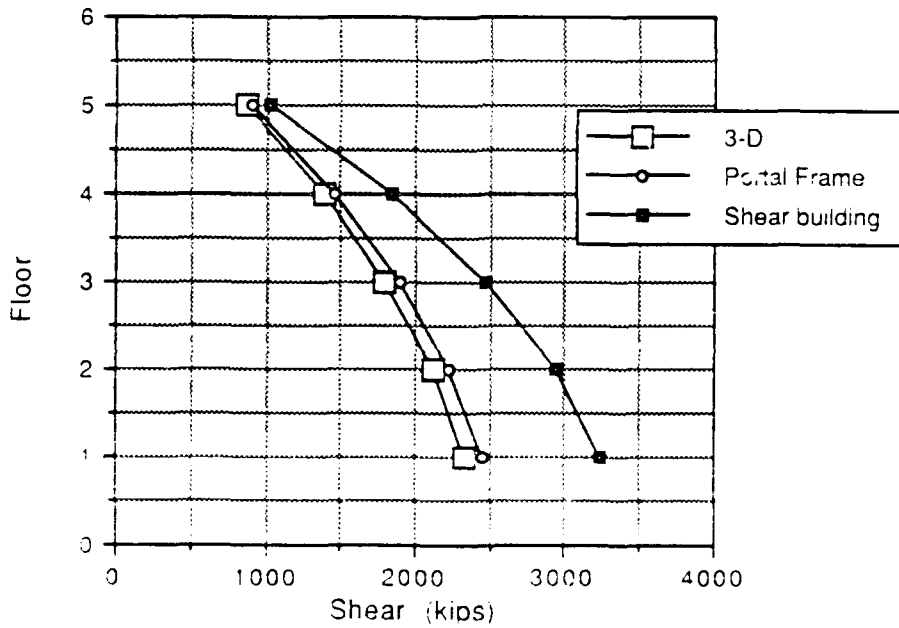


Figure A.30 Total column shear (series 5/1.75:1/0500/E-C)

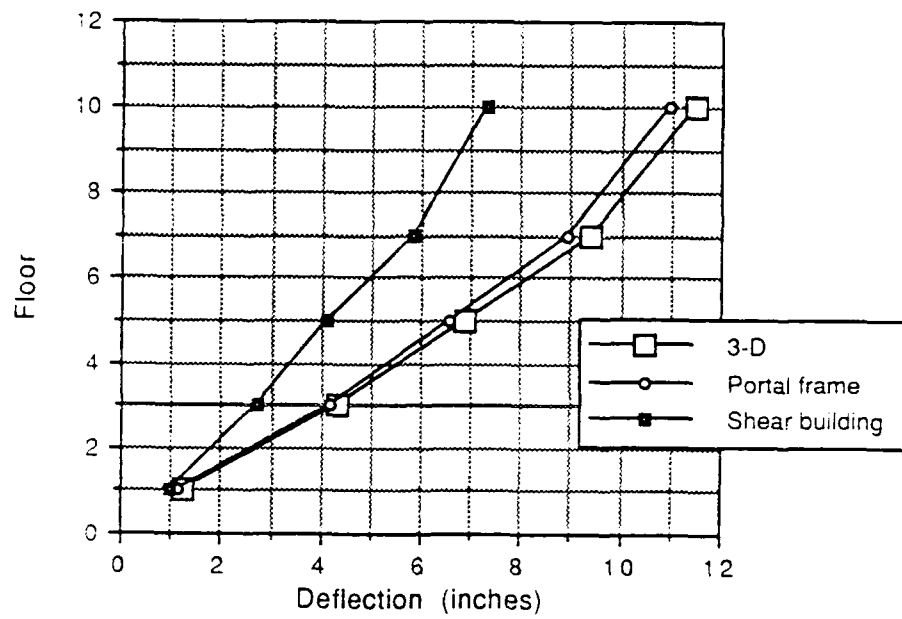


Figure A.31 Horizontal floor deflection  
(series 10/1.75:1/0500/E-C)

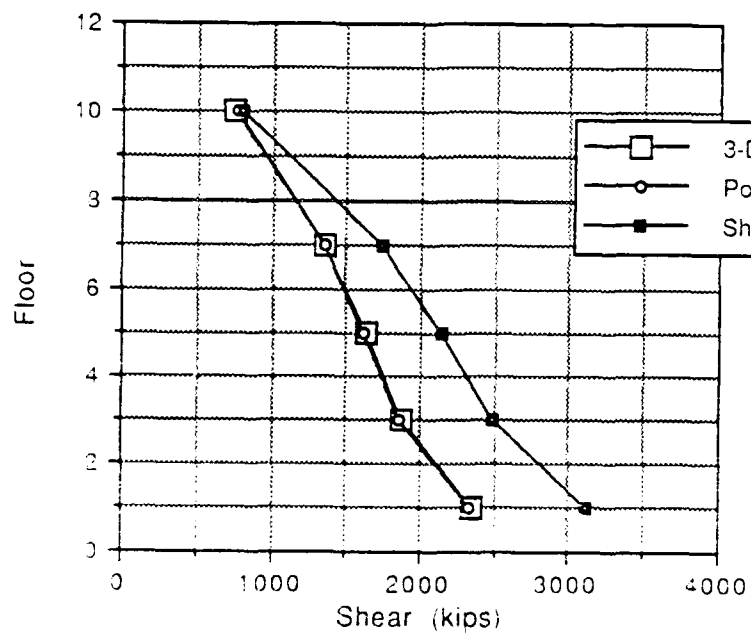


Figure A.32 Total column shear  
(series 10/1.75:1/0500/E-C)

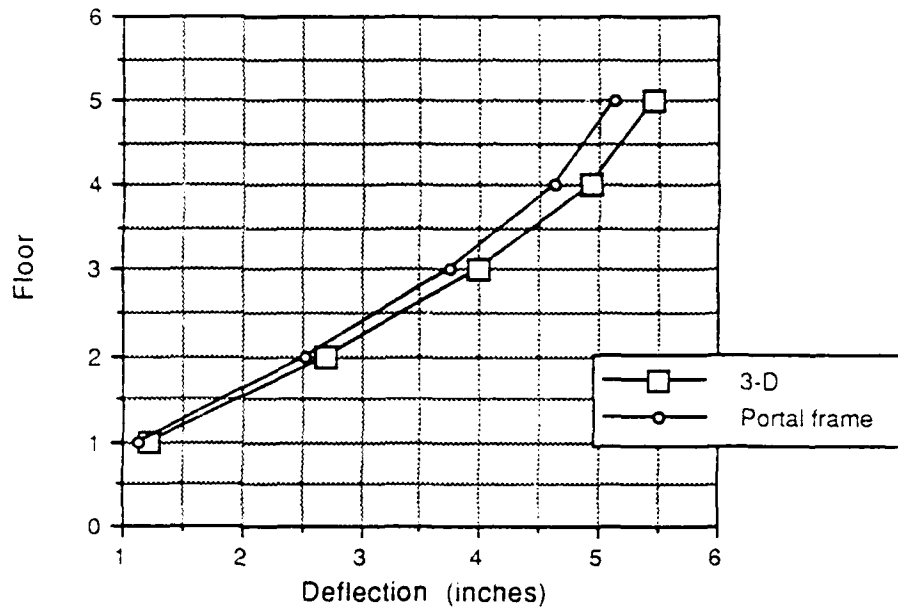


Figure A.33 Horizontal floor deflection (x)  
(series 5/1:1/0500/E-C{1,1})

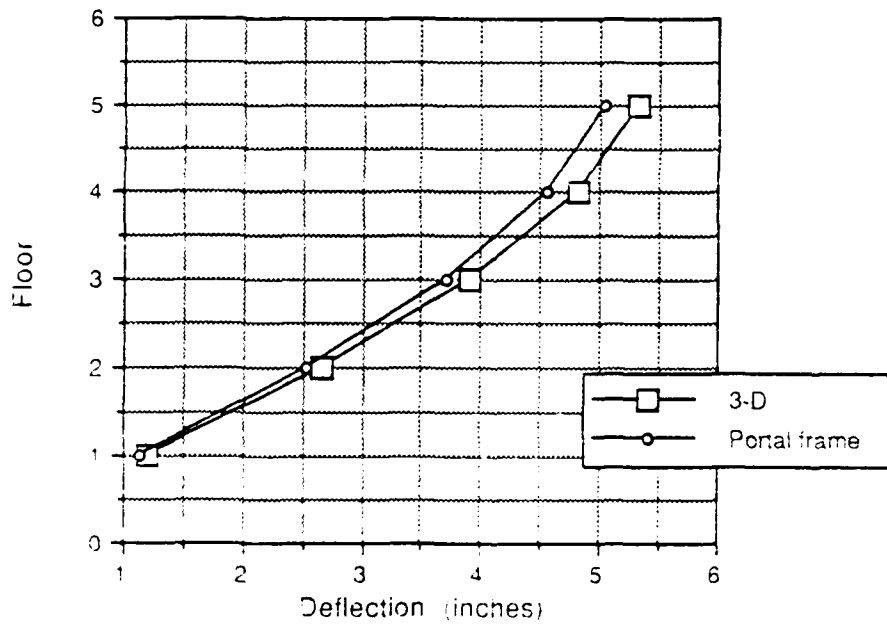


Figure A.34 Horizontal floor deflection (z)  
(series 5/1:1/0500/E-C{1,1})

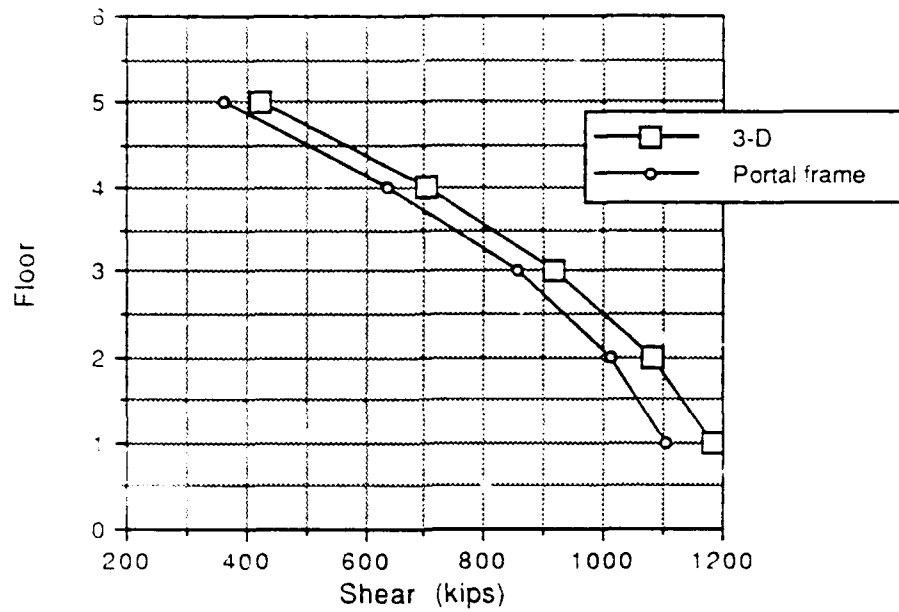


Figure A.35 Total floor shear (x)  
(series 5/1.1/0500/E-C{1,1})

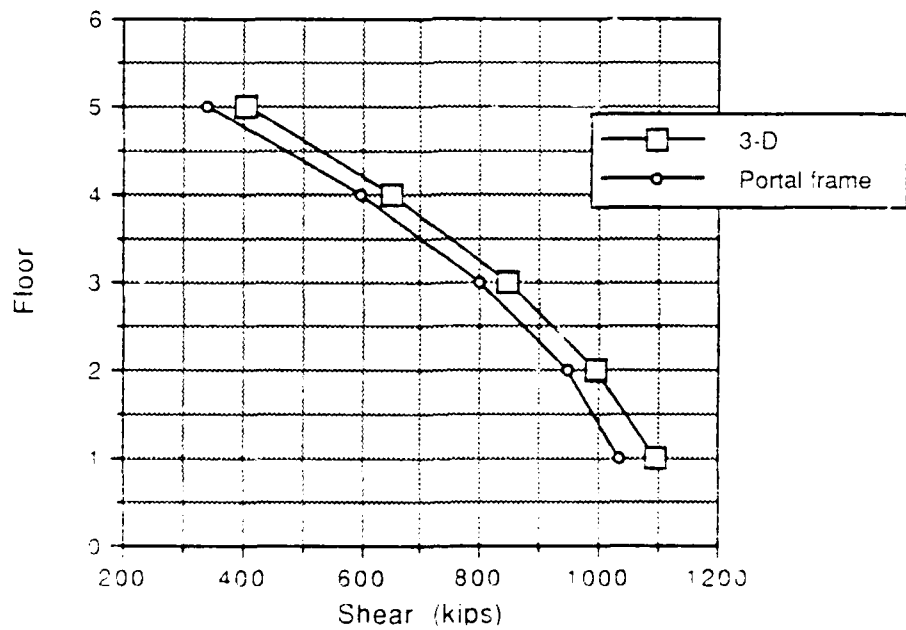


Figure A.36 Total floor shear (z)  
(series 5/1.1/0500/E-C{1,1})

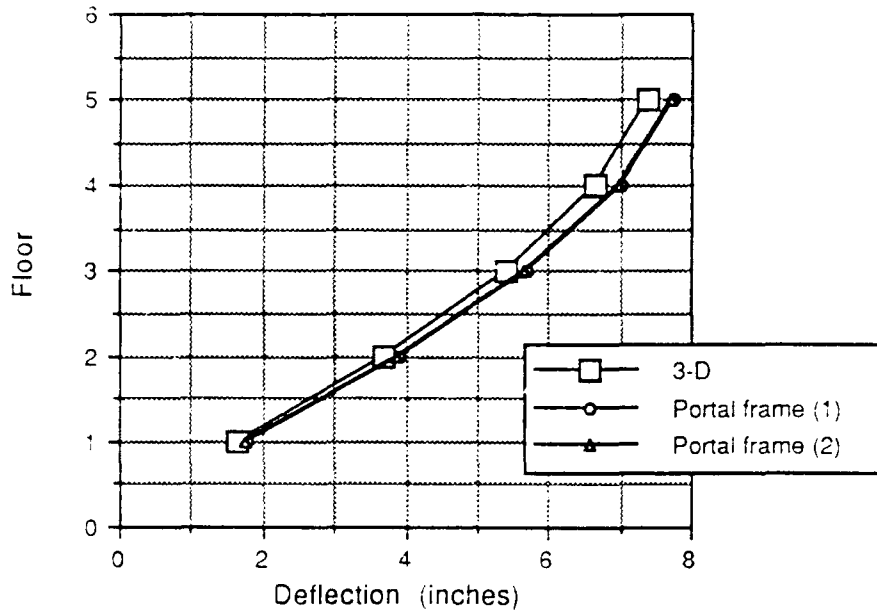


Figure A.37 Horizontal floor deflection (z)  
(series 5/1:1E/0500/E-C{0,1})

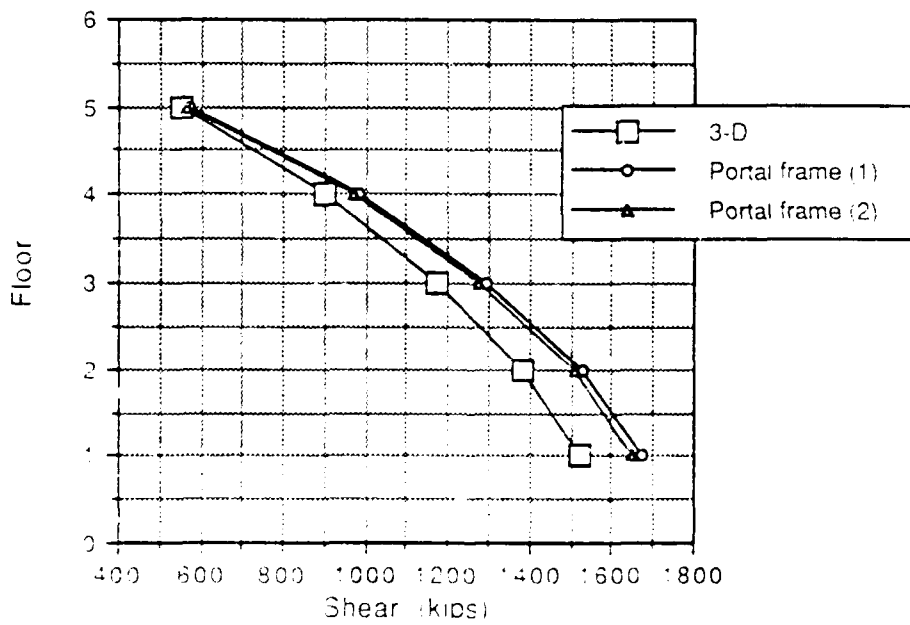


Figure A.38 Total floor shear (z)  
(series 5/1:1E/0500/E-C{0.1})

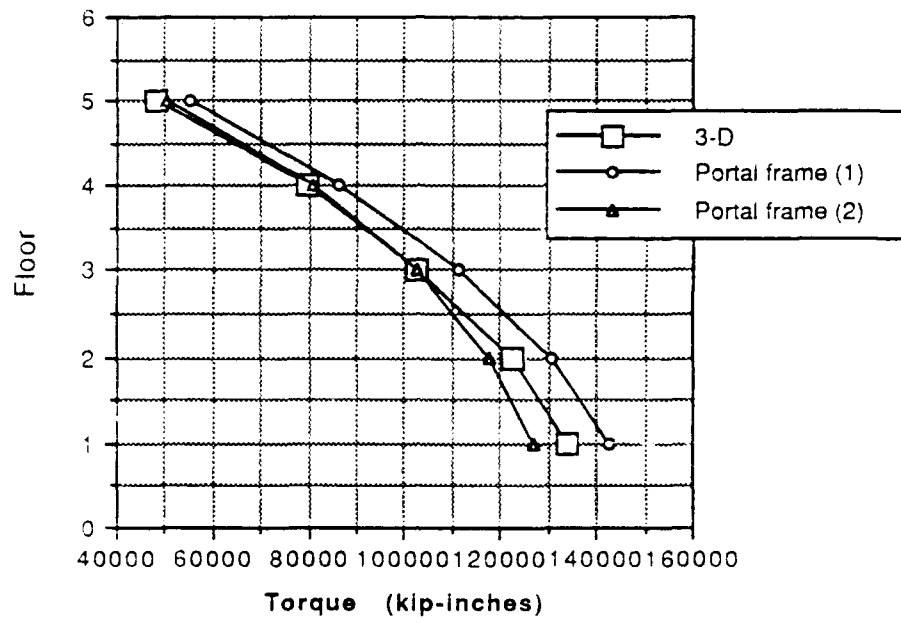


Figure A.39 Total floor torque  
(series 5/1:1E/0500/E-C{0,1})

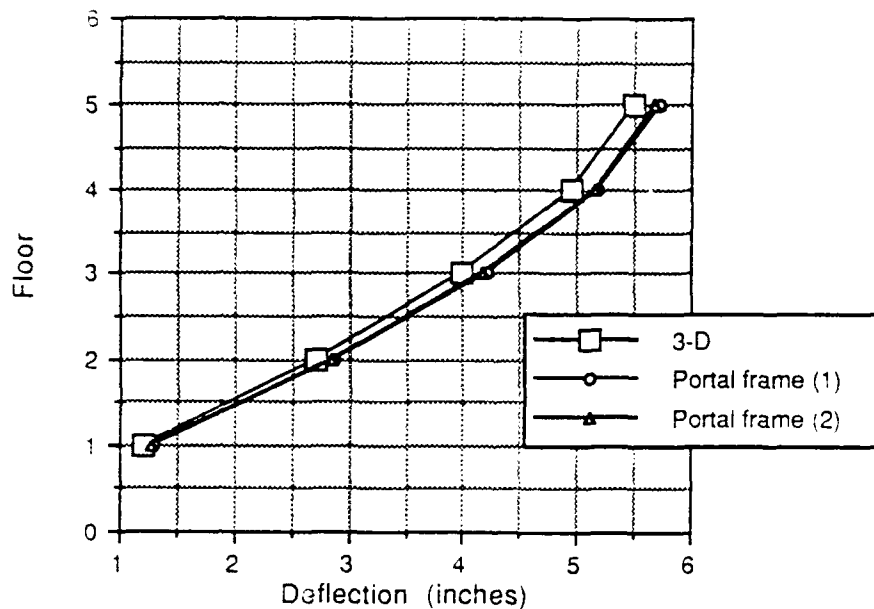


Figure A.40 Horizontal floor deflection (x)  
(series 5/1:1E/0500/E-C{1,1})

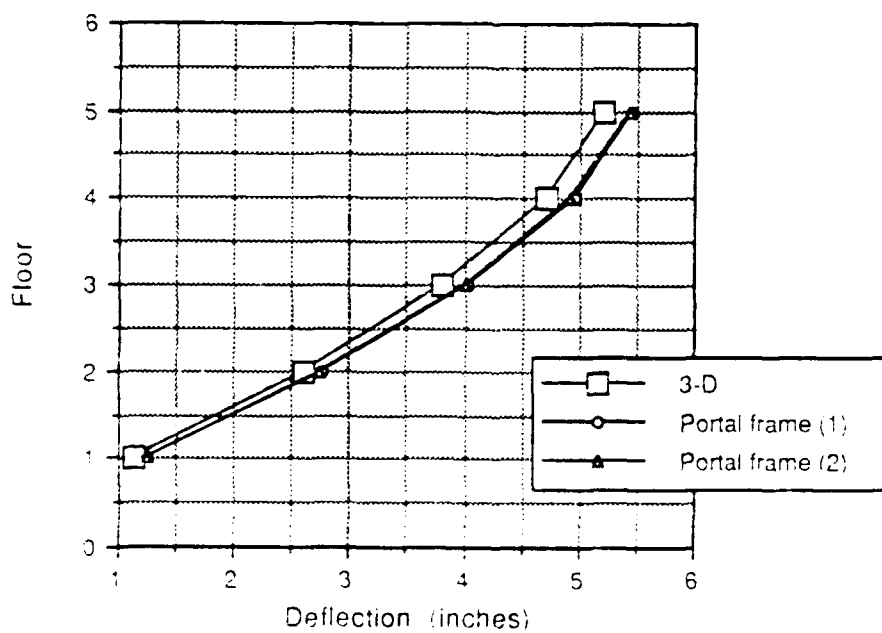


Figure A.41 Horizontal floor deflection (z)  
(series 5/1:1E/0500/E-C{1,1})

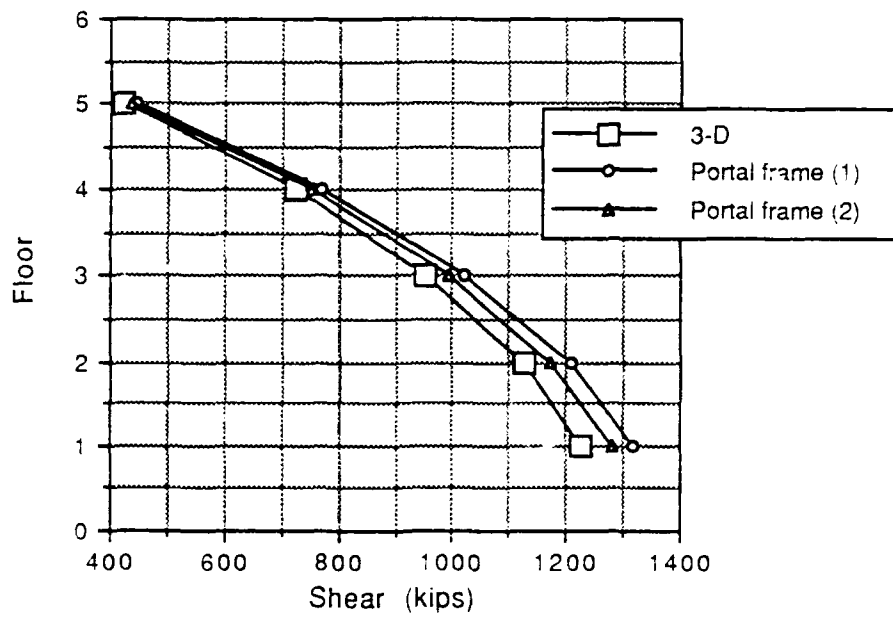


Figure A.42 Total floor shear (x)  
(series 5/1:1E/0500/E-C{1,1})

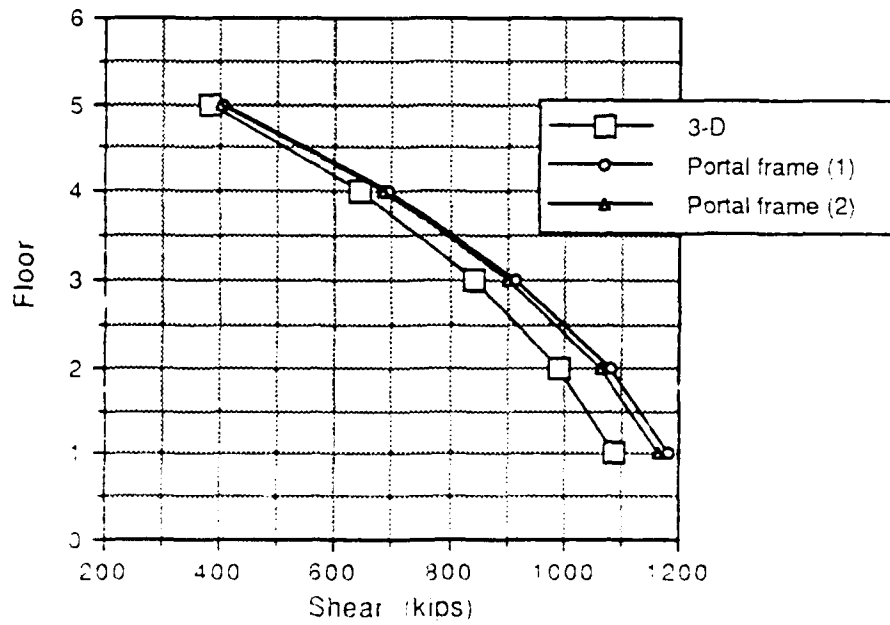


Figure A.43 Total floor shear (z)  
(series 5/1:1E/0500/E-C{1,1})

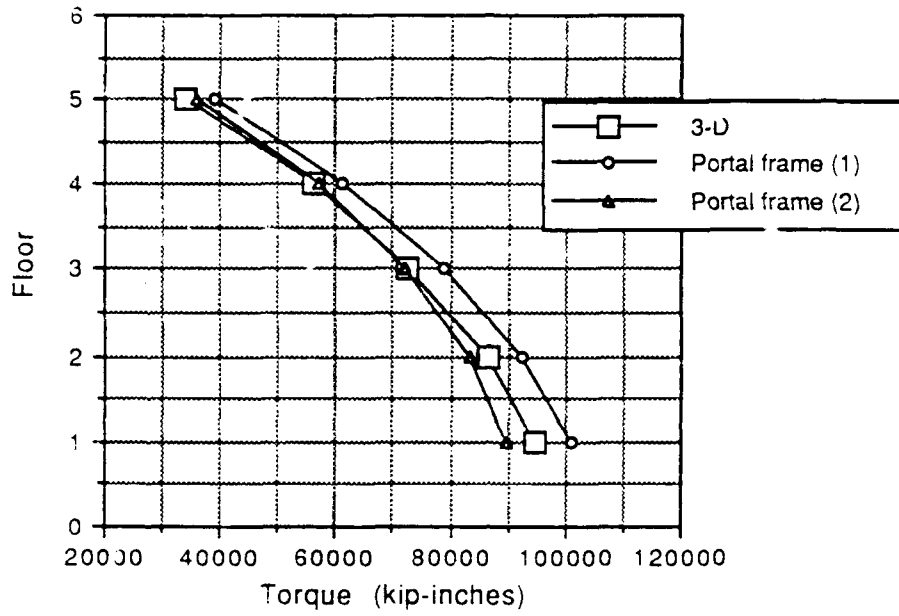


Figure A.44 Total floor torque  
(series 5/1:1E/0500/E-C{1,1})

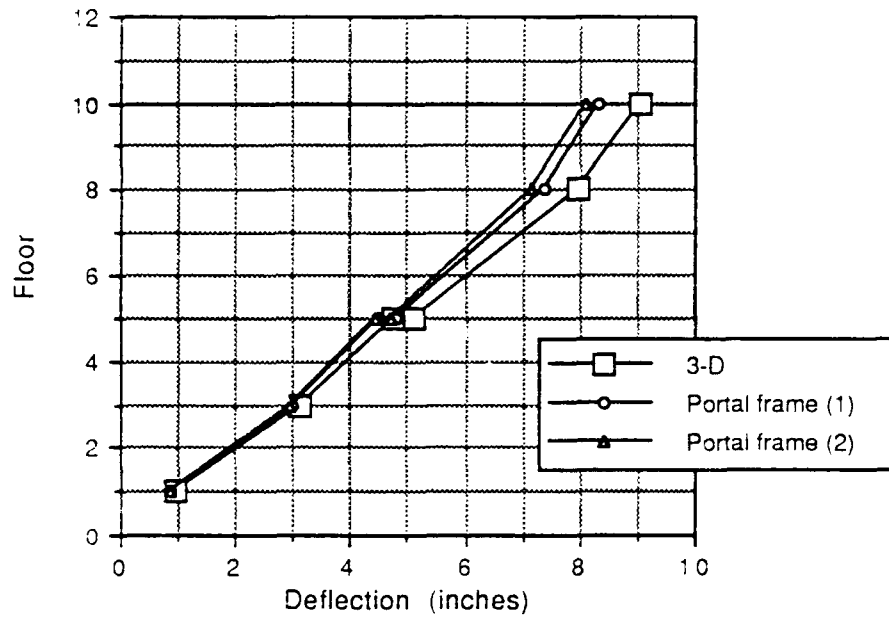


Figure A.45 Horizontal floor deflection (z)  
(series 10/1:1ESB/0500/E-C{0,1})

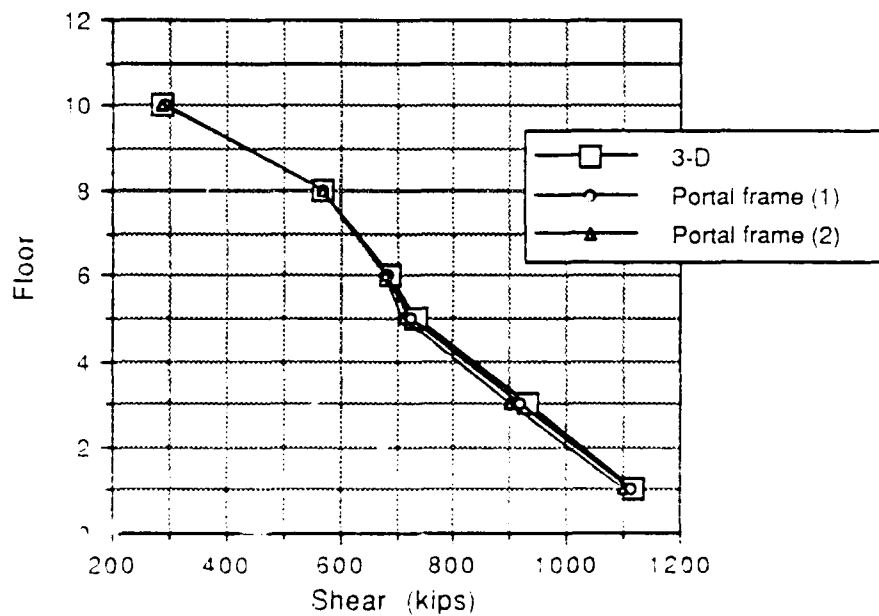


Figure A.46 Total floor shear (z)  
(series 10/1:1ESB/0500/E-C{0 1})

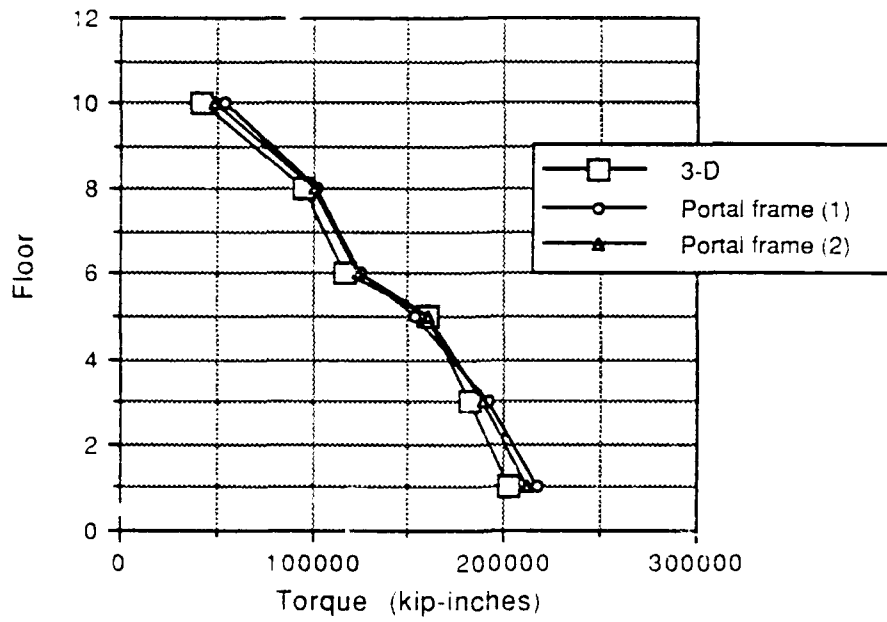


Figure A.47 Total floor torque  
(series 10/1:1ESB/0500/E-C{0,1})

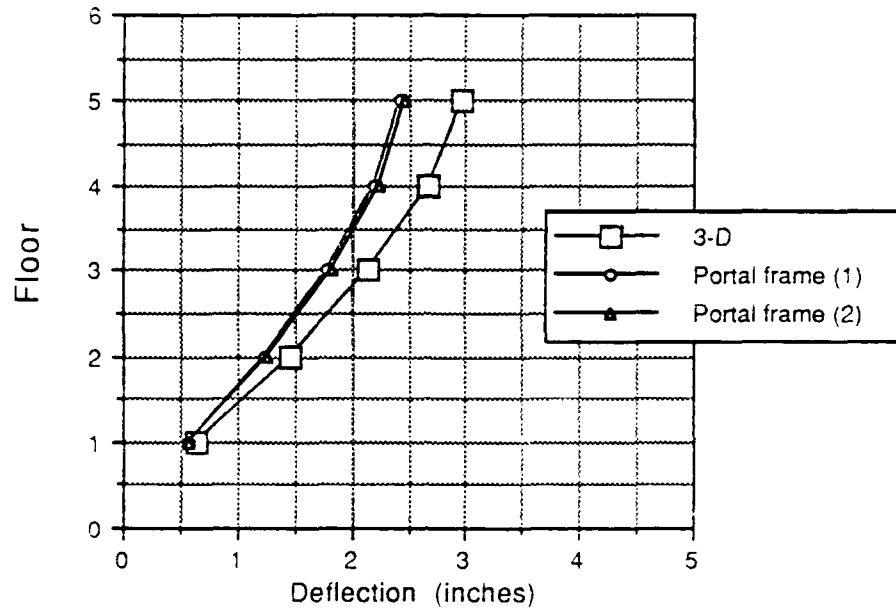


Figure A.48 Horizontal floor deflection (x)  
CQC modal combination  
(series 5/3:2L/0500/E-C{.5625,-1.0})

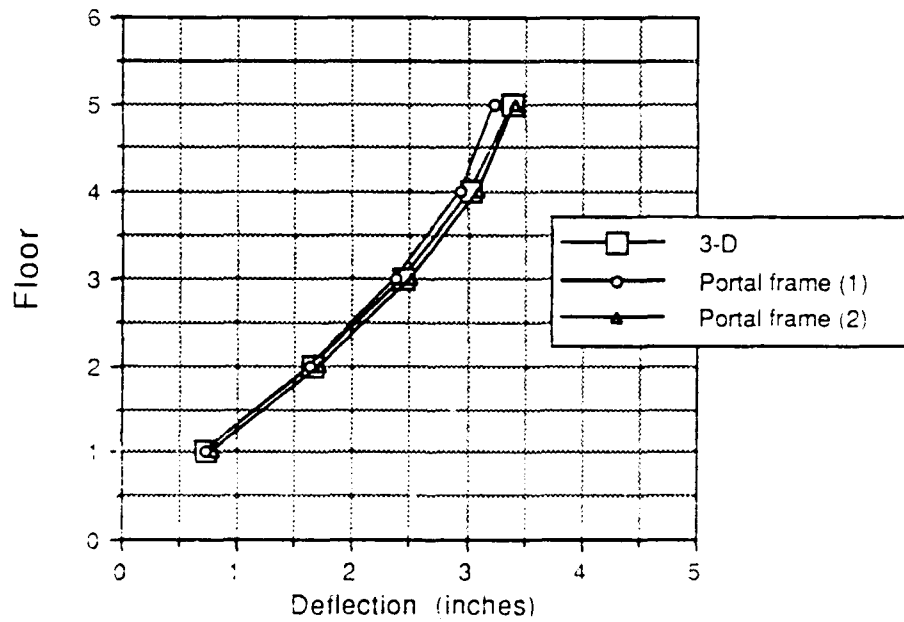


Figure A.49 Horizontal floor deflection (z)  
CQC modal combination  
(series 5/3:2L/0500/E-C{.5625,-1.0})

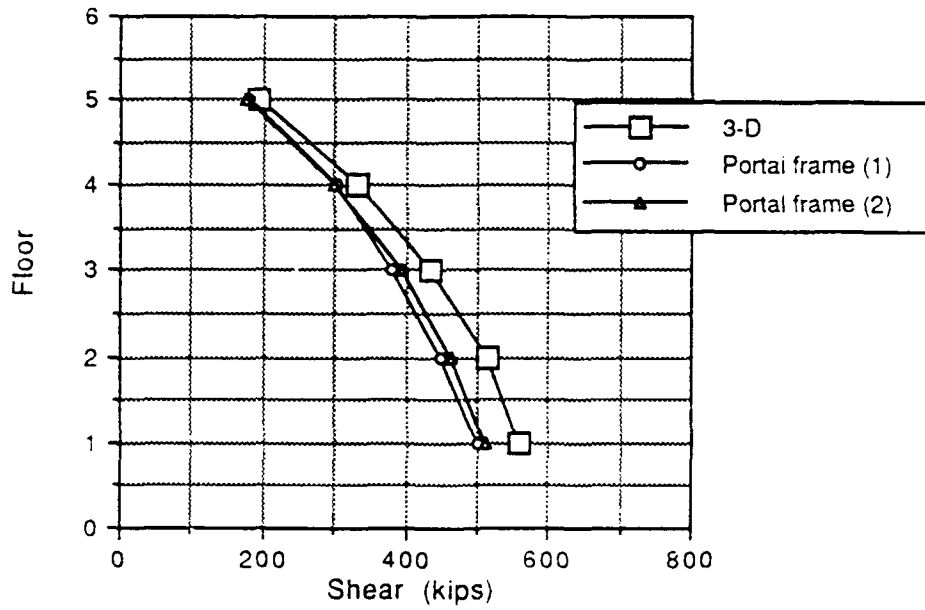


Figure A.50 Total floor shear (x)  
 CQC modal combination  
 (series 5/3:2L/0500/E-C{.5625,-1.0})

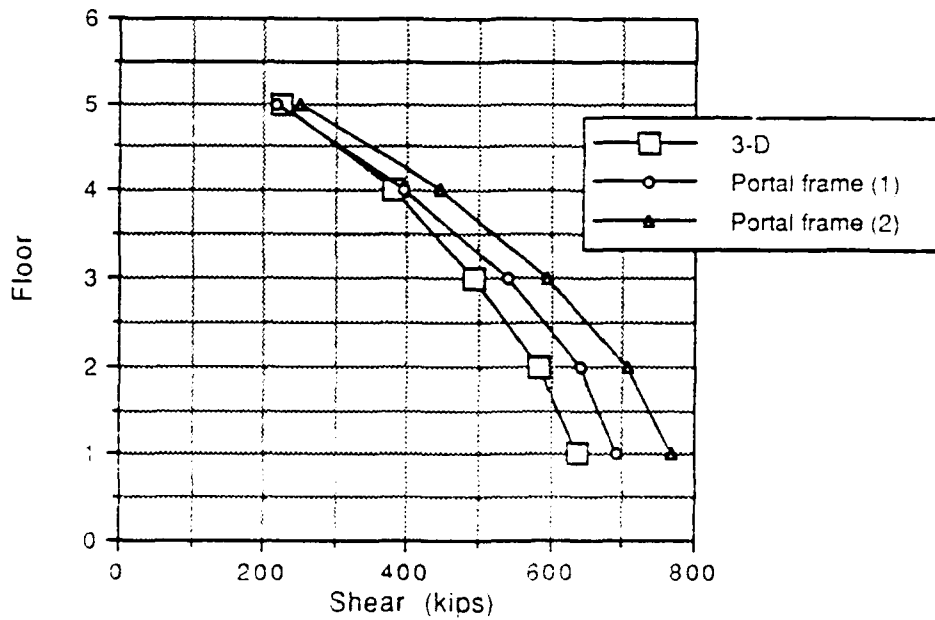


Figure A.51 Total floor shear (z)  
 CQC modal combination  
 (series 5/3:2L/0500/E-C{.5625,-1.0})

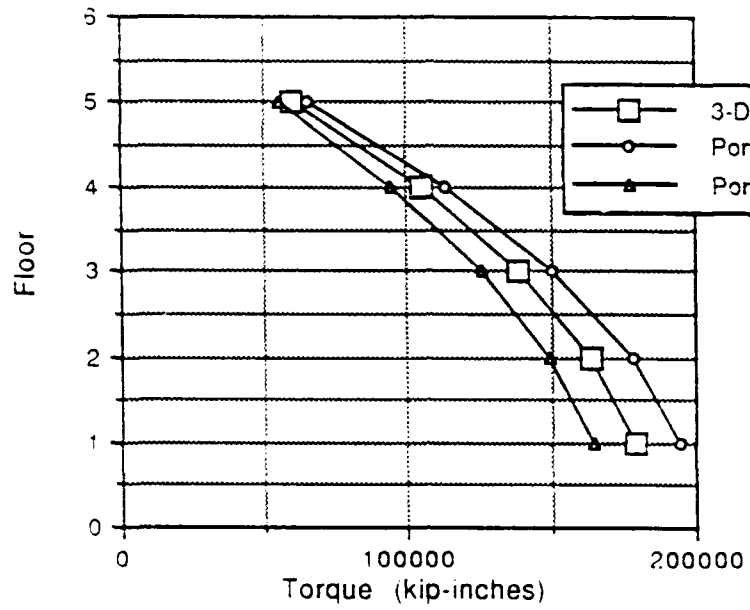


Figure A.52 Total floor torque  
CQC modal combination  
(series 5/3:2L/0500/E-C{.5625,-1.0})

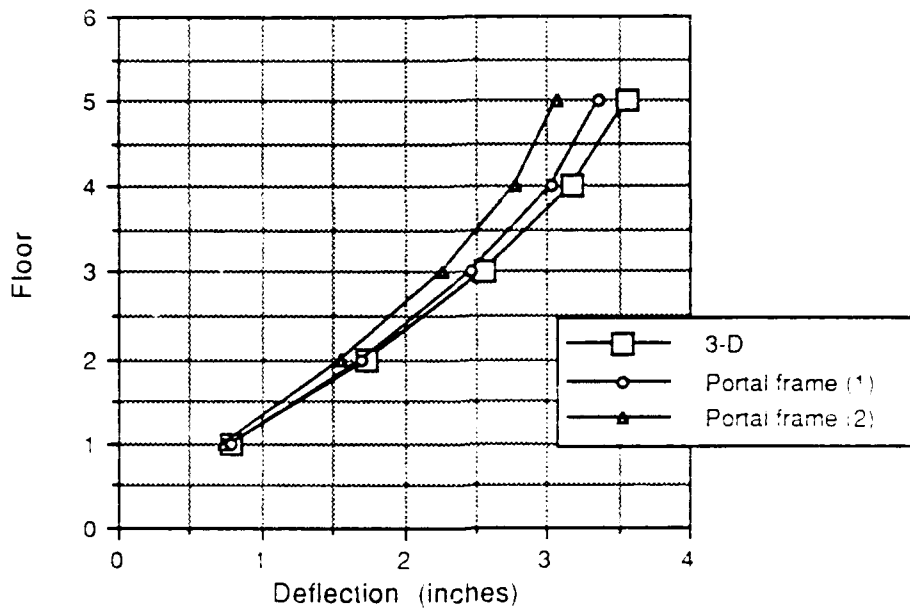


Figure A.53 Horizontal floor deflection (x)  
 SRSS modal combination  
 (series 5/3:2L/0500/E-C{1.0,.5625})

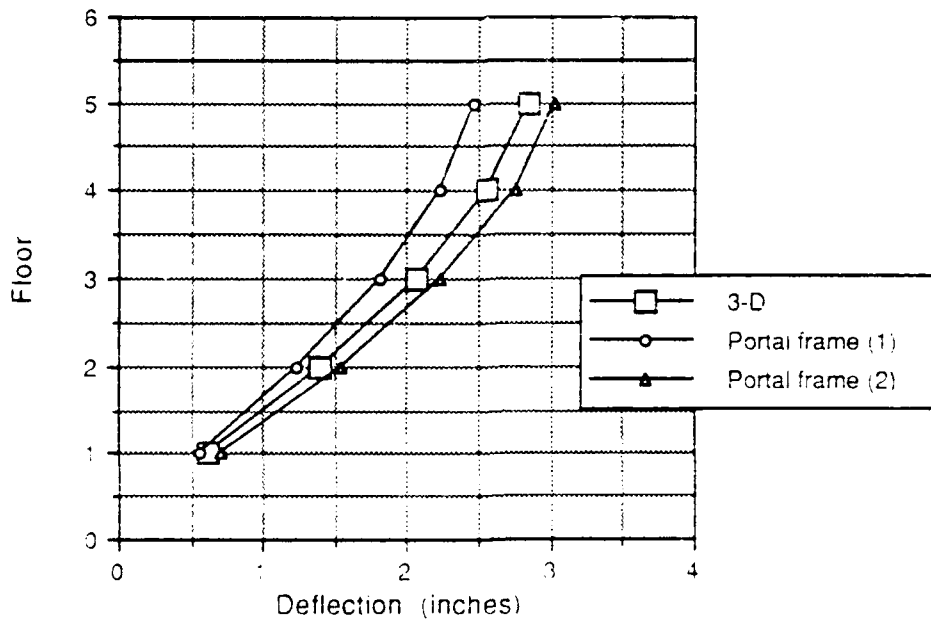


Figure A.54 Horizontal floor deflection (z)  
 SRSS modal combination  
 (series 5/3:2L/0500/E-C{1.0,.5625})

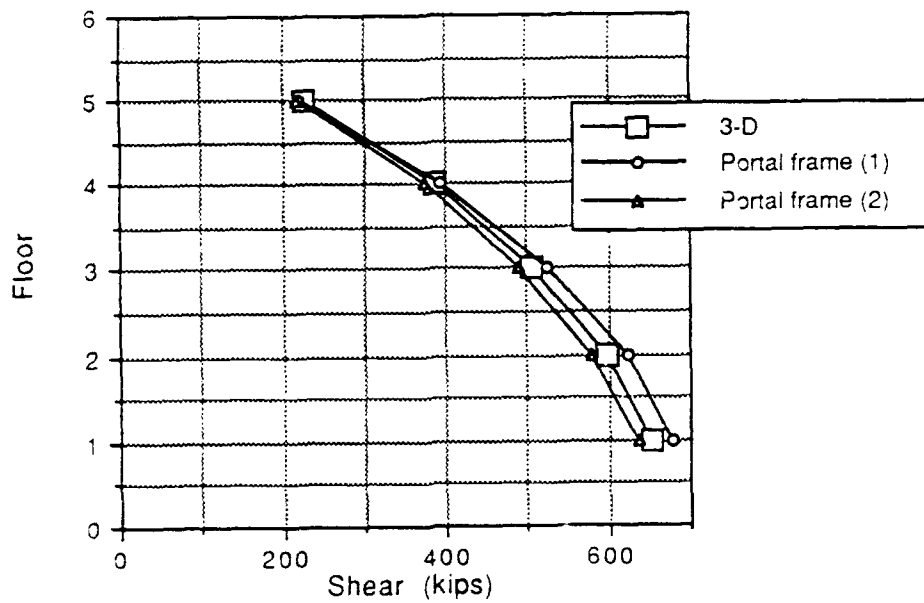


Figure A.55 Total floor shear (x)  
 SRSS modal combination  
 (series 5/3:2L/0500/E-C{1.0,.5625})

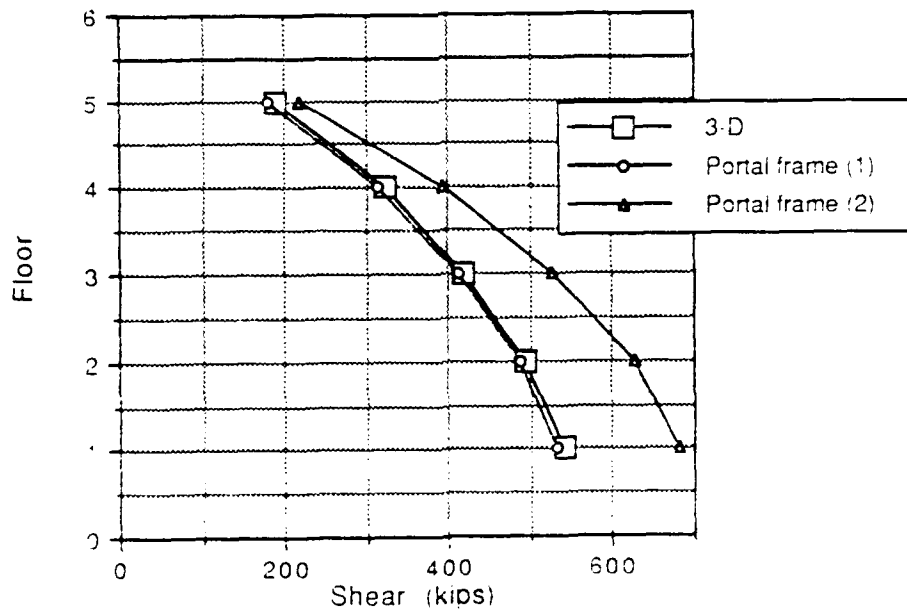


Figure A.56 Total floor shear (z)  
 SRSS modal combination  
 (series 5/3:2L/0500/E-C{1.0,.5625})

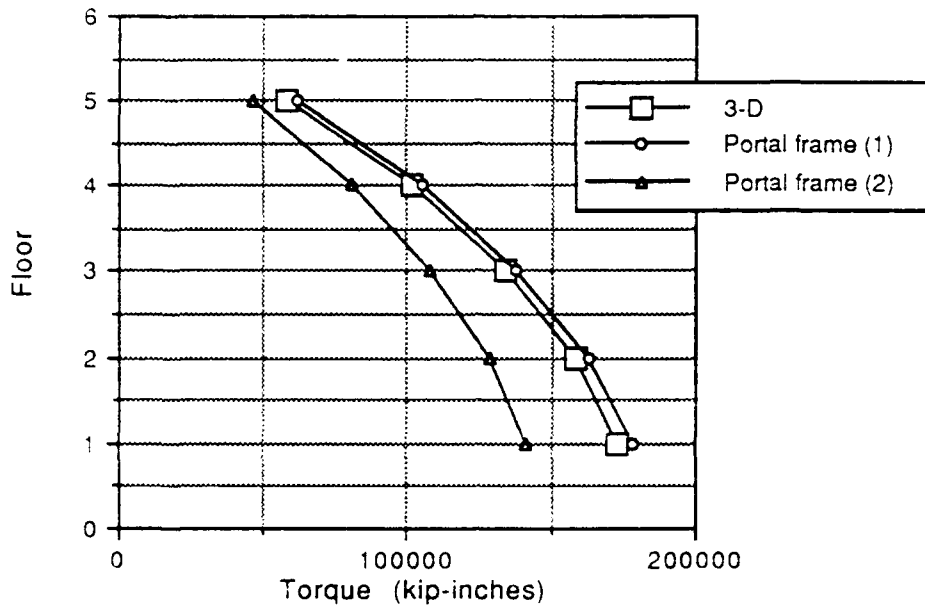


Figure A.57 Total floor torque  
SRSS modal combination  
(series 5/3:2L/0500/E-C{1.0,.5625})

## APPENDIX B

### MAT VERTICAL DEFLECTION PROFILES

This appendix summarizes mat vertical deflection profiles for all calculations on the softest and hardest soils studied ( $v_s = 500$  fps and 1500 fps). All frames are doubly symmetric, and deflections are displayed in two views for one quadrant of the uplifted half of the mat. These space frames were loaded in the x-direction and therefore rock about the z-axis with the coordinate origin located at the mat center.

Legend notes:

**b** and **c** are the mat dimensions in the x and z directions. Solid line graphs display results of earthquake loadings. Dashed line graphs display results of harmonic loadings applied to a structure supported by a soil volume. The harmonic loadings were applied as a preliminary calculations require to evaluate equivalent soil springs (see Chapter II). Profiles for harmonic loads are given for centerline nodes in the x-direction and for the nodal line in the z direction tending to generate maximum negative deflections for the given mat aspect ratio.

Series nomenclature: (N/X:Z/kkkk/E-Q{x,z})

**N** equals number of frame floors

**X:Z** equals floor plan ratio of dimensions in x and z directions (load applied in x direction)

**kkkk** equals soil shear wave velocity in feet/sec

**E-Q** implies earthquake (E-Q for El Centro and M-C for Mexico City)

**{x,z}** vector identifying the horizontal direction of earthquake loading

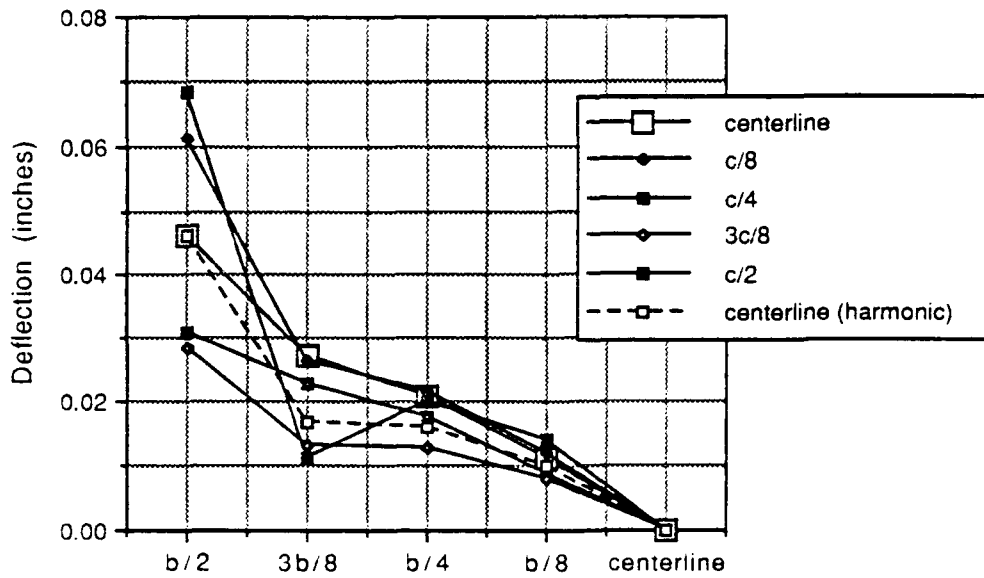


Figure B.1 Mat vertical deflection profile z-axis view (3/1:1/0500/E-C)

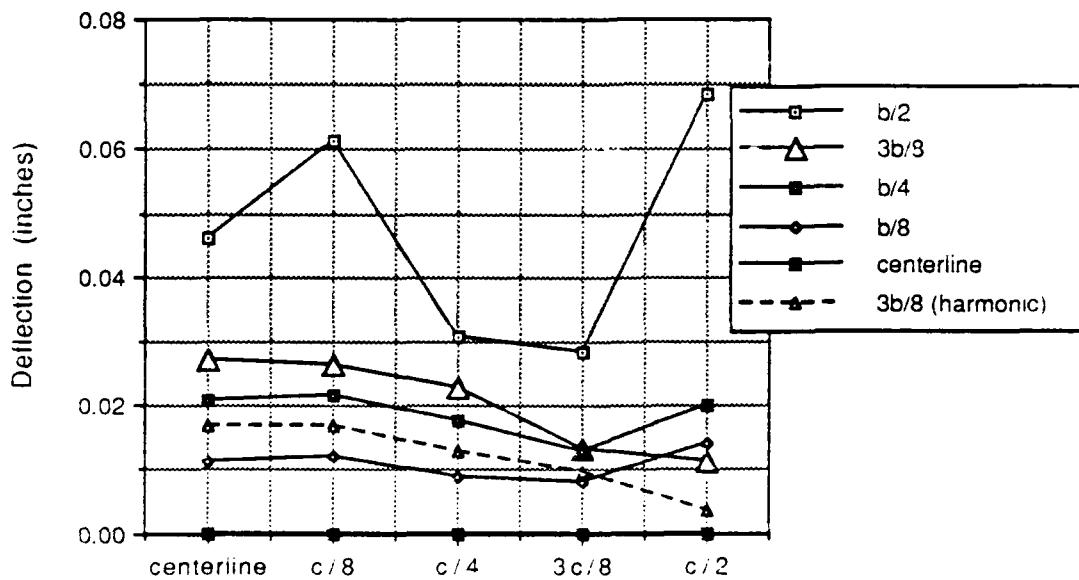


Figure B.2 Mat vertical deflection profile x-axis view (3/1:1/0500/E-C)

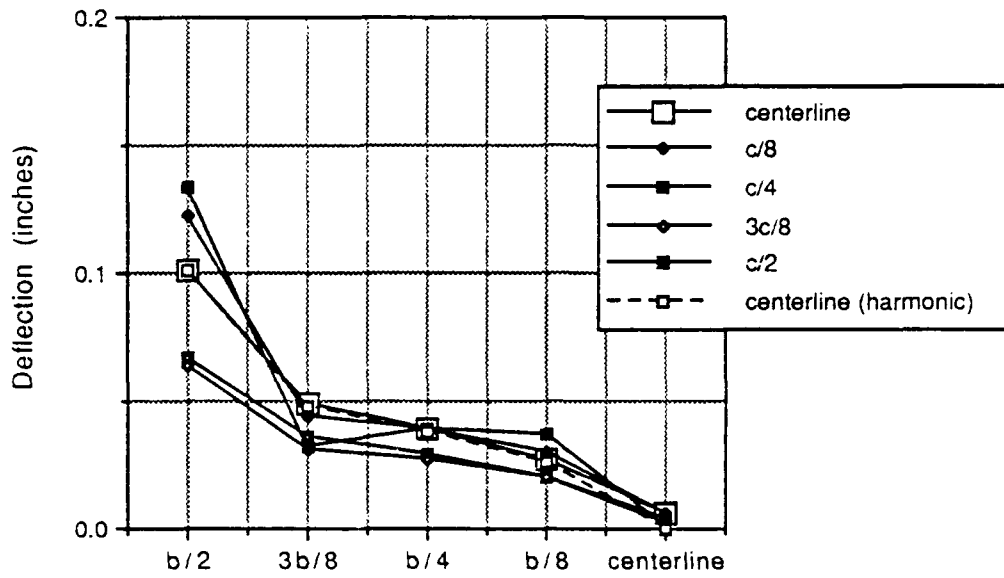


Figure B.3 Mat vertical deflection profile z-axis view (5/1:1/0500/E-C)

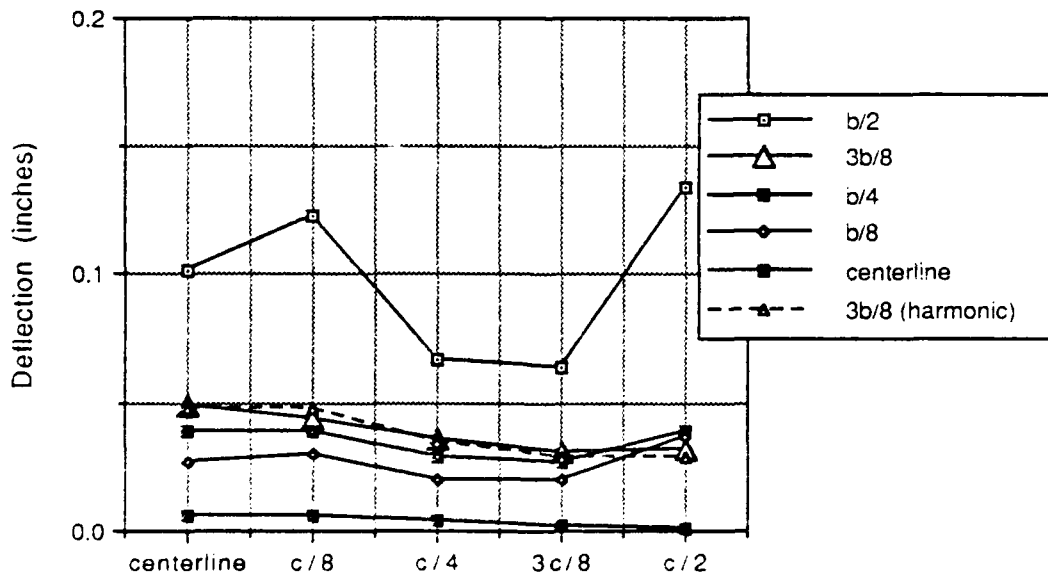


Figure B.4 Mat vertical deflection profile x-axis view (5/1:1/0500/E-C)

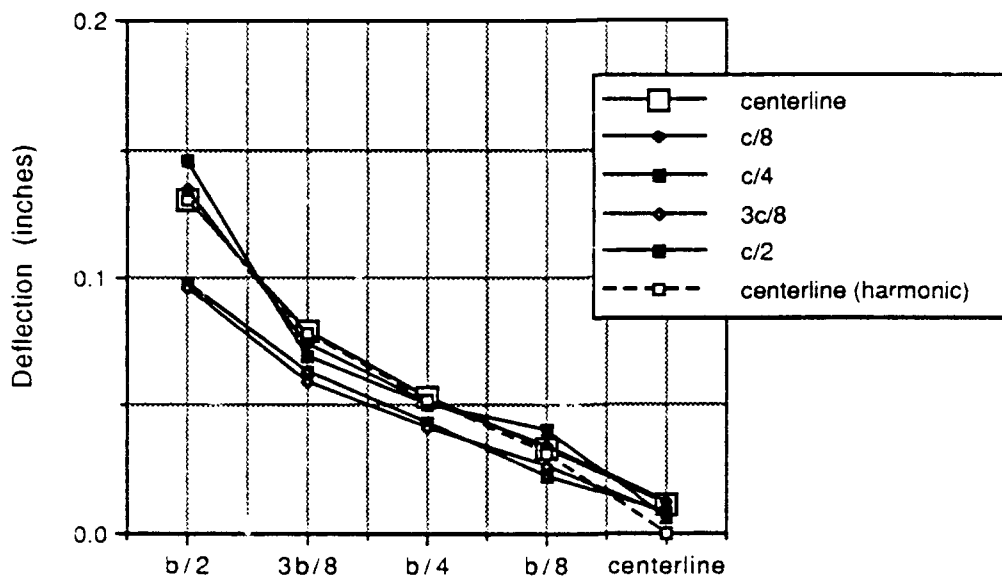


Figure B.5 Mat vertical deflection profile  
z-axis view (10/1:1/0500/E-C)

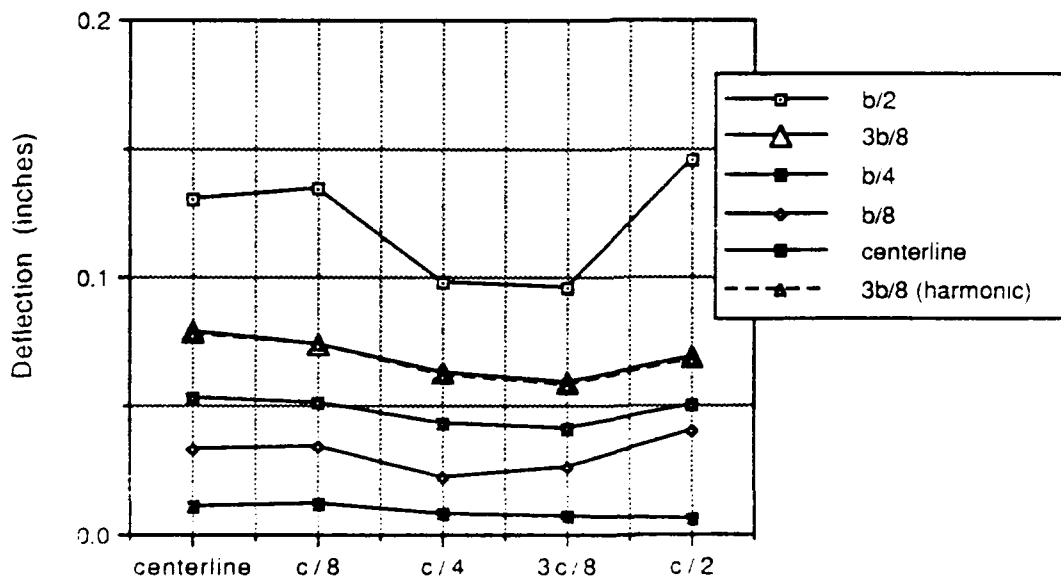


Figure B.6 Mat vertical deflection profile  
x-axis view (10/1.1/0500/E-C)

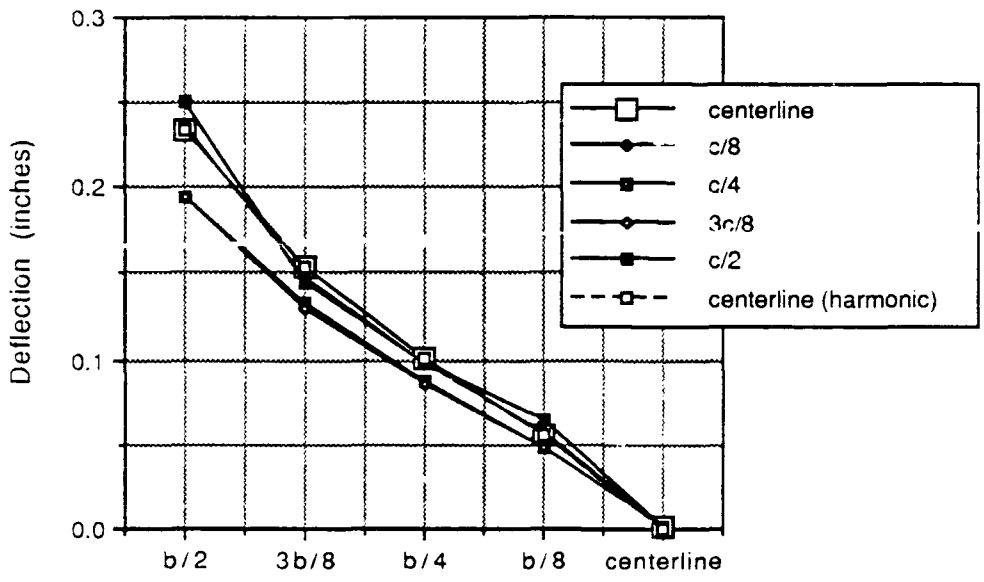


Figure B.7 Mat vertical deflection profile z-axis view (15/1:1/0500/E-C)

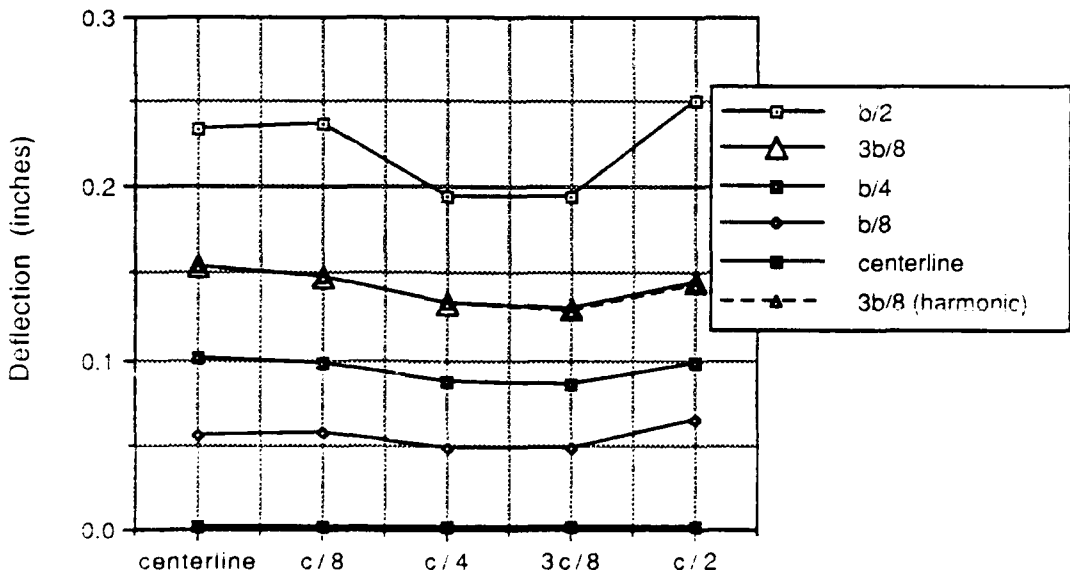


Figure B.8 Mat vertical deflection profile x-axis view (15/1:1/0500/E-C)

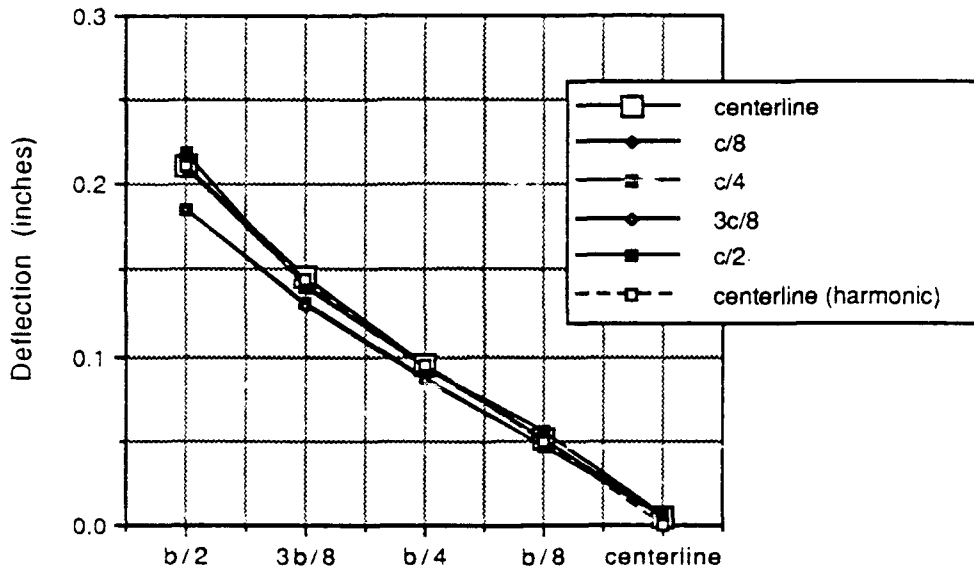


Figure B.9 Mat vertical deflection profile z-axis view (20/1:1/0500/E-C)

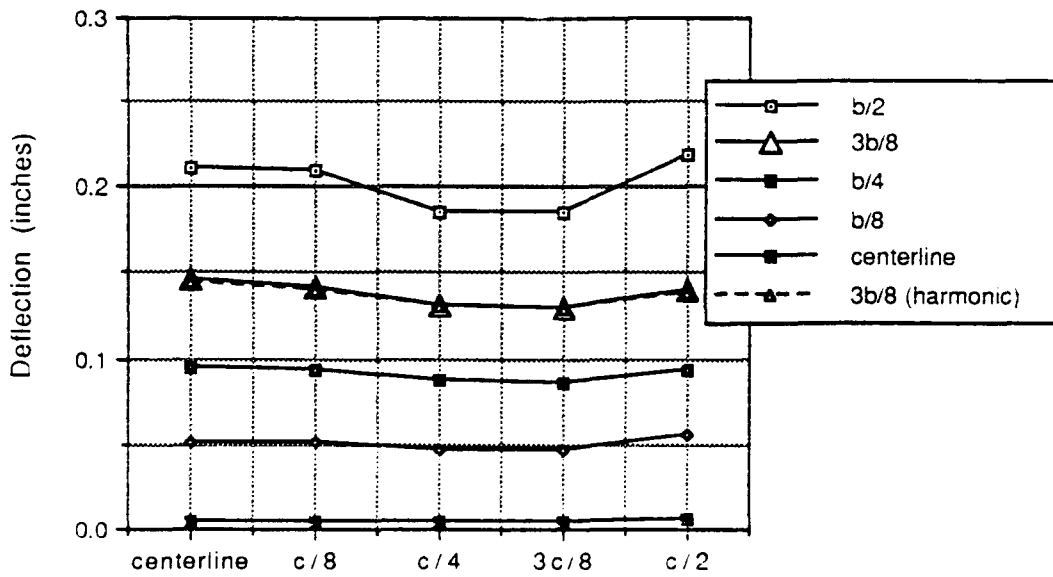


Figure B.10 Mat vertical deflection profile x-axis view (20/1:1/0500/E-C)

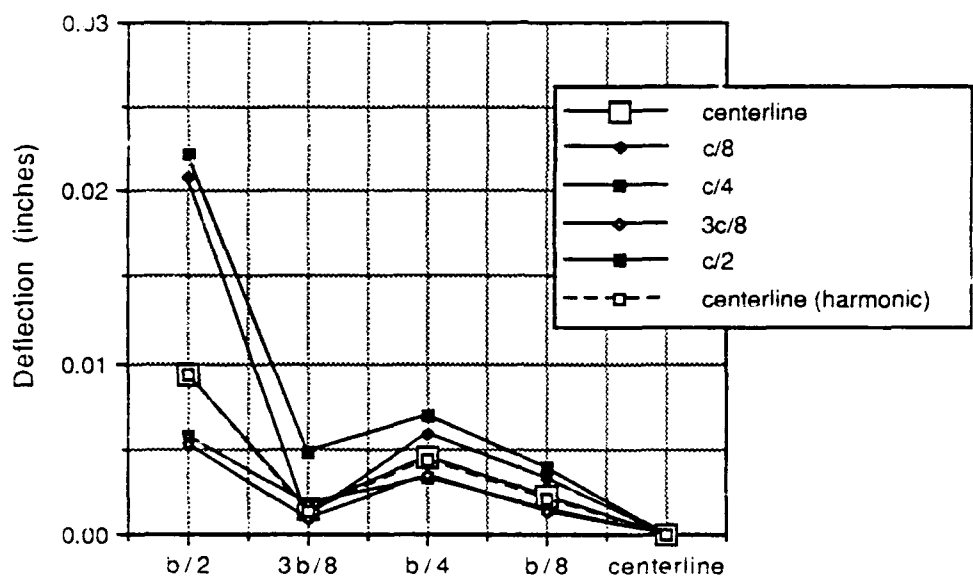


Figure B.11 Mat vertical deflection profile z-axis view (3/1:1/1000/E-C)

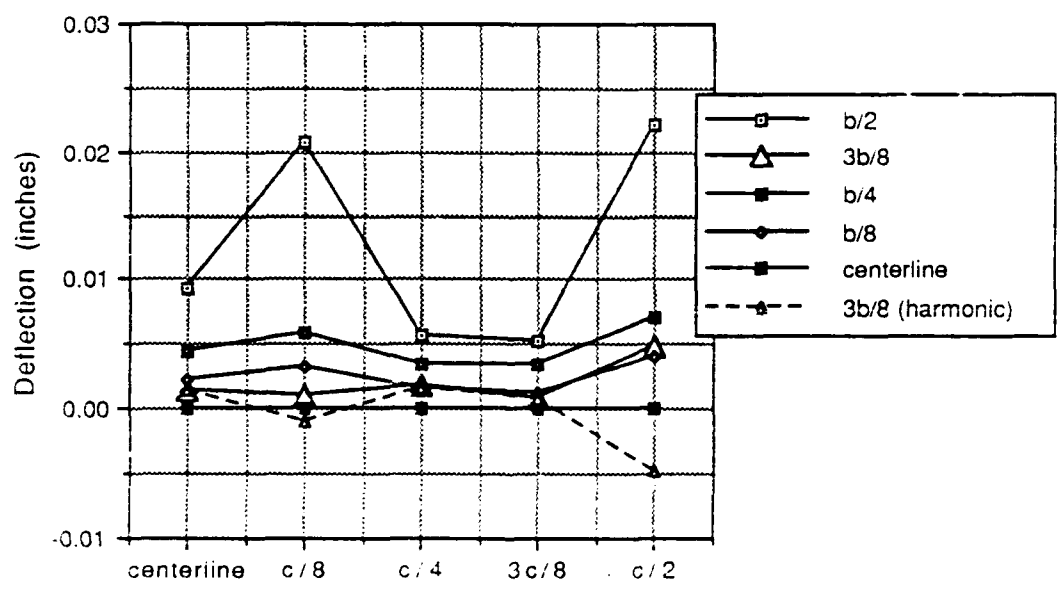


Figure B.12 Mat vertical deflection profile x-axis view (3/1:1/1000/E-C)

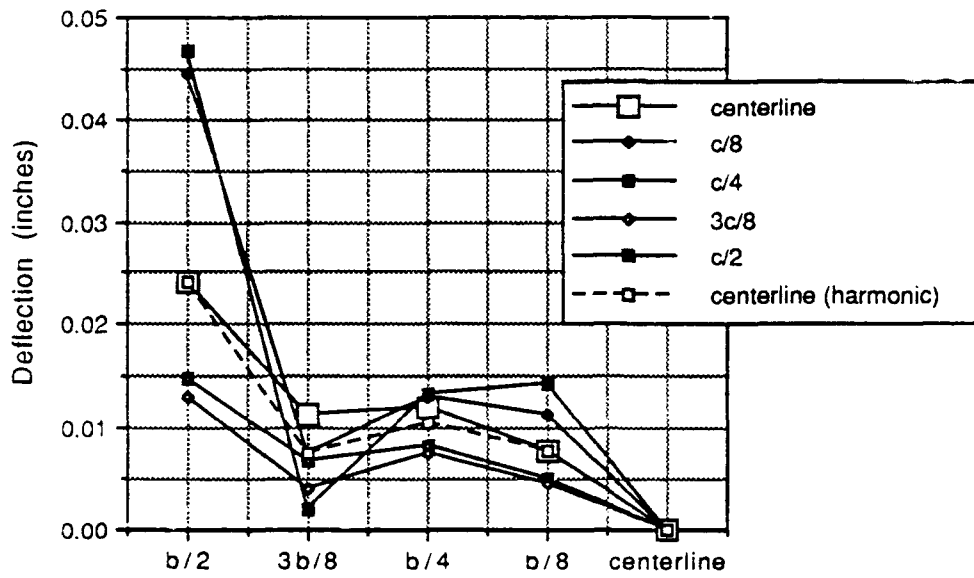


Figure B.13 Mat vertical deflection profile  
z-axis view (5/1:1/1000/E-C)

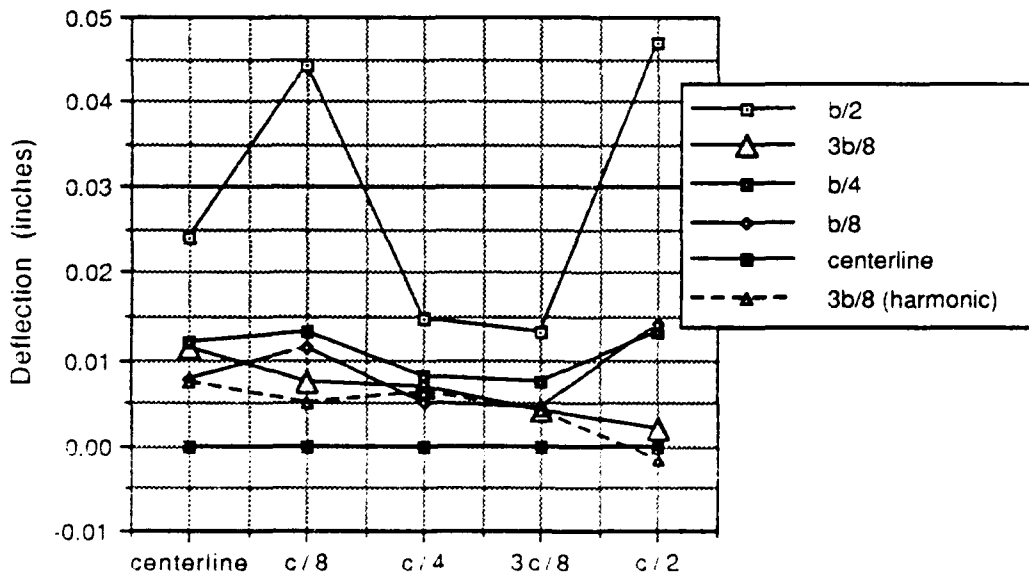


Figure B.14 Mat vertical deflection profile  
x-axis view (5/1:1/1000/E-C)

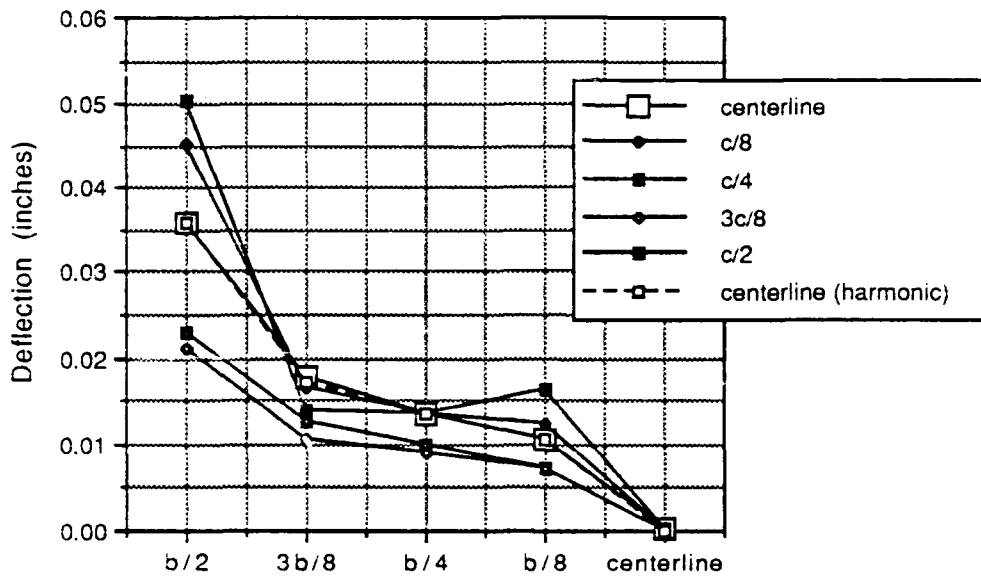


Figure B.15 Mat vertical deflection profile z-axis view (10/1:1/1000/E-C)

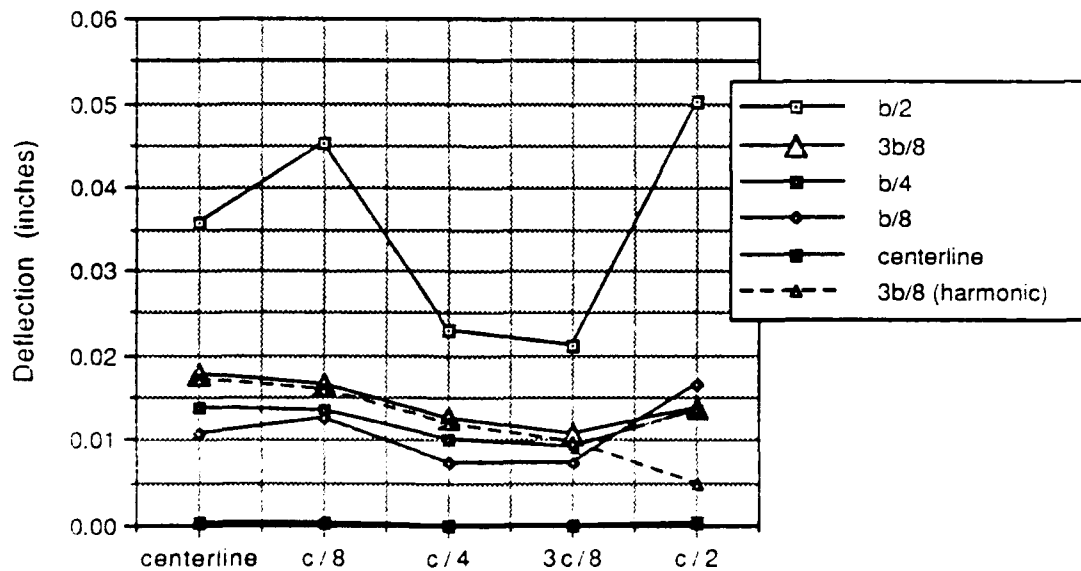


Figure B.16 Mat vertical deflection profile x-axis view (10/1:1/1000/E-C)

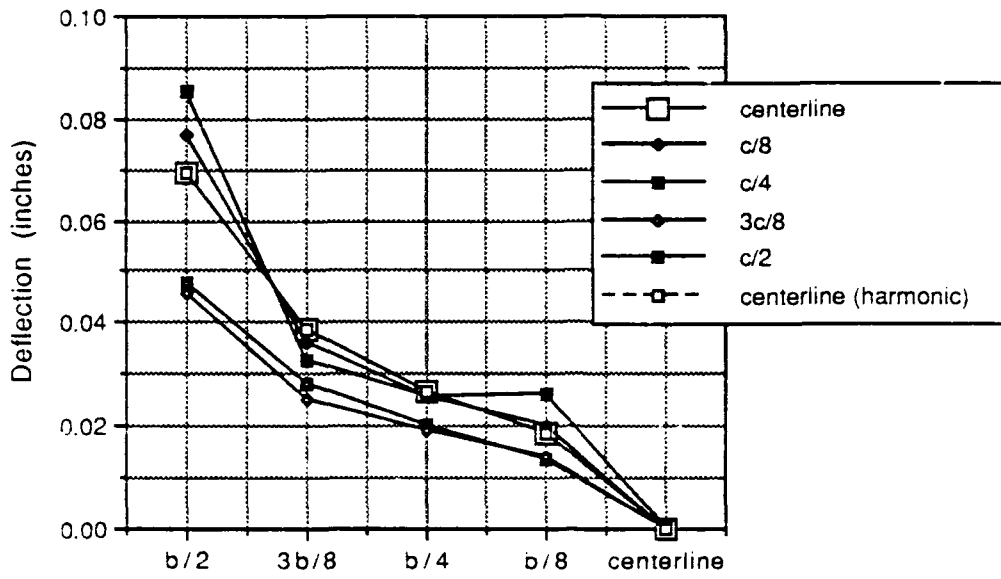


Figure B.17 Mat vertical deflection profile z-axis view (15/1:1/1000/E-C)

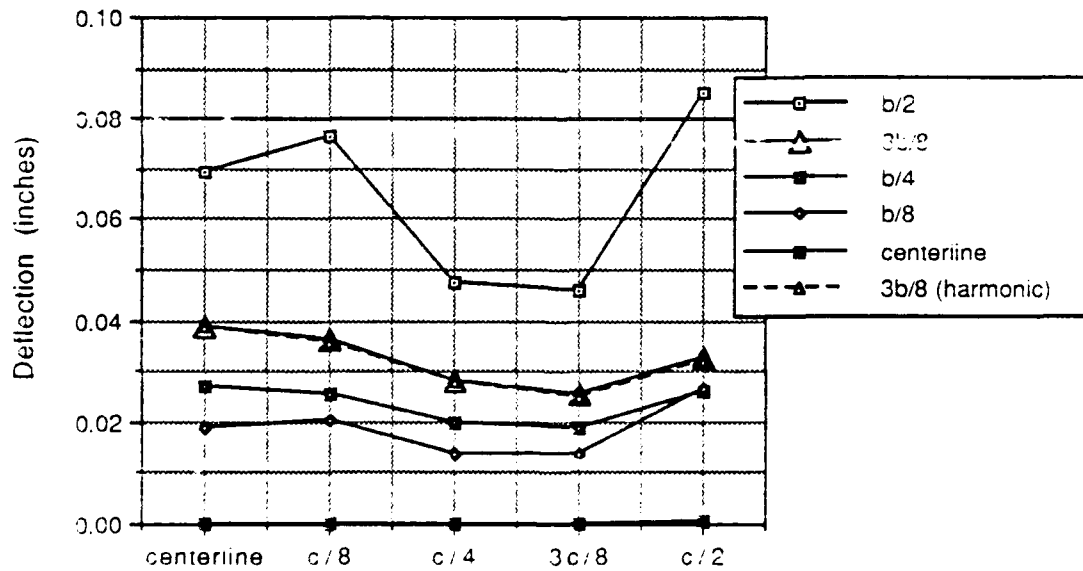


Figure B.18 Mat vertical deflection profile x-axis view (15/1:1/1000/E-C)

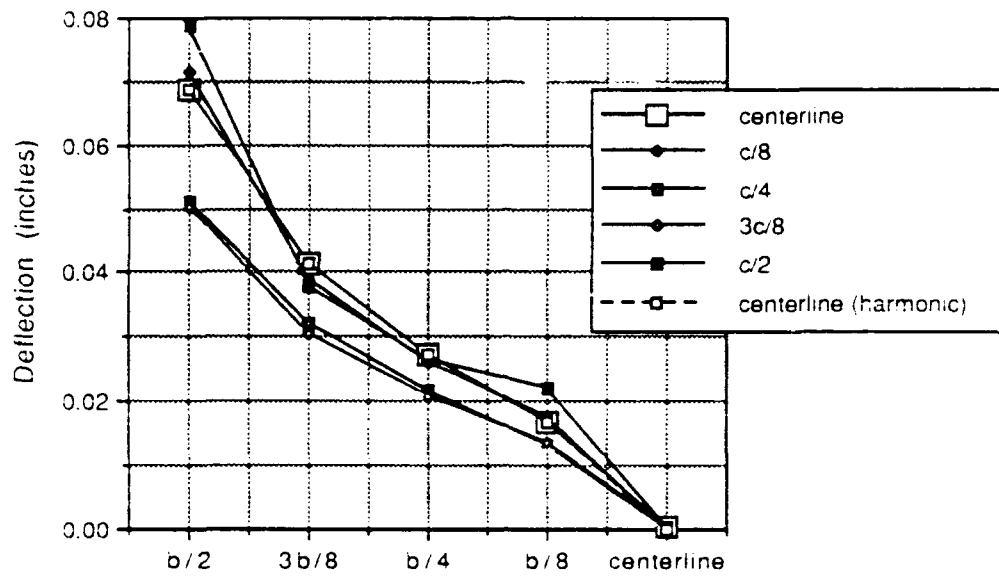


Figure B.19 Mat vertical deflection profile  
z-axis view (20/1:1/1000/E-C)

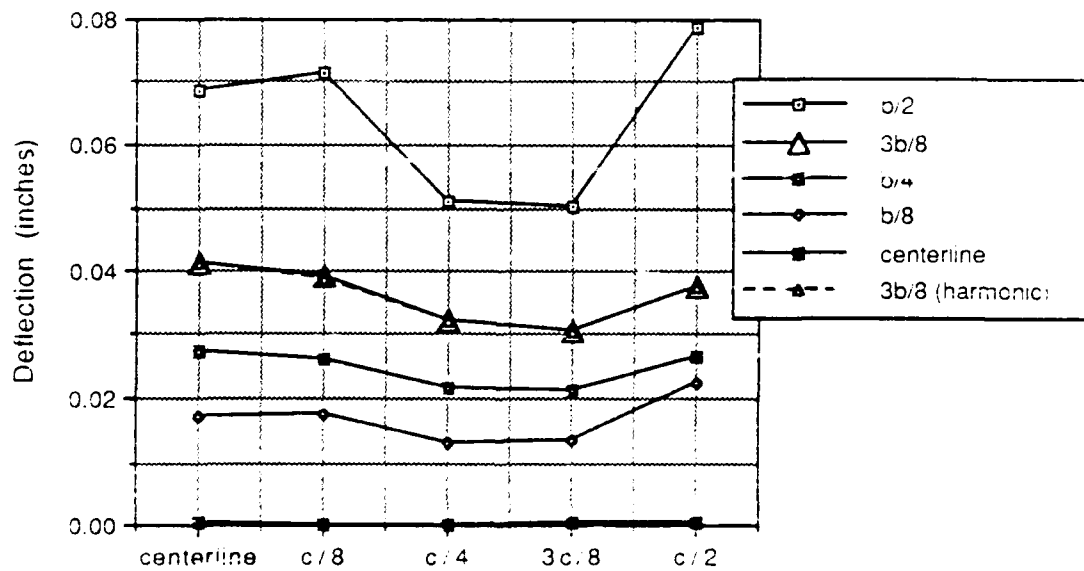


Figure B.20 Mat vertical deflection profile  
x-axis view (20/1:1/1000/E-C)

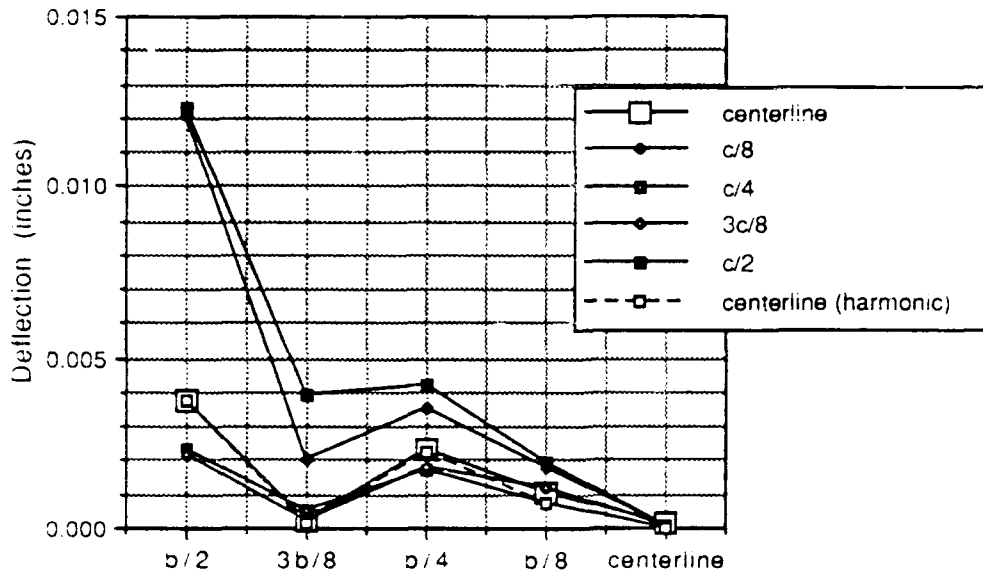


Figure B.21 Mat vertical deflection profile  
z-axis view (3/1:1/1500/E-C)

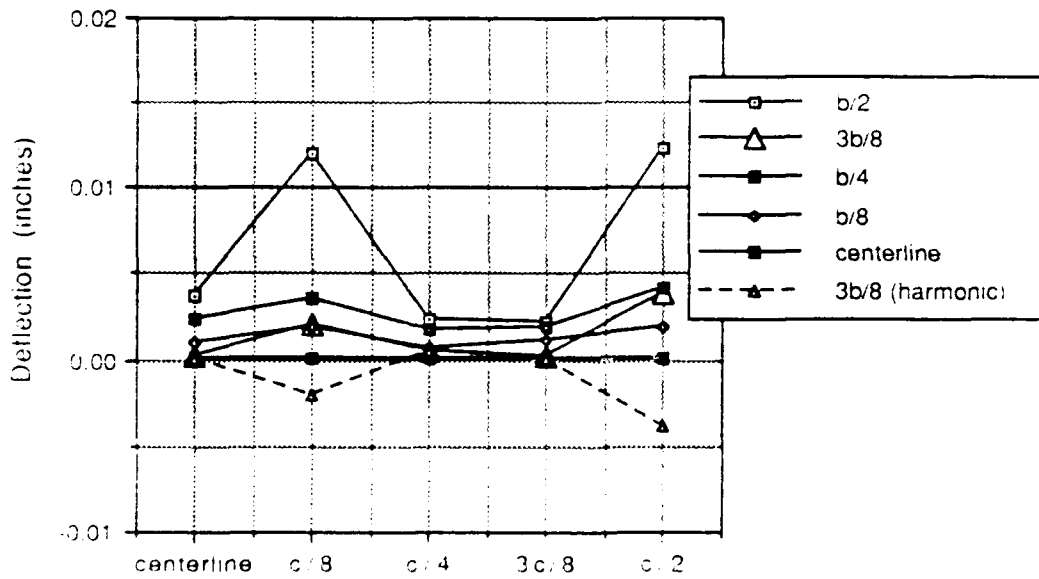


Figure B.22 Mat vertical deflection profile  
x-axis view (3/1:1/1500/E-C)

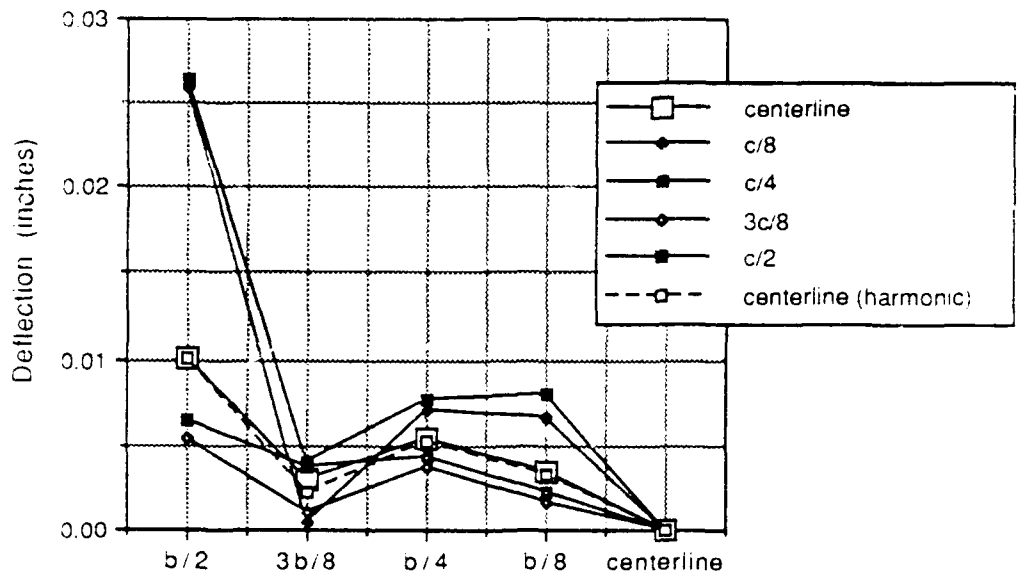


Figure B.23 Mat vertical deflection profile z-axis view (5/1.1/1500/E-C)

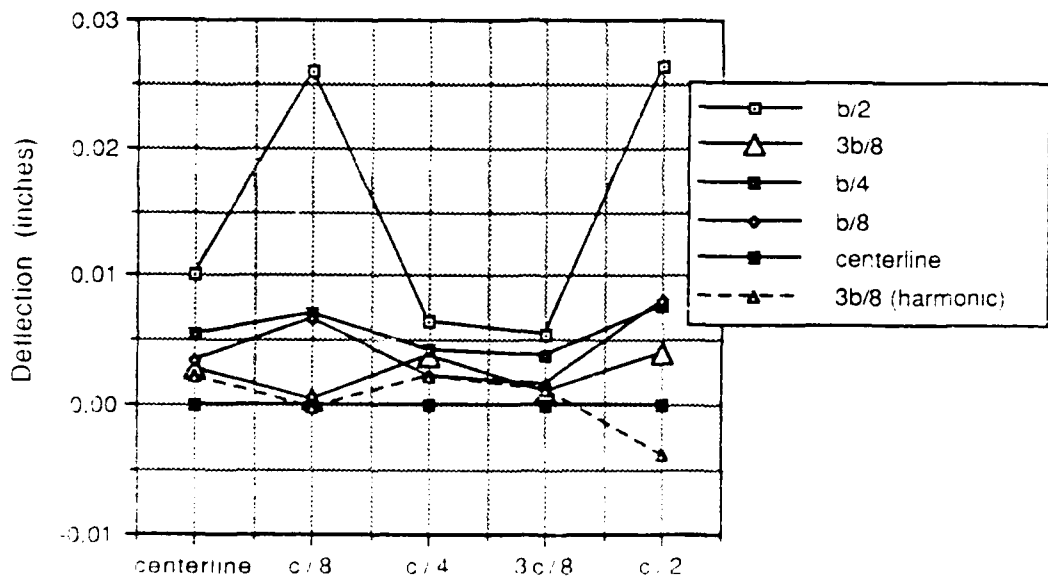


Figure B.24 Mat vertical deflection profile x-axis view (5/1.1/1500/E-C)

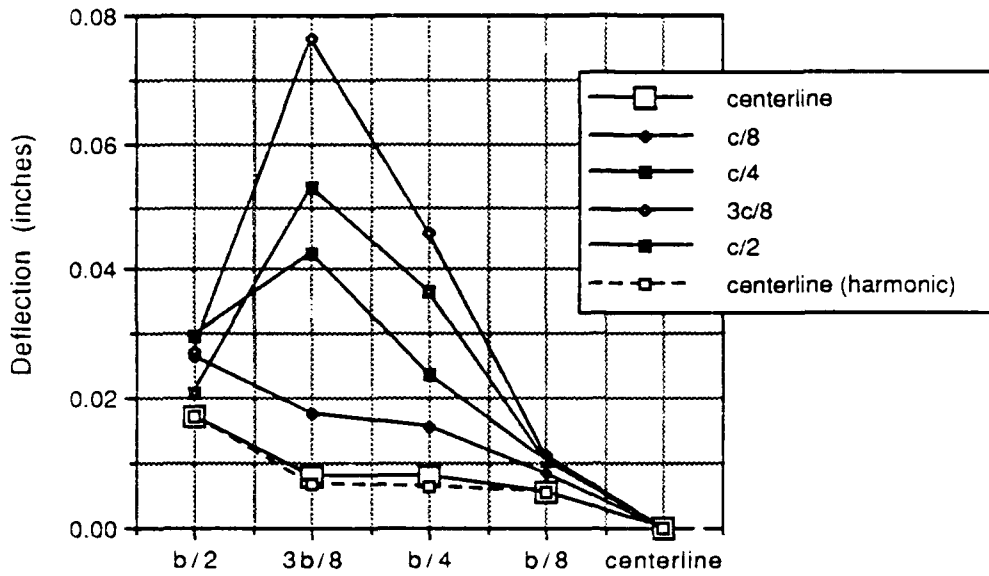


Figure B.25 Mat vertical deflection profile z-axis view (10/1:1/1500/E-C)

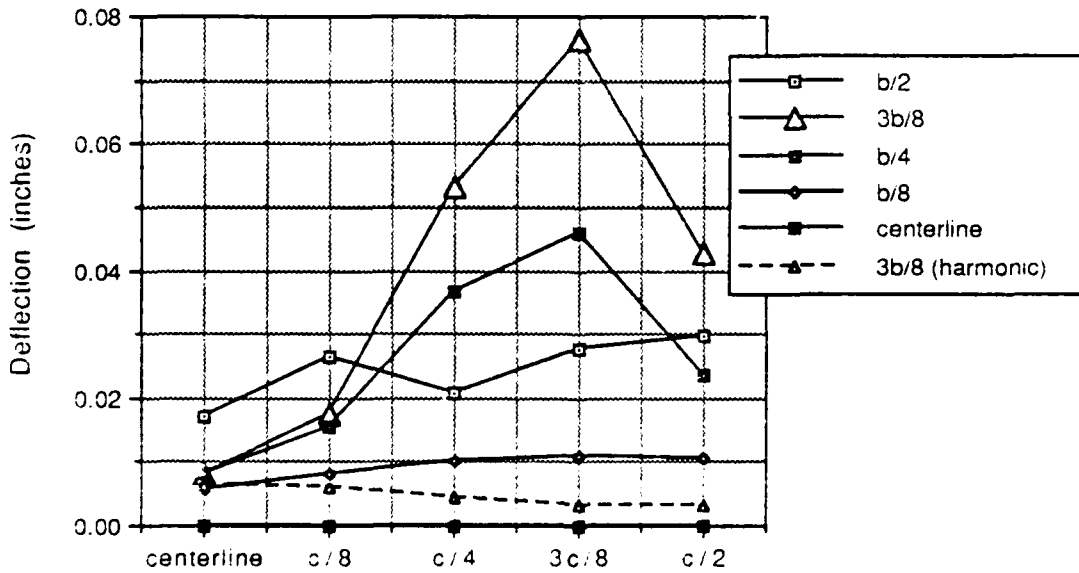


Figure B.26 Mat vertical deflection profile x-axis view (10/1:1/1500/E-C)

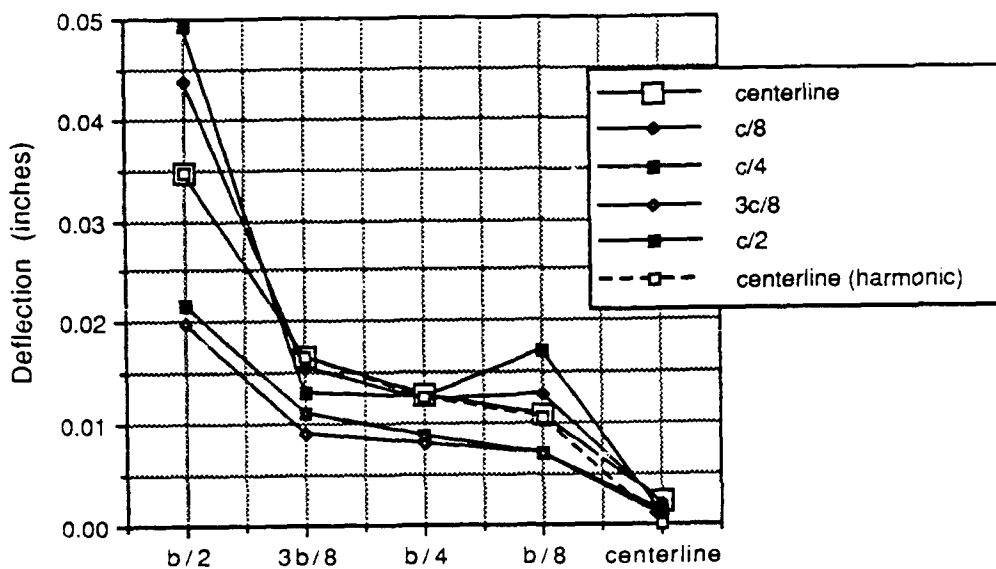


Figure B.27 Mat vertical deflection profile z-axis view (15/1:1/1500/E-C)

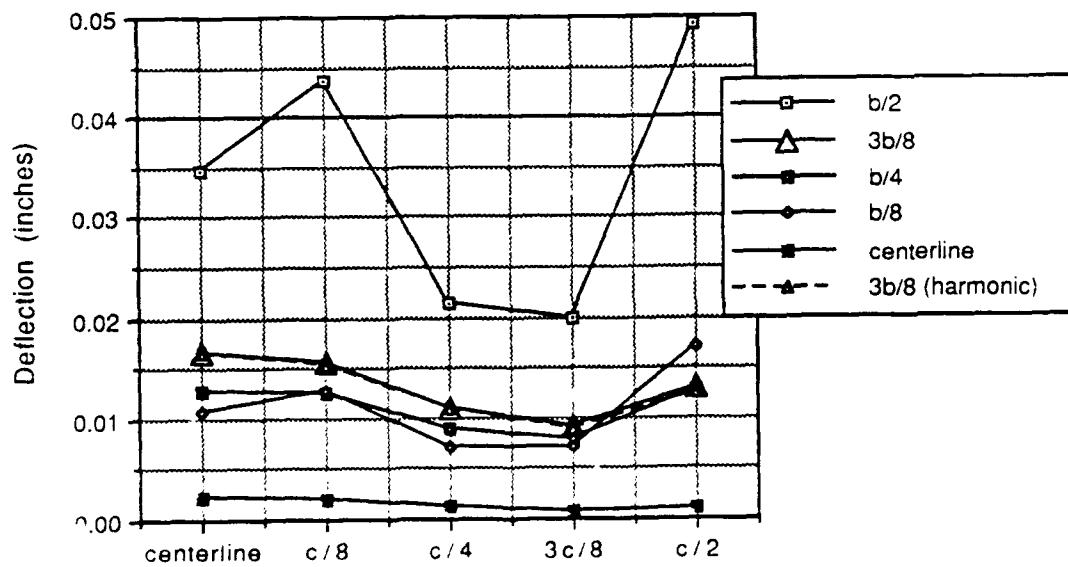


Figure B.28 Mat vertical deflection profile x-axis view (15/1:1/1500/E-C)

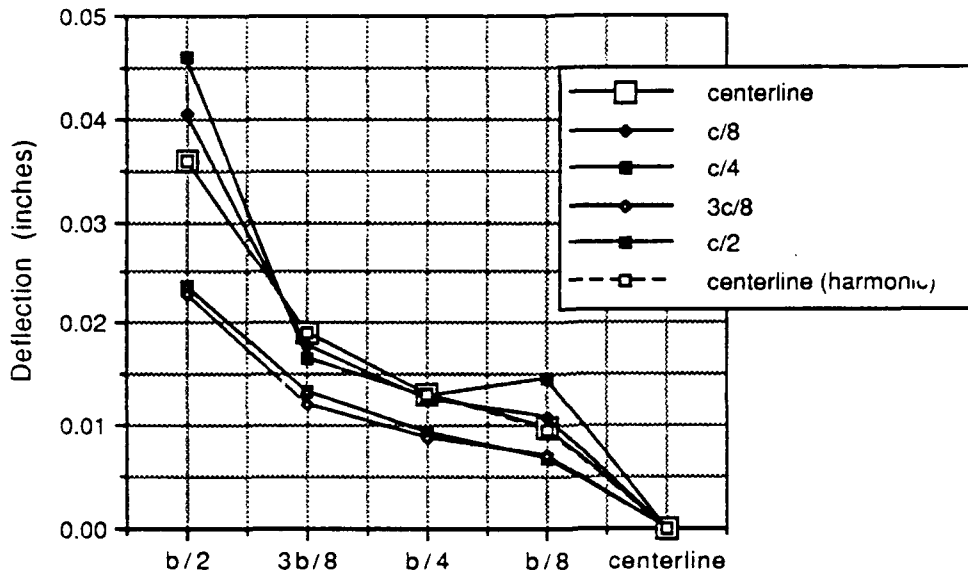


Figure B.29 Mat vertical deflection profile z-axis view (20/1:1/1500/E-C)

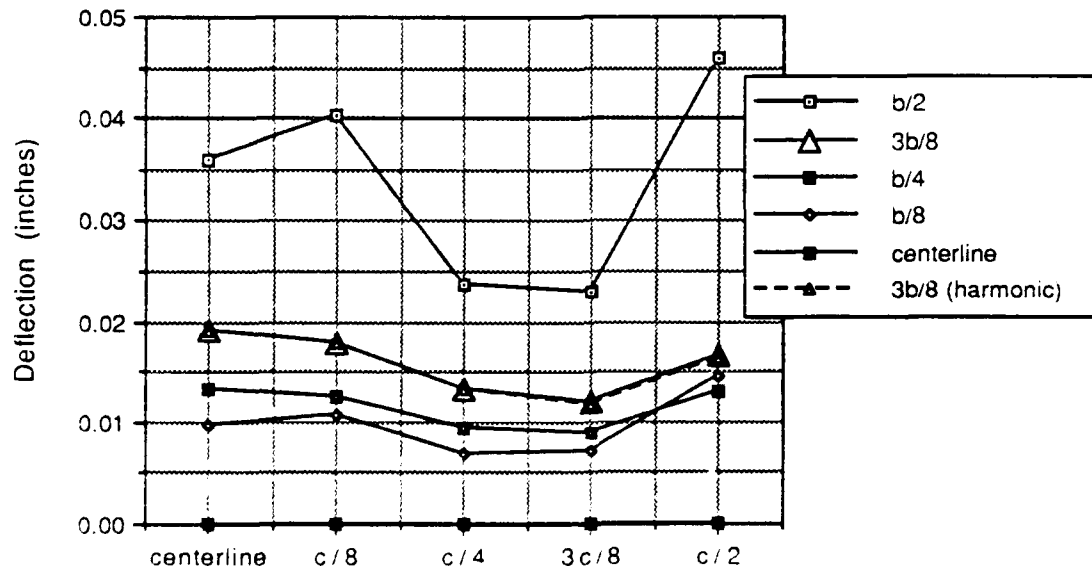


Figure B.30 Mat vertical deflection profile x-axis view (20/1:1/1500/E-C)

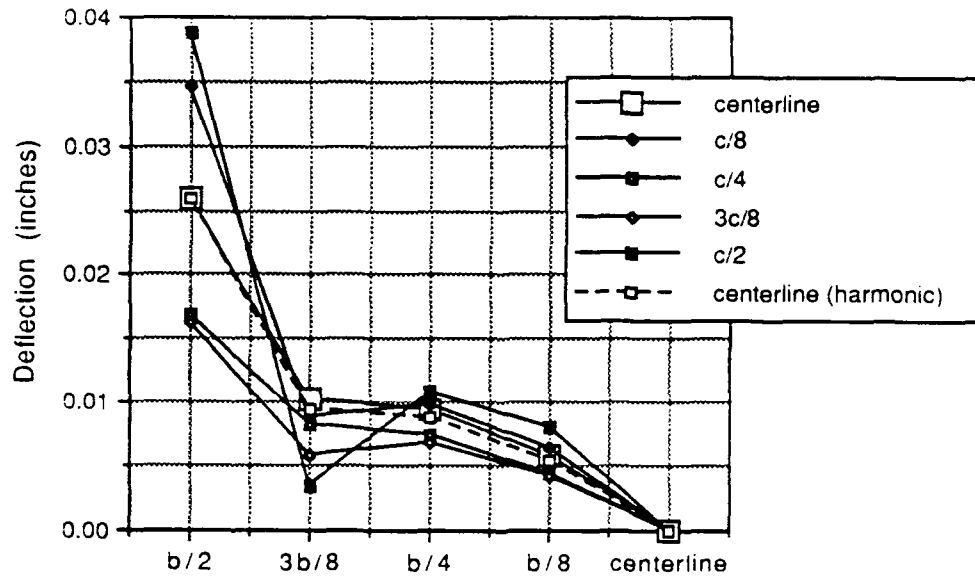


Figure B.31 Mat vertical deflection profile z-axis view (3/1:1/0500/M-C)

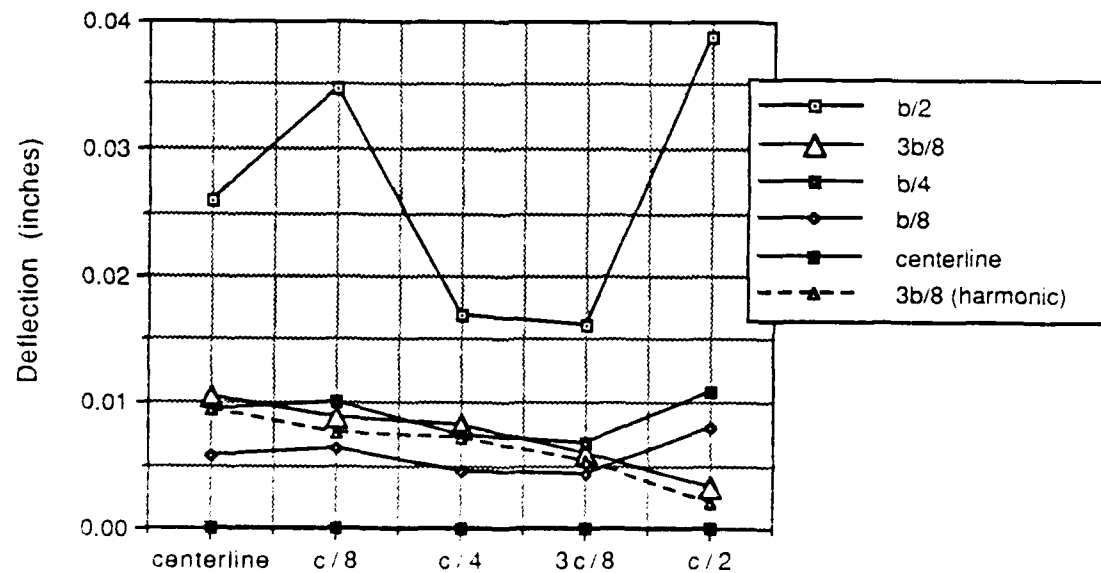


Figure B.32 Mat vertical deflection profile x-axis view (3/1:1/0500/M-C)

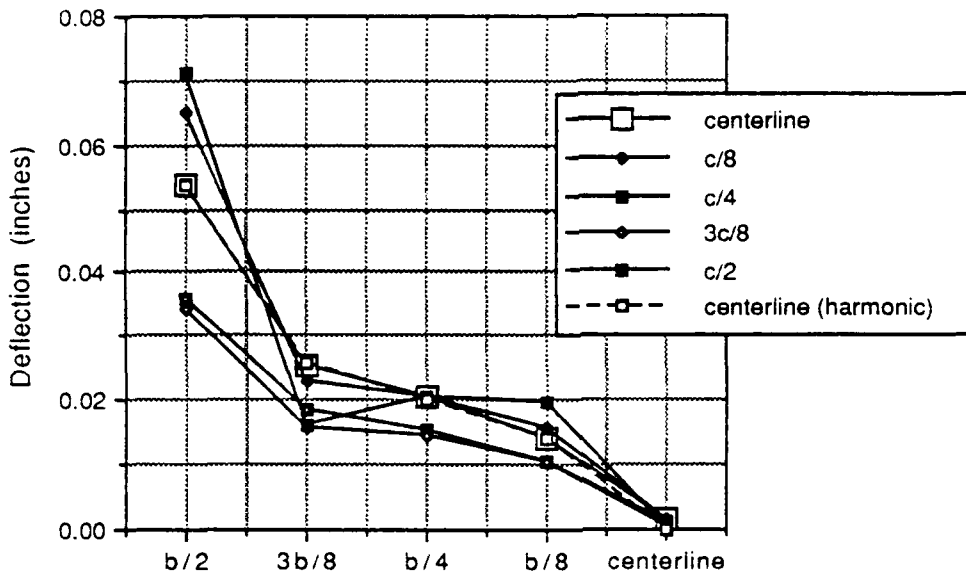


Figure B.33 Mat vertical deflection profile z-axis view (5/1:1/0500/M-C)

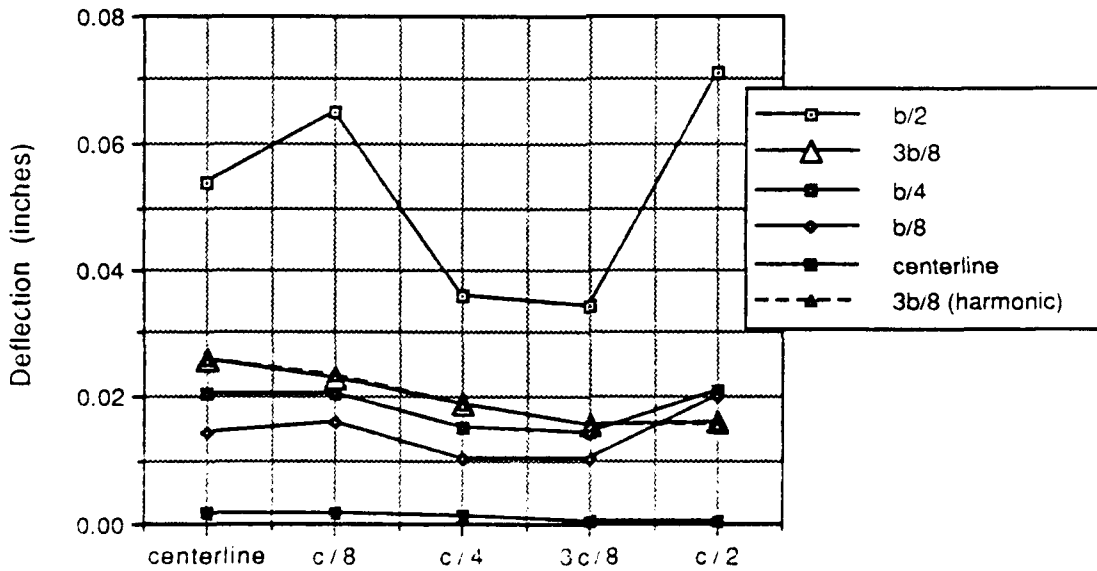


Figure B.34 Mat vertical deflection profile x-axis view (5/1:1/0500/M-C)

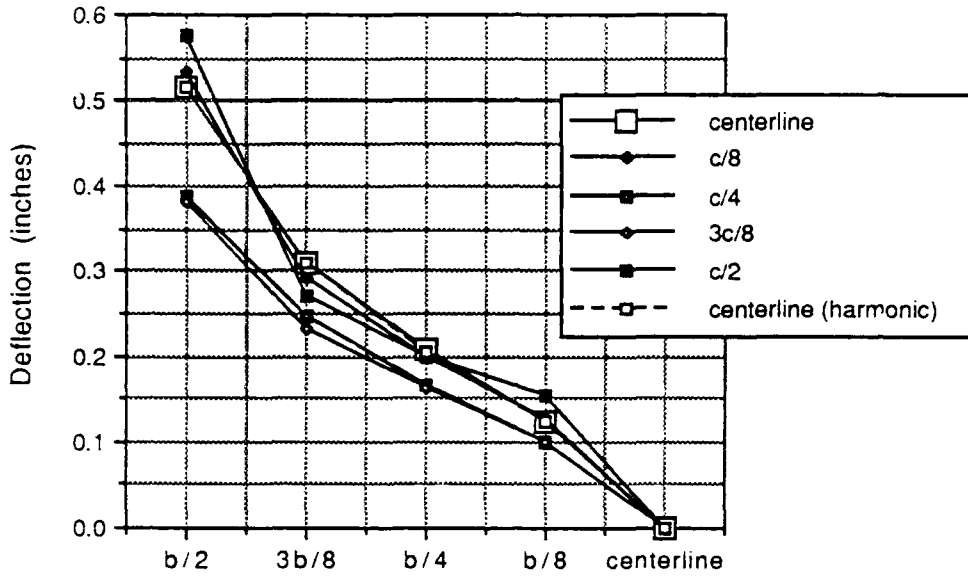


Figure B.35 Mat vertical deflection profile z-axis view (10/1:1/050U/M-C)

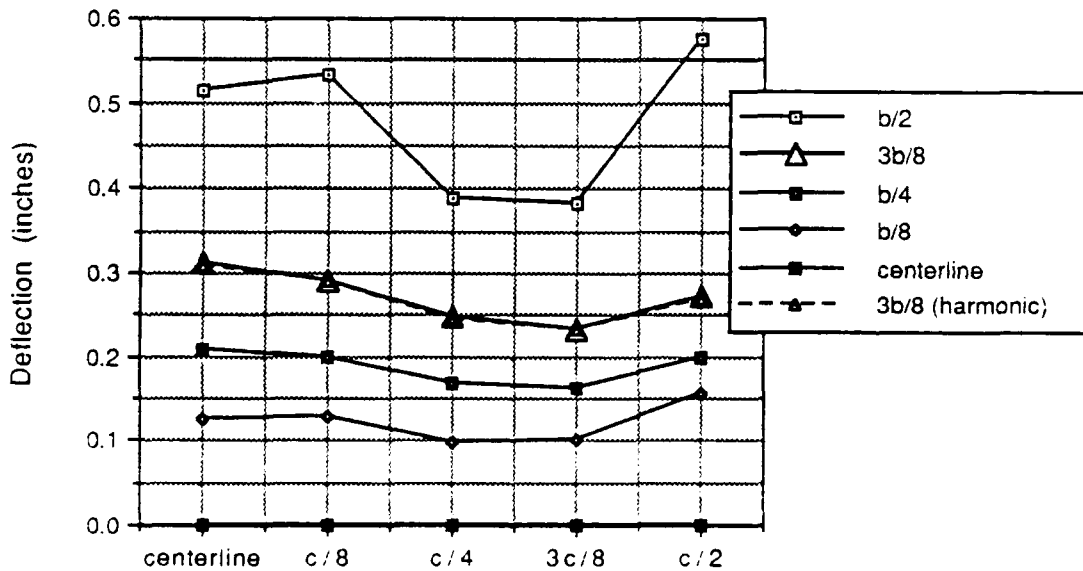


Figure B.36 Mat vertical deflection profile x-axis view (10/1:1/0500/M-C)

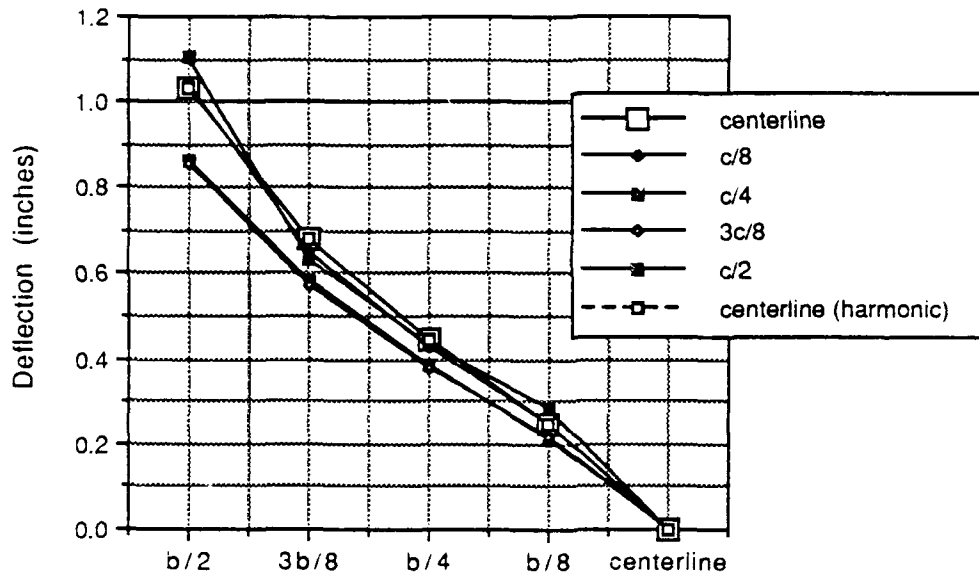


Figure B.37 Mat vertical deflection profile z-axis view (15/1:1/0500/M-C)

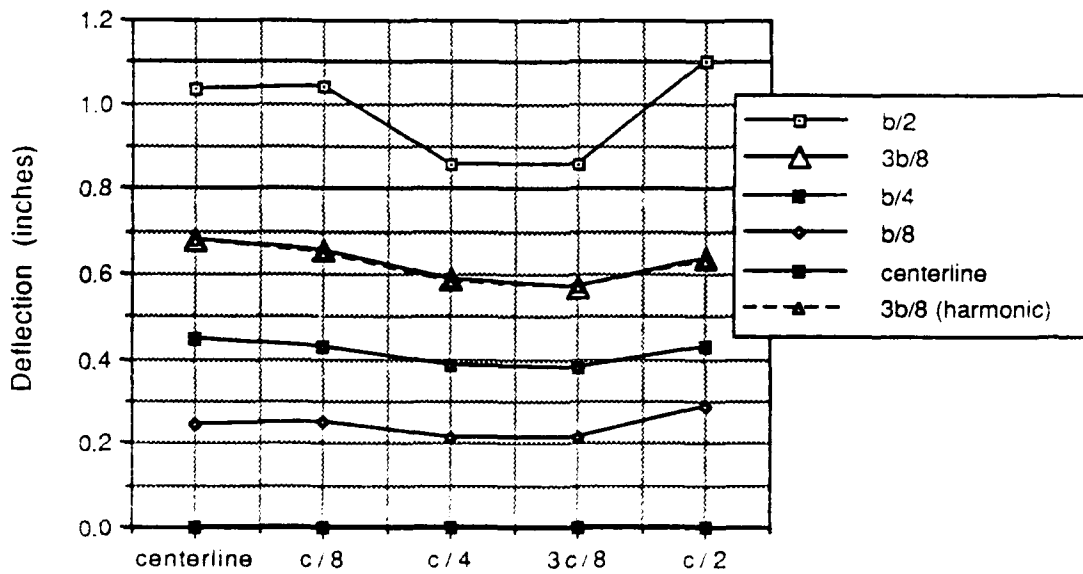


Figure B.38 Mat vertical deflection profile x-axis view (15/1:1/0500/M-C)

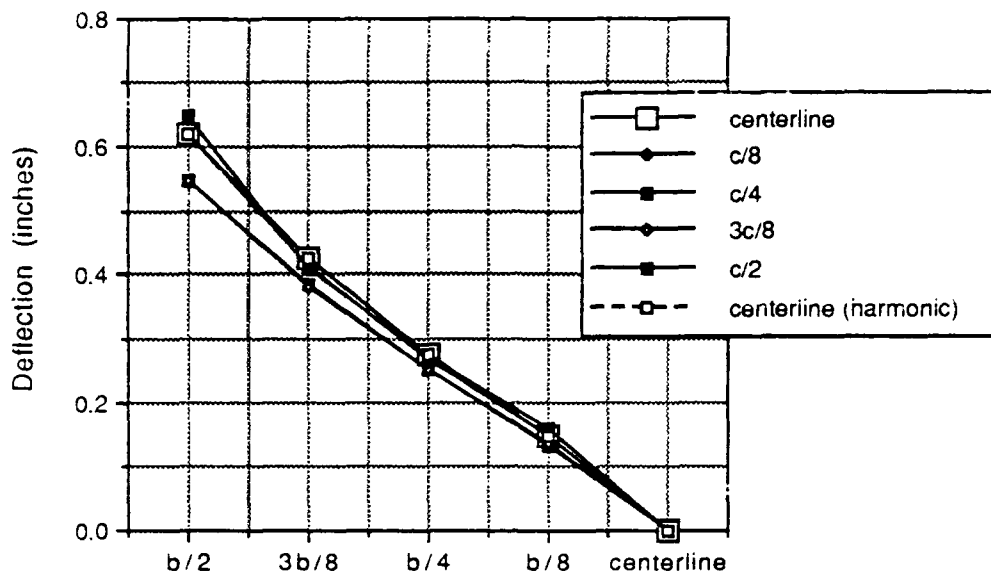


Figure B.39 Mat vertical deflection profile  
z-axis view (20/1:1/0500/M-C)

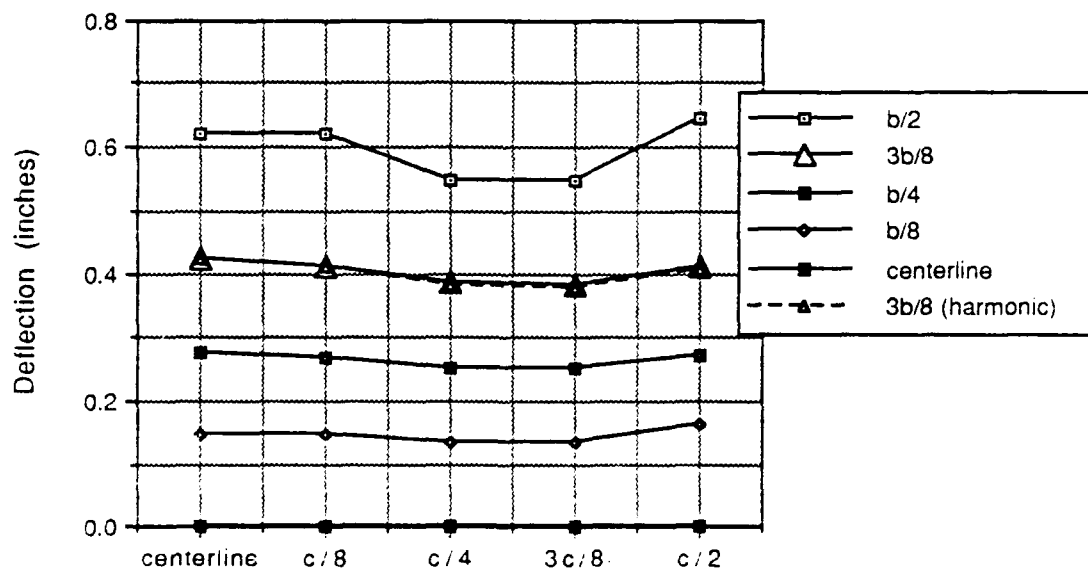


Figure B.40 Mat vertical deflection profile  
x-axis view (20/1:1/0500/M-C)

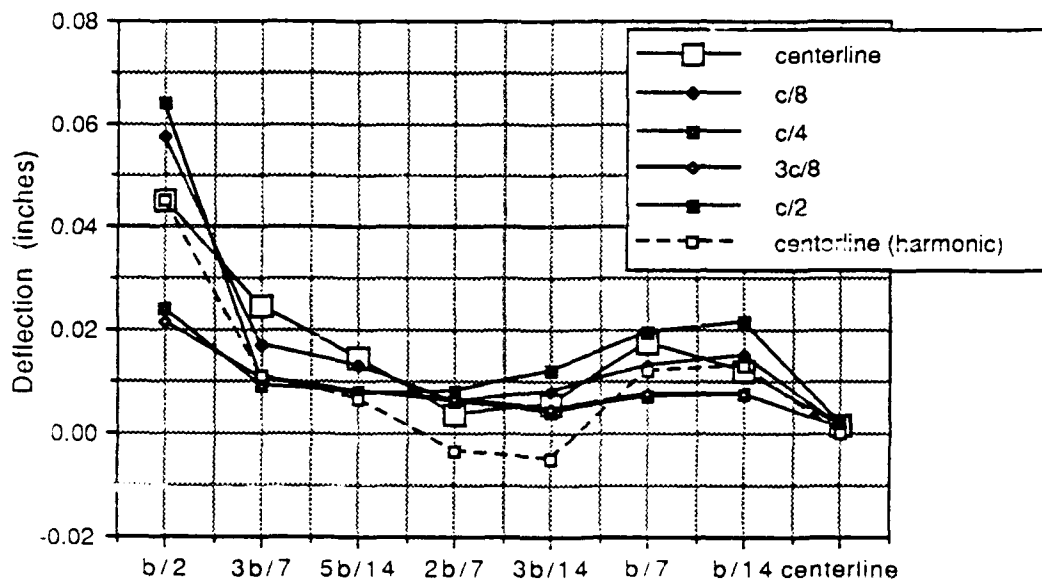


Figure B.41 Mat vertical deflection profile z-axis view (3/1.75:1/0500/E-C)

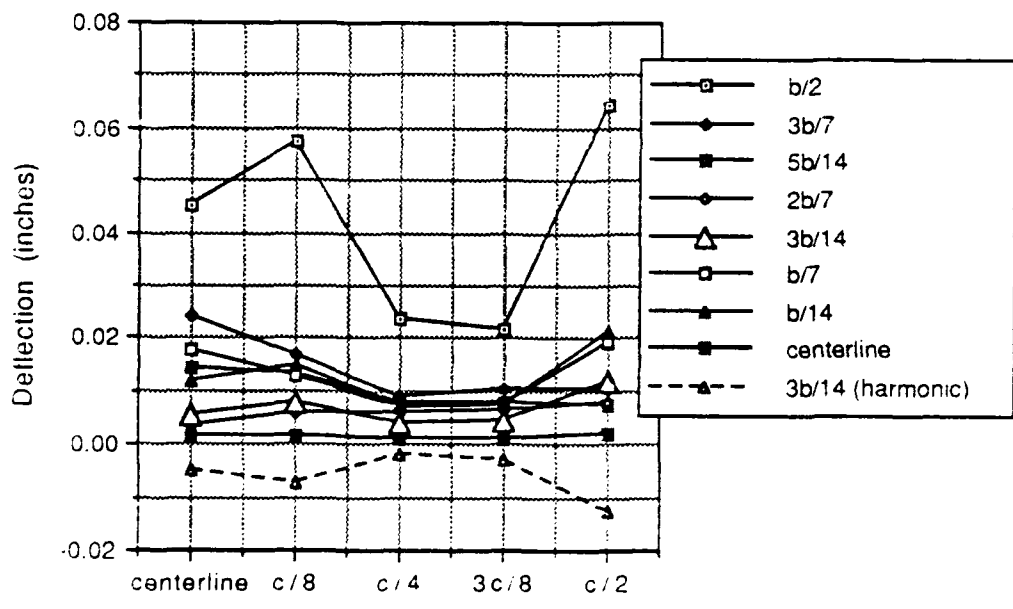


Figure B.42 Mat vertical deflection profile x-axis view (3/1.75:1/0500/E-C)

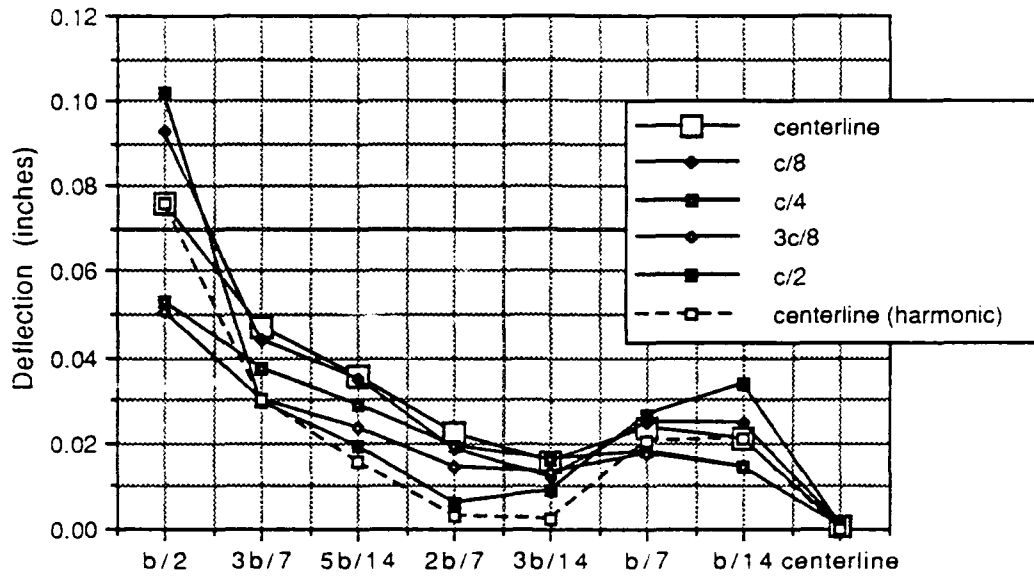


Figure B.43 Mat vertical deflection profile z-axis view (5/1.75:1/0500/E-C)

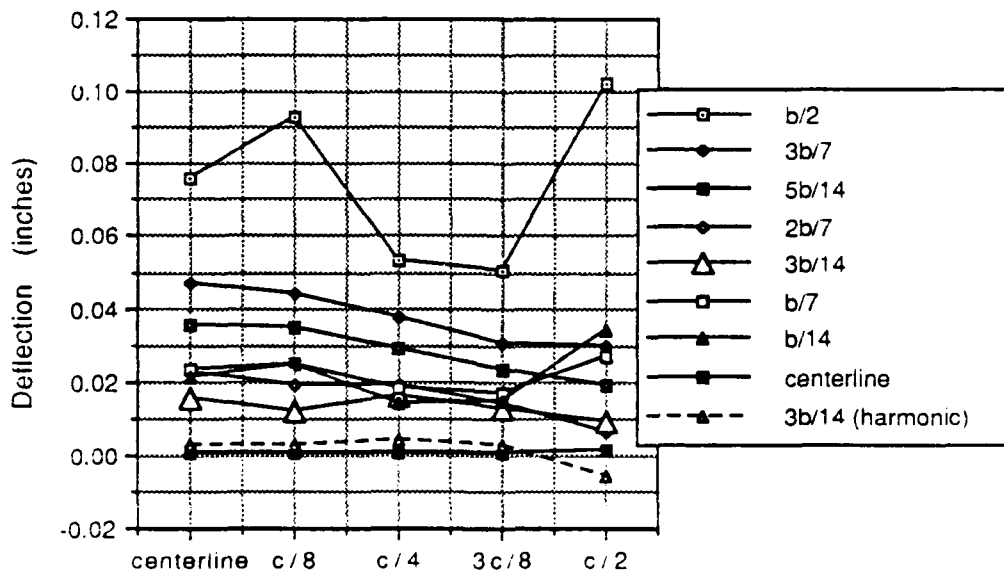


Figure B.44 Mat vertical deflection profile x-axis view (5/1.75:1/0500/E-C)

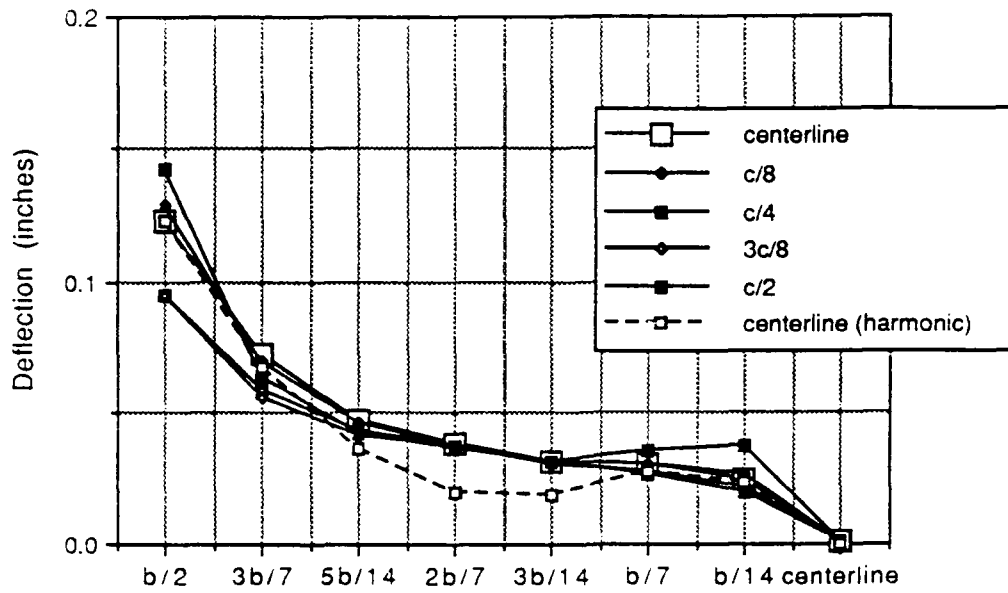


Figure B.45 Mat vertical deflection profile z-axis view (10/1.75:1/0500/E-C)

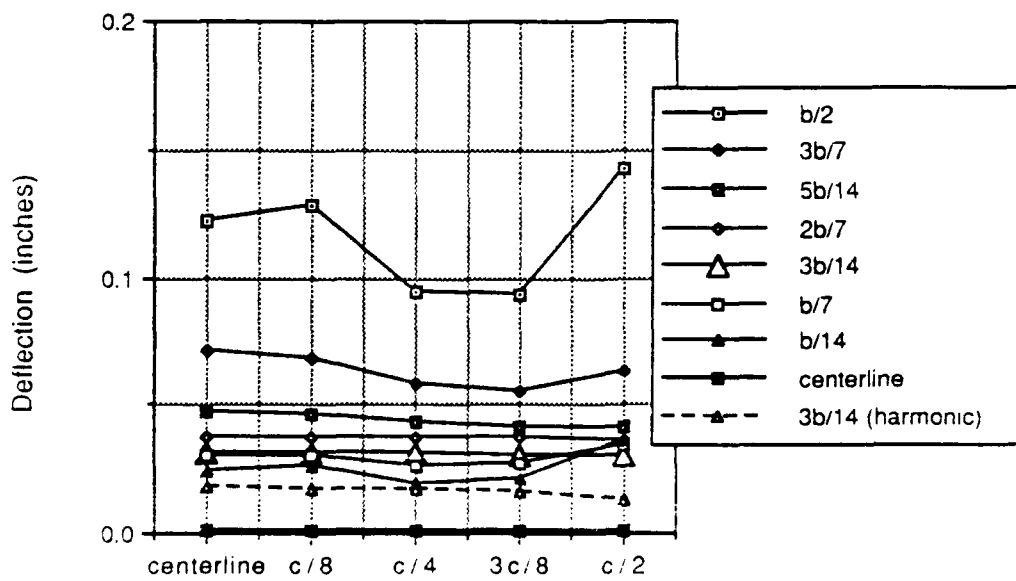


Figure B.46 Mat vertical deflection profile x-axis view (10/1.75:1/0500/E-C)

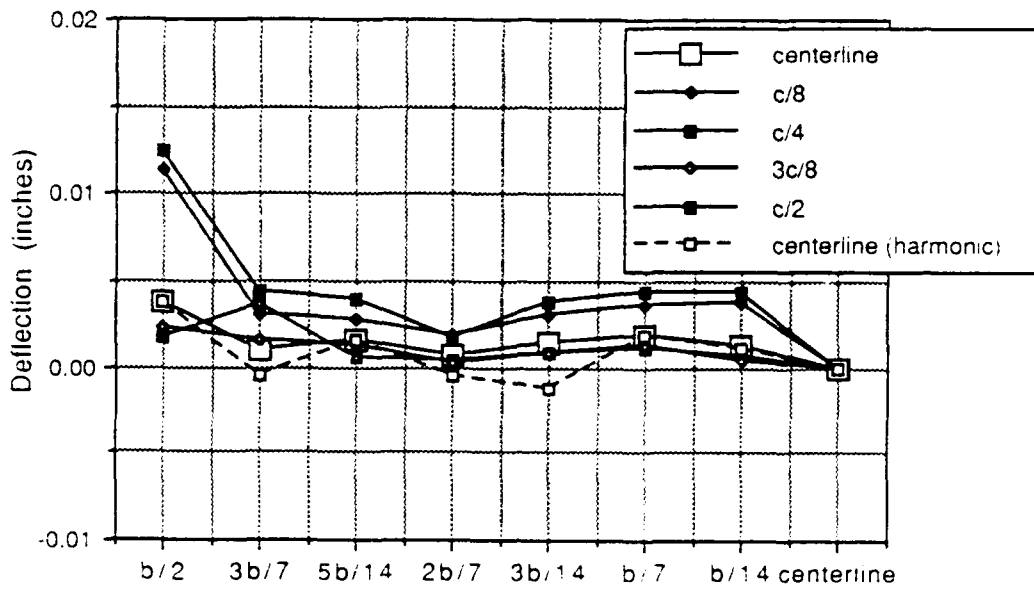


Figure B.47 Mat vertical deflection profile z-axis view (3/1.75:1/1500/E-C)

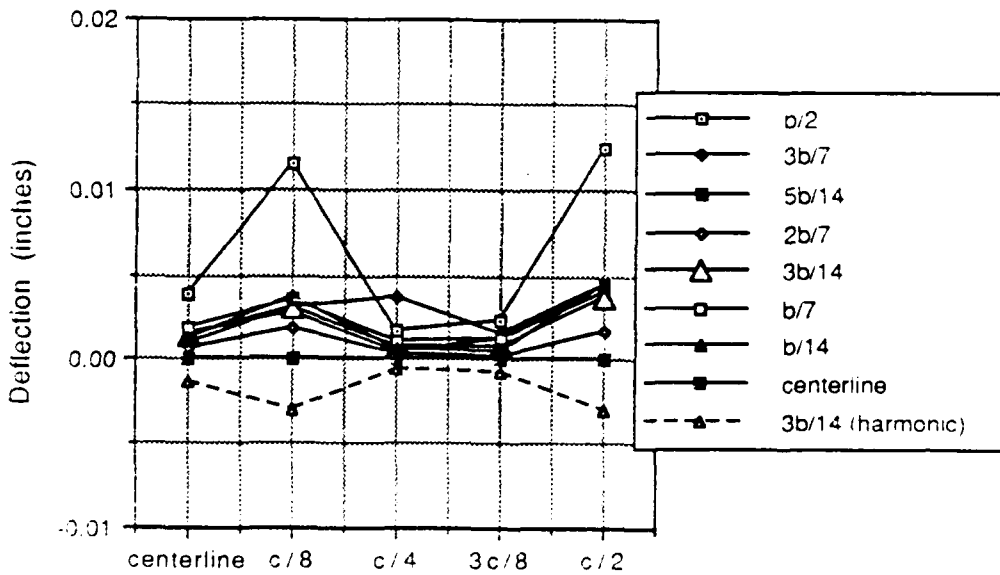


Figure B.48 Mat vertical deflection profile x-axis view (3/1.75:1/1500/E-C)

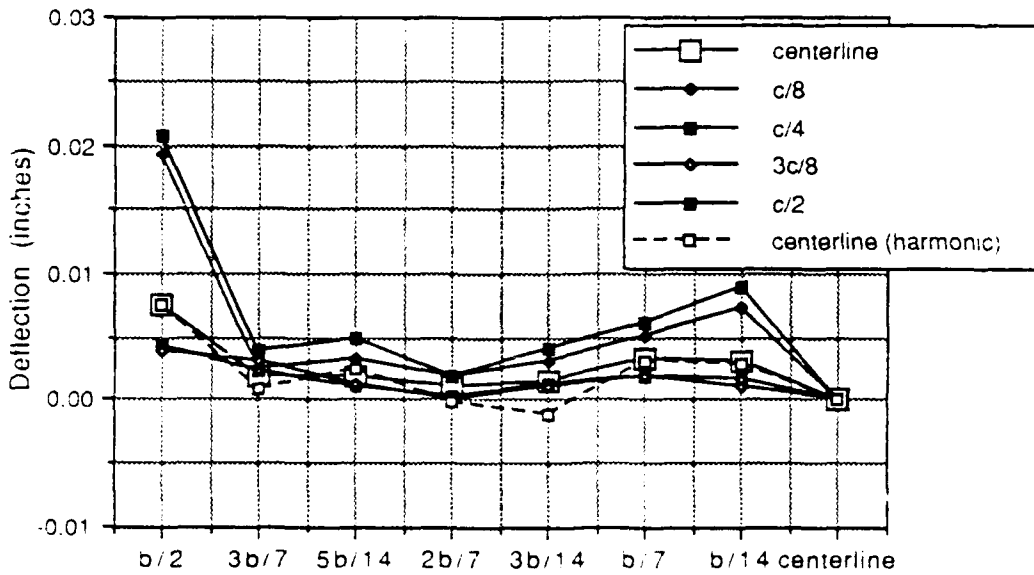


Figure B.49 Mat vertical deflection profile  
z-axis view (5/1.75:1/1500/E-C)

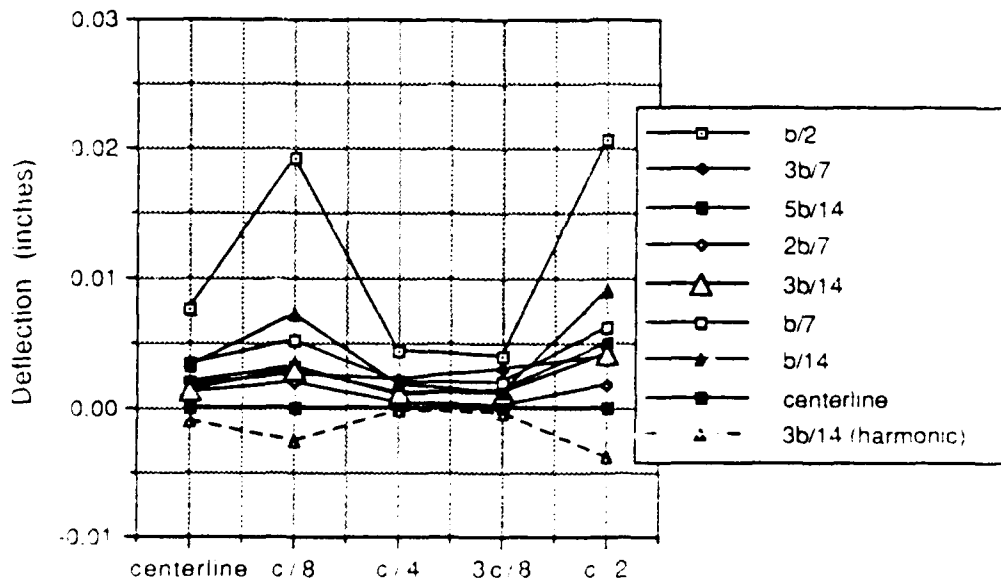


Figure B.50 Mat vertical deflection profile  
x-axis view (5/1.75:1/1500/E-C)

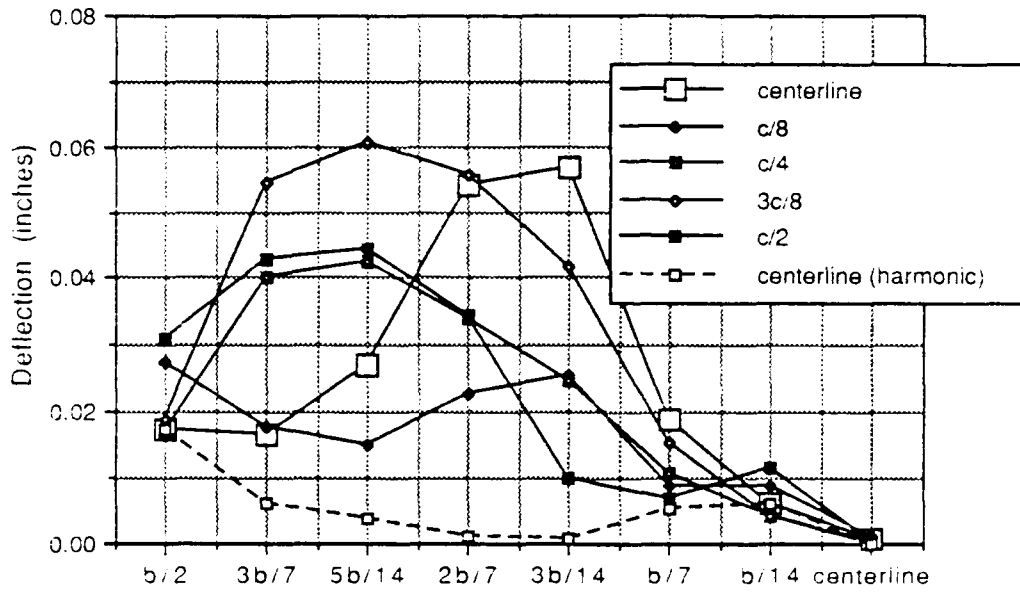


Figure B.51 Mat vertical deflection profile z-axis view (10/1.75:1/1500/E-C)

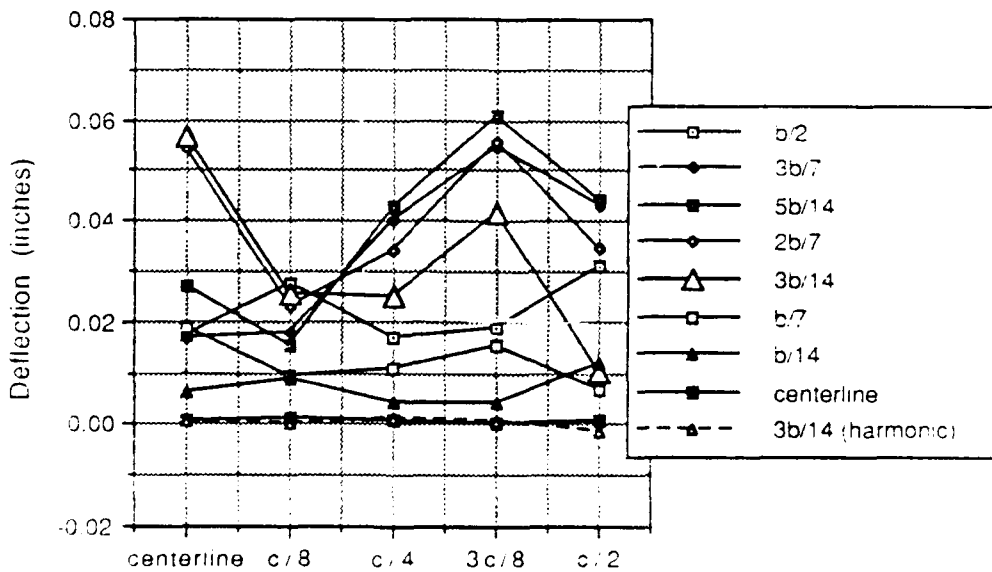


Figure B.52 Mat vertical deflection profile x-axis view (10/1.75:1/1500/E-C)

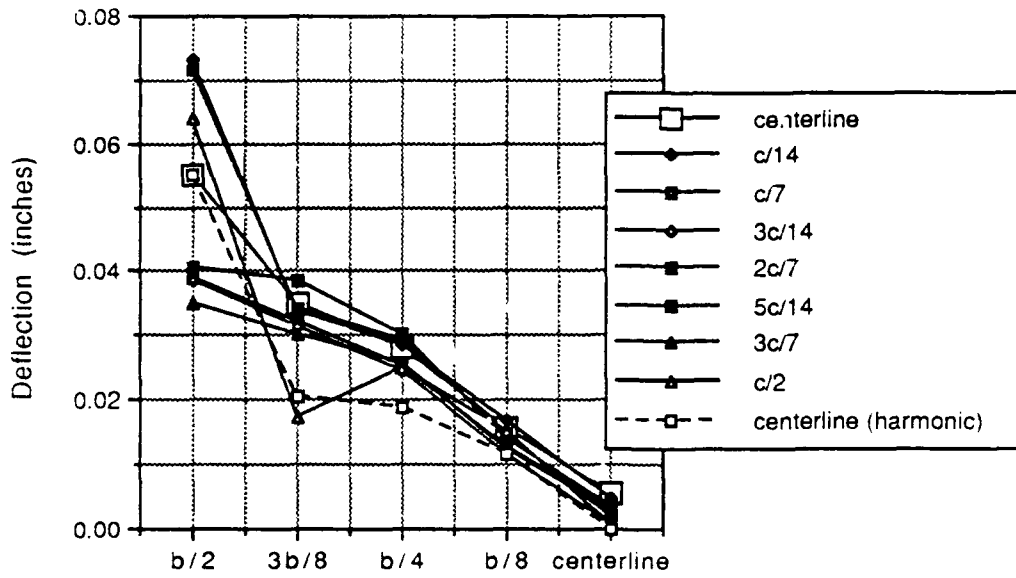


Figure B.53 Mat vertical deflection profile  
z-axis view (3/1:1.75/0500/E-C)

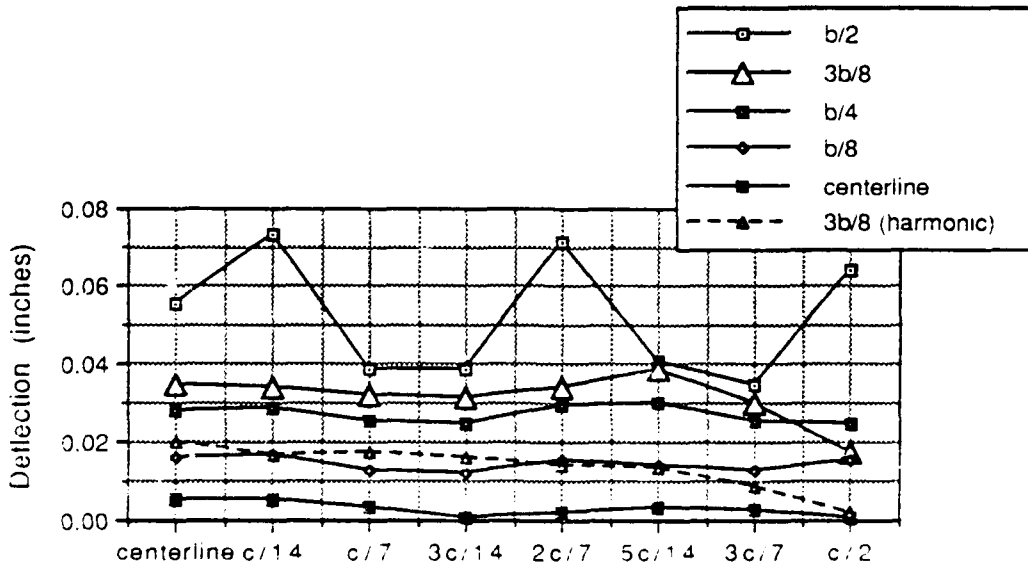


Figure B.54 Mat vertical deflection profile  
x-axis view (3/1:1.75/0500/E-C)

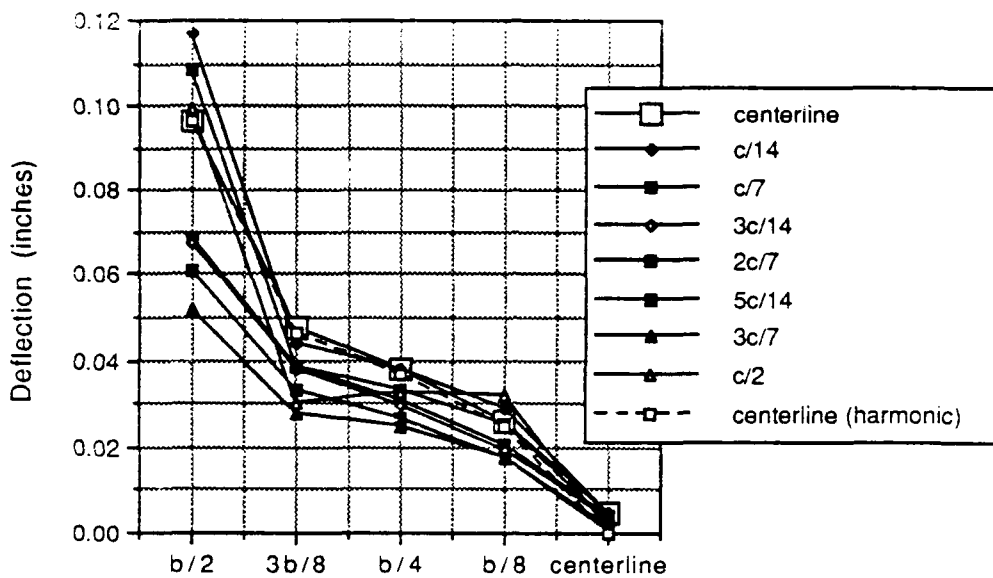


Figure B.55 Mat vertical deflection profile z-axis view (5/1:1.75/0500/E-C)

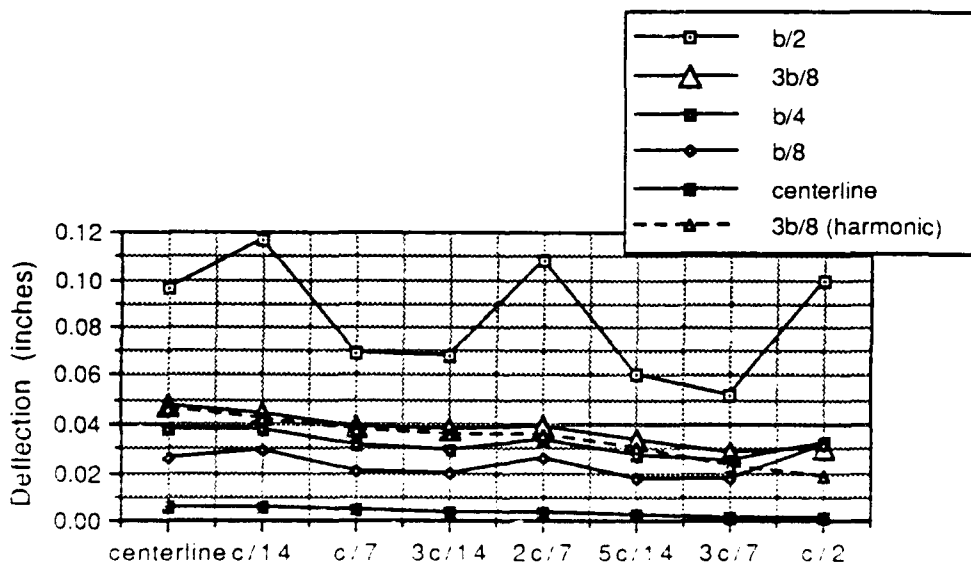


Figure B.56 Mat vertical deflection profile x-axis view (5/1:1.75/0500/E-C)

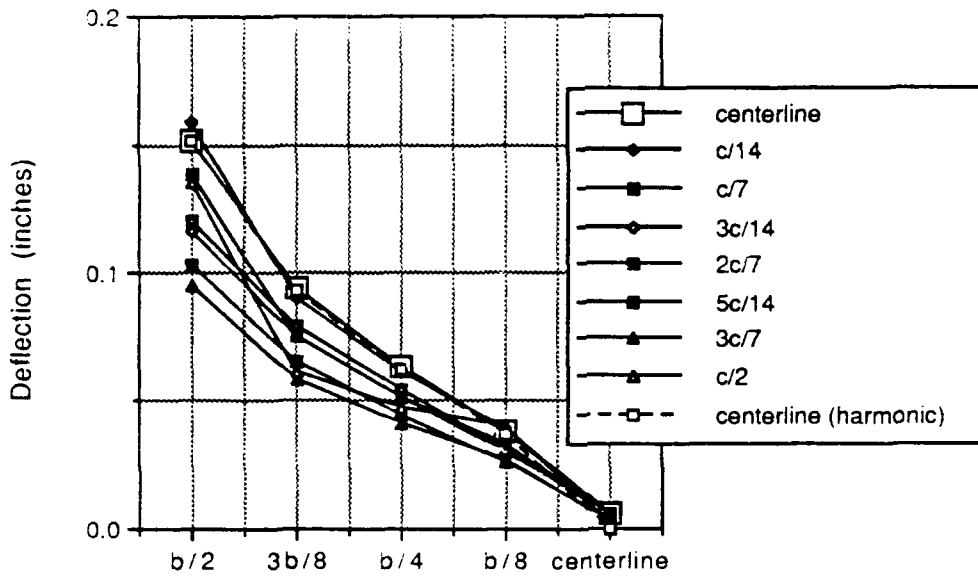


Figure B.57 Mat vertical deflection profile  
z-axis view (10/1:1.75/0500/E-C)

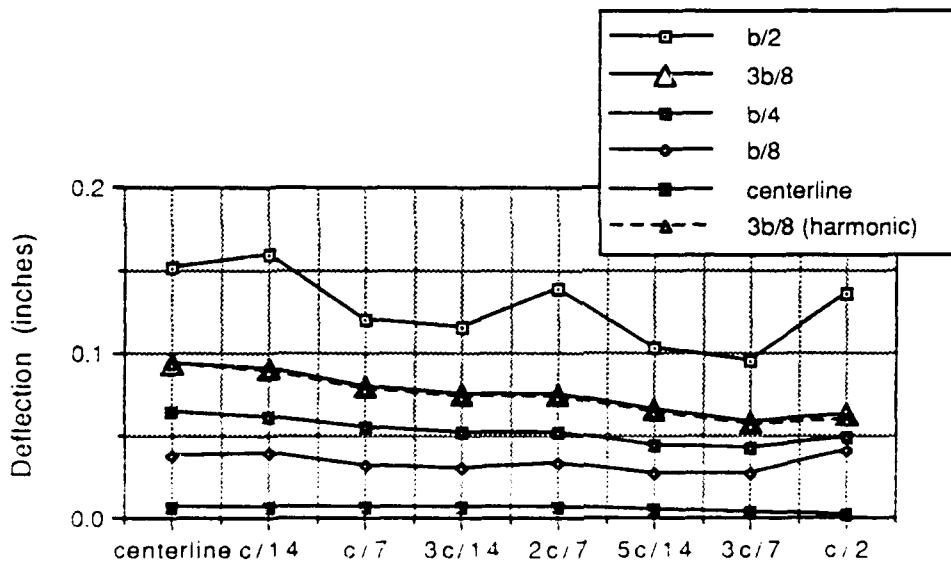


Figure B.58 Mat vertical deflection profile  
x-axis view (10/1:1.75/0500/E-C)

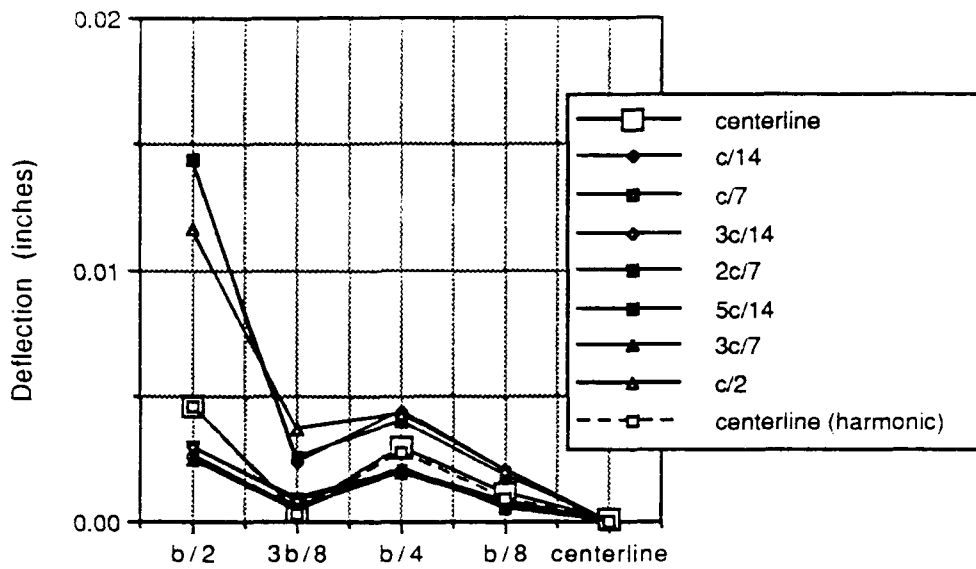


Figure B.59 Mat vertical deflection profile  
z-axis view (3/1:1.75/1500/E-C)

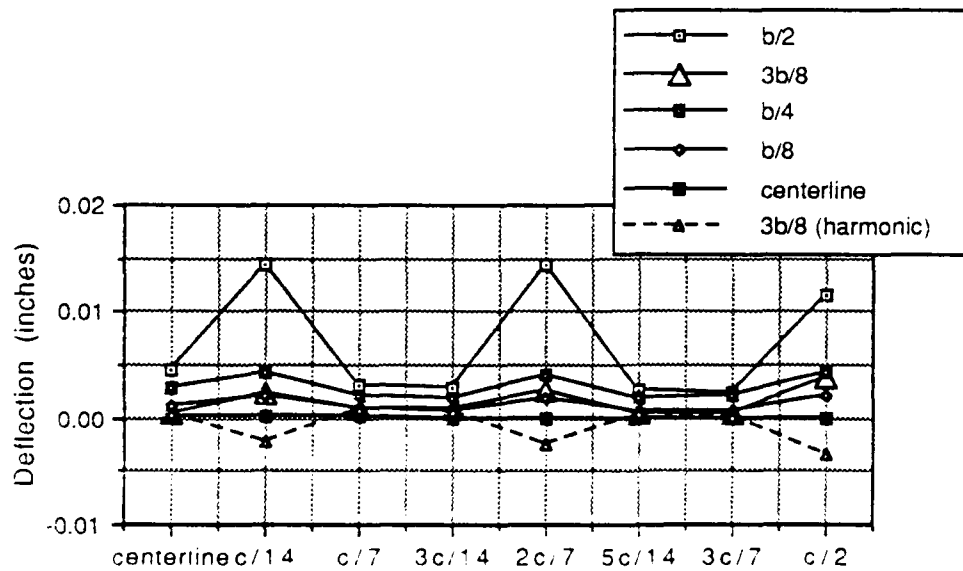


Figure B.60 Mat vertical deflection profile  
x-axis view (3/1:1.75/1500/E-C)

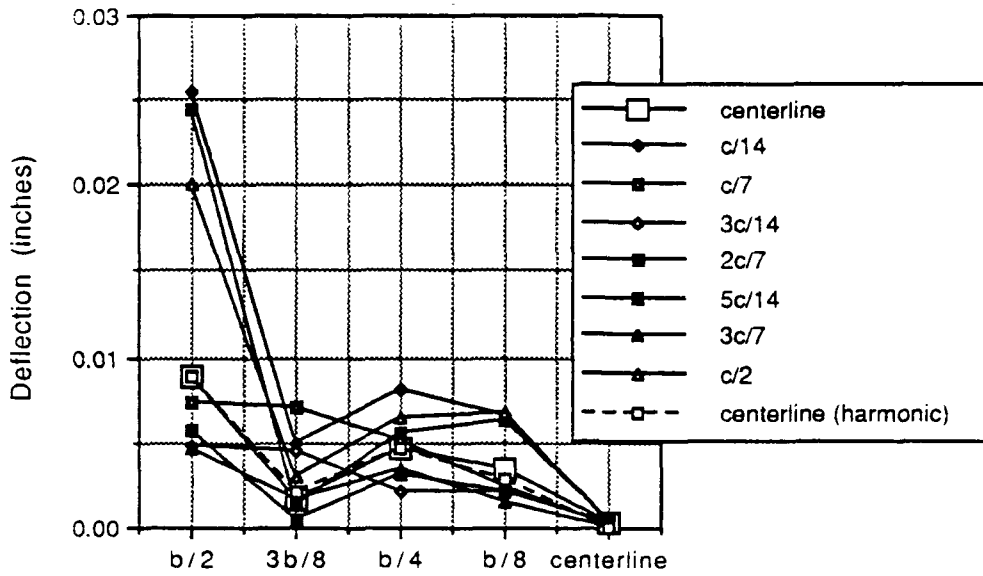


Figure B.61 Mat vertical deflection profile  
z-axis view (5/1:1.75/1500/E-C)

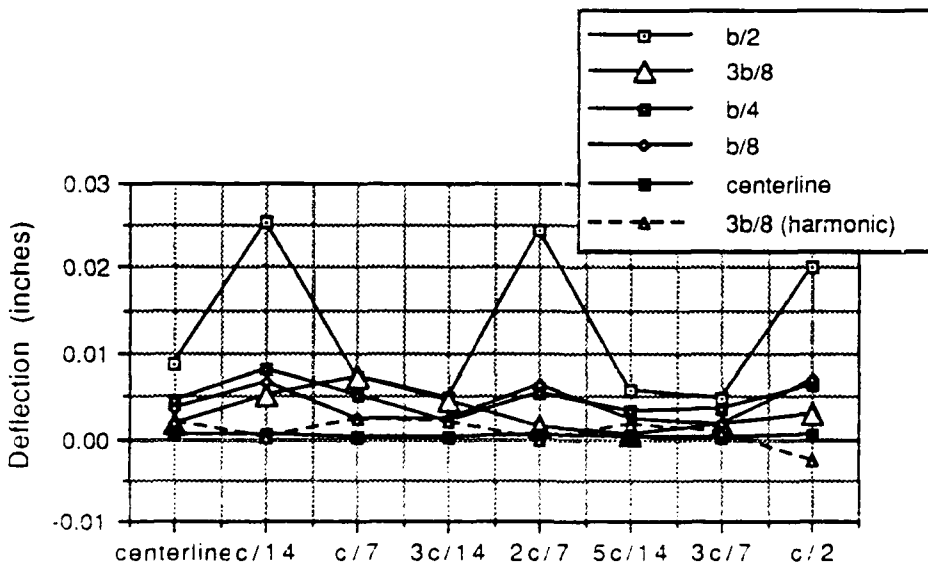


Figure B.62 Mat vertical deflection profile  
x-axis view (5/1:1.75/1500/E-C)

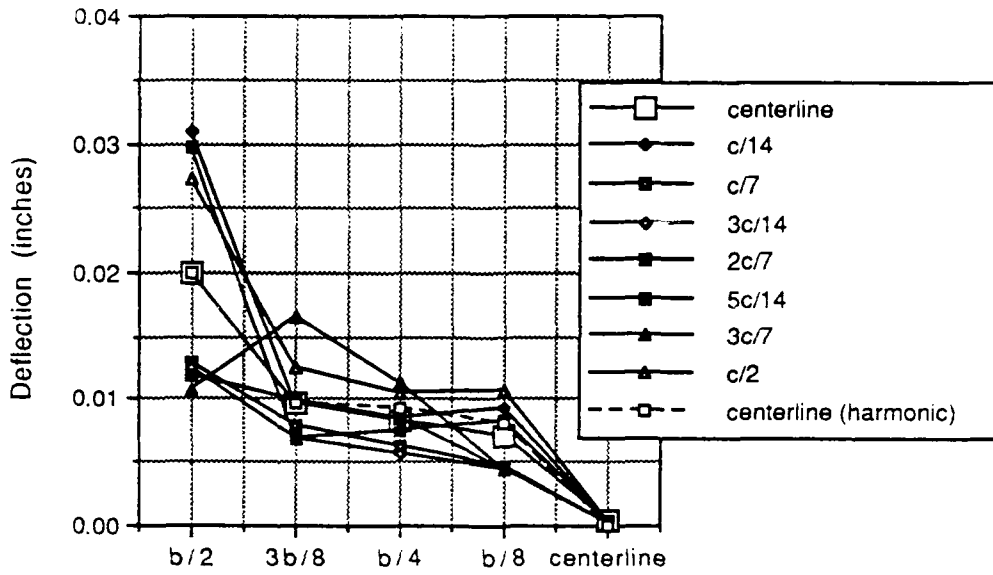


Figure B.63 Mat vertical deflection profile z-axis view (10/1:1.75/1500/E-C)

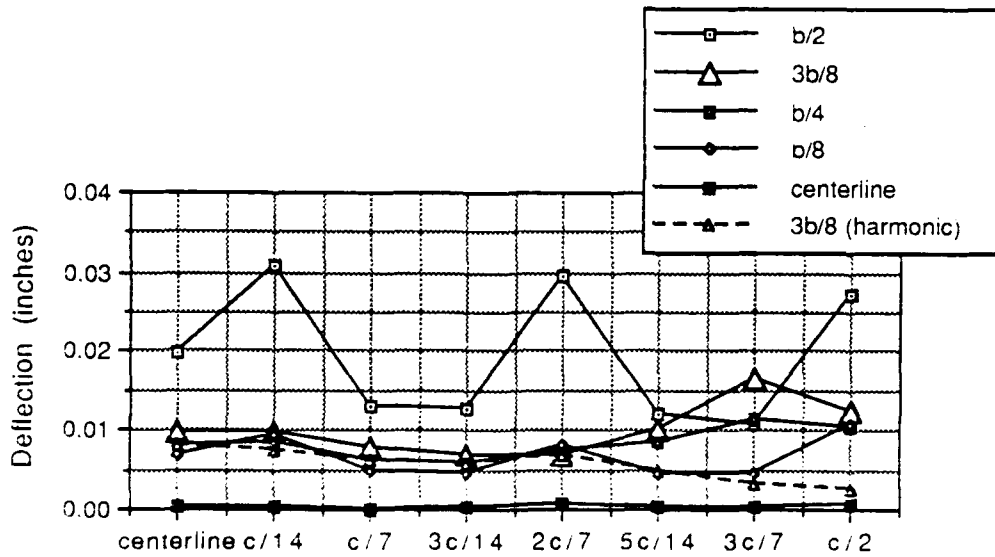


Figure B.64 Mat vertical deflection profile x-axis view (10/1:1.75/1500/E-C)

## APPENDIX C

### EQUIVALENT SOIL SPRING STIFFNESS

This appendix summaries equivalent soil spring stiffness profiles for selected calculations on the softest and hardest soils studied ( $v_s = 500$  fps and 1500 fps). All frames are doubly symmetric, and soil springs are displayed in two views for one quadrant of the uplifted half of the mat. These space frames were loaded in the x-direction and therefore rock about the z-axis with the coordinate origin located at the mat center.

Legend notes:

The mat dimensions in the x and z directions are designated **b** and **c**. Solid line graphs display results of earthquake loadings. No springs are computed at the axis of rocking.

Series nomenclature:

**(N/X:Z/kkkk/E-Q{x,z})**

**N** equals number of frame floors

**X:Z** equals floor plan ratio of dimensions in x and z directions (load applied in x direction)

**kkkk** equals soil shear wave velocity in feet/sec

**E-Q** implies earthquake (E-C for El Centro and M-C for Mexico City)

**{x,z}** vector identifying the horizontal direction of earthquake loading

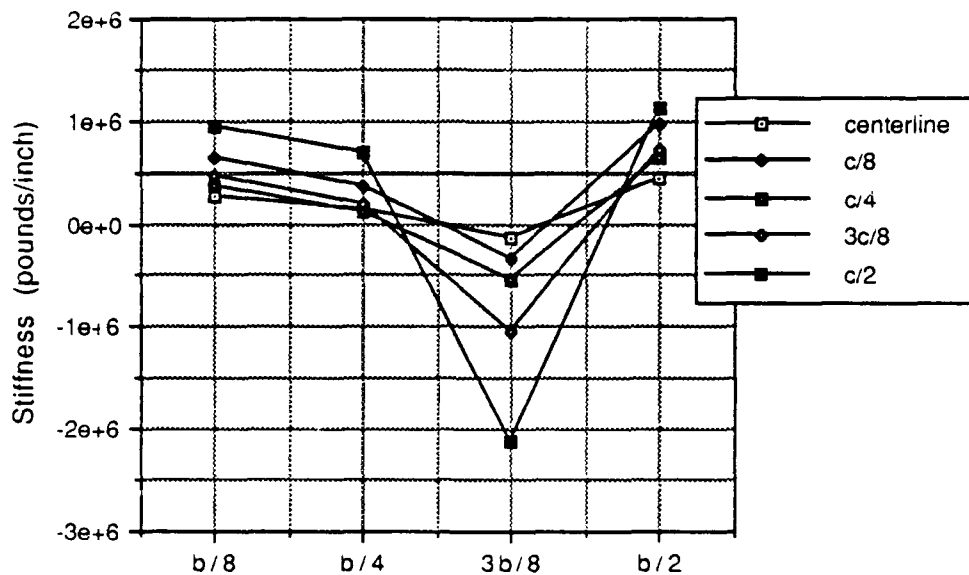


Figure C.1 Equivalent soil spring stiffness z-axis view (3/1:1/0500)

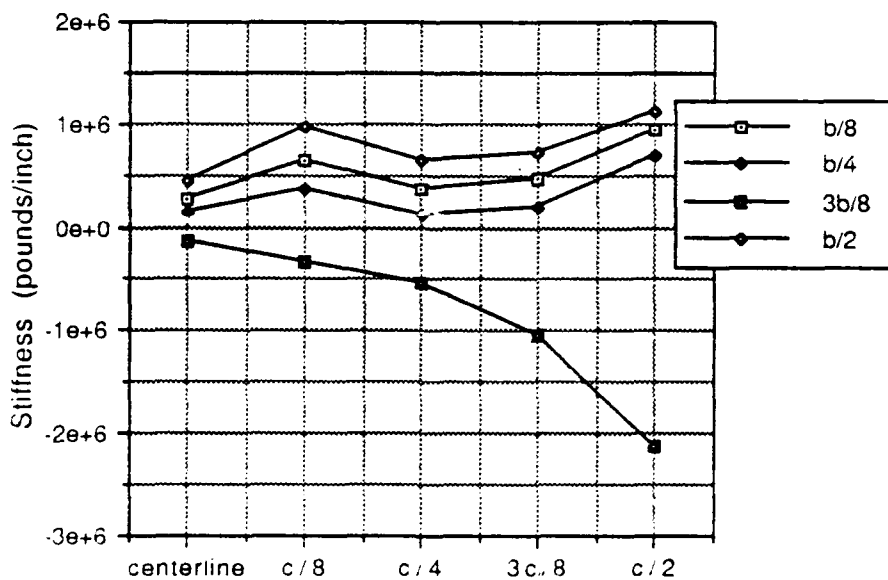


Figure C.2 Equivalent soil spring stiffness x-axis view (3/1:1/0500)

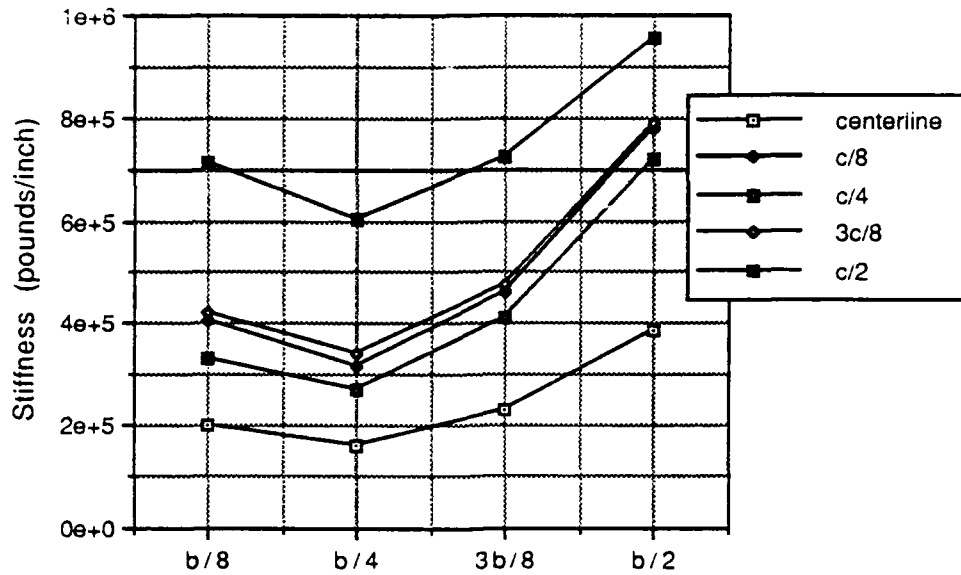


Figure C.3 Equivalent soil spring stiffness  
z-axis view (20/1:1/0500)

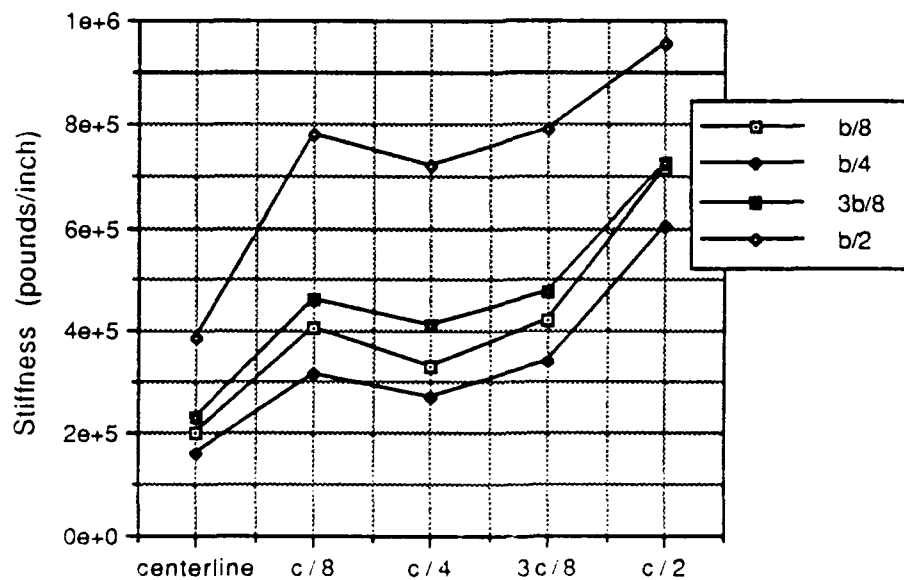


Figure C.4 Equivalent soil spring stiffness  
x-axis view (20/1:1/0500)

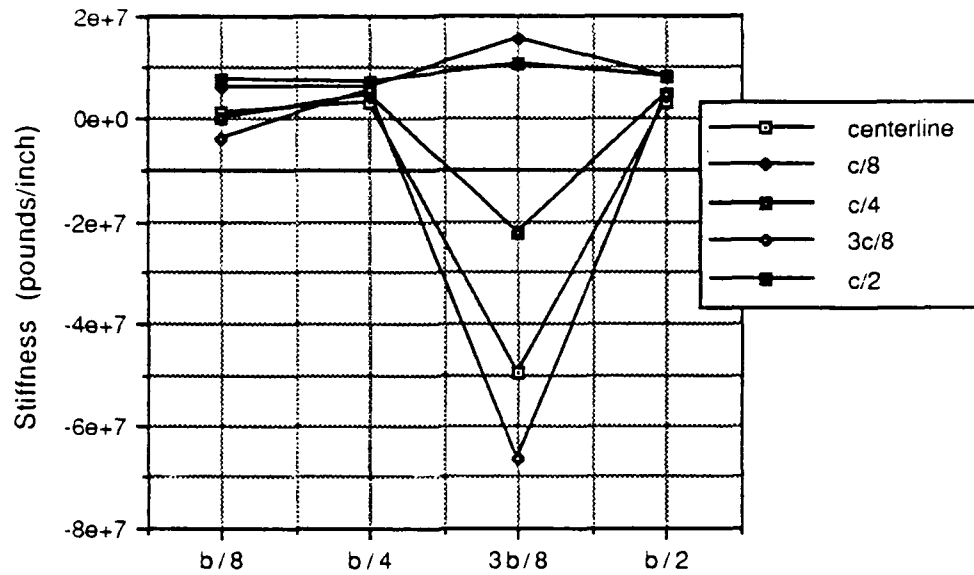


Figure C.5 Equivalent soil spring stiffness  
z-axis view (3/1:1/1500)

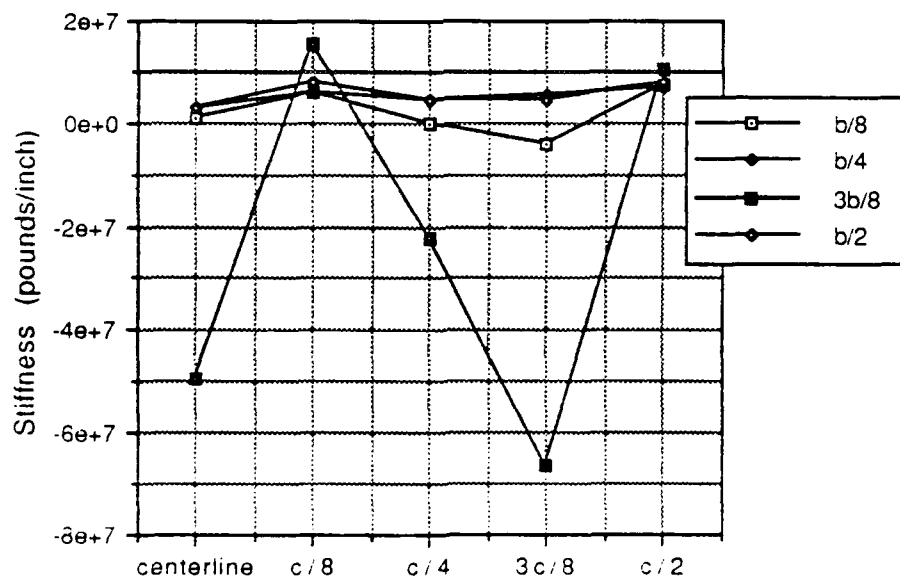


Figure C.6 Equivalent soil spring stiffness  
x-axis view (3/1:1/1500)

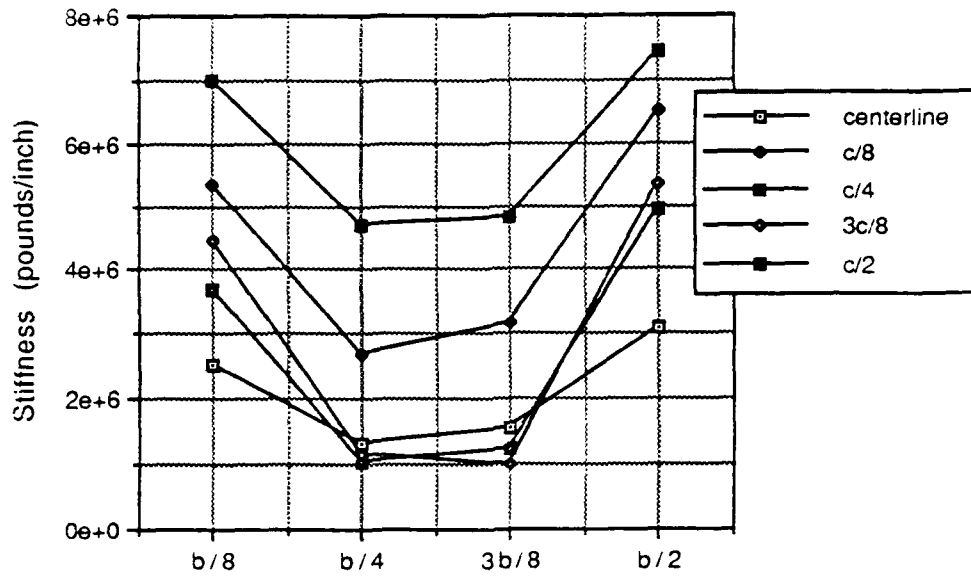


Figure C.7 Equivalent soil spring stiffness  
z-axis view (20/1:1/1500)

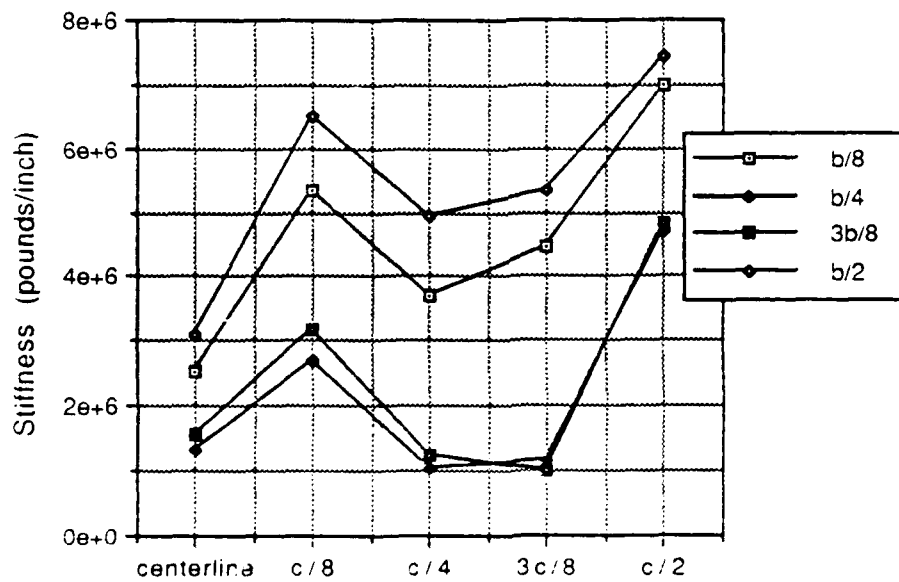


Figure C.8 Equivalent soil spring stiffness  
x-axis view (20/1:1/1500)

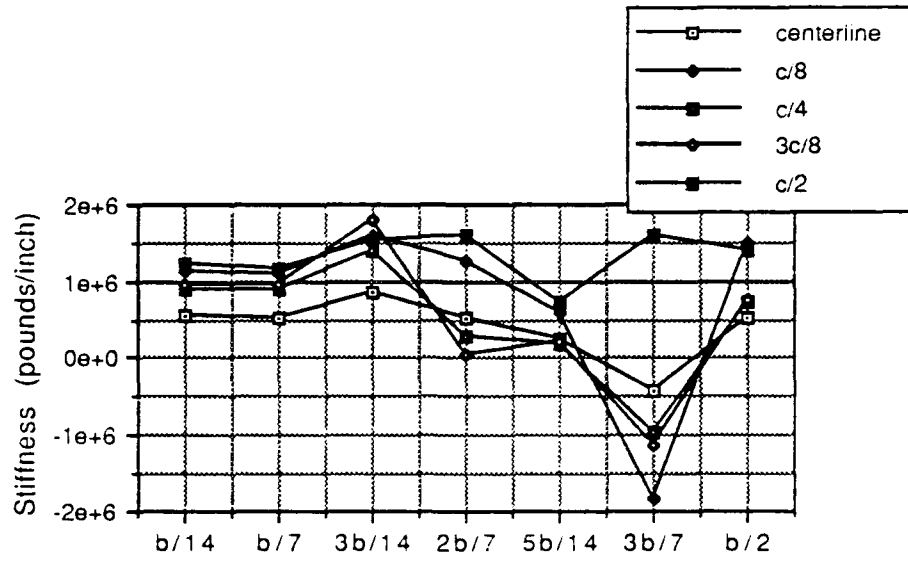


Figure C.9 Equivalent soil spring stiffness z-axis view (3/1.75:1/0500)

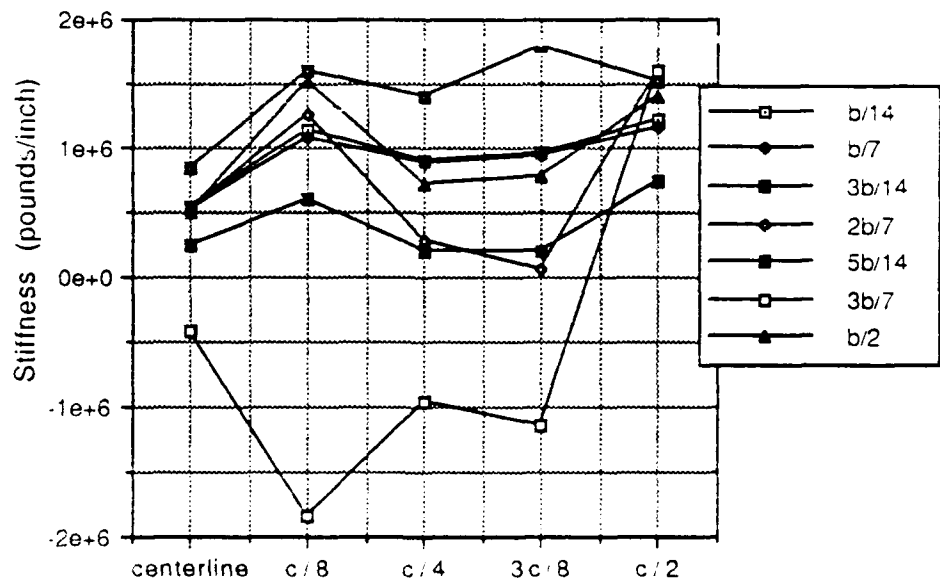


Figure C.10 Equivalent soil spring stiffness x-axis view (3/1.75:1/0500)

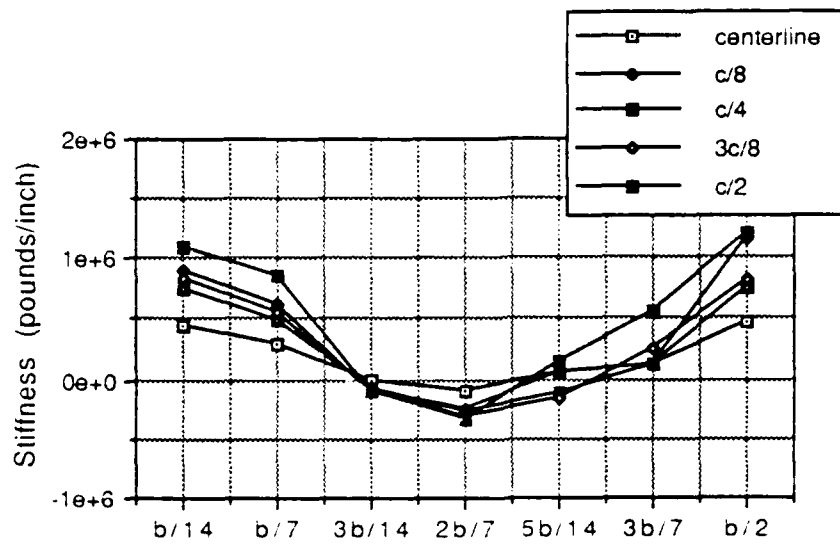


Figure C.11 Equivalent soil spring stiffness z-axis view (10/1.75:1/0500)

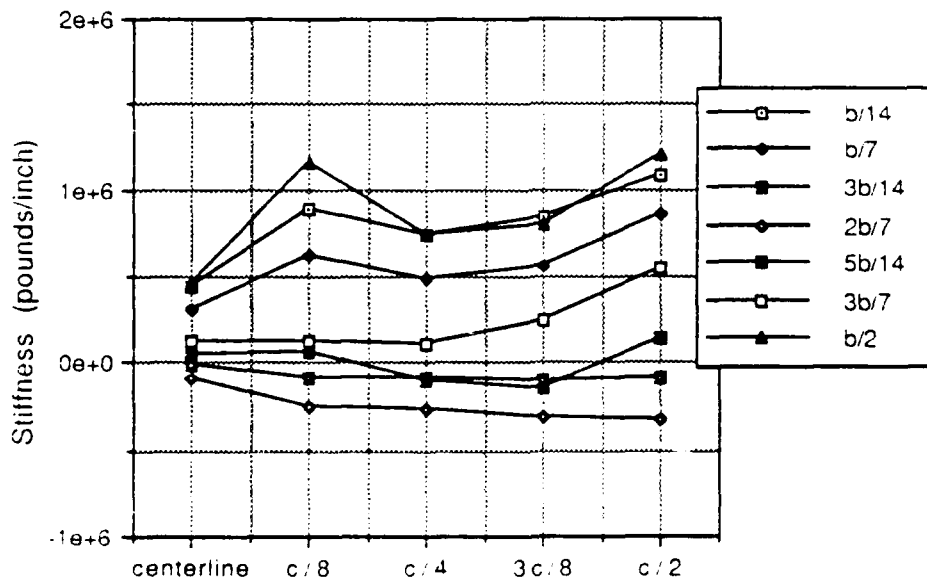


Figure C.12 Equivalent soil spring stiffness x-axis view (10/1.75:1/0500)

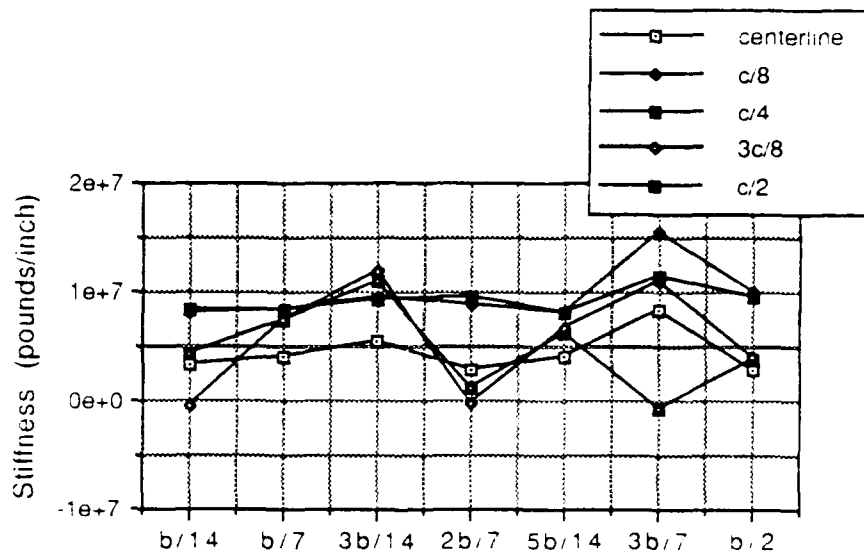


Figure C.13 Equivalent soil spring stiffness z-axis view (3/1.75:1/1500)

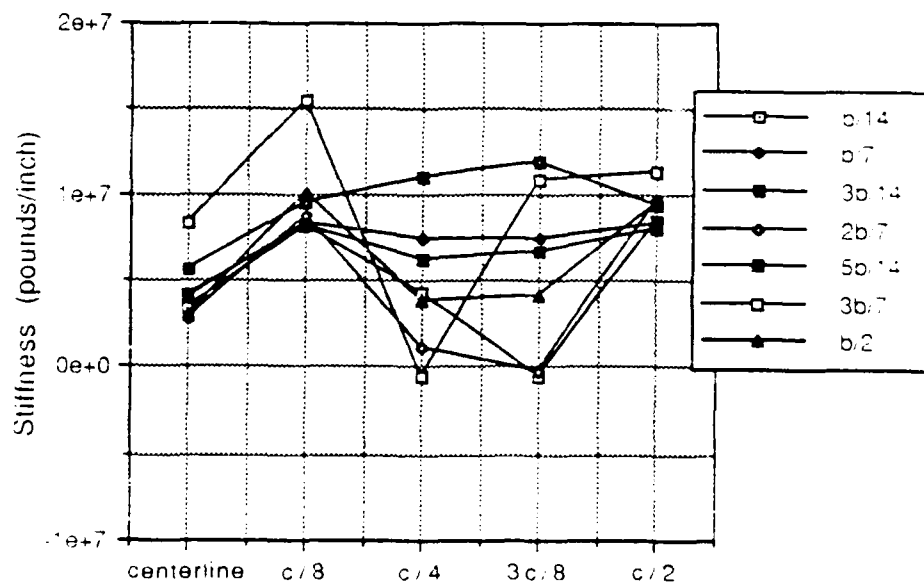


Figure C.14 Equivalent soil spring stiffness x-axis view (3/1.75:1/1500)

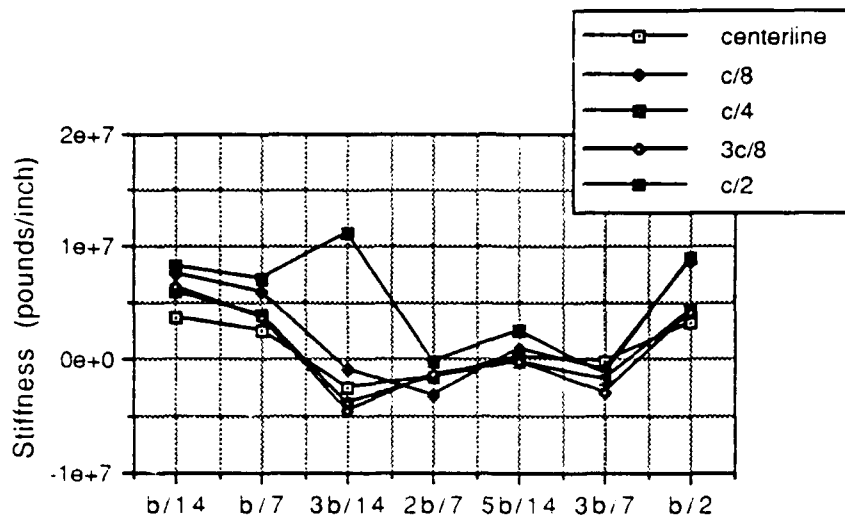


Figure C.15 Equivalent soil spring stiffness  
z-axis view (10/1.75:1/1500)

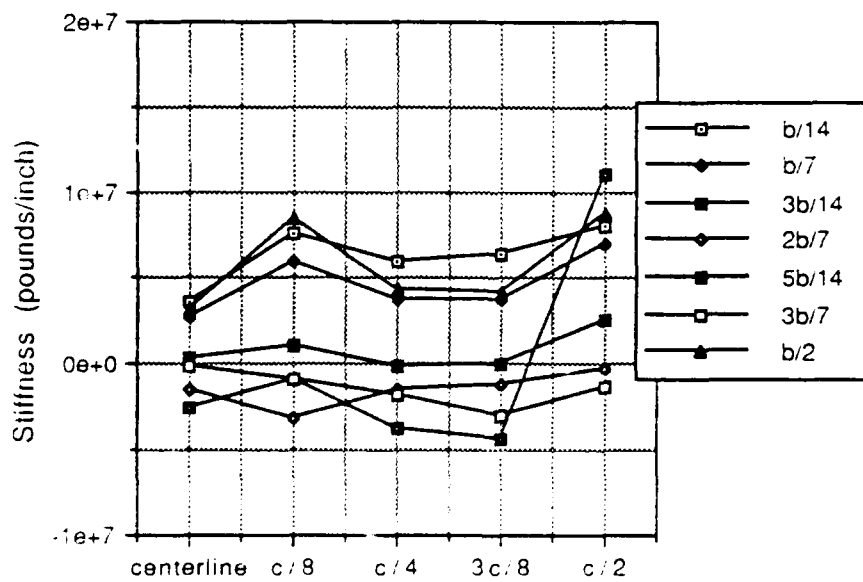


Figure C.16 Equivalent soil spring stiffness  
x-axis view (10/1.75:1/1500)

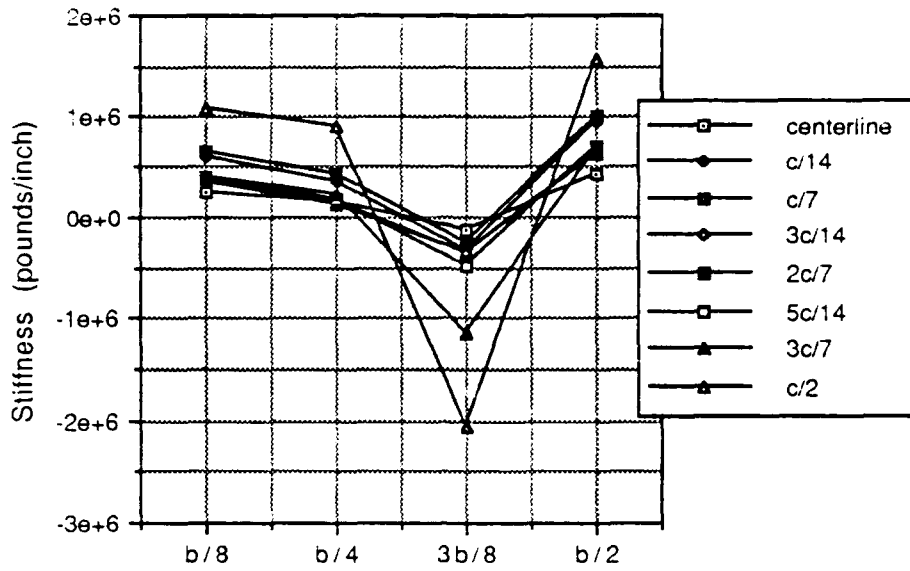


Figure C.17 Equivalent soil spring stiffness  
z-axis view (3/1:1.75/0500)

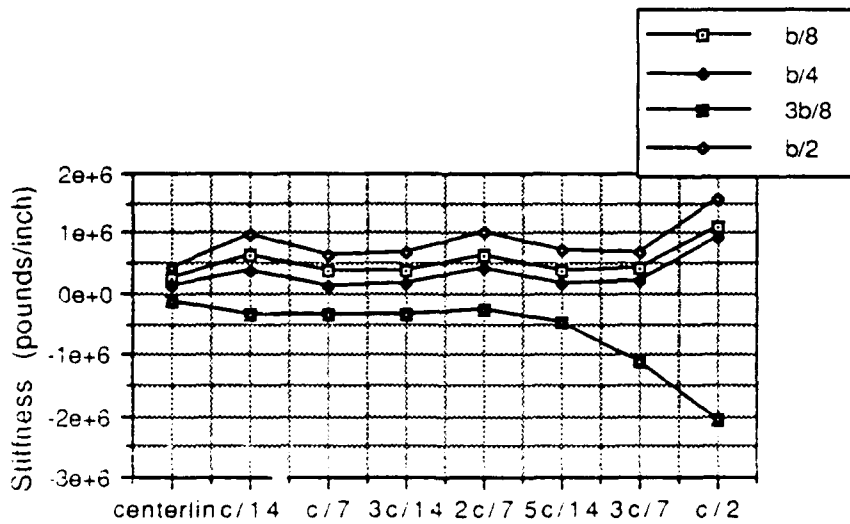


Figure C.18 Equivalent soil spring stiffness  
x-axis view (3/1:1.75/0500)

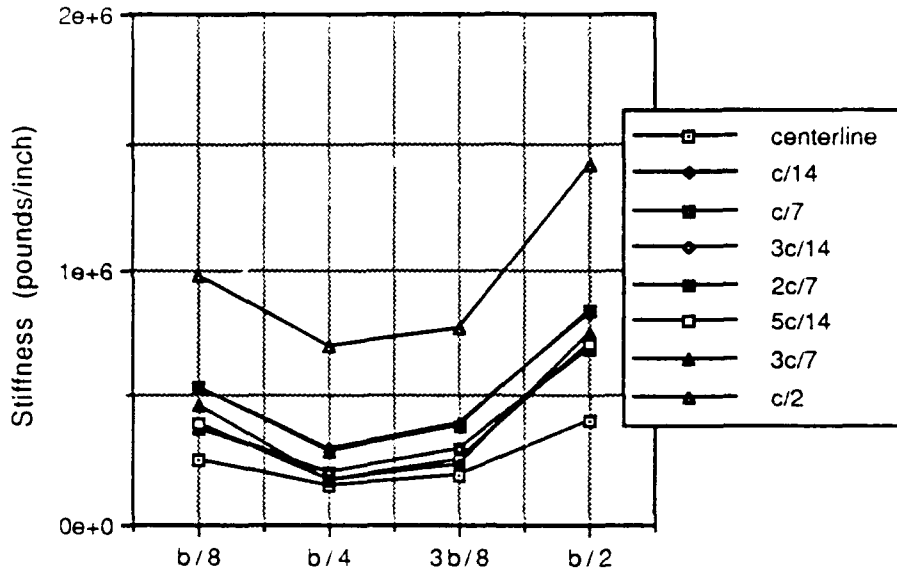


Figure C.19 Equivalent soil spring stiffness z-axis view (10/1:1.75/0500)

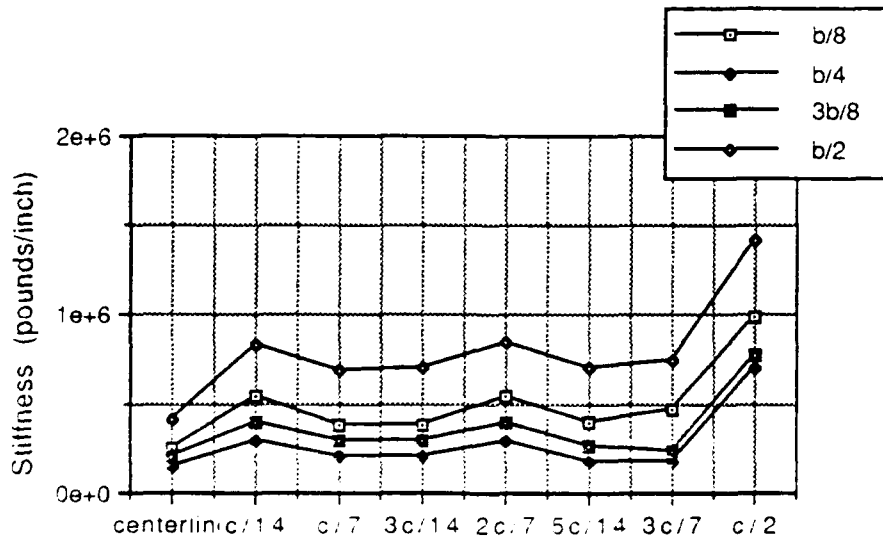


Figure C.20 Equivalent soil spring stiffness x-axis view (10/1:1.75/0500)

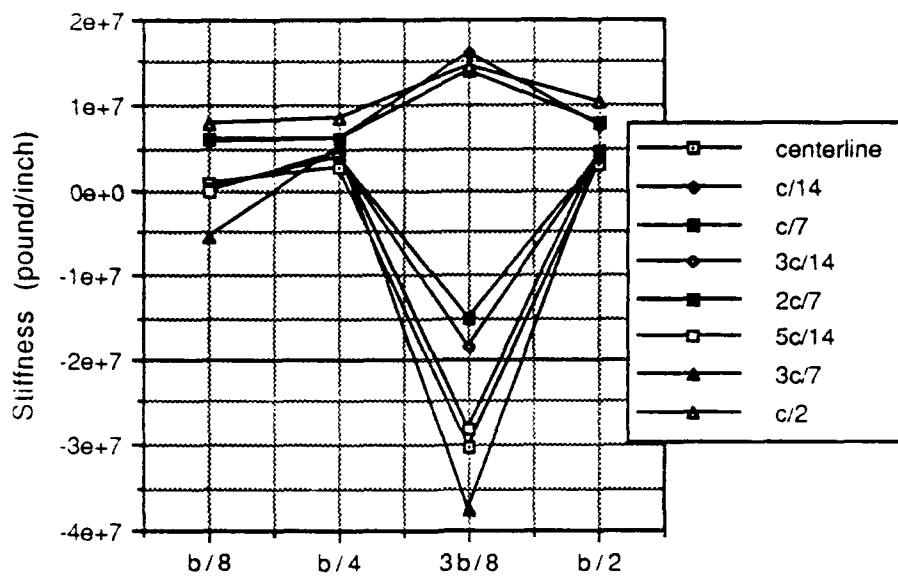


Figure C.21 Equivalent soil spring stiffness  
z-axis view (3/1:1.75/1500)

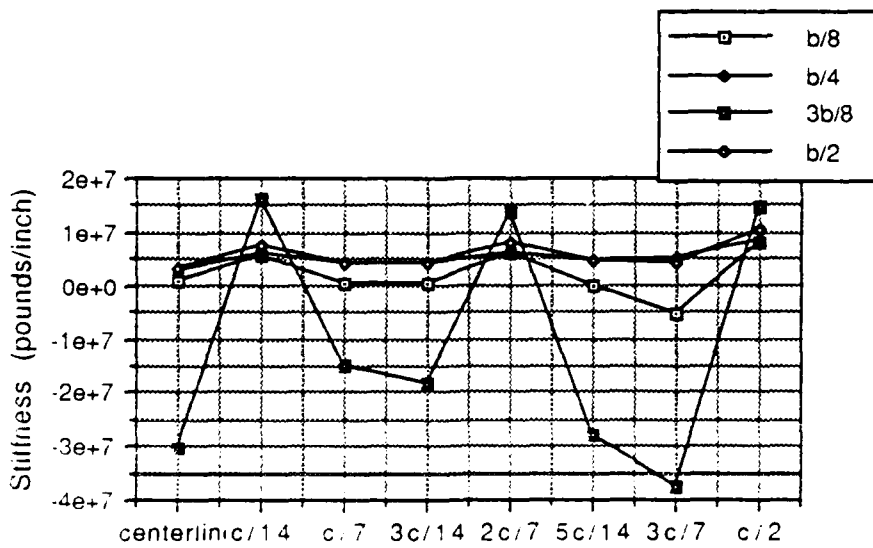


Figure C.22 Equivalent soil spring stiffness  
x-axis view (3/1:1.75/1500)

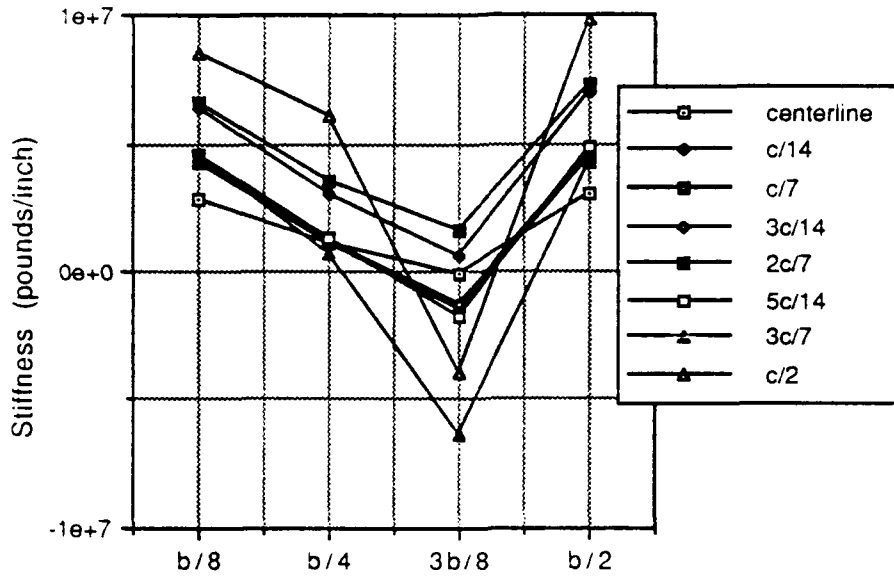


Figure C.23 Equivalent soil spring stiffness  
z-axis view (10/1:1.75/1500)

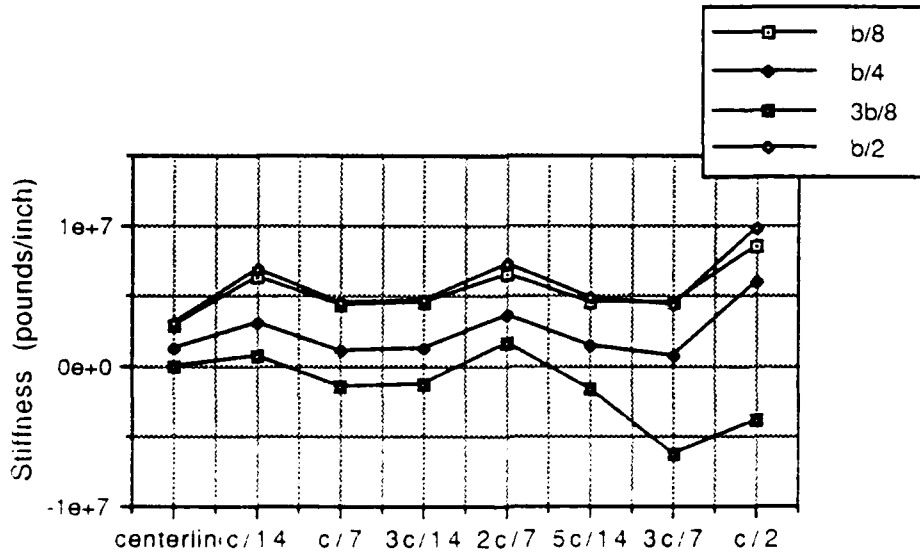


Figure C.24 Equivalent soil spring stiffness  
x-axis view (10/1:1.75/1500)

## **APPENDIX D**

### **SUMMARY OF ANSYS ANALYSIS PROCEDURES**

This appendix summarizes important features the ANSYS finite element code and the manner in which these features were applied to this study. For a thorough explanation of all practical and theoretical aspects of these features refer to the ANSYS Engineering Analysis System User's Manual (24), from which the following information is extracted.

### REDUCED MODAL ANALYSIS

Natural frequencies and mode shapes derive from the following equation:

$$([\mathbf{K}] - \omega_i^2 [\mathbf{M}]) \{\psi\}_i = 0 \quad \text{eq. D.1}$$

where  $[\mathbf{K}]$  is the reduced stiffness matrix of the structure,  $[\mathbf{M}]$  is the reduced mass matrix of the structure,  $\omega_i = 2\pi f_i$  is the natural frequency of mode  $i$ , and  $\{\psi\}_i$  is the reduced mode shape vector of mode  $i$ .  $\{\psi\}_i$  is normalized such that  $\{\psi\}_i^T [\mathbf{M}] \{\psi\}_i = [\mathbf{I}]$ , where  $[\mathbf{I}]$  is the identity matrix. The Guyan reduction technique, described below, reduces mass, stiffness and damping matrices to master degrees of freedom prescribed by the user. The ANSYS default procedure (Householder mode extraction) extracts the first  $n$  eigenvectors and eigenvalues. Here  $n$  is equal to the number of master degrees of freedom selected for matrix reduction.

### DIRECT HARMONIC RESPONSE ANALYSIS

The present study used this modal analysis form to obtain equivalent soil springs. Harmonic horizontal forcing functions, applied at each story level, developed a rocking response an explicitly modeled soil-structure system (see Chapter II). With this analysis the entire structure must be linear. All loads must vary sinusoidally at a specified frequency. For the purposes of this study, all loads acted in phase with one another to promote

fundamental mode response. Thus, simplified equations of motion for this problem are as follows:

$$[\mathbf{M}] \{\mathbf{u}''\} + [\mathbf{K}] \{\mathbf{u}\} = \{\mathbf{F}(t)\} \quad \text{eq. D.2}$$

These calculations contain no damping terms. The displacement vector  $\{\mathbf{u}\}$  is of the form:

$$\{\mathbf{u}\} = \{\mathbf{u}_{\max} e^{i\phi t}\} e^{i\Omega t} = \{\mathbf{u}_1 + i \mathbf{u}_2\} e^{i\Omega t} \quad \text{eq. D.3}$$

where  $\mathbf{u}_{\max}$  is the displacement vector amplitude,  $\phi$  is the displacement vector phase shift,  $\Omega$  is the specified natural frequency of the force vector (radians/sec),  $\{\mathbf{u}_1\} = \{\mathbf{u}_{\max} \cos\phi\}$  and  $\{\mathbf{u}_2\} = \{\mathbf{u}_{\max} \sin\phi\}$ , and  $t$  is time. Similarly, the force vector  $\{\mathbf{F}(t)\}$  is of the form:

$$\{\mathbf{F}(t)\} = \{\mathbf{F}_{\max}\} e^{i\Omega t} \quad \text{eq. D.4}$$

where  $\mathbf{F}_{\max}$  is the force vector amplitude. With no damping, force and displacement vectors act with the same vector phase components,  $\phi$ .

Making the appropriate substitutions and factoring out the time dependent term,  $e^{i\Omega t}$ , a simplified matrix equation follows:

$$(( [\mathbf{K}] - \Omega^2 [\mathbf{M}]) \{\mathbf{u}_1 + i \mathbf{u}_2\} = \{\mathbf{F}_{max}\} \quad \text{eq. D.5}$$

Solution of this equation in the displacement pass yields the vector  $\{\mathbf{u}_1 + i \mathbf{u}_2\}$ . Similarly, typical finite stress calculations yield complex member forces and stresses.

### PUESDO-VELOCITY SPECTRUM RESPONSE

The present study applied this modal analysis to obtain response of frames supported by equivalent soil springs subjected to earthquake velocity spectrums. Here also, the structure must be linear. ANSYS allows no more than twenty frequencies in the user definition of the loading spectrum. Logarithmic interpolation provides estimates for intermediate frequency spectrum values. This study defined velocity spectrums over a range of .1 to 10 Hz. A truncated solution of equation D1 provided significant classical mode shapes for frequencies as high as 10 or 25 Hz, depending upon the fundamental frequency and relative stiffness of the structure in question. Participation factor  $\lambda_i$  for mode  $i$  is as follows:

$$\lambda_i = \{\psi\}_i [\mathbf{M}] \{\mathbf{D}\} \quad \text{eq. D.6}$$

where  $\{\mathbf{D}\}$  is a unit direction vector for the spectral excitation. The reduced displacement vector  $\{\mathbf{u}\}_i$  for mode  $i$  is computed as follows:

$$\{\mathbf{u}\}_i = \frac{S_{vi} \lambda_i}{\omega_i} \{\psi\}_i \quad \text{eq. D.7}$$

where  $S_{vi}$  is the interpolated spectral velocity of mode  $i$ , which has natural frequency  $\omega_i = 2\pi f_i$ .

Modal combination solutions included modes of frequencies as high as 10 Hz, provides the following significance criterion was met:

$$\text{M.C.}_i = \frac{S_{vi} \lambda_i}{\omega_i} \geq .001$$

where  $\text{M.C.}_i$  is the mode coefficient ratio, or significance level, of the  $i^{\text{th}}$  mode.

#### Modal Combination

Depending upon the relative spacing of significant mode frequencies, this study selected one of two modal combination options. In problems not inducing coupled torsion, the square root of the sum of squares (SRSS) method determined approximate structure response. With torsional coupling, significant frequencies were generally more closely spaced. In these cases complete quadratic combination method (CQC) determined approximate structure response.

--SRSS Combination

For this method the total modal response for a given displacement, force or stress,  $R_a$ , is as follows:

$$R_a = \sqrt{\sum_{i=1}^N (m_i^s)^2 (R_i)^2} \quad \text{eq. D.8}$$

where  $R_i$  is the maximum modal response of the  $i^{\text{th}}$  mode.

The spectral multiplier for the  $i^{\text{th}}$  mode,  $m_i^s$ , is as follows:

$$m_i^s = \frac{S_{vi}}{S_{vi}^0} \quad \text{eq. D.9}$$

where  $S_{vi}$  is the interpolated spectral velocity at mode frequency  $i$  and damping value  $d_i$ .  $S_{vi}^0$  is the spectral velocity at mode frequency  $i$  evaluated at the lowest damping value specified.

--CQC Combination

For this method the total modal response,  $R_a$ , is as follows:

$$R_a = \sqrt{\left| \sum_{i=1}^N \sum_{j=1}^N k \epsilon_{ij} m_i^s m_j^s R_i R_j \right|} \quad \text{eq. D.10}$$

where  $k=1$  for  $i=j$  and  $k=2$  for  $i \neq j$ .

The coupling coefficient  $\epsilon_{ij}$  is as follows:

$$\epsilon_{ij} = \frac{8 (\xi_i \xi_j)^{1/2} (\xi_i + r \xi_j) r^{3/2}}{(1-r^2)^2 + 4 \xi_i \xi_j r (1+r^2) + 4 (\xi_i + \xi_j^2) r^2} \quad \text{eq. D.11}$$

where  $r = \omega_j/\omega_i$  and  $\xi_k$  is the effective damping ratio for mode  $k = i$  or  $j$ . The coupling coefficient approaches zero for independent modes and approaches one with increasing dependency.

### **Guyan Reduction to Specified Master Degrees of Freedom and Superelement Formation**

To insure feasible runtimes, all three-dimensional frame calculations required this method of limiting degrees of freedom. With this procedure the user selects certain degrees of freedom to be active (master degrees of freedom). The remaining degrees of freedom become dependent (slaved) to these selected master degrees of freedom. Where a collection of elements can act as a single element (superelement) in multiple calculations, Guyan reduction can also limit the number of master degrees of freedom. The resulting mass, stiffness, and damping matrices of the superelement are stored for future applications. In this way, significant savings in element formation costs accrue.

Total mass, stiffness, and damping matrices partition as follows:

$$[\Gamma] = \begin{bmatrix} [\Gamma_{mm}] & [\Gamma_{sm}] \\ [\Gamma_{ms}] & [\Gamma_{ss}] \end{bmatrix} \quad \text{eq. D.12}$$

where m represents master degrees of freedom and s represents slaved degrees of freedom.

With Guyan reduction, the general form of the equations of motions:

$$[\mathbf{M}]\{\mathbf{u}''\} + [\mathbf{C}]\{\mathbf{u}'\} + [\mathbf{K}]\{\mathbf{u}\} = \{\mathbf{F}\}, \quad \text{eq. D.13}$$

simplifies to a reduced system of the form:

$$[\hat{\mathbf{M}}]\{\hat{\mathbf{u}}''\} + [\hat{\mathbf{C}}]\{\hat{\mathbf{u}}'\} + [\hat{\mathbf{K}}]\{\hat{\mathbf{u}}\} = \{\hat{\mathbf{F}}\}, \quad \text{eq. D.14}$$

where  $\hat{\mathbf{u}}$  is the reduced displacement vector of master degrees of freedom. The ANSYS program specifies the reduced stiffness  $[\hat{\mathbf{K}}]$ , force  $[\hat{\mathbf{F}}]$ , mass  $[\hat{\mathbf{M}}]$ , and damping  $[\hat{\mathbf{C}}]$  matrices as follows:

$$[\hat{\mathbf{K}}] = [\mathbf{K}_{mm}] - [\mathbf{K}_{ms}][\mathbf{K}_{ss}]^{-1}[\mathbf{K}_{sm}] \quad \text{eq. D.15}$$

$$[\hat{\mathbf{F}}] = [\mathbf{F}_m] - [\mathbf{K}_{ms}][\mathbf{K}_{ss}]^{-1}[\mathbf{F}_s] \quad \text{eq. D.16}$$

$$\begin{aligned} [\hat{\mathbf{M}}] &= [\mathbf{M}_{mm}] - [\mathbf{K}_{ms}][\mathbf{K}_{ss}]^{-1}[\mathbf{M}_{sm}] - [\mathbf{M}_{ms}][\mathbf{K}_{ss}]^{-1}[\mathbf{K}_{sm}] \\ &\quad + [\mathbf{K}_{ms}][\mathbf{K}_{ss}]^{-1}[\mathbf{M}_{ss}][\mathbf{K}_{ss}]^{-1}[\mathbf{K}_{sm}] \end{aligned} \quad \text{eq. D.17}$$

$$\begin{aligned} [\hat{\mathbf{C}}] &= [\mathbf{C}_{mm}] - [\mathbf{K}_{ms}][\mathbf{K}_{ss}]^{-1}[\mathbf{C}_{sm}] - [\mathbf{C}_{ms}][\mathbf{K}_{ss}]^{-1}[\mathbf{K}_{sm}] \\ &\quad + [\mathbf{K}_{ms}][\mathbf{K}_{ss}]^{-1}[\mathbf{C}_{ss}][\mathbf{K}_{ss}]^{-1}[\mathbf{K}_{sm}] \end{aligned} \quad \text{eq. D.18}$$

The reduced stiffness and force matrices are exact; however, the mass and damping matrices are approximate.

## APPENDIX E

### EXAMPLE PORTAL FRAME ANALYSIS

This appendix presents an example problem demonstrating the portal frame analysis technique for a mono-symmetric frame loaded for maximum self-induced torque. The simplified analysis technique, employing equations 2.8 and 2.14, is used to determine gross structure response--horizontal floor deflections, net column shears, and net column torques. Comparison is made to results of a corresponding space frame analysis.

### Example dynamic stick frame analysis using portal frame approximations:

#### Problem statement:

Determine the maximum dynamic roof deflection, base shear, and base torque using portal frame analysis for the structure and loading previously identified as 5/1:1E/0500/E-C{0,1}.

#### Detailed description:

A description of the features of the structure and load alluded to by the previous nomenclature is:

5	floors (12 ft in height)
1:1	square floor plan
E	eccentric arrangement of columns
0500	soil shear wave velocity in ft/sec
E-C	EI-Centro north-south earthquake component
{0,1}	soil pseudo-velocity spectral loading oriented along z axis

Based on the physical descriptions of Chapter II, member properties are as follows:

#### Columns

$$I_{zz} = 750 \text{ in}^4$$

$$I_{xx} = 677 \text{ in}^4$$

$$A = 33.4 \text{ in}^2$$

#### Mat

$$t = 25 \text{ in}$$

$$\rho = .000225 \text{ lb-sec}^2/\text{in}^4$$

$$(150 \text{ lb}/\text{in}^3)$$

$$m = 5184 \text{ lb-sec}^2/\text{in}$$

$$J_{yy} = 7.963\text{E}8 \text{ lb-sec}^2\text{-in}$$

#### Beams

$$I_{zz} = 1330 \text{ in}^4$$

$$I_{xx} = 58 \text{ in}^4$$

$$A = 18.3 \text{ in}^2$$

#### Floor

$$t = 8.25 \text{ in}$$

$$\rho = .000219 \text{ lb-sec}^2/\text{in}^4$$

$$(100 \text{ lb}/\text{ft}^2 \text{ -- DL}+50\%\text{LL})$$

$$m = 1654.4 \text{ lb-sec}^2/\text{in}$$

$$J_{yy} = 2.544\text{E}8 \text{ lb-sec}^2\text{-in}$$

Steel properties

$$E = 30E6 \text{ lbs/in}^2$$

$$\nu = .3$$

Concrete properties

$$E = 3.12 \text{ lbs/in}^2$$

$$G = 1.20 \text{ lbs/in}^2$$

$$\nu = .2$$

Soil properties

$$v_s = 500 \text{ ft/sec}$$

$$G = 6469 \text{ lb/in}^2$$

$$\nu = .333$$

$$\rho = .000180 \text{ lb-sec}^2/\text{in}^4$$

$$(120\text{lb/in}^3)$$

Here 16 columns are located at the intersection of beam lines shown in the plan view (Figure E.1). Full continuity of all beam and column joints is assumed.

Computing stiffness of equivalent springs of the portal frame:

To build the portal frame stick model (Figure 2.3), the following parameters must first be computed: five soil springs, two horizontally oriented torsional springs to represent the effects of floor stiffness at each column joint, and the torsional stiffness of each floor of columns. The last two components (torsional floor springs and equivalent column torsional stiffness) are computed once, since all floors of this structure are identical. Note that the axial rotations of far-field nodes of the torsional floor springs must be coupled to the corresponding rotations of the mat foundation if a soil model with rocking springs is provided. Otherwise, the axial rotations of far-field nodes of the torsional floor springs should be completely fixed.

The soil springs of this example are computed from the recommendations of Dobry and Gazetas (14) as follows (using the symbols defined in reference (14)):

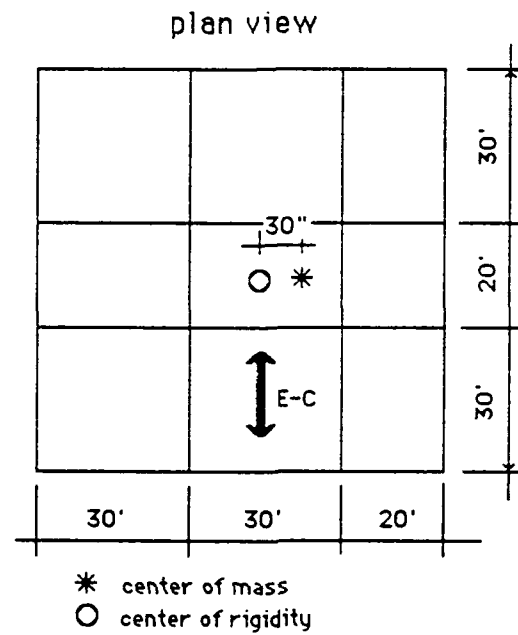


Figure E.1 Plan view of structure and loading (5/1:1E/0500/E-C{0,})

Horizontal translation--

$$K_x = S_x \frac{2LG}{2-\nu} = 4.5 \frac{(2)(480)(6469)}{(2-.333)} = 16.8E6 \text{ lb/in}$$

$$S_x = 4.5 \left( \frac{A}{4L^2} \right)^{.75} = 4.5 (1)^{.75} = 4.5$$

From Figure 10 of reference (14),  $\tilde{K}_x$  is found graphically after computing the ordinate  $a_0$  at the approximate mode one frequency of the structure:

$$\tilde{K}_x = (.96)K_x = 16.2E6 \text{ lb/in} = \tilde{K}_y$$

$$a_0 = \frac{\omega L}{v_s} = \frac{(8.33)(480)}{(500)(12)} = .666$$

$$\omega = 2\pi \{C_T(h_n)^{.75}\}^{-1} = 2\pi \{.035(60\text{ft})^{.75}\}^{-1} = 8.33 \text{ rad/sec}$$

where  $\omega$  is derived from eq. 9B of ANSI A58.1-1982.

Rocking about horizontal axes--

$$K_{rx} = S_{rx} \frac{G}{1-\nu} (I_x)^{.75} = 3.2 \frac{(6469)}{(1-.333)} \left( \frac{(960)^4}{12} \right)^{.75}$$

$$= 4.26E12 \text{ in-lb/in}$$

From Figure 7a of reference (14),  $\tilde{K}_{rx}$  is found graphically for ordinate  $a_0$  as above:

$$\tilde{K}_{rx} = (.93) K_{rx} = 3.96E12 \text{ in-lb/in} = \tilde{K}_{ry}$$

Torsion about vertical axis--

$$K_t = S_t G(J)^{.75} = 3.8(6469) \left( \frac{2(960)4}{12} \right)^{.75} = 5.67E12 \text{ in-lb/in}$$

From Figure 8 of reference (14),  $\tilde{K}_t$  is found graphically for ordinate  $a_0$  as above:

$$\tilde{K}_t = (.94) K_t = 5.33E12 \text{ in-lb/in}$$

Effective torsional floor springs are computed as described for eq. 2.8 above. Arbitrary column shears are applied to hinged mid-column locations according to the tributary span of beams framing into each column (refer to Figure E.2 for typical floor frame in x-direction). Normalizing stiffness factors  $\gamma_i$  (for column  $i$ ) are found by scaling arbitrary column shears to the ratio of the sum of column moments at the floor joints and the sum of column moments at the floor joints for a corresponding frame of equal spans. The corresponding frame has the same length and number of spans, but each end span carries a unit shear, thus each interior span carries a shear of 2.0 (force units).

Thus for the frame of Figure E.2 the  $\gamma_i$  values are computed as follows:

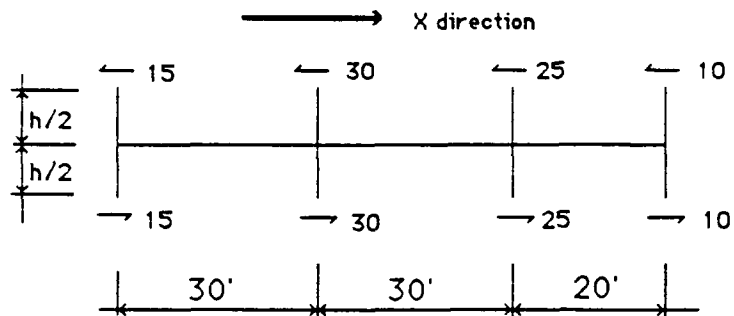
Sum of the moments of the frame are--

$$2 \left( \frac{h}{2} \right) (15 + 30 + 25 + 10) = 80h$$

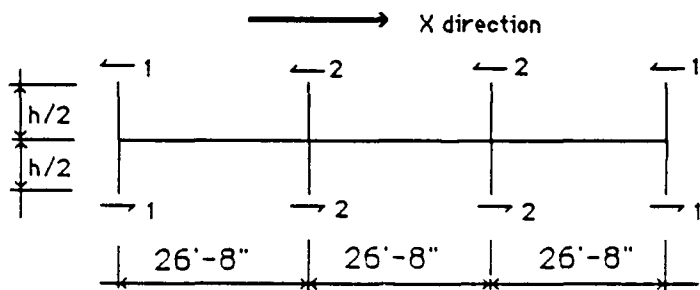
Sum of the moments of the corresponding equal span frame are--

$$2 \left( \frac{h}{2} \right) (1 + 2 + 2 + 1) = 6h$$

Thus the normalizing factors  $\gamma_i$  are--



typical floor - portal frame  
arbitrary shears



corresponding equal span portal frame  
unit end shears

Figure E.2 Portal frame analysis of  
typical floor frame (x-direction)

$$\gamma_3 = .075(25) = 1.875$$

$$\gamma_4 = .075(10) = .75$$

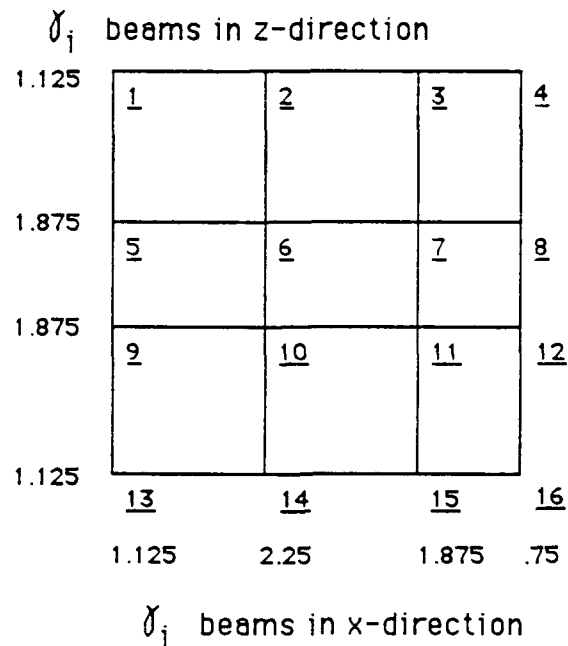
In Figure E.3,  $\gamma_i$  values are given for frames oriented in both the x and z direction. From eq. 2.8, the sum of beam rotational stiffnesses at all column faces are computed as follows:

beams in x-direction--

$$\begin{aligned} K_T &= \frac{(4)(1.125)(6)(30E6)(1330)}{(30)(12)} \\ &+ \frac{(8)(2.25)(6)(30E6)(1330)}{(30)(12)} \\ &+ \frac{(4)(1.875)(6)(30E6)(1330)}{(30)(12)} \\ &+ \frac{(4)(1.875)(6)(30E6)(1330)}{(20)(12)} \\ &+ \frac{(4)(.75)(6)(30E6)(1330)}{(20)(12)} \\ &= 3.04E10 \text{ in-lb/in} \end{aligned}$$

beams in z-direction--

$$\begin{aligned} K_T &= \frac{(8)(1.125)(6)(30E6)(1330)}{(30)(12)} \\ &+ \frac{(8)(1.875)(6)(30E6)(1330)}{(30)(12)} \\ &+ \frac{(8)(1.875)(6)(30E6)(1330)}{(20)(12)} \\ &= 3.09E10 \text{ in-lb/in} \end{aligned}$$



n — column reference number  
used in TK!Solver calculation  
of  $J_{eff}$

Figure E.3 Normalizing factors used  
computing effective floor stiffness and  
effective polar moment of inertia  
of columns

The effective column torsional stiffness is computed from eq. 2.14. The stiffness of individual column joints (required in eq. 2.10) are computed from eq. 2.10 as follows:

$$K_{\theta jx} = \frac{(1.125)(6)(30E6)(1330)}{(30)(12)} = 7.481E8 \text{ in-lb/in}$$

(where  $j = 1, 5, 9, \text{ and } 13$ )

$$K_{\theta jx} = \frac{(2)(2.25)(6)(30E6)(1330)}{(30)(12)} = 29.925E8 \text{ in-lb/in}$$

(where  $j = 2, 6, 10, \text{ and } 14$ )

$$K_{\theta jx} = \frac{(1.875)(6)(30E6)(1330)}{(30)(12)} + \frac{(1.875)(6)(30E6)(1330)}{(20)(12)} = 31.171E8 \text{ in-lb/in}$$

(where  $j = 3, 7, 11, \text{ and } 15$ )

$$K_{\theta jx} = \frac{(.75)(6)(30E6)(1330)}{(20)(12)} = 7.481E8 \text{ in-lb/in}$$

(where  $j = 4, 8, 12, \text{ and } 16$ )

$$K_{\theta jz} = \frac{(1.125)(6)(30E6)(1330)}{(30)(12)} = 7.481E8 \text{ in-lb/in}$$

(where  $j = 1, 2, 3, 4, 13, 14, 15, \text{ and } 16$ )

$$K_{\theta jz} = \frac{(1.875)(6)(30E6)(1330)}{(30)(12)} + \frac{(1.875)(6)(30E6)(1330)}{(20)(12)} = 31.171E8 \text{ in-lb/in}$$

(where  $j = 5, 6, 7, 8, 9, 10, 11, \text{ and } 12$ )

Additionally, the effective stiffness and area of the column is found by summing the inertias (in each direction) and the areas of all columns of a single floor, thus:

$$I_{kx} = (16)(677) = 10832 \text{ in}^4$$

$$I_{kz} = (16)(750) = 12000 \text{ in}^4$$

$$A_k = (16)(33.4) = 534 \text{ in}^2$$

The calculation of  $K_t$  (eq. 2.14) is easily implemented on microcomputer spread sheet programs or general math programs capable of utilizing columns of numbers. In this instance the program TK!Solver was used to obtain  $J_{\text{eff}} = 2.697\text{E}6 \text{ in}^4$  (as demonstrated in Tables E.1 through E.3 and Figure E.4).

Also, individual column shears were estimated by eq. 2.20. This analysis, as implemented with TK!Solver is demonstrated in Tables E.4 and E.5 and Figure E.5.

Comparison of results:

The roof node of the portal frame model at the center of rigidity (top column node) is 25, while the corresponding mat node is 20. The first floor column of this model is element 8, with end nodes 20 and 21. Comparing important forces and displacements for this model to results of the corresponding space frame model:

<u>parameter**</u>	<u>portal frame</u>	<u>space frame</u>	<u>difference</u>
roof deflection*	7.69 in	7.37	+4.1%
base shear	1648 kips	1519 kips	+8.5%
base torque	1270E6 kips/in	1339 kip/in	-5.1%
max. column $V_x$	14.767 kip	17.3 kip	-14.3%
max. column $V_z$	143.8 kip	118.0 kip	21.8%

\*relative to mat

\*\* also see Figures A.37 through A.39

Table E.1 Summary of column deflection stiffness (kx and kz) and torsion stiffness (K) contributions (TK!Solver solution)

column	kx	kz	K
1	748100000	748100000	1.926E10
2	2992500000	748100000	1.556E10
3	3117100000	748100000	1.656E10
4	748100000	748100000	1.695E10
5	748100000	3117100000	1.863E10
6	2992500000	3117100000	2.4803E9
7	3117100000	3117100000	3.99E9
8	748100000	3117100000	1.463E10
9	748100000	3117100000	1.863E10
10	2992500000	3117100000	2.4803E9
11	3117100000	3117100000	3.99E9
12	748100000	3117100000	1.463E10
13	748100000	748100000	1.926E10
14	2992500000	748100000	1.556E10
15	3117100000	748100000	1.656E10
16	748100000	748100000	1.695E10

Table E.2 Summary of column coordinates (Cartesian and polar) (TK!Solver solution)

column	xi	zi	ai	ri
1	-480	-480	-136.736	700.3571
2	-120	-480	-107.354	502.8916
3	240	-480	-66.3706	523.9275
4	480	-480	-46.8476	657.9514
5	-480	-120	-166.759	523.9275
6	-120	-120	-141.34	192.0937
7	240	-120	-29.7449	241.8677
9	480	-120	-14.9314	465.7252
9	-480	120	166.7595	523.9275
10	-120	120	141.3402	192.0937
11	240	120	29.74488	241.8677
12	480	120	14.93142	465.7252
13	-480	480	136.7357	700.3571
14	-120	480	107.354	502.8916
15	240	480	66.37062	523.9275
16	480	480	46.84761	657.9514

Table E.3 Summary of TK!Solver variable sheet for calculation of  $J_{eff}$  (J in this table)

St	Input	Name	Output	Unit	Comment
		ai	178.02507	deg	angle--x-axis to radius ri
L	1	kx		in-lb/in	floor rotational stiffness at column i (x-rotation)
L	1	kz		in-lb/in	floor rotational stiffness at column i (z-rotation)
L		K	.08121142	in-lb/in	column i torsional stiffness
	30000000	E		lb/in <sup>2</sup>	column elastic modulus
	11538500	G		lb/in <sup>2</sup>	column shear modulus
	677	Ix		in <sup>4</sup>	column moment of inertia (x)
	750	Iz		in <sup>4</sup>	column moment of inertia (z)
	144	L		in	column length
		f	3.1071236	rad	
		J	2697327.3	in <sup>4</sup>	effective column polar moment of inertia
L		ri	29.017236	in	radius--origin to column i
L	1	xi		in	x-coordinate of column i
	30	xc		in	x-coordinate of center of rigidity
L	1	zi		in	z-coordinate of column i
	0	zc		in	z-coordinate of center of rigidity
		K1	.00009645		
		K2	.08111497		

```

S Rule=
* f = 2*pi()/360*ai
* K = K1 + K2
* K1 = (12*E*Ix*kx)*ri^2*(sin(f))^2/(kx*L^3+6*E*Ix*L^2)
* K2 = (12*E*Iz*kz)*ri^2*(cos(f))^2/(kz*L^3+6*E*Iz*L^2)
* ri^2 = (xi-xc)^2+(zi-zc)^2
* f = atan2(zi-zc,xi-xc)
* J = SUM(K)*L/G

```

Figure E.4 Summary of TK!Solver rule sheet for calculation of  $J_{eff}$  (J in this figure)

Table E.4 Summary of TKISolver input portal frame load factors and output individual column shears

column	gx	gz	Ys	Zs
1	1.125	1.125	11219.0813	89170.2739
2	2.25	1.125	14767.4419	81864.8256
3	1.875	1.125	13888.8889	71173.6111
4	.75	1.125	9045.58405	68769.765
5	1.125	1.875	3540.36574	143796.554
6	2.25	1.875	5081.62612	135102.033
7	1.875	1.875	4674.6172	120569.42
8	.75	1.875	2716.46133	118563.27
9	1.125	1.875	-3540.3657	143796.554
10	2.25	1.875	-5081.6261	135102.033
11	1.875	1.875	-4674.6172	120569.42
12	.75	1.875	-2716.4613	118563.27
13	1.125	1.125	-11219.081	89170.2739
14	2.25	1.125	-14767.442	81864.8256
15	1.875	1.125	-13888.889	71173.6111
16	.75	1.125	-9045.584	68769.765

Table E.5 Summary of TK!solver variable sheet for calculation of individual column shears

St	Input	Name	Output	Unit	Comment
L		Xs	-9045.584		total column x-shear
L		Zs	-18499.74		total column v-shear
L		Xt			column x-shear component of T
L		Zt			column z-shear component of T
L		Xv			column x-shear component of Ux
L		Zv			column z-shear component of Uz
L	1	Gx			2nd moment of gamma x
L	1	Gz			2nd moment of gamma z
L	1	x			column x coordinate
L	1	z			column z coordinate
L	1	gx			gamma x
L	1	gz			gamma z
	-1.27E8	T			net torque
	0	Ux			net shear (x)
	1648000	Uz			net shear (z)
	2937600	Gsx			sum Gx
	3175200	Gsz			sum Gz
	30	xc			center of rigidity (x)
	0	zc			center of rigidity (z)
L	1	n			floor number

```

S Rule
  "Gx = gx*(y-yc)^2
  "Gy = gy*(x-xc)^2
  "Gsx = sum('Gx)
  "Gsy = sum('Gy)
  * Xt = T/( Gsx/(gx*(z-zc)) + (x-xc)/(z-zc)*Gsz/(gz*(x-xc)) )
  * Zt = (x-xc)/(z-zc)*Xt
  * Xv = gx/sum('gx)*Ux
  * Zv = gz/sum('gz)*Uz
  * Ys = Xt + Xv
  * Zs = Zt + Zv

```

Figure E.5 Summary of TK!Solver rule sheet for calculation of individual column shears

The input file for the ANSYS dynamic portal frame analysis is as follows:

```

/PREP7
/TITLE, 5/1:1E/0500/E-C{0.1}
KAN,2
KAY,2,-1
KSE,1
DMPRAT,0.02

C*** SOIL DAMPERS
ET,20,14          * HORIZONTAL
ET,19,14          * ROCKING
DAMP,20,0.10
R,20,16.2E6        * HORIZONTAL TRANSLATION
R,19,3.96E12      * ROCKING
R,18,5.33E12      * TORSION
C*** FLOOR STIFFNESS
C*** X-AXIS ROTATION
R,61,3.09E10
R,62,3.09E10
R,63,3.09E10
C*** Y-AXIS ROTATION
R,64,3.04E10
R,65,3.04E10
R,66,3.04E10

KEYOPT,20,3,0      * 3-D LONGITUDINAL
KEYOPT,19,3,1      * 3-D TORSIONAL

C*** MASSES
ET,1,21
C*** FLOORS
R,81,1656.4,0,1656.4,0,2.544E8,0 * NO VERTICAL INERTIA
R,82,1656.4,0,1656.4,0,2.544E8,0 * NO VERTICAL INERTIA
R,83,1656.4,0,1656.4,0,2.544E8,0 * NO VERTICAL INERTIA

C*** MAT
R,5,5184,0,5184,0,7.963E8,0      * NO VERTICAL INERTIAL CONTRIBUTIONS
KEYOPT,1,3,0          * 3-D ROTARY INERTIA

C*** COLUMNS
ET,2,4
EX,2.30E6
NUXY,2,.30
DENS,2.1E-8
RSIZE,10
R,41,534,12000,10832.6,13,6.27,
RMORE,0.2.697E6
R,42,534,12000,10832.6,13,6.27,

```

RMORE,0,2.697E6  
R,43,534,12000,10832,6.13,6.27,  
RMORE,0,2.697E6  
R,45,1000,1E8,1E8,10,10,  
RMORE,0,1E10  
R,46,1000,1E8,1E8,10,10,  
RMORE,0,1E10  
R,47,1000,1E8,1E8,10,10,  
RMORE,0,1E10

C\*\*\* NODE DEFINITION

CSYS,0  
N,1,-100,0  
N,2,0,0,-100  
N,3,-100  
N,10  
N,15,0,720  
FILL  
N,20,30,0  
N,25,30,720  
FILL  
N,41,-100,144  
N,45,-100,720  
FILL  
N,61,30,144,-100  
N,65,30,720,-100  
FILL

C\*\*\* ELEMENT GENERATION

C\*\*\* FOUNDATION

TYPE,20  
REAL,20  
MAT,20  
E,1,10  
E,2,10  
TYPE,19  
REAL,19  
MAT,20  
E,1,10  
E,2,10  
REAL,18  
E,3,10

C\*\*\* SUPERSTRUCTURE

TYPE,1  
REAL,5  
E,10  
TYPE,2  
MAT,2  
REAL,45  
E,10,20

REAL,41  
 E,20,21  
 REAL,45  
 E,21,11  
 TYPE,19  
 MAT,19  
 REAL,61  
 E,21,41  
 REAL,64  
 E,21,61  
 TYPE,1  
 REAL,81  
 E,11  
 EGEN,2,1,-5,,,,,1  
 EGEN,3,1,-5  
 EGEN,2,1,-5,,,,,1

C\*\*\* CREAT MASTER DEGREES OF FREEDOM

M,10,ALL,15  
 M,20,ALL,25

WSORT,Y

C\*\*\* CONSTRAIN SOIL FAR-FIELD

D,1,ALL,,,3

C\*\*\* CONSTRAIN MAT VERTICAL DISPLACEMENT

D,10,UY

C\*\*\* LINK FLOOR SPRING AND MAT ROTATIONS (RIGID BODY MOTION)

CPSIZE,30

CP,1,ROTZ,10

CPNGEN,1,ROTZ,61.65,1

CP,2,ROTX,10

CPNGEN,2,ROTX,41.45,1

C\*\*\* SPECTRAL LOADING

EXTMOD,0,10

EXMODE,0,10,.001

SED,0,0,0,0,1,0 \* LOADING DIRECTION VECTOR

SVTYP,0

MCOMB,4 \* CQC MODAL COMBINATION

FREQ,1,126,158,2,251,316,398,501,631

FREQ,794,1,0,1,259,1,585,1,995,2,512,3,162,3,981,5,012

FREQ,6,310,10,0

SV,02,10,74404,10,41552,16,27039,10,78914,12,25910,23,09483,31,6868,27,9666

8,23,2336SV,02,26,4339,41,5602,31,12429,34,13453,31,32267,21,09132,20,80643

18,58266,11,10242

SV,02,6,8755,4,99404

SV,05,9,30424,8,14082,11,09237,9,22775,11,26828,19,68481,27,04603,21,76371,

18,98671

SV,.05,21.44260,31.64747,26.92249,30.27422,25.40870,15.25333,13.70017,14.247  
82,7.9174

SV,.05,5.08803,3.49641

SV,.10,7.48453,5.92197,7.31063,7.5869,9.83444,16.30909,21.4464,18.12219,15.59  
801

SV,.10,16.46297,21.52373,21.41171,25.44367,21.37437,11.51369,10.13662,10.108  
05,6.5517

SV,.10,4.98344,2.94805

LWRITE

AFWRIT

FINISH

The output file for the ANSYS dynamic portal frame analysis (with modal frequency data, nodal displacements and element nodal forces) is as follows:

\*\*\*\*\* RESPONSE SPECTRUM CALCULATION SUMMARY \*\*\*\*\*

MODE	CUMULATIVE		PARTIC.FACTOR	MODE COEF.	M.C. RATIO
	FREQUENCY	SV			
	EFFECTIVE MASS	MASS FRACTION			
1	0.9577 7211.06	38.1780 0.535503	84.92	538.8	1.000000
2	0.9903 0.380515E-06	40.7708 0.535503	-0.6169E-03	-0.4042E-02	0.000008
3	1.315 54.9871	31.6693 0.539586	-7.415	-28.43	0.052763
4	2.938 991.560	20.8966 0.613221	-31.49	-35.65	0.066159
5	3.040 0.124532E-07	20.8543 0.613221	0.1116E-03	0.1218E-03	0.000000
6	3.841 11.5354	18.9126 0.614077	-3.396	-2.662	0.004940
7	4.938 521.227	11.3813 0.652784	22.83	8.376	0.015545
8	5.142 0.756735E-09	10.4401 0.652784	0.2751E-04	0.8889E-05	0.000000
9	6.067 14.7678	7.4495 0.653881	3.843	0.7510	0.001394
10	6.798 447.836	6.5292 0.687138	21.16	3.235	0.006004
11	7.134 0.531341E-10	6.3141 0.687138	-0.7289E-05	-0.1027E-05	0.000000
12	7.827 60.7115	5.9201 0.691646	7.792	0.9380	0.001741
13	8.179 333.824	5.7423 0.716437	18.27	2.042	0.003789
14	8.656 0.701884E-08	5.5206 0.716437	0.8378E-04	0.8504E-05	0.000000
15	8.983 434.345	5.3800 0.748692	20.84	1.986	0.003687
16	9.412 3384.11	5.2085 1.00000	-58.17	-5.123	0.009509
17	9.505 0.144746E-05	5.1733 1.00000	0.1203E-02	0.1042E-03	0.000000

SUM OF EFFECTIVE MASSES= 13466.0

SIGNIFICANCE FACTOR FOR EXPANDED MODES = 0.10000E-02

## MODAL MULTIPLIERS INCLUDING DAMPING

MODE	FREQUENCY	DAMPING		SPECTRUM		SPECTRAL	
		ASSUMED	ACTUAL	ASSUMED	REQUIRED	MULTIPLIER	
1	0.958	0.0200	0.0233	38.1780	37.2026	0.974453	
3	1.315	0.0200	0.0215	31.6693	31.4613	0.993431	
4	2.938	0.0200	0.0222	20.8966	20.4050	0.976476	
6	3.841	0.0200	0.0215	18.9126	18.6826	0.987838	
7	4.938	0.0200	0.0232	11.3813	10.9514	0.962222	
9	6.067	0.0200	0.0214	7.4495	7.3537	0.987130	
10	6.798	0.0200	0.0251	6.5292	6.2350	0.954939	
12	7.827	0.0200	0.0218	5.9201	5.8227	0.983548	
13	8.179	0.0200	0.0255	5.7423	5.4457	0.948357	
15	8.983	0.0200	0.0288	5.3800	4.9222	0.914907	
16	9.412	0.0200	0.0932	5.2085	3.2290	0.619958	

## \*\*\*\*\* POST1 NODAL DISPLACEMENT LISTING \*\*\*\*\*

LOAD STEP 1 ITERATION= 1 SECTION= 1  
 FREQ= -1.0000 LOAD CASE= 1

THE FOLLOWING X,Y,Z DISPLACEMENTS ARE IN NODAL COORDINATES

NODE	UX	UY	UZ	ROTX	ROTY	ROTZ
1	0.0000E+00	0.0000E+00	0.0000E+00	0.0000E+00	0.0000E+00	0.0000E+00
2	0.0000E+00	0.0000E+00	0.0000E+00	0.0000E+00	0.0000E+00	0.0000E+00
3	0.0000E+00	0.0000E+00	0.0000E+00	0.0000E+00	0.0000E+00	0.0000E+00
10	0.1479E-05	0.0000E+00	0.1086		0.2087E-03	0.1744E-04
11	0.1404E-04	0.1591E-05	1.894		0.6980E-02	0.6050E-03
12	0.2979E-04	0.1455E-05	4.018		0.6554E-02	0.1127E-02
13	0.4223E-04	0.1091E-05	5.810		0.5321E-02	0.1556E-02
14	0.5116E-04	0.7049E-06	7.122		0.3677E-02	0.1867E-02
15	0.5604E-04	0.2816E-06	7.852		0.1647E-02	0.2035E-02
20	0.1489E-05	0.4724E-07	0.1082		0.2087E-03	0.1849E-04
21	0.1404E-04	0.4718E-07	1.879		0.6980E-02	0.6048E-03
22	0.2979E-04	0.4717E-07	3.989		0.6554E-02	0.1127E-02
23	0.4223E-04	0.4717E-07	5.770		0.5321E-02	0.1555E-02
24	0.5116E-04	0.4717E-07	7.074		0.3677E-02	0.1866E-02
25	0.5604E-04	0.4717E-07	7.800		0.1647E-02	0.2035E-02
41			0.2087E-03			
42			0.2087E-03			
43			0.2087E-03			
44			0.2087E-03			
45			0.2087E-03			
61					0.1569E-08	
62					0.1569E-08	
63					0.1569E-08	

64	0.1569E-08
65	0.1569E-08

## MAXIMUMS

NODE	15	11	15	11	15	11
VALUE	0.5604E-04	0.1591E-05	7.952	0.6980E-02	0.2035E-02	0.5462E-07

## \*\*\*\*\* POST1 ELEMENT NODE FORCE LISTING \*\*\*\*\*

LOAD STEP 1 ITERATION= 1 SECTION= 1  
 FREQ= -1.0000 LOAD CASE= 1

THE FOLLOWING X,Y,Z FORCES ARE IN NODAL COORDINATES

ELEM= 1 FX FY FZ  
 1 23.96 0.0000E+00 0.0000E+00  
 10 23.96 0.0000E+00 0.0000E+00

ELEM= 2 FX FY FZ  
 2 0.0000E+00 0.0000E+00 0.1759E+07  
 10 0.0000E+00 0.0000E+00 0.1759E+07

ELEM= 3 MX MY MZ  
 1 0.8265E+09 0.0000E+00 0.0000E+00  
 10 0.8265E+09 0.0000E+00 0.0000E+00

ELEM= 4 MX MY MZ  
 2 0.0000E+00 0.0000E+00 6215.  
 10 0.0000E+00 0.0000E+00 6215.

ELEM= 5 MX MY MZ  
 3 0.0000E+00 0.9298E+08 0.0000E+00  
 10 0.0000E+00 0.9298E+08 0.0000E+00

ELEM= 6 FX FY FZ MX MY MZ  
 10 0.0000E+00 0.0000E+00 0.0000E+00 0.0000E+00 0.0000E+00 0.0000E+00

ELEM= 7 FX FY FZ MX MY MZ  
 10 12.68 0.2209E-01 0.1648E+07 0.1338E+09 0.8950E+08 1045.  
 20 12.68 0.2209E-01 0.1648E+07 0.1338E+09 0.1270E+09 1044.

ELEM= 8 FX FY FZ MX MY MZ  
 20 12.68 0.6209E-02 0.1648E+07 0.1338E+09 0.1270E+09 1045.  
 21 12.68 0.6209E-02 0.1648E+07 0.1035E+09 0.1270E+09 781.7

ELEM= 9 FX FY FZ MX MY MZ  
 21 3.236 0.2348E-01 0.3688E+06 14.22 0.4791E+08 0.5901  
 11 3.236 0.2348E-01 0.3688E+06 14.22 0.4743E+08 0.1227

ELEM= 10 MX MY MZ

21 0.2093E+09 0.0000E+00 0.0000E+00  
41 0.2093E+09 0.0000E+00 0.0000E+00

ELEM= 11 MX MY MZ

21 0.0000E+00 0.0000E+00 1618.  
61 0.0000E+00 0.0000E+00 1618.

ELEM= 12 FX FY FZ MX MY MZ

11 0.0000E+00 0.0000E+00 0.0000E+00 0.0000E+00 0.0000E+00 0.0000E+00

ELEM= 13 FX FY FZ MX MY MZ

21 11.99 0.1009E-02 0.1507E+07 0.1075E+09 0.1176E+09 852.4  
22 11.99 0.1009E-02 0.1507E+07 0.1095E+09 0.1176E+09 874.5

ELEM= 14 FX FY FZ MX MY MZ

22 3.982 0.5586E-02 0.4408E+06 15.32 0.6710E+08 0.1671  
12 3.982 0.5586E-02 0.4408E+06 15.32 0.6660E+08 0.1183

ELEM= 15 MX MY MZ

22 0.1961E+09 0.0000E+00 0.0000E+00  
42 0.1961E+09 0.0000E+00 0.0000E+00

ELEM= 16 MX MY MZ

22 0.0000E+00 0.0000E+00 1479.  
62 0.0000E+00 0.0000E+00 1479.

ELEM= 17 FX FY FZ MX MY MZ

12 0.0000E+00 0.0000E+00 0.0000E+00 0.0000E+00 0.0000E+00 0.0000E+00

ELEM= 18 FX FY FZ MX MY MZ

22 8.987 0.5901E-04 0.1274E+07 0.8905E+08 0.1022E+09 617.6  
23 8.987 0.5901E-04 0.1274E+07 0.9448E+08 0.1022E+09 676.7

ELEM= 19 FX FY FZ MX MY MZ

23 3.027 0.1555E-02 0.4577E+06 16.61 0.7029E+08 0.3296  
13 3.027 0.1555E-02 0.4577E+06 16.61 0.6812E+08 0.3593

ELEM= 20 MX MY MZ

23 0.1581E+09 0.0000E+00 0.0000E+00  
43 0.1581E+09 0.0000E+00 0.0000E+00

ELEM= 21 MX MY MZ

23 0.0000E+00 0.0000E+00 1109.  
63 0.0000E+00 0.0000E+00 1109.

ELEM= 22 FX FY FZ MX MY MZ

13 0.0000E+00 0.0000E+00 0.0000E+00 0.0000E+00 0.0000E+00 0.0000E+00



**VITA**

**JOHN EUGENE HIGGINS, JR.**  
CAPTAIN, United States Air Force  
Box 123A Route 2  
Gladewater, TX 75647

**MILITARY EXPERIENCE**

Ph.D. CANDIDATE in civil engineering with emphasis on structure dynamics, assigned to Texas A&M University, College Station, TX, under the Air Force Institute of Technology (AFIT) Civilian Institutions Program. (Degree received May 1990.)

PROJECT OFFICER for enhanced superhard missile silo development, assigned to Ballistic Missile Office (BMO), Norton AFB, CA. Managed design and testing of prototype hardened silos for Peacekeeper and Small Missile systems. (Nov 82 - Aug 86)

**CIVILIAN EXPERIENCE**

SALES MANAGER for construction chemicals in western United States for Sika, Corp., Lyndhurst, NJ (Nov 80 - Jul 82)

QUALITY ASSURANCE MANAGER for Stanley Works (Division of Stanley Tools), Denver, CO. (Nov 78 - Sep 80)

DESIGN ENGINEER/INSPECTOR for Ross H. Bryan, Inc., Nashville, TN. (Sep 74 - Sep 78)

**EDUCATION**

MASTER OF SCIENCE in civil engineering with emphasis on structure analysis--Vanderbilt University, Nashville, TN. (Completed May 74)

BACHELOR OF ARTS in mathematics/physics (double major)--Vanderbilt University, Nashville, TN. (Completed May 72)